Decisional Tools for Optimising Process Economics, Capacity Sourcing and Portfolio Management for Biotherapeutics

Thesis submitted to University College London for the degree of Doctor of Engineering (EngD) in Biochemical Engineering

By

Annabel Lyle, BEng, MRes

The Advanced Centre for Biochemical Engineering

Department of Biochemical Engineering

UCL

WC1E 6BT

September 2023

Declaration

I, **Annabel Lyle**, confirm that the work presented in this thesis is my own. Where information has been derived from other sources, I confirm that this has been indicated in the thesis.

Abstract

Biopharmaceutical industry portfolios have diversified from ones centred on protein therapeutics to inclusion of a myriad of novel modalities, such as cell and gene therapies (CGTs). These biotherapeutics have the ability to address unmet medical needs and potentially be curative. However, their nascency brings several complexities and uncertainties to their development, manufacturing and ultimately commercialisation. This thesis aims to create a decisional tool that integrates cost modelling with multi-objective optimisation to aid manufacturing and capacity decisions at the process, drug development and enterprise level for both protein and gene therapy modalities.

This was approached by generating a decisional tool comprising the following key elements, (a) an adeno-associated virus (AAV) process economics model for the evaluation of AAV manufacturing options, (b) a drug development lifecycle cost model for the evaluation of overall research & development (R&D) budgets and (c) a stochastic multi-objective optimisation model for portfolio management and capacity planning of mixed-modality portfolios.

Each component of the tool was used to approach industrially-relevant case studies. The first key novel contribution involved investigation of the cost-effectiveness and purity performance of AAV flowsheets, with a particular focus on the impact of traditional versus scalable alternatives. Secondly, the drug development cost model was used for the estimation of overall R&D budgets for protein and CGT products and to provide benchmark contributions for process development and manufacturing activities. Finally, the overall decisional tool provided a novel means to address a portfolio and capacity optimisation case study for mixed-modality drug pipelines. This reconciled both risk and reward as objective functions and provided the first study to consider the dynamic impact of clinical success rates on both portfolio composition and capacity. This initially focused on mAbs and ADCs, investigating the impact of batch versus continuous-next generation manufacturing on the profitability. The study was

extended to evaluate the impact of CGT injection upon the portfolio characteristics. Overall, the decisional tool outlined within this thesis addressed both a novel set of computational methods and case studies, tackling some of the significant challenges biotherapeutic developers currently face.

Impact statement

Decisional tools have been utilised frequently within the biopharmaceutical industry to address a myriad of process and business-related questions, for a range of therapeutic modalities. The work conducted in this thesis involved construction of a decisional tool to address the perceived challenges associated with the manufacturing and development of cell and gene therapy products, as well as assessment of the profitability of mixed-modality portfolios in a dynamic environment. The outputs of each individual tool component aid industry in various decision-making practices early on in the development timeline. This aids in selection of processes or portfolio management strategies without practical implementation, thus reducing the use of material, labour and ultimately expenditure.

The benefits of implementing the tools described in this thesis have been acknowledged by a series of industry specialists, who were involved in providing and benchmarking assumptions or sponsorship of the work. Particularly for the AAV process economics work, Thomas Linke, Ph.D. (Principal Scientist, Purification Process Sciences at AstraZeneca, Gaithersburg, USA) expressed that, “Adeno-associated virus (AAV)-based vectors have emerged as the leading platform to deliver therapeutic genes into a patient’s cells. However, high treatment costs present a serious obstacle for the future of AAV-based gene therapies, and significant improvements in productivity and yields are required to achieve reduced manufacturing costs. Annabel has developed a decisional tool that can be used to inform and guide upstream and downstream development strategies toward the most cost-effective manufacturing process while meeting drug substance purity targets. Annabel’s case study clearly demonstrates how the decisional tool identified the optimal AAV manufacturing flow chart from many options in terms of purity, scalability, and process economics. The results from the EngD collaboration between AstraZeneca and UCL can guide us in prioritising our process development efforts and has the potential to save approximately 12 man-months in process development that translates into approximately £150k. The work described in this thesis is an important contribution toward bringing AAV-based therapeutics to market and providing patients

equitable access to gene therapies.” This was further reinforced with a statement from Albert Schmelzer Ph.D. (Executive Director, Cell Culture & Fermentation Sciences, AstraZeneca, Gaithersburg, USA), who stated “Annabel has developed an informative decisional tool that can enable process development scientists to identify opportunities to reduce cost of goods. The case studies identify a strategy for achieving at least a 40% reduction in cost of goods manufactured compared to traditional AAV production methods. These strategies translate to savings of $12M or more per year at peak commercial demand for AAV-based therapies. Through the framework developed here, process development can proceed more efficiently, as cost of goods considerations are at the forefront of strategy rather than as an after-thought. Following a similar approach, anyone can apply this work to their manufacturing processes.”

Furthermore, Brad Matanin (Director, Global Network Strategy for Biologics, AstraZeneca, Gaithersburg, USA) stated that “Biopharma portfolios are becoming increasingly complex with growth in both new modalities and standard mAbs. Through this collaboration, we have gained access to Annabel’s portfolio analysis tool to help support decisions on how best to optimize R&D portfolio prioritization and asset capacity planning considering the balance between batch versus continuous manufacturing platforms and mAbs versus new modalities. This could help us prioritise investment decisions into new manufacturing facilities for next generation platforms and new modalities. This is key to delivering robust supply while maximizing profitability.”

Acknowledgements

I would firstly like to express my sincere gratitude to my supervisor, Professor Suzy Farid, for the level of both personal and professional support provided throughout the EngD project. Her mentorship and guidance has truly shaped me as a student. I would also like to show my appreciation to my postdoctoral supervisor Dr. Christos Stamatis for his immense support, particularly with respect to development of my Python skills. I would also like to thank the UCL Biochemical Engineering department and in particular, the Decisional Tools group for consistent feedback on results and methodologies employed.

I must also acknowledge and express a huge thank you to AstraZeneca for the financial support, resources and knowledge provided to shape the work outlined in this thesis. In particular, thanks go out to Richard Turner, Julia Thompson, James Savery, Albert Schmelzer, Martyn Hulley, Jon Coffman, Brad Metanin and Lekan Daramola. A very special thanks must go to Thomas Linke, who provided consistent communication, resources and support on the AAV process economics work – I could not have developed the case study without his team's input. I would also like to convey further gratitude to the Engineering and Physical Sciences Research Council (EPSRC) for the financial support.

The completion of this thesis could not have been done without the personal support of so many in my life. A huge thank you goes out to my parents, who have always stood by my professional decisions with beaming pride, even if Dad often forgets I do Biochemical Engineering and not Maths and Physics (close enough). I wish to say a huge thank you to Lauren, and even little Rufus, for all the love, patience and even trying to understand what an AAV and a GA were when writing up. Thank you to the folk in the vineyard office at UCL, particularly Libby, Georgia, Haneen and Jordan, for riding the highs and lows together for the last four years and the last minute "we need a holiday" trips. To my best friends, who endured the journey of this EngD also, thank you to Shaz, Harriett, Lewis, Caitlin and Dougie.

UCL Research Paper Declaration Form
referencing the doctoral candidate's own published work(s)

Please use this form to declare if parts of your thesis are already available in another format, e.g. if data, text, or figures:

- *have been uploaded to a preprint server*
- *are in submission to a peer-reviewed publication*
- *have been published in a peer-reviewed publication, e.g. journal, textbook.*

This form should be completed as many times as necessary. For instance, if you have seven thesis chapters, two of which containing material that has already been published, you would complete this form twice.

1. **For a research manuscript that has already been published** (if not yet published, please skip to section 2)

   a) **What is the title of the manuscript?**

   Process economics evaluation and optimization of adeno-associated virus downstream processing.

   b) **Please include a link to or doi for the work**

   https://doi.org/10.1002/bit.28402

   c) **Where was the work published?**

   Biotechnology and Bioengineering

   d) **Who published the work?** (e.g. OUP)

   Wiley

   e) **When was the work published?**

   22 April 2023

   f) **List the manuscript's authors in the order they appear on the publication**

   Annabel Lyle, Christos Stamatis, Thomas Linke, Martyn Hulley, Albert Schmelzer, Richard Turner, Suzanne S. Farid

   g) **Was the work peer reviewed?**

   Yes

   h) **Have you retained the copyright?**

   Yes, Wiley allows the right to reuse the full text of the publishes article as part of a thesis if I am the author.

   i) **Was an earlier form of the manuscript uploaded to a preprint server?** (e.g. medRxiv). If 'Yes', please give a link or doi)

   If 'No', please seek permission from the relevant publisher and check the box next to the below statement:

   ☒

   *I acknowledge permission of the publisher named under **1d** to include in this thesis portions of the publication named as included in **1c**.*

2. **For a research manuscript prepared for publication but that has not yet been published** (if already published, please skip to section 3)

   a) **What is the current title of the manuscript?**

b) **Has the manuscript been uploaded to a preprint server?** (e.g. medRxiv; if 'Yes', please give a link or doi)

c) **Where is the work intended to be published?** (e.g. journal names)

d) **List the manuscript's authors in the intended authorship order**

e) **Stage of publication** (e.g. in submission)

3. **For multi-authored work, please give a statement of contribution covering all authors** (if single-author, please skip to section 4)

Annabel Lyle - Conceptualisation, data curation, formal analysis, investigation, visualisation, modelling, methodology, paper writing (original draft and review and editing)

Suzanne Farid – Conceptualisation, funding acquisition, resources, supervision, visualisation, validation, writing (review and editing)
Christos Stamatis – Resources, supervision, modelling, visualisation, writing (review and editing)
Martyn Hulley – Resources, supervision and validation
Thomas Linke – Resources, supervision and validation
Albert Schmelzer - Resources, supervision and validation
Richard Turner – Conceptualisation, resources, supervision and validation

4. **In which chapter(s) of your thesis can this material be found?**

Chapter 1 and 3

5. **e-Signatures confirming that the information above is accurate** (this form should be co-signed by the supervisor/ senior author unless this is not appropriate, e.g. if the paper was a single-author work)

Candidate 

Date:

24/08/2023

Supervisor/ Senior Author (where appropriate)

Suzanne Farid

Date

24/08/2023

Contents

Declaration **2**

Abstract **3**

Impact statement **5**

Acknowledgements **7**

UCL Research Paper Declaration Form **8**

List of Tables **14**

List of Figures **16**

Abbreviations **24**

1 Scope and Background **26**

1.1 Introduction 26

1.2 Biopharmaceutical drug development 28

1.2.1 Conventional drug development pathway 28

1.2.2 Expedited development pathways (FDA) 30

1.3 Manufacture of mAbs and ADCs 33

1.4 Gene therapy 35

1.4.1 Introduction to adeno-associated viruses (AAV) 35

1.4.2 Viral vector market and clinical trials 37

1.4.3 AAV manufacturing 38

1.4.4 Development and manufacturing challenges 45

1.5 Computational methods for optimisation 51

1.5.1 Mathematical programming 51

1.5.2 Heuristics and meta-heuristics 52

1.5.3 Single and multi-objective optimisation 57

1.5.4 Use of computational methods in decision-support tools 61

1.6 Decisional tools 63

1.6.1 Applications of decisional tools 63

1.6.2 Decisional tools for novel modalities 69

1.7 Aims and organisation of thesis 71

2 Decisional tool: Problem requirements and structure **74**

2.1 Overview 74

2.2 Problem definition 77

2.2.1 Requirements and capabilities 77

2.3 Selection of software and overall model design 79

2.3.1 AAV process economics 80

2.3.2 Derivation of R&D budgets for mAbs, ADCs, AAVs and CAR T 82
2.3.3 Portfolio management and capacity planning for mAbs, ADCs, AAVs and CAR T 84
2.4 Conclusion 87

3 Process economic evaluation and optimisation of adeno-associated virus manufacturing 88
3.1 Introduction 88
3.2 Materials and methods 90
3.2.1 Overview and description of decisional tool 90
3.2.2 Process models 91
3.2.3 Process economics 104
3.2.4 Uncertainty analysis 110
3.2.5 Optimisation 111
3.3 Case study setup 115
3.3.1 Case study overview 115
3.3.2 Process outline 115
3.3.3 Key assumptions 117
3.3.4 Monte Carlo assumptions 118
3.3.5 Optimisation assumptions 118
3.4 Results and discussion 123
3.4.1 What is the COG/dose breakdown for the traditional versus scalable AAV flowsheets? 123
3.4.2 How does dose size impact COG/dose? 125
3.4.3 How does uncertainty impact the robustness of the strategies? 127
3.4.4 What is the optimal purification strategy in terms of meeting cost and purity targets? 130
3.4.5 How does the optimal polishing strategy change with AEX yield and empty capsid removal? 133
3.4.6 What is the optimal AAV flowsheet in terms of cost and purity targets? 137
3.4.7 How does the critical lysis point impact cost and impurity release? 140
3.5 Conclusion 143

4 Estimation of research & development budgets for novel modalities 145
4.1 Introduction 145
4.2 Drug development lifecycle 146
4.3 Methodology 151
4.3.1 Overview 151
4.3.2 Process development 152

4.3.3 Manufacturing 153
4.3.4 Clinical trials 154
4.3.5 Transition success rates 154
4.3.6 Total budgets and capitalised equivalents 155
4.4 Case study setup 155
4.4.1 Key assumptions 156
4.5 Results and discussion 168
4.5.1 What is the CMC contribution towards the R&D cost? 168
4.5.2 What is the impact of assuming different success rates between modalities? 173
4.5.3 Sensitivity analysis 174
4.6 Conclusion 182

5 Portfolio optimisation and capacity planning for mixed modality portfolios 184
5.1 Introduction 184
5.2 Model formulation 186
5.2.1 Problem-specific notation 186
5.2.2 Case study terminology 187
5.2.3 Overview 188
5.2.4 GA theory 192
5.2.5 Chromosome-encoding strategy 197
5.2.6 Candidate portfolio structure 199
5.2.7 Objective functions 201
5.2.8 Optimisation algorithm 205
5.2.9 Uncertainty 221
5.2.10 Bernoulli event-based simulation 221
5.3 Case study setup 224
5.3.1 Case study definition 224
5.3.2 Portfolio outline 227
5.3.3 Key portfolio assumptions 229
5.3.4 Optimisation structure and assumptions 232
5.3.5 Constraints 234
5.3.6 Uncertainty assumptions 237
5.3.7 Bernoulli-event based simulation 237
5.4 Results and Discussion 240
5.4.1 What is the appropriate choice of GA parameters? 240
5.4.2 What is the optimal portfolio structure when different batch: continuous ratios are assumed? 248
5.4.3 How does risk dynamically impact the portfolio? 258
5.4.4 How does the injection of CGTs impact the portfolio characteristics? 262

5.4.5 How does the portfolio structure change if CGTs are injected at the same rate as mAbs? ... 264
5.4.6 How does the portfolio structure change if risk is favoured over reward? 266
5.5 Conclusion ... 270

6 Conclusions and future work ... **272**
6.1 Introduction ... 272
6.2 Process economic evaluation and optimisation of AAV manufacturing ... 272
6.2.1 Summary of findings ... 272
6.2.2 Future work ... 273
6.3 Estimation of CMC budgets for novel modalities ... 275
6.3.1 Summary of findings ... 275
6.3.2 Future work ... 276
6.4 Portfolio management and capacity planning for mixed modality portfolios 277
6.4.1 Summary of findings ... 277
6.4.2 Future work ... 278
6.5 Summary ... 279

7 Commercialisation ... **280**
7.1 Introduction ... 280
7.2 Tool appraisal for industrial practices ... 280
7.2.1 Hiding Jupyter code ... 280
7.2.2 Implementation of widgets ... 283
7.2.3 Performance ... 283
7.2.4 Supporting documentation for usage ... 284
7.2.5 Revenue ... 285

Bibliography ... **286**

Appendices ... **286**

A: Process economic evaluation and optimisation of AAV manufacturing ... 311

B: Estimation of research & development budgets for novel modalities ... 328

C: Portfolio optimisation and capacity planning for mixed modality portfolios ... 331

Papers by the author ... **345**

List of Tables

Table 1.1 Breakdown of expedited regulatory programs designated by the FDA. 32

Table 1.2 Common adherent technologies utilised for AAV production and the range of sizes that can be typically found in industry. 39

Table 1.3 Summary of optimisation methods alongside benefits and limitations of implementation..... 54

Table 1.4 Glossary of key genetic algorithm terms. 56

Table 1.5 A selection of convergence metrics used in multi-objective optimisation. 59

Table 1.6 Summary table of the application of decision-support tools to novel therapeutics. 69

Table 2.1 Breakdown of results chapter by the model components used. 76

Table 3.1 Cost of goods per year breakdown and equations utilised in model (Suzanne S. Farid, 2002). 106

Table 3.2 AAV flowsheet combinations considered in the deterministic analysis and the associated assumptions for each. 119

Table 3.3 Key AAV process assumptions for the case-study. 119

Table 3.4 Purification assumptions utilised in the process economics model. 120

Table 3.5 Constraints considered in the brute-force optimisation work. 122

Table 4.1 Process development personnel breakdown by category and relevant definition. 156

Table 4.2 Estimated FTE requirements for process development activities for mAbs and ADCs. 158

Table 4.3 Estimated FTE requirements for process development activities for viral vectors and CAR T. 159

Table 4.4 Key manufacturing inputs for the protein process economics model 162

Table 4.5 Key manufacturing inputs for the viral vector and CAR T process economics models. 164

Table 4.6 Clinical success rates for each modality by phase and the corresponding number of projects required overall. 166

Table 5.1 Characteristics of the drugs in the starting portfolio. 230

Table 5.2 Ranges of assumptions used for drugs in the pipeline..... 231

Table 5.3 Key inputs used for the GA-based optimisation work and corresponding values. 234

Table 5.4 Future facility options and manufacturing capacities. 236

Table 5.5 Summary of capacity options available for each modality. 236

Table 5.6 Uncertain parameters utilised in the portfolio management tool. 237

Table 5.7 Probabilities of transition success for each modality by phase and the corresponding number of projects required overall. 239

Table 5.8 Key model results across algorithm generations. 244

Table 5.9 Key model results across population sizes evaluated. 247

Table 5.10 Key outputs for top performing candidate portfolios in the 20% study. 251

Table 5.11 Key outputs for top performing candidate portfolios in the 80% study. 255

Table 5.12 Change in eNPV and portfolio size when repair strategy is implemented. 258

Table 5.13 Risk-adjusted results for both continuous pipeline scenarios. 259

List of Figures

Figure 1.1 Drug discovery and development pathway for typical biopharmaceuticals. Here, a split is determined between research or studies that are conducted in-vitro or in animals and those that are carried out in human volunteers..... 31
Figure 1.2 Key advantages and disadvantages of using AAV as a gene delivery vehicle, relative to LV, another popular choice of vector in gene therapy (Clark, 2002; Daya & Berns, 2008; Mountain, 2000). 36
Figure 1.3 Breakdown by indication of AAVs used in clinical trials. This is further broken down to highlight the number of projects targeting a particular indication in each clinical trial phase (Cell and Gene Therapy Catapult, 2022)..... 38
Figure 1.4 Overview of AAV gene delivery mechanisms into mammalian cells. The green tick symbolises the genetic material that is innately contained within the cells, whereas the red cross signifies that which is not innately present and therefore needs to be supplied, typically by means of transfection or infection. 40
Figure 1.5 General process flowsheet for AAV manufacture, supplemented with the function of each step. 42
Figure 1.6 Schematic highlighting the methods of increasing culture volume for AAV production. On the left, roller bottles, an example of an adherent culture technology, whereby scaling out is required to permit an increase in culture volume. On the right, a single use bioreactor as an example of a suspension culture technology; in this case, scale up is possible. Note: bioreactor images sourced from Sartorius, roller bottle images sourced from Sigma Aldrich. 47
Figure 1.7 Graphic representation of the generalised procedure undertaken during a GA. As highlighted, those elements integrated within the cyclic portion of the diagram refer to steps that are repeated across the number of algorithm generations. Those tasks that appear outside of this are steps required to initialise the algorithm and are only repeated when multiple runs of the algorithm are carried out. More distinct definitions of the terms involved in a GA are outlined in Chapter 5. 55
Figure 1.8 Adapted from Farid (2012). Typical analytical stages and techniques employed in decision making. 64
Figure 2.1 Schematic of the interaction between chapters within the thesis. The red contour indicates the tool component used in the AAV process economics work. The blue contour indicates those used within the drug development lifecycle cost model work. The black contour represents the overall decisional tool, incorporating the portfolio management and capacity sourcing elements also. 76

Figure 2.2 Example of class design in the AAV process economics model in Python 3.8, using chromatography as an example unit operation. All classes were coded in Spyder (IDE) and objects were instantiated in Jupyter Notebook (GUI). The structure of classes always took the following: class definition (e.g. chromatography), definition of relevant attributes (e.g. DBC, resin type) and the set of methods or calculations related to the class (e.g. mass balancing and sizing equations for chromatography)..... 81
Figure 2.3 Example of class design in the drug development lifecycle model in Python 3.8, using the stage as an example. All classes were coded in Spyder (IDE) and objects were instantiated in Jupyter Notebook (GUI). The structure of classes always took the following: class definition (e.g. a given stage), definition of relevant attributes (e.g. activity type (process development, manufacturing or clinical trials), modality under consideration or phase (e.g. I, II, III, regulatory review) and the set of methods or calculations related to the class (calculation of the costs for the activity, phase and modality under consideration). 83
Figure 2.4 Example of class design in the portfolio optimisation tool in Python 3.8, using the genetic algorithm as an example. All classes were coded in Spyder (IDE) and objects were instantiated in Jupyter Notebook (GUI). The structure of classes always takes the following: class definition (e.g. genetic algorithm), definition of relevant attributes (e.g. GA parameters) and the set of methods or calculations related to the class (steps involved in evolving candidate solutions). 85
Figure 3.1 Example generic string for optimisation algorithm..... 112
Figure 3.2 Architecture of brute force optimisation algorithm and the relationship with the base-case process economics model. 113
Figure 3.3 Viral vector process flowsheet for adeno-associated virus (AAV) vector product. The dendrograms illustrate the key differences between the four flowsheets initially evaluated in the cell culture (adherent versus suspension) and polishing (ultracentrifugation versus chromatography) stages. AEX, anion-exchange chromatography; UC, ultracentrifugation. 117
Figure 3.4 COG/dose breakdown by category within USP and DSP process stages for four AAV flowsheet options with adherent or suspension culture for USP and AEX or UC for polishing. The boxes on the right of each bar represent key sizing metrics; the top number highlights the number of cell culture units or the bioreactor volume (for adherent or suspension scenarios respectively). The bottom number represents the number of parallel ultracentrifuges used or the AEX column diameter (for UC or AEX scenarios respectively). The second set of boxes located to the right of the bars highlights the USP: DSP cost of goods ratios for each scenario. The percentages next to each bar represent the COG/dose reduction for each flowsheet relative to the traditional flowsheet of adherent-ultracentrifugation. The demand was assumed to be 1,000 doses/year, with a dose size of 1 x 10^{14} vg/dose. The facility was resized for each set of inputs. Ad, adherent culture; AAV, adeno-associated virus; AEX, anion-

exchange chromatography; COG, cost of goods; DSP, downstream processing; Susp, suspension culture; UC, ultracentrifugation; USP, upstream processing. 125
Figure 3.5 Scatter plots displaying the COG/dose change with increasing dose size. The demand was assumed to be 1,000 doses/year. The facility was resized for each set of inputs. 127
Figure 3.6 Uncertainty analysis results from the Monte Carlo simulation showing (a) violin plots of the COG/dose distributions for each scenario under uncertainty, (b) key probabilistic output parameters for each scenario, (c) uncertain process input parameters and their distributions evaluated in the Monte Carlo simulations. The demand was assumed to be 1,000 doses/year, with a dose size of 1 x 10^{14} vg/dose. The facility was resized for each set of inputs. 130
Figure 3.7 Brute-force outputs for AAV purification scenarios where **a)** differing target levels of empty capsid removal are encountered, **b)** different starting levels of host cell proteins (HCP) and **c)** different starting levels of DNA are defined. The $ symbols represent the most cost-effective option when less than 75% empty capsid removal is achieved or low starting levels of HCP or DNA ($2x10^{-7}$ ng/vg and $6x10^{-10}$ ng/vg) are assumed. For **a)**, M = optimal solution when at least 75% removal of empty capsids is required and H = optimal solution when at least 90% removal of empty capsids are required. For **b)** and **c),** H = optimal solution when a high impurity load is used ($2x10^{-5}$ ng/vg and $6x10^{-8}$ ng/vg). The contours represent the following; (- - -) meet target for a moderate impurity level, (——) meet target for a high impurity level. Grey box = breach constraints (see **Figure A4** for details). The demand was assumed to be 1,000 doses/year, with a dose size of 1 x 10^{14} vg/dose. 134
Figure 3.8 a) Optimal polishing purification choice in terms of COG/g across a matrix of scenarios with different combinations AEX yields and purity targets. A "/" sign in each box is used to represent solutions that fall within a 5% COG/dose difference from the optimal solution. Lighter shading represents solutions that do not contain AEX in the winning solution. Darker shading represents solutions that do contain AEX in the winning solution, **b)** Feasible solutions remaining in brute-force optimisation choices at each purity target. The demand was assumed to be 1,000 doses/year, with a dose size of 1 x 10^{14} vg/dose. The facility was resized for each set of inputs. 136
Figure 3.9 Brute-force optimisation outputs for full flowsheet scenarios. The $ symbol represents the most cost-effective option when less than 75% empty capsid removal is achieved. M = best performing solutions when at least 75% removal of empty capsids is required. H = best performing solutions when at least 90% removal of empty capsids are required. The contours represent the following; (- - -) meet the 75% target, (——) meet the 90% target. Grey coloured areas = breach constraints. The demand was assumed to be 1,000

doses/year, with a dose size of 1 x 10^{14} vg/dose. The facility was resized for each set of inputs. 139
Figure 3.10 Heatmap generated for comparison of lysis point. Three demands (in doses) are presented, which are found on the y-axis. The x-axis refers to the extracellular scenario in question, e.g. 90% refers to a scenario where 90% of the AAV is secreted and 10% is retained in the cell. **a)** the percentages refer to the difference between the scenario under consideration and the case where a fully (100%) extracellular AAV was assumed (scale provided by the ladder on the right of the figure). The black dotted line is placed to give the critical lysis point, which is defined as the point beyond which a significant COG/dose difference is exhibited (significant being deemed 10%)**, b)** upstream sizing for each scenario, where the first number is how many bioreactors were required and the second is the bioreactor model used**, c)** for a multi-model and AEX purification platform, what the overall LRV would be in cases of lysis or no lysis. 142
Figure 4.1 Representation of the dependencies between process development (PD), manufacturing (MFG) and clinical trials (Trials) activities. The example used here is the trajectory of a mAb product. Colours are used to distinguish between activities pertaining to a specific phase, e.g. the shade of blue used for Phase I is used for the corresponding PD and MFG activities. 149
Figure 4.2 a) Key inputs and outputs into the decisional tool, divided by key cost category, including process development, manufacturing and clinical trial activities, **b)** specifics of each activity broken down by development phase. Included here is quantitative data related to the inputs outlined in **a).** 150
Figure 4.3 Out-of-pocket cost schematic depicting the development pathway and cost breakdown by development activity and phase for **a)** mAbs and **b)** ADCs. The clinical success rates (overall rate of 12% assumed for **a)** and **b)**) were used to calculate the number of projects required at each stage of the development pathway to achieve a market success. The process development and manufacturing activities were costed at-risk based on the number of projects. The number of projects at each phase are shown about the cost breakdowns. [Style of figure presentation adapted from Nie (2015) and Farid et al. (2020)]. 169
Figure 4.4 Out-of-pocket cost schematic depicting the development pathway and cost breakdown by development activity and phase for **a)** AAVs and **b)** CAR T cells. The clinical success rates (overall rate of 12% assumed for **a)** and **b)**) were used to calculate the number of projects required at each stage of the development pathway to achieve a market success. The process development and manufacturing activities were costed at-risk based on the number of projects. The number of projects at each phase are shown about the cost breakdowns. [Style of figure presentation adapted from Nie (2015) and Farid et al. (2020)]. 170

Figure 4.5 CMC out-of-pocket cost breakdown per success for each modality. The overall success rate was assumed to be equal across modalities (at 12% LOA from Phase I). PD = process development, MFG = manufacturing. 172
Figure 4.6 Out-of-pocket cost breakdowns per success when **a)** the same clinical success rates were assumed across modalities and **b)** different clinical success rates were assumed for each modality, sourced from (QLS, 2021). 175
Figure 4.7 Sensitivity analysis output when considering success rate scenarios by modality type. The y-axis refers to the modality under consideration and the x-axis represents what success rate scenario was being considered. Each box corresponds to the total out-of-pocket cost per success for the given scenario. The ladder on the right-hand side is a Python 3.8 generated scale for the heatmap, where the darker shading relates to higher costs and lower costs for lighter shades. The best, base and worst scenarios reflect the data in **Table 4.6**, where the base case refers to the same used in **Figure 4.6 b)** 177
Figure 4.8 a) The sensitivity analysis output for each indication. The x-axis gives key inputs (LOA from Phase I and Ph I: III projects) and the modalities under consideration. The optimal modality in terms of budget is highlighted with the dotted contours around corresponding budget values. The y-axis represents the indication under consideration. The ladder on the right-hand side is a Python 3.8 generated scale for the heatmap, where the darker blue relates to higher costs and lower costs for lighter shades of blue. Each box corresponds to the total out-of-pocket cost per success for the given scenario. The base case from **Figure 4.4** was used as a reference point, **b)** total out-of-pocket cost distribution across all phases for each modality. The bars are annotated with the specific percentage contributions..... 181
Figure 4.9 Change in total out-of-pocket cost with overall LOA from Phase I success rate across modalities. The red dotted line represents the critical overall success rate at which the optimal in terms of budget changes..... 182
Figure 5.1 Overall tool architecture for the portfolio management and capacity planning case study. Grey shaded boxes located outside the dotted contours relate to assumptions or key model inputs. Simulation-based steps (i.e. generating cost data from process economics and drug development cost models) are contained within the red dotted contours or are shaded orange. Optimisation-based (i.e. use of the modified GA) are contained within the black dotted contours or are shaded blue. The step labelled “Evaluation of fitness” is contained within the optimisation procedure, but draws upon the outputs from the simulation part of the model, hence lies within a red contour. The green shaded box represents the success-failure simulation, which is an independent part of the tool. 191
Figure 5.2 Examples of chromosome-encoding strategies employed when using GA-based algorithms, where **a)** is binary-encoding, **b)** permutation-encoding / integer representation and **c)** value-encoding. 194

Figure 5.3 Illustration of how value encoding can be converted to binary. The number of bits was assumed to be 3, hence each gene is represented in triplets, shown by the contour lines drawn. 195
Figure 5.4 Generic chromosome structure for the case study. Notation: ds, i = candidate drug i from candidate solution (s), $i \in Ndpipe$, ms, i = commercial manufacturing strategy for drug i (in-house, CMO or future facility), $i \in Ndpipe$, $s \in Npop$. 199
Figure 5.5 Derivation of the objective functions within the tool. Within each box, an indication of the Python data structure used for coding the datasets, e.g. list or dictionary, is provided. Boxes shaded in grey represent datasets that are constructed outside of the optimisation algorithm loop, thus were not confined to any form of time complexity that arose from running over multiple iterations. Boxes shaded light blue represent datasets that vary across each iteration or generation within the algorithm, hence were re-generated during each loop. The solid contour ( ) was used to highlight the grouping of the expenses and revenues for any given candidate solution, though values were expressed in separate lists (income versus outgoings). The dotted contour (- - -) was used to group the income and outgoings after the impact of drug failures were applied, if the Bernoulli event-based simulation was conducted. 204
Figure 5.6 General tool architecture for the modified genetic algorithm. The dotted boxes further highlight the changes occurring to the population size throughout the procedure... 206
Figure 5.7 Creation of new population at each generation in the optimisation algorithm. P_g and O_g together depict the combined parent and offspring population. The next stage highlights the procedure of non-dominated sorting, where the combined population are divided into a series of Pareto ranks or fronts (front 1 is the optimal set). The next parent population is half of the combined population in the previous generation and therefore, any relevant splitting of a particular Pareto front / rank is handled by crowding distance sorting, which seeks to reject a portion of the front which is considered more crowded. Furthermore, P_{g+1} reflects the new population created for the next generation. 210
Figure 5.8 Illustrative example of the hypervolume calculation. The axes represent an illustrative example of an objective function 1 (f_1) and objective function 2 (f_2), where it is desirable to maximise f_1 and minimise f_2. The dotted lines show how the rectangles are formed for the calculation of the overall hypervolume. The reference point is highlighted in blue. . 212
Figure 5.9 Examples of the crossover and mutation procedures followed in the tool (**b**) and their differences between single-point and bit-point crossover and mutation, **a)** single-point crossover and bit-point mutation procedure for matrix-style chromosomes and **b)** uniform crossover and mutation for matrix-style chromosomes. In both **a)** and **b),** the split between crossover and mutation is defined. The solid contours in the parent chromosomes represent the crossover point(s) and the impact is shown in the “after crossover” chromosomes, shaded

grey to depict the swapping of genes. The dashed contours highlight the mutation points(s), where the blue shading in the offspring highlighted the result of a gene mutation. 215
Figure 5.10 Illustrative examples of chromosome encoding and the translation to the corresponding product IDs. The dotted contours around certain drugs highlight their exclusion and hence a 0-value assigned during binary encoding. 233
Figure 5.11 Progression of the objective space over generations, **a)** generation number 1**, b)** generation number 5**, c)** generation number 10**, d)** generation number 15**, e)** generation number 20, **f)** generation number 25, **g)** generation number 30, **h)** generation number 35, **i)** generation number 40. 243
Figure 5.12 Change in the weighted objective functions with the number of algorithm generations. A secondary axis of computational time is provided to show the increased computational intensity required to achieve fitter solutions. Red dotted line = boundary defined where the optimal solution is +/-5% of the maximum value achieved in the study. 243
Figure 5.13 Progression of the objective space across population sizes, **a)** population size = 20**, b)** population size = 40**, c)** population size = 60**, d)** population size = 80**, e)** population size = 100, **f)** population size = 120, **g)** population size = 140, **h)** population size = 160, **i)** population size = 180. 246
Figure 5.14 Change in weighted objective value with the population size. A secondary axis of computational time is provided to show the increased computational intensity required to achieve fitter solutions. The optimal line represents the fittest solution achieved after successive algorithm iterations. Red dotted line = boundary defined where the optimal solution is +/-5% of the maximum value achieved in the study. 247
Figure 5.15 Plot of the objective space from generation 30. Circled solutions are part of the non-dominated frontier or Pareto rank 1 and were hence selected to further analyse on a drug-by-drug basis. As discussed in Section 5.2, candidate solutions are generally represented by sg,p, where g = generation number and p = solution index in the population. 251
Figure 5.16 Structure of the candidate portfolios highlighted in **Figure 5.14**. Each set of two rows represents a single candidate portfolio, as denoted in the figure. M = mAb product and A = ADC product. I = in-house, C = CMO and F = future facility. Orange shading = internal capacity options selected (in-house), blue shading = outsourcing to CMO and green shading = future facility. Grey shading = products that are manufactured continuously and white shading = products that are manufactured in batch mode. 252
Figure 5.17 Plot of the objective space from generation 30. Circled solutions are part of the non-dominated frontier (or Pareto rank 1) and were hence selected to further analyse on a drug-by-drug basis. As discussed in Section 5.2, candidate solutions are generally represented by sg,p, where g = generation number and p = solution index in the population. 255

Figure 5.18 Structure of the candidate portfolios highlighted in **Figure 5.16**. Each set of two rows represents a single candidate portfolio, as denoted in the figure. M = mAb product and A = ADC product. I = in-house, C = CMO and F = future facility. Orange shading = internal capacity options selected (in-house), blue shading = outsourcing to CMO and green shading = future facility. Grey shading = products that are manufactured continuously and white shading = products that are manufactured in batch mode. 256
Figure 5.19 a) Profitability of selected candidate solutions compared with the overall LOA from Phase I (%). The data is split corresponding to the percentage of failures that occur early, i.e. in Phase I, **b)** raw data corresponding to that plotted in **a).** 261
Figure 5.20 Sensitivity analysis results when three risk profiles are considered in the portfolio optimisation framework. The probabilities of transition success used across scenarios are found in **Table 5.7**. The red shading represents the worst-case. The white shading is the base-case. The blue shading is the best-case. 264
Figure 5.21 Optimal portfolio composition across different CGT injection rates when success rate (risk scenario) is also varied. Within each box, the top value represents the ratio of protein products to CGT products within the final portfolio and the bottom value highlights the ratio of in-house to CMO to future facility capacity selected. The shading (key in the top-left) represents those solutions that fall below or above a set NPV threshold, defined here as $8bn. The risk scenarios represent those presented in **Table 5.7**. 266
Figure 5.22 a) Top ranking solutions plotted by each objective when different weightings were assigned to each objective function and **b)** the percentage of CGTs that appeared in the top performing portfolios in each weighting scenario. The bar colour in **b)** correspond to the lines in **a).**..... 269
Figure 7.1 Snapshot of the GUI for the decisional tool on Jupyter notebook. The blue circle highlights the hide code tab installed through “NbExtensions” and the red circle highlights a shortcut to access this hide code feature. 281
Figure 7.2 Resulting GUI from enabling the hide code feature. The only remaining displays are any input widgets or outputs from the functioning of the hidden code..... 282
Figure 7.3 Syntax relating to the input of the number of Monte Carlo trials. Input is an in-built Python 3.8 function for entering numerical data if paired with int()..... 283

Abbreviations

AAV	Adeno-associated virus
ADC	Antibody drug conjugate
AEX	Anion exchange
BHK	Baby hamster kidney
CAGR	Compound annual growth rate
CAR	Chimeric antigen receptor
CEX	Cation exchange
CGT	Cell and gene therapies
CHO	Chinese hamster ovary
CMO	Contract manufacturing organisation
COG	Cost of goods
CMO	Contract manufacturing organisation
CRO	Contract research organisation
CsCl	Caesium chloride
CT	Clinical trials
DES	Discrete-event simulation
DNA	Deoxyribonucleic acid
DSP	Downstream processing
EMA	European Medicines Agency
FCI	Fixed capital investment
FDA	Food and drug administration
FF	Future facility
FTE	Full-time equivalent
GA	Genetic algorithm
GOI	Gene of interest
GUI	Graphical user interface
HEK	Human-embryonic kidney
IDE	Integrated development environment
IEX	Ion exchange
IH	In-house
IND	Investigational new drug
LCA	Leber’s congenital amaurosis
LOA	Likelihood of approval
LV	Lentivirus
mAb	Monoclonal antibody

MCDM	Multi-criteria decision making
MFG	Manufacturing
MILP	Mixed integer linear programming
MMC	Multi-model chromatography
MOO	Multi-objective optimisation
MSC	Mesenchymal stem cells
NDA	New Drug Application
NPV	Net present value
eNPV	Expected net present value
sdNPV	Standard deviation of net present value
NSGA-II	Non-dominated sorting algorithm II
PCC	Periodic counter current
PD	Process development
PSO	Particle Swarm Optimisation
R&D	Research and development
RNA	Ribonucleic acid
SEC	Size exchange chromatography
SMA	Spinal muscular atrophy
SOO	Single-objective optimisation
SS	Stainless steel
SU	Single-use
USP	Upstream processing

1 Scope and Background

1.1 Introduction

The development pathway through which biological drugs traverse to achieve market status is often characterised by large expense and relatively low overall probabilities of success. The nascency of the field with respect to emerging modalities and technologies, as well as the many complexities existing at a molecular level often necessitate the injection of substantial research and development (R&D) budgets to finance key activities along the drug development pathway, notably process development efforts, drug manufacturing and the conductance of clinical trials. Estimates of these capitalised budgets have been placed in the range of $3 – 4bn (DiMasi et al., 2016; Farid et al., 2020) with overall timings from pre-clinical phase to commercialisation around 10 to 15 years. It is therefore critical that the various stage costs encountered along the pathway and ultimately R&D budgets are estimated early on, with the impact of risk upon investment playing a pivotal role in financial projections. Furthermore, at a dynamic level, consideration of a company's finite resources and how best to allocate them amongst a plethora of drugs within the portfolio is also significant to ensure delays or manufacturing restrictions are not encountered.

Whilst the aforementioned challenges are representative of biological drugs in general, they are particularly pronounced when considering the more novel biologics which have achieved less success to date in being commercialised. Particularly in comparison to more established modality groups like that of monoclonal antibodies (mAbs), cell and gene therapies (CGT) present significant and unique developmental challenges at both a process and business level. The relative complexity in production of these therapies have generated high cost of goods (COG) at a manufacturing level and often bring about increased early-phase process development effort (compared to mAbs). Furthermore, the long-term impact of utilising these treatments is still uncertain, hence patient follow-up is a more lengthy and costly process than for protein therapeutics.

In summary, this suggests that there is an importance in deriving a comprehensive and integrated tool capable of addressing the critical features of drug development, alongside the current challenges in both manufacturing and development. The use of decisional tools has historically been significant in deriving solutions to several of the process and business challenges (Farid, 2012). As a result, the aim of the work conducted in this thesis is the development and utilisation of a decisional tool that integrates process economic modelling with cash-flow and profitability analysis.

To establish knowledge on the scope of research already conducted on the topics already outlined, including modelling techniques, this chapter presents a review of the relevant literature and explores areas where investigation is necessary. Section 1.2 gives an overview of the conventional drug development lifecycle for a biopharmaceutical, followed by a review of expedited pathways designed, in general, for more novel modalities. Section 1.3 provides detail about the manufacture of protein therapeutics, in particular monoclonal antibodies (mAbs) and antibody-drug conjugates (ADCs). Section 1.4 discusses the use of viral vectors in *in-vivo* gene therapy applications, specifically AAV. This section includes market data, as well as information on the various manufacturing strategies employed to produce AAVs and the corresponding challenges necessary to combat. Furthermore, Section 1.5 discusses an array of computational methods that have previously been employed in biopharmaceutical modelling and optimisation, with particularly focus given to meta-heuristics. Section 1.6 provides a breakdown of the typical techniques employed in the decisional tools space, as well as various examples of their specific application within a bioprocessing context. This is narrowed down further to include the use of these tools for comparatively more novel modalities in comparison to mAbs.

1.2 Biopharmaceutical drug development

Biopharmaceuticals are a subset of pharmaceuticals which are derived from biological sources, as opposed to chemical synthesis. These biopharmaceuticals generally may be small biomolecules, protein or nucleic acid-based, however in recent years, the field has expanded to include a wealth of other entities, including stem cells, gene therapies and combination therapies (Mokhtari et al., 2017). For the purposes of this review, as well as the work conducted in the thesis as a whole, monoclonal antibodies (mAbs), antibody drug-conjugates (ADCs), adeno-associated viruses (AAVs) and chimeric antigen receptor T-cells (CAR T cells) are specifically focused upon.

1.2.1 Conventional drug development pathway

1.2.1.1 Pre-discovery and drug discovery

The pathway from drug discovery to market for a biopharmaceutical centres around three stages; drug discovery, development and commercialisation (Pérez-Escobedo et al., 2011). **Figure 1.1** highlights the breakdown of this lifecycle; initiated before drug discovery, a preliminary stage whereby R&D teams aim to better understand a chosen indication and its effect on the body (Lo & Field, 2010; Schenone et al., 2013). This initial research may take place within the company itself, or may be in partnership with a contract research organisation (CRO). Following this, a wealth of relevant biomolecules are assessed in their ability to target a particular disease or condition (Chorghade, 2006). This iterative research process can typically last for 1 - 2 years, with the number of potential drug candidates decreasing as time goes on. A disease target (hypothesised to be the root cause of a given indication) is typically identified at this point. Most significantly, validation must be carried out to ensure that the desired target is able to be treated by a candidate therapy (Lo & Field, 2010).

Progression from this point involves R&D teams searching for a potential therapeutic candidate to address the indication, by harnessing compounds found either as wild-type molecules or those that have been engineered for a particular use (recombinant). Through a

variety of initial screening techniques, lead candidates are narrowed down via an optimisation process, the objective being to select the drug that displays the highest preliminary level of safety and efficacy. In particular, virtual screening methods have advanced in efforts to reduce drug discovery costs and time impacts, through incorporation of machine learning or deep learning methodologies (Oliveria et al. 2023). These have the ability to rapidly evaluate large numbers of molecular structures and hence accelerate the overall discovery phase.

Moreover, the pre-clinical trial stage involves the testing of the identified lead compounds either *in-vitro* (usually in cells or tissue culture) or *in-vivo*, by using animal models (Lo & Field, 2010). The purpose of these studies is to determine preliminary information regarding the toxicity levels, pharmacokinetics, pharmacodynamics and the safety of the dosing regimen for the drug (Mundae & Ostor, 2010; Schmidt & Grossmann, 1996). If successful in this phase and in order to enable the development process of a potential therapeutic to begin, an investigational new drug (IND) application must be submitted to the FDA (if in the US), enabling companies to begin clinical trials in humans participants (Nitin Kashyap et al., 2013; Umscheid et al., 2011). The regulatory process is not dissimilar to that with the European Medicines Agency (EMA); instead of an IND, an investigational medicinal product dossier is filed (Nitin Kashyap et al., 2013).

1.2.1.2 Drug development

This portion of the drug development lifecycle involves the first testing in human volunteers. The period is initiated with Phase I, whereby around 20 - 100 healthy participants are recruited (Lo & Field, 2010), with the purpose of identifying the safety, tolerability and pharmacokinetics of the drug (Mundae & Ostor, 2010). The number of participants is increased to around 100 - 300 following entry into Phase II of clinical trials. This particular phase can be divided into two halves; Phase IIa and IIb, however the overall aim of the trial is proof of concept; that is, the efficacy of the drug at the particular dosing level (Yuan et al., 2016). It has been well documented that the transition from Phase II to III of clinical trials is a critical point in the development lifecycle of a drug, largely due to the clinical success rate being far lower than

for bridging the gap between other phases (Paul et al., 2010). Multiple possibilities for the lower success rate associated with this point in development have been suggested. Given the much higher costs associated with Phase III, companies may choose not to embark on the next phase, as it may not be financially feasible for them to continue the development (Basu et al., 2017). Alternatively, and from a drug effectiveness standpoint, Phase II represents the stage in which the drug is first tested for its extent of functionality. Whilst many drug candidates can prove safety, many fall short at providing significant levels of efficacy (Van Norman, 2019). Nevertheless, perhaps the most common reason for the termination of Phase II trials is the lack of participant recruitment or retention (Basu et al., 2017).

Phase III trials have a similar overall aim to Phase II, however the participant pool is far larger, with recruitment numbers of around 300 - 3,000 volunteers (Mundae & Ostor, 2010). More specific objectives of this phase include identification of side effects and patients who are exempt, therefore also forms the basis of the appropriate instructions and packaging corresponding to the therapy. After successful completion of clinical trials, a New Drug Application (NDA) is filed and submitted to the appropriate regulatory body, containing data collected from all trials, thus the main objective of the application is to provide the relevant authorities with sufficient evidence to permit market approval of the therapy.

1.2.2 Expedited development pathways (FDA)

Given the estimated time to market for a therapeutic often exceeds 10 years, the applicability of the conventional drug development pathway can hamper the rapid and effective treatment of a subset of serious and life-threatening indications. As such, many of these indications have yet to be addressed by the biopharmaceutical industry. Thus, in order to expedite their development and approval, the FDA has, since 1988, introduced a series of programs to facilitate and accelerate either the development or review of therapies that can be used to treat “serious conditions” (FDA, 2014). The FDA defines serious or life-threatening condition as one that can result in mortality or greatly impedes the patient’s quality of life (FDA, 2014). Another pertinent attribute required by therapies taking an expedited pathway is that they

provide treatment to indications yet to be focused upon; alternatively, if evidence is supplied that they are an improvement over existing therapies, this is also sufficient. The general heuristic is the potential benefits of bringing the drug to market early warrant the risks associated with rapid approval (FDA, 2014). These expedited pathways can be grouped by those that alter the time for review and those that speed up development. **Table 1.1** highlights this split.

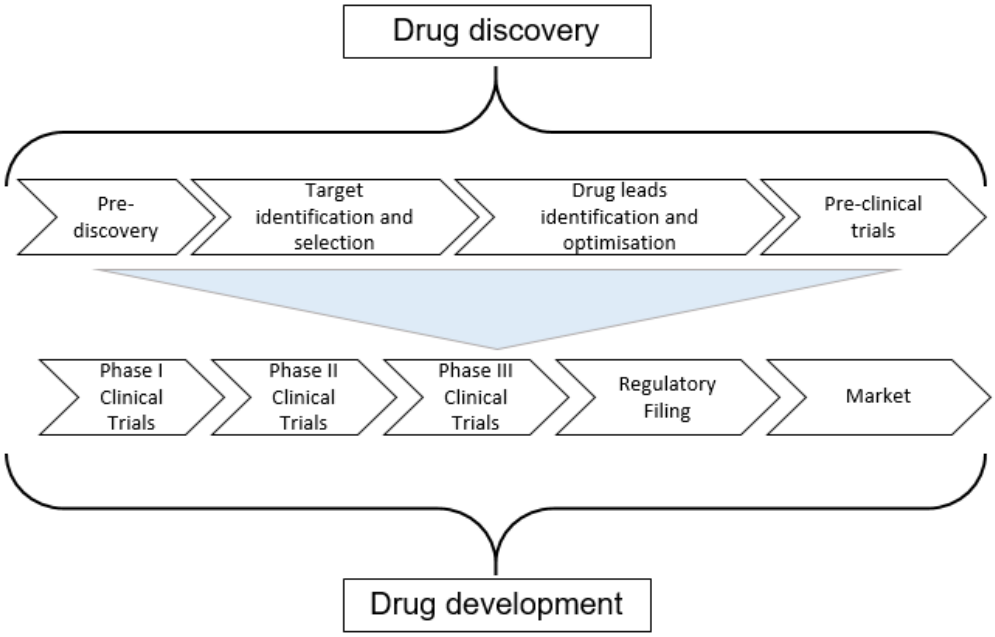

Figure 1.1 Drug discovery and development pathway for typical biopharmaceuticals. Here, a split is determined between research or studies that are conducted in-vitro or in animals and those that are carried out in human volunteers.

1.2.2.1 Orphan drug designation

By definition, a drug with orphan status is considered to address a particularly rare indication. In quantitative terms and specifically in Europe, an indication is permitted orphan status if it affects 1 in 2000 people or less (Abozaid et al., 2022). Upon a therapy achieving orphan drug designation, access is granted to various financial, market and assistance-based incentives.

Table 1.1 Breakdown of expedited regulatory programs designated by the FDA.

Pathway	Eligibility criteria	Impact on development	Examples
Accelerated approval	Therapy must treat a serious condition and there must be early data that shows the advantage of the therapy over currently available others.	Approval conditionally granted based upon Phase II/III data.	Herceptin, Gleevec
Fast-Track	Therapy must treat a wide range of serious conditions. Either clinical or non-clinical data can be supplied, provided it evidences the therapeutic potential of the drug and addresses an unmet medical need.	Ability to engage in frequent communication with FDA and gain access to advice on clinical trial design and how best to facilitate product development. Additionally, the data in question can be submitted on a rolling basis.	Zolgensma
Breakthrough	Meaningful early clinical data must be supplied evidencing the superiority of the candidate over current available therapies.	Gain access to intensive regulatory guidance on drug development. The development process is condensed.	Kymriah, Yescarta, Zolgensma
Priority Review	Candidate drug must show a clear improvement with respect to safety and efficacy in comparison to currented available therapies.	Review process for therapy is reduced to six months (from ten months).	Luxturna, Zolgensma

Note: The colour coding signifies those pathways that alter development time and those that alter review time (green is review time and orange is development time). Adapted from: (Monge et al., 2022).

Financially, designation enables a reduction in the fees associated with clinical trials, namely a 50% tax credit on such expenditure (DiMasi & Grabowski, 2007). From a market perspective, it allows drugs market exclusivity for a period of seven years (US) and ten years (EU) (Nagai, 2019), thus inhibiting the introduction of any competitive therapies. Furthermore, aid is provided to orphan drug manufacturers in the form of advice on how to ameliorate their development process. It must be noted that a drug being granted orphan drug designation does not necessary fall into the category of an expedited pathway, however in general, orphan

drug status innately yields many of the same benefits as expedited pathways, in particular accelerated approval (Nagai, 2019).

As will be discussed later, many cell and gene therapies often target rare or ultra-rate diseases. Consequently, it can be inferred from the pathways mapped out in **Table 1.1**, as well as the various incentives provided by the Orphan Drug Act, that it is possible for companies to achieve a profit from a relatively moderate sales level of these so-called orphan drugs, as was outlined by (DiMasi & Grabowski, 2007).

1.3 Manufacture of mAbs and ADCs

mAbs are a type of biological drug that have been frequently used in the treatment of a multitude of indications. The global mAb market was valued in 2022 at $210bn, with a compound annual growth rate (CAGR) of ~11% (Grand View Research, 2022). In contrast, ADCs are a more targeted application of antibodies. Structurally, an ADC is comprised of a mAb molecule connected via a linker to a cytotoxic drug. The whole complex presents specificity as well as cytotoxicity to kill antigenic cells (Fu et al., 2022).

In general, mAbs have a well-established manufacturing process. mAb production occurs in mammalian cells, specifically Chinese hamster ovary (CHO) cells (Li et al., 2010). This has been traditionally conducted using fed-batch cell culture, typically using stainless steel facilities. However, more recently, continuous manufacturing and namely perfusion cell culture has attracted increased interest, particularly governed by its ability to achieve higher productivities and thus smaller downstream volumes overall (Pollock et al., 2013). This ultimately offers the potential for smaller facility footprints over fed-batch culture. Other continuously operated steps have been implemented in mAb manufacturing, such as continuous protein A chromatography. This often takes the form of periodic counter current (PCC) chromatography, which involves cycling a number of smaller columns rather than just one (Gomis-Fons et al., 2020). In particular, Pollock et al. (2017) investigated the economic

impact of implementing perfusion cell culture and continuous capture for mAb manufacture, comparing and contrasting results with a fully batch flowsheet as a base-case. This highlighted that commercial use of continuous manufacturing (USP and capture) was not competitive in comparison to batch, but presented cost benefits throughout clinical manufacture (for pre-clinical to Phase III). In contrast and more recently, there has been evidence of the benefits to implementing fully-continuous mAb flowsheets, termed end-to-end continuous. This was evaluated by Mahal et al. (2021), which presented a COG analysis comparing batch, end-to-end continuous and a hybrid process. This detailed the potential commercial cost savings that can be achieved through implementation of single-use continuous facilities over stainless steel batch, in particular when annual demands are below 500kg. Greater demands (particularly those in the region of 1,000kg or higher) indicated smaller cost benefits (< 10%).

mAbs are typically expressed extracellularly, thus do not require inclusion of a lysis phase to break open the CHO cells. Instead, recovery of the product involves centrifugation followed by depth filtration, although manufacturers may install multiple filtration steps (with differing filter grades) depending on the level of clarification desired (Kelley, 2009). For purification of the clarified product fluid, Protein A chromatography is first employed, offering high specificity and capacity to capture the mAbs. This step has also been reported to achieve high yields and purities (Liu et al., 2010). Elution of the product from the protein A resin involves low-pH conditions, which secondarily serves to inactivate any viruses present. Conventional mAb purification includes another two chromatography stages, such as cation-exchange (CEX) and anion-exchange (AEX). CEX is performed in bind-and-elute mode whilst AEX captures impurities and is hence operated in flow-through mode (Du et al., 2012).

In ADC manufacture, production of the mAb component remains the same as if the mAb itself was the final medicinal product. However, for ADC therapies, several additional steps are required for production of the whole molecule. Most significantly, modification and conjugation steps are essential to attach the linker-drug complex to the mAb component, to generate the

ADC (Tsuchikama & An, 2018). Further purification stages are undertaken to remove any product-related impurities introduced during these stages.

1.4 Gene therapy

Gene therapy can be defined as the therapeutic introduction of genetic material to cells with the intention to correct a defective gene or replace a missing one (Gonçalves & Paiva, 2017). There are two definitive categories that gene therapy can be divided into, with each characterised by whether the genetic material is delivered to cells inside the body (*in-vivo)* or conversely, after the cells are removed from the body *(ex-vivo).*

1.4.1 Introduction to adeno-associated viruses (AAV)

Viral vectors have been shown to be a competent delivery system of genetic material into cells. In general, viral vectors may feature as the final product for *in-vivo* application or can be produced as a reagent for use in genetically modifying *ex-vivo* therapies (e.g. retrovirus or lentivirus). Given their inherent infectivity, viruses readily deliver DNA or RNA into mammalian cells and for those with a different tropism, a myriad of other cells. Whilst this is a general advantage of viruses for use in a gene therapy application, AAV in particular are rapidly becoming a clinical favourite (Naso et al., 2017).

AAV originate from the parvoviridae family and are non-enveloped, DNA viruses (Kay et al., 2001; Maier et al., 2010), typically falling in the size range of 20-25nm. They are additionally classed as helper-dependent viruses, thereby to achieve productive infection, require the addition of a much larger, helper virus (usually an adenovirus or herpes simplex virus) (Booth et al., 2004). Helper-dependent viruses are innately replication-defective and in contrast to a replication-competent virus, they are generally deemed to be safer for use in gene therapy. This can be attributed to the absence of the necessary genes to promote viral replication without aid. The inherent lack of pathogenicity and thereby safety of the AAV is paramount, making them an attractive end-product for gene therapy (Arnett et al., 2012). Nevertheless,

there are a wealth of other positive aspects of the AAV vector, which are further highlighted in **Figure 1.2**. For illustrative purposes, AAV were compared to lentiviruses (LV) in terms of their advantages as a gene therapy vector.

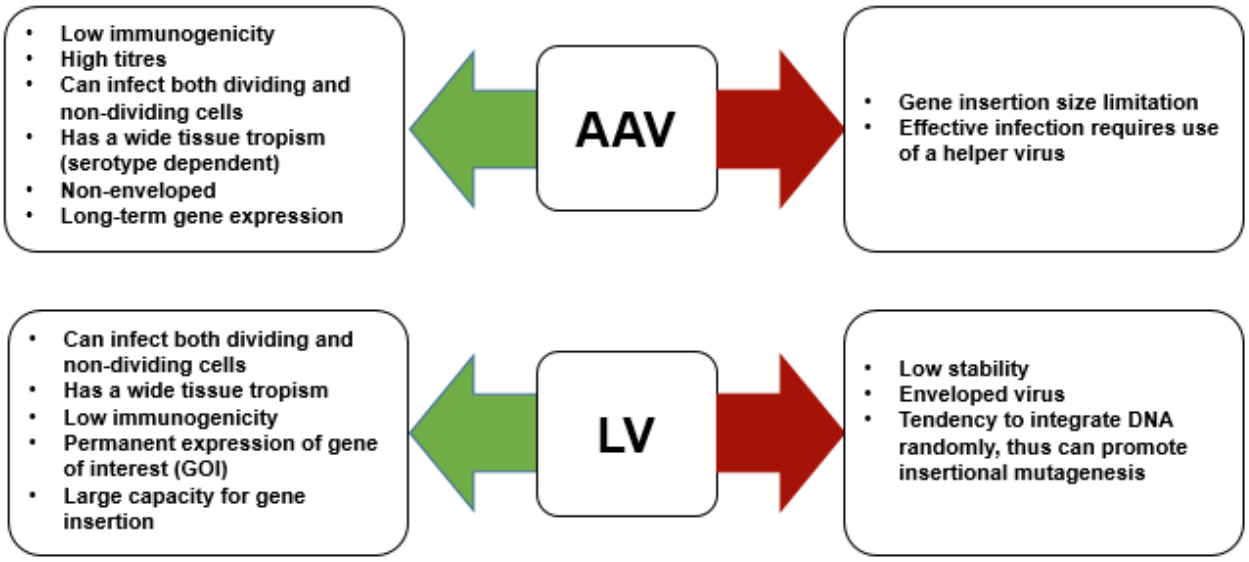

Figure 1.2 Key advantages and disadvantages of using AAV as a gene delivery vehicle, relative to LV, another popular choice of vector in gene therapy (Clark, 2002; Daya & Berns, 2008; Mountain, 2000).

As indicated in **Figure 1.2**, 12 human serotypes of AAV exist, which collectively results in a very broad tissue tropism. As a whole, this means AAV have the ability to infect a variety of tissue types and evidently be utilised for a wealth of indications. Moreover, unlike LV, AAV is non-enveloped and is instead enclosed with a capsid. Enveloped viruses are generally regarded as less stable than non-enveloped, due to a lower tolerance to environments such as high temperatures, salt, pH or the presence of chemical denaturants. This is attributable to the composition of the envelope being a lipid bilayer (Lucas, 2010).

AAVs are also a non-integrating vector, where transient expression of the transgene is exhibited. Transient expression inherently infers that subsequent daughter cells will not contain the transgene, therefore in the context of a gene therapy, the potency of the treatment will diminish over time. Having said this, it has not been documented as a major disadvantage

of the AAV, as cell division in adult somatic cells is not frequent, thus AAV degradation is generally minimal over time. It has further been reported that expression of the necessary gene is often sustained even in these cases (Mountain, 2000). Thus in summary, whilst AAVs transiently express the gene of interest (GOI), this does not in actuality curtail its therapeutic potential.

1.4.2 Viral vector market and clinical trials

In the forecast period of 2019 to 2027, the viral vector manufacturing market is estimated to grow at a CAGR of 27.4% (Mordor Intelligence, 2022). AAV success has been recognised with the approval of *in-vivo* therapies in areas of ophthalmology, haematology and neuromuscular diseases. Specifically, the current commercialised AAV products are Luxturna (Spark Therapeutics, PA, USA), Zolgensma (AveXis, IL, USA), Hemgenix (CSL Behring, PA, USA), Roctavian (BioMarin, CA, US) and Upstaza (PTC Therapeutics, NJ, USA).

Aside from those that are commercialised, there are a number of *in-vivo* AAV projects in clinical trials, addressing a multitude of therapeutic areas. This is illustrated in **Figure 1.3**, where 2022 clinical trial data from the Cell and Gene Therapy Catapult was compiled and considered by clinical phase and indication. This highlights the progress towards commercialisation in ophthalmology, neuromuscular diseases and haematology, as it is shown that these are the only disease areas to have candidates in Phase III. This correlates with the success in these areas from AAV commercialised products, as discussed earlier. Additionally, **Figure 1.3** also gives rise to the surplus of untapped disease areas, exemplifying that there still exist a myriad of uncertainties likely impeding the universal use of AAVs as a product.

As discussed in Section 1.2.2, many therapies for non-chronic indications are granted the ability to take one or more expedited pathways during drug development, likely then enabling a shorter development timeline. This is seen in action with Luxturna and Zolgensma, which were both assigned orphan drug status. Additionally, Luxturna received priority review and Zolgensma granted priority review, fast-track and breakthrough designations by the FDA.

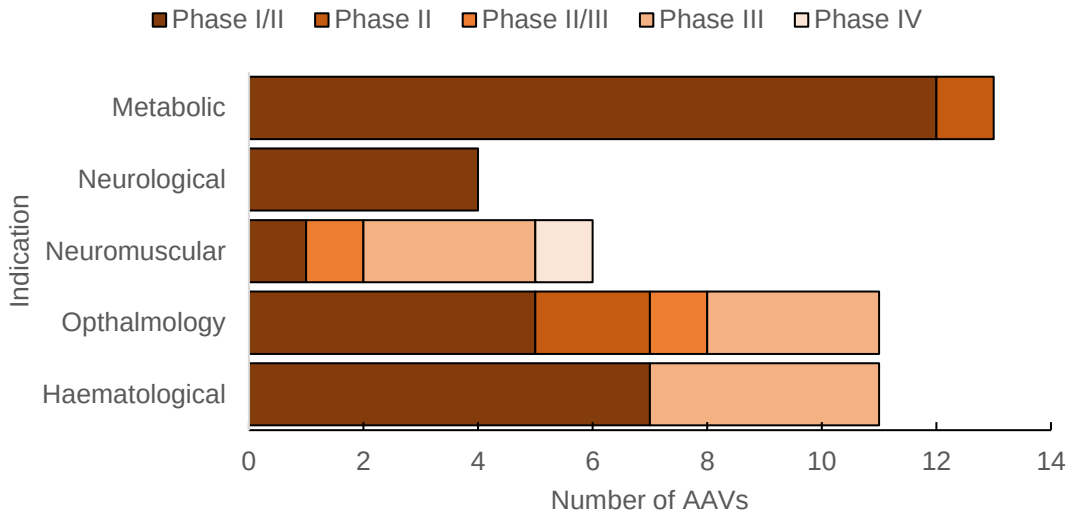

Figure 1.3 Breakdown by indication of AAVs used in clinical trials. This is further broken down to highlight the number of projects targeting a particular indication in each clinical trial phase (Cell and Gene Therapy Catapult, 2022)

1.4.3 AAV manufacturing

1.4.3.1 Upstream processing (USP)

Traditionally, recombinant AAVs have had success in being produced to high titres in a laboratory setting, particularly using adherent human embryonic kidney (HEK) 293 cells (Xiao et al., 1998). Adherent mode refers to culturing cells that are attached to the vessel surface, with no free movement. Detachment of cells is necessary post-culture via trypsin. This is in contrast to suspension cell culture, where cells grow suspending in the cell culture media.

There are a number of adherent cell culture technologies available in AAV manufacturing and a selection have been highlighted in **Table 1.2**. As a result, the majority of such lab procedures have been directly translated for use in a commercial setting, despite the use of adherent technologies characteristically being laborious and costly to maintain at the large scale (van der Loo & Wright, 2016).

Table 1.2 Common adherent technologies utilised for AAV production and the range of sizes that can be typically found in industry.

Technology	Surface area availability (cm^2)	Reference
Roller bottles	490, 850, 1750	(Merten et al., 2014b)
Multilayer cell factories	1, 2, 4, 10, 40 stacks of 636cm^2 each layer	(Merten et al., 2014b)
Fixed bed reactor	66,000, 133,000, 333,000	Pall
T-flasks	75, 150, 175, 225	(Strobel et al., 2019; Wang et al., 2012)

Note: Whilst T-flasks are rarely used for relatively large production volumes, they are frequently found in the seed train for a multitude of adherent technologies.

AAV production in adherent HEK293 cells is typically achieved via transient transfection, whereby three plasmids are taken up by the cells. The plasmids contain the necessary genetic material for the construction of an AAV particle; one plasmid contains the *rep* and *cap* genes, which provide packaging (with respect to the virus genetic material) and structural functions (formation of the capsid) respectively (Grieger et al., 2016). A second plasmid provides helper virus material to regulate and facilitate the replication of the AAV within the HEK cell, as innately, they are a replication deficient and helper-dependant virus. Thus, the presence of a helper virus promotes AAV gene expression, enabling effective replication within the host cell (Kay et al., 2001). Finally, the third plasmid contains the gene of interest (GOI), thereby is the vehicle conferring therapeutic potential to the viral vector. Whilst it is most common to use a three plasmid system when opting for transient transfection as a gene delivery method, some two plasmid systems have been reported (Allay et al., 2011). Here, both the plasmids containing the *rep* and *cap* genes and the GOI are transfected, however the helper virus DNA is delivered via infection to the mammalian cells. Having said this, using a tri-plasmid system

offers process benefits, such as a removal of the need to heat inactivate live helper viruses, thus preventing the risk of contamination by such (Ayuso et al., 2010; Kay et al., 2001)

An alternative to transfection can take the form of stable packaging or producer cell lines for use in suspension culture. Generally, packaging and producer cell lines utilise infection via a helper virus, with the difference between the two being that packaging requires transfection with the plasmid containing the GOI and a producer cell line does not (Wang et al., 2012). Regarding hosts, there has been published use of HeLa cells (Martin et al., 2013) and baby hamster kidney (BHK) cells (Thomas et al., 2009) as either packaging or producer cell lines.

A summary of the gene delivery methods is given in **Figure 1.4.** It must also be noted that a plasmid-free system has been reported by the gene therapy company CEVEC Pharmaceuticals. In this case, a producer cell system requiring no plasmids and no helper viral infections was generated (Faust, 2023). This circumvents the need to purify out the helper virus by introducing a helper free stable producer cell line.

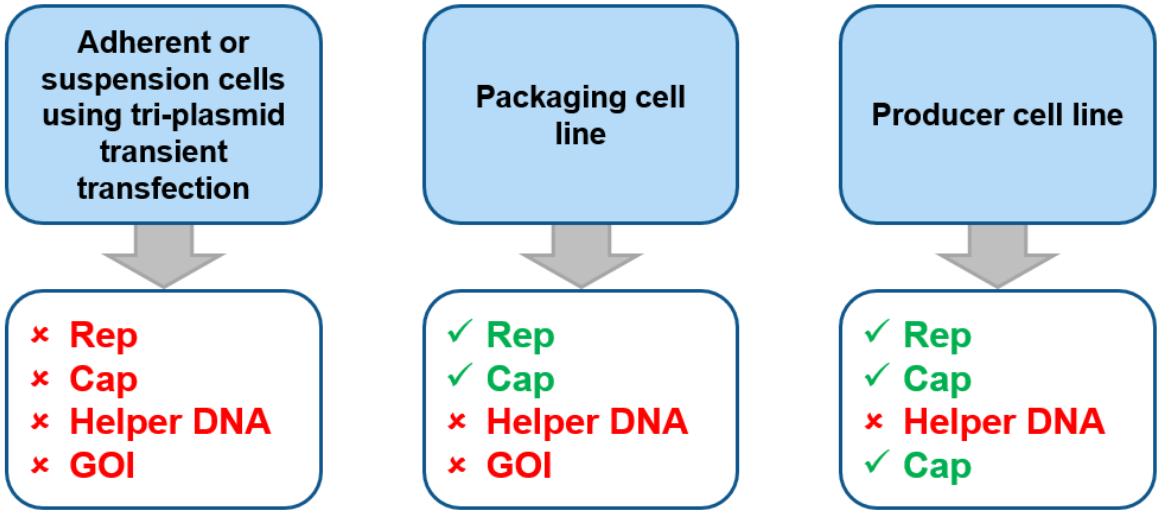

Figure 1.4 Overview of AAV gene delivery mechanisms into mammalian cells. The green tick symbolises the genetic material that is innately contained within the cells, whereas the red cross signifies that which is not innately present and therefore needs to be supplied, typically by means of transfection or infection.

1.4.3.1.1 Insect cells

Though mammalian cells are arguably a favoured host for AAV production, an alternative method is the use of Sf9 insect cells in suspension. To induce AAV production, a specific insect parasite known as the baculovirus is used to infect host cells. This production system has gained prominence due to the relative ease of culturing insect cells and the high titres associated with recombinant baculovirus-induced AAV production per cell (Wang et al., 2012).

In general, the production process involves Sf9 cells being infected by three separate baculoviruses; one responsible for providing the *rep* gene, another for the *cap* gene and a final construct with the intent to provide the GOI, as reported by Moreno et al. (2022). Recent advancements have allowed for a “OneBac” system to be used Aslanidi et al. (2009), where the Sf9 insect cells are modified in the same way as a producer cell line would be, to provide the AAV genetic functions innately; only one baculoviral infection is necessary to integrate helper virus material. The method developed here however was only applicable to two viral serotypes (AAV1 and AAV2). The term “OneBac” later became coined to describe a similar protocol, but had been refined for application to all human recombinant AAV serotypes (Mietzsch et al., 2014).

1.4.3.2 Downstream processing (DSP)

As with any bioprocess, efficient harvest and purification of the therapeutic product is imperative to ensuring a safe, potent and high purity payload is transferred into patients. Whilst these product attributes are vital, a balance must be satisfied with maximising the overall process yield so as to limit product losses and thus not impact the process economics so detrimentally. In general, and as with the USP portion of the process, the downstream section of AAV manufacturing often follows protocol that is standard in a laboratory setting (Merten et al., 2014a). As a summary, **Figure 1.5** highlights the usual train of unit operations that feature during AAV DSP. It must be noted that the flowsheet outlined here is rather general and as outlined by Clément and Grieger (2016), production of AAVs across the field suffers from a

lack of uniformity regarding production protocols (this paper identified twelve greatly different flowsheets at the time of publication).

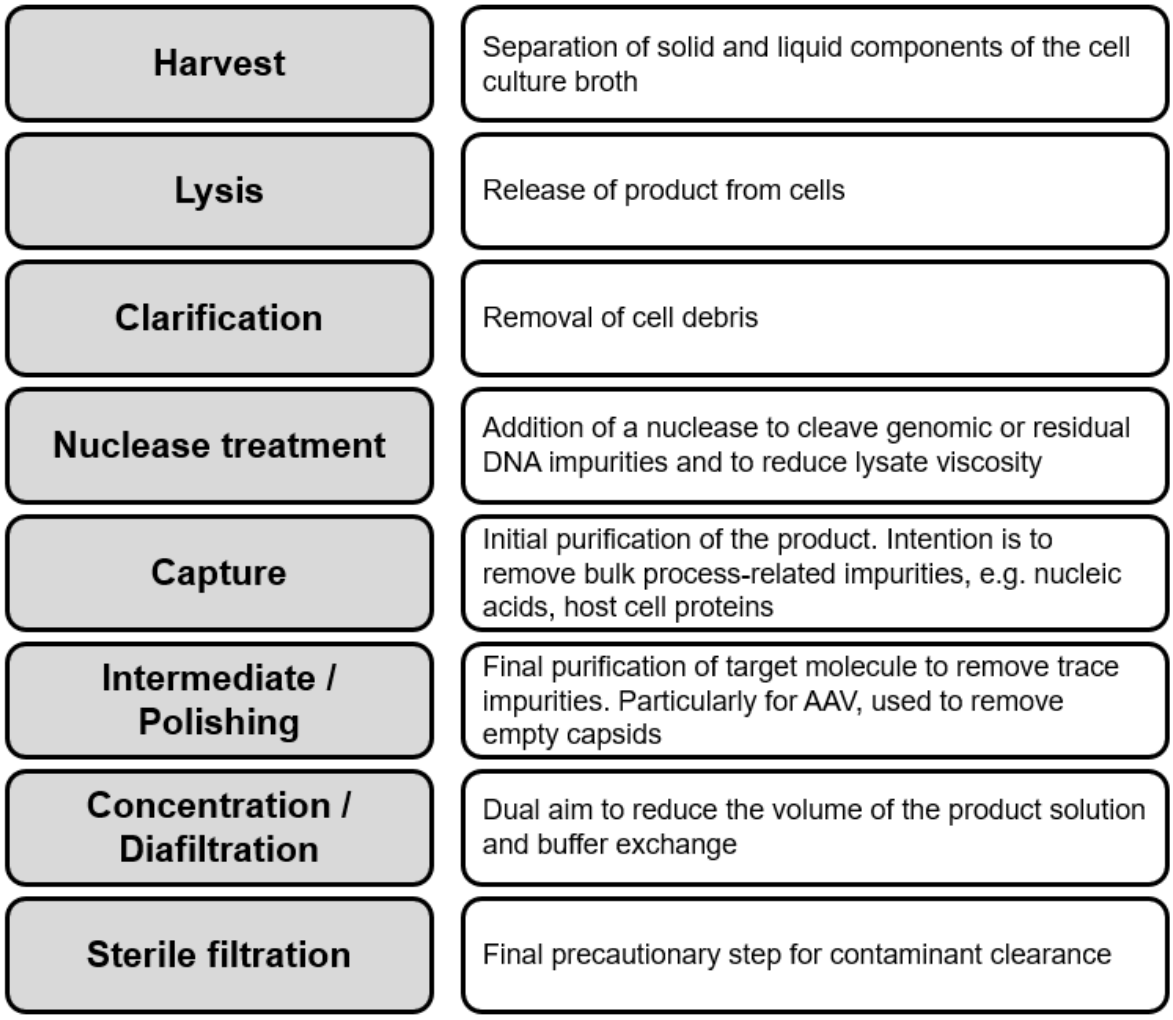

Figure 1.5 General process flowsheet for AAV manufacture, supplemented with the function of each step.

1.4.3.2.1 Harvest

Regardless of the upstream method utilised, cells must be harvested to remove the cell culture broth. In contrast to other vector types, such as the lentivirus, certain AAV serotypes are located intracellularly (Wright, 2008), thus the extracellular medium is eliminated following cell culture. Having said this, extracellular AAV products have been reported and more regularly, those that are partially intracellular or extracellular. Crude harvest is typically performed by centrifugation at lab scale, thereby exploiting density differences between the cells and culture

medium or by filtration, namely depth, at large scale (Vandenberghe et al., 2010). An important consideration is that the clarification stage employed is highly dependent on the nature of the upstream technology and / or the AAV serotype behaviour. For example, the outflow stream of adherent technologies will contain no or very little cell quantities as this is prior to trypsinization, whereas suspension outflow streams contain a mixture of cells and broth, thus such a cell density could impact filter performance if a sub-optimal type is selected (Hebben, 2018). Similarly, an intracellular AAV would typically require a tangential flow filtration (TFF) stage to retain cells and remove broth, whereas depth filtration is better suited to cases where the AAV is predominately extracellularly expressed.

In cases where the AAV is intracellularly expressed, inclusion of a lysis step is necessary, to release the product from cells. This simultaneously releases impurities from the cells, such as host cell proteins (HCP) and host cell DNA (hcDNA). A multitude of techniques have been reported as a means of lysis, including microfluidization, chemical lysis via detergent treatment, heat-shock, freeze-thaw and sonication (Clément & Grieger, 2016; Merten et al., 2014a; van der Loo & Wright, 2016). In general, larger manufacturing scales avoid techniques such as freeze-thaw, sonication and heat-shock due to limited scalability. Post-lysis, the impurity burden upon later downstream processing steps is typically lightened by addition of a nuclease employed in tandem with lysis, however generally is utilised as a step on its own (Segura et al., 2011), with the most frequent reagent used being Benzonase. This stage has an additional benefit in reducing lysate viscosity (Hebben, 2018).

1.4.3.2.2 Purification

In general, purification lacks the greatest consistency across AAV manufacturing. In part, this is attributable to the great diversity of AAV serotypes that are utilised in gene therapy and as such, processes often require re-design according to serotype and therefore indication. As with mAb bioprocessing, AAVs can be purified by a wide range of properties, including net surface charge, hydrophobicity, size or by affinity to a specific ligand (Merten et al., 2014a). A fairly standard and well-established purification protocol is the use of gradient density

ultracentrifugation, either by an iodixanol or caesium chloride (CsCl) gradient (Segura et al., 2011). This method has shown impressive impurity removal profiles, with no bias towards AAV serotype (Strobel et al., 2015), however lacks the ability to be scaled by standard means and therefore must be scaled-out instead of up (Segura et al., 2011). With a natural industry drive towards increasing vector demands and ultimately larger scale manufacturing, chromatographic purification is a feasible alternative. This provides a scalable strategy and is highly specific, particularly that of affinity, given that the resin utilised is largely dependent on the serotype of AAV being produced. For example, Poros (Thermo Fisher, MA, US) distribute a specific affinity resin for AAV8 and AAV9, however AAVX has been developed to address the call for a more standardised resin that can work for a wide range of serotypes (this works for AAV1 through to AAV8). Moreover, as a means to overcome a serotype dependency on chromatography choice, a universal purification method was developed designed for compatibility with a myriad of AAV serotypes (Nass et al., 2018).

IEX in particular is useful as either a capture or polishing stage, as it has the ability to satisfy the purification requirements of both types of step; it has the capacity and selectivity to remove bulk impurities and for the latter, has empty capsid removal capabilities, due to a slight charge difference between these and full capsids. Unlike lentiviruses and adenoviruses, AAVs exhibit a net positive charge at a neutral pH (Burova & Ioffe, 2005), allowing for binding if using a cation exchange (CEX) resin, which exhibit ligands that are negatively charged and hence bind positively charged cations. In contrast, using anion exchange (AEX) would typically allow for binding of negatively charged anions as resin ligands are positively charged. Additionally, utilised as a polishing stage over capture, multimodal chromatography (MM) is useful as it harnesses both size exclusion, hydrophobic and ionic capabilities. The molecular weight of an AAV particle is ~3,750kDa, thus commercially available MM platforms such as CaptoCore 400 or 700 (Cytiva, Marlborough, US), with molecular weight cut-offs of 400kDa and 700kDa respectively, can be used in flow-through mode. Nevertheless, it must be recognised that whilst SEC or MMC are often referred to as polishing stages throughout the literature (Burova

& Ioffe, 2005; Merten et al., 2014a; Qu et al., 2015; Terova et al., 2018), they do not satisfy the definition of a polishing stage shown in **Figure 1.5**; this is because they lack empty capsid removal capabilities.

Furthermore, chromatography yields for AAV purification are greatly variable. CEX yields have been reported to be higher than 90% (Burova & Ioffe, 2005; Qu et al., 2015) and AEX yields have shown to be lower than 10% in certain cases (Burova & Ioffe, 2005), yet in other studies, this number is elevated to 60-70% (Wang et al., 2012). Moreover, affinity or immuno-affinity yields tend to vary greatly across serotypes; as outlined by (Nass et al., 2018), yields range from 55-92% across serotypes.

1.4.4 Development and manufacturing challenges

1.4.4.1 Challenges in upstream processing

Though transient transfection using adherent technologies has had much success in AAV production (with two marketed products i.e. Luxturna and Zolgensma following this vector generation method (Wright, 2008), manufacturing inherently encounters scalability issues, whereby traditional scale up is limited by the surface area available of the technology. To combat this, scale out is used to increase culture surface area as illustrated in **Figure 1.6**, potentially resulting in hundreds of units of the technology, as reported by (Wright et al., 2010), for companies manufacturing large vector quantities for clinical trials or for a chronic indication. As discussed in Section 1.4.3.1, the use of adherent cell lines is still used in both research and industry, therefore the cell culture technologies utilised are generally limited to, in the case of AAVs, roller bottles, multilayer cell factories or the more scalable fixed bed reactor. Overall, this scale out procedure rapidly becomes financially and logistically infeasible as it results in a large facility footprint, a requirement for copious labour and processing times and thus ultimately expenditure. However, it must be noted that the scalability issue is not a pressing matter for companies in the orphan drug space seeking to leverage the prompt development pathways associated with this novel subset of biopharmaceuticals; rather, this challenge is

particularly pronounced in the development and manufacture of AAVs for more prevalent indications.

Irrespective of whether adherent or suspension cells are used, transfection as a method itself is met with variability, particularly concerned with the efficiency of the step (Merten et al., 2014b); that is, the proportion of cells in the population that successfully took up the plasmids to express genetic material. Variability is also magnified due to the lack of automation with adherent cell processing, introducing the consistent issue of operator errors being introduced. Furthermore, whilst the inherent obstacle in increasing volume has been addressed through the use of suspension technologies, the economic viability of transfection as an approach lessens as the suspension culture volume increases. This specifically relates to the adaptation of the plasmid transfection method to use in suspension, where it has been found that transfection efficiency greatly reduces upon scaling up (Collard, 2021).

Moreover, other suspension cell culture methods are fraught with their own challenges, despite satisfying the requirement for a more scalable and less manual approach. The use of Sf9 cells with baculoviral infection runs the risk of baculovirus contamination (Penaud-Budloo et al., 2018), thereby necessitating increased purification to achieve sufficient deactivation or removal of such and ultimately additional, robust analytics. Besides this, in the general case of any packaging or producer cell line, seed generation can be an tedious process, with the cell line requiring a long lead time (Wang et al., 2012). From a commercial perspective, the process by which a cell line is developed is characteristically costly, particularly relating to licensing applications for the new cell (Smith, 2017). Furthermore, cell banking and subsequent quality testing is a costly and timely process. Development and creation of a master and working cell bank, as well as analytical testing can amount to €1.5 million (approximately $1.65 million) (Lawson et al. 2021).

Figure 1.6 Schematic highlighting the methods of increasing culture volume for AAV production. On the left, roller bottles, an example of an adherent culture technology, whereby scaling out is required to permit an increase in culture volume. On the right, a single use bioreactor as an example of a suspension culture technology; in this case, scale up is possible. Note: bioreactor images sourced from Sartorius, roller bottle images sourced from Sigma Aldrich.

1.4.4.2 Challenges in downstream processing

Many of the issues with viral vector DSP have arisen from the industry's inability to derive and optimise platform recovery and particularly purification technologies for specific use in producing viral vectors. It is arguably this type of development that has allowed mAbs to become a widely manufactured and used biopharmaceutical product, thus necessitating the same drive-in viral vector manufacturing. Whilst clear efforts have been made to address such an issue, this has often involved the transfer of the typical mAb purification platform over, resulting in viral vector purification being carried out in sub-optimal conditions (Lundgren, 2019).

Furthermore and in general for all viral vector products, production processes have consistently endured relatively poor downstream processing performance in terms of recovery, with 50% AAV yields generally considered plausible (Masri et al., 2019). Much of the difficulty here is that such loss accumulates after a train of suboptimal process steps, thus no single unit operation can be specifically deemed to be the major problem (Glover et al., 2019). Low yields however, are a particular issue for steps such as chromatography, whereby the conditions typically encountered (i.e. pH or conductivity extremes) can render many viral particles ineffective, thereby their ability to infect target cells is impaired (Potter et al., 2014). Traditional viral vector purification technologies, such as CsCl gradient density ultracentrifugation, encounter similar recovery and AAV infectivity losses, however achieve plausible impurity reduction levels. Iodixanol gradient partially satisfies the issue of infectivity reduction, as shown by and presents a low-toxicity alternative to CsCl gradient (Moleirinho et al., 2019). However, when process scale up is desired and large product demands are necessary, gradient density ultracentrifugation in general can become economically infeasible. Such a technology cannot be scaled in the same manner as other steps such as chromatography, thus manufacturers must often resort to scaling out, that is, to linearly increase the number of ultracentrifuges employed. The cost implications of doing this can be drastic, however companies manufacturing material for the market still reportedly employ this

as a polishing stage (Wright, 2008). Therefore, there exists a vital need for the effective translation of the purification performance achieved with technologies such as gradient density ultracentrifugation at the lab scale, to a more scalable technology that can cope economically in a commercial setting.

Following on from this, a significant and somewhat unique impurity issue that arises with vector manufacturing is the generation of vector particles lacking fully packaged genetic material, referred to as empty capsids. As a result, this type of viral particle cannot provide the same clinical benefit as a full capsid and it is thought that in some cases, administration of such may provoke an increased immune response (Fraser Wright, 2014a) and through such, can reduce the expression of the desired gene (Hebben, 2018). The empty capsid issue is exacerbated by certain methods of vector generation, generally adherent over suspension (Merten, 2016), and presents an additional impurity that must be removed during downstream processing. The challenge industry faces with such an impurity is that they are structurally closely related to the full capsids (Qu et al., 2015), thereby making it difficult to utilise some chromatographic procedures and exploit molecular and structural differences between impurities. This is greatly exemplified by the inability of affinity chromatography to remove empty capsids, as the ligand cannot distinguish between the two types of particle due to identical capsid properties (Nass et al., 2018). It has been shown that IEX can adequately address this impurity issue (Nass et al., 2018; Urabe et al., 2006), as there is a subtle pI difference between full and empty capsids (approximately 0.4) (Qu et al., 2015), however as discussed previously, IEX has encountered great variability in yield when utilised in AAV purification and it is thought that purification performance is somewhat dependant on AAV serotype.

Furthermore, steps such as ultracentrifugation have demonstrated success in removal of empty particles, independent of AAV serotype (Crosson et al., 2018). However, as discussed previously, whilst surmounting one key issue, one is faced still with the lack of scalability of the ultracentrifuge as a purification method.

1.4.4.3 Additional challenges

Some general challenges faced include the characteristic stickiness of AAV capsids (Choong et al., 2016). This becomes a problem particularly during formulation and ultimately vial storage, as contact with glass surfaces can promote nonspecific adsorption of the AAV (Wright, 2008). Whilst it has been reported that certain reagents such as Pluronic F68 help to stabilise vector yields during formulation and limit vial adherence (Bennicelli et al., 2008), the extent of this challenge is largely dependent on the serotype of AAV, therefore present a more prominent issue in some cases.

On the analytical front, there is a necessity for rapid and high throughput techniques for measuring AAV critical quality attributes at numerous stages throughout the whole manufacturing process. Particularly relevant to AAVs are the product-related impurities that bear multiple similarities both in terms of structure and size to the AAV product, bringing additional complexities to the purification and thus analytical procedures (Fraser Wright & Zelenaia, 2011). However, development of these analytical techniques is hindered by the very initiatives that are designed to alleviate some of the developmental burdens upon newer modalities such as AAV; that is, expedited pathways and orphan drug designation. Because of these, AAV development timelines often become too short to have sufficient time to develop adequate analytical support and ultimately evaluate process performance. Thus, a trade-off arises between rapid commercialisation of a product and exclusivity in a particular disease space and developing a robust bioprocess, with a set of equally plausible analytics to ensure safety, purity, identity and potency of the product. Evidently, a fundamental part of this challenge lies in where focus should be directed.

Whilst progress is consistently observed in AAV manufacturing, it is evident that a wealth of challenges and process-business trade-offs remain to be addressed, thus inciting a need for the establishment of methods to alleviate some of the pressures associated with decisions faced by biopharmaceutical manufacturers.

1.5 Computational methods for optimisation

1.5.1 Mathematical programming

At a glance, mathematical programming is the use of mathematical models to address optimisation problems, ultimately with the purpose of aiding industrial decision-making. The foundations of mathematical programming are traced to publications in the 1950s and 1960s (Dantzig and Wolfe, 1960; Neumann and Morgenstern, 1953). It has since been widely applied in tackling optimisation problems related to capacity scheduling and portfolio management, in particular mixed-integer linear programming, which is a variation of linear programming (Jankauskas, 2019). By nature, this technique seeks to solve optimisation problems where both the objective function(s) and constraint are linear.

The application of MILP involves expressing the objective function(s) and constraints as linear expressions. This means that in cases where these elements cannot inherently be formulated as linear expression, linearisation is required, which can be a complex process in large-scale applications. As is a general rule of optimisation-based problems, the objective function represents the quantity (or in cases of multi-objective optimisation, quantities) that must be minimised or maximised, subject to a variety of imposed constraints. Constraints define the limits within the region of the decision space that is deemed feasible, where feasibility is typically defined in the context of the specific problem. Whilst the goal of using MILP may often be to find the global optimum of a solution set, this is not necessarily guaranteed, particularly in the case of complex combinatorial optimisation problems. In these cases, finding the optimum may not be possible within a reasonable timeframe.

One such simplistic example of mathematical programming is brute-force optimisation, which involves enumerating through all possible decision variable combinations in order to characterise the objective space. For deterministic problems with a small number of possible combinations, brute-force optimisation has been proven to be an efficient means to guarantee optimality. In the context of bioprocessing problems, particular those related to manufacture

of biotherapeutics, brute-force algorithms have been implemented previously in the literature. In particular, Jenkins et al. (2016) implemented a brute-force optimisation algorithm for rapid evaluation of various process configurations within stem cell manufacturing.

However, due to the computationally demanding nature of this technique, it rapidly becomes an infeasible option in larger scale applications. A more common approach to MILP problems is branch and bound. In these cases, the feasible decision space is iteratively portioned into a smaller subsets (Huang et al., 2021). The organisation of these resembles a tree structure. The branch element refers to the splitting of the objective space in this hypothetical tree, whilst the bound is the procedure of determining the branches that may lead to infeasible subsets of the objective space (Huang et al., 2021).

1.5.2 Heuristics and meta-heuristics

As an alternative to mathematical programming, the field of heuristics and more commonly meta-heuristics have also been widely used as optimisation methods. They are able to alleviate several of the key limitations that would prevent implementation of mathematical programming, namely dealing with non-linearities in the model equations and generating solutions in a timely manner.

Heuristic and meta-heuristic algorithms, in comparison to mathematical programming, are concerned with generating solutions that may or may not be the true optimal from the decision space. Though there is no guarantee of optimality, the algorithm performance is often dependent on the flexibility in the solutions across iterations and in cases of multi-objective optimisation, the reconciliation of conflicting objective functions. In cases where the decision space is near infinite (i.e. those employing stochastic elements), heuristic-based methods are far better suited to providing good quality solutions. A summary of the benefits and limitations of using either optimisation method is outlined in **Table 1.3**.

1.5.2.1 Genetic algorithms

One of the most commonly used meta-heuristic optimisation algorithms is the genetic algorithm (GA), introduced by Holland (1975). These belong to a class of methods referred to as evolutionary algorithms, which build upon Darwinism and the theory of evolution to drive changes in solutions across iterations. In general, the process of biological evolution is followed, whereby the algorithms seek to select the fittest members of a given population and through elitism, pass these characteristics on to future generations. To introduce diversity into the population, typical genetic processes are also mimicked by the algorithm, including crossover and mutation of genes. These are typically expressed as a probabilistic rate (e.g. between 0 and 1) and the choice of both can greatly impact solution quality and the likelihood of premature algorithm convergence.

The key terminology associated with genetic algorithms has been compiled in **Table 1.4.** Candidate solutions can more contextually be referred to as chromosomes, which are a string of genes that when combined, encode a unique strategy to the problem under consideration.

The traditional procedure followed in running a GA is outlined in **Figure 1.7**, which highlighted a flowsheet of steps. There have been significant modifications or additions to this more traditional methodology since the algorithm's development in the 1970s, however the generic steps have remained relatively the same. More recent published works have reported changes to the established GA structure, namely in regard to the chromosome-encoding strategy, selection method and crossover and / or mutation methods. These are outlined in greater detail within relevant chapters (i.e. Chapter 5), providing a rationale behind the methods selected and examples of their use in published studies.

Table 1.3 Summary of optimisation methods alongside benefits and limitations of implementation.

Optimisation method	Benefits	Limitations
Heuristic and meta-heuristics	• Less computationally expensive to run for large-scale applications • Useful in handling non-linearities	• Does not guarantee optimality • Optimisation parameters govern algorithm performance • Requires a high computational time to converge to better solutions
Mathematical programming	• More likely to achieve the global optimum for linear problems than meta-heuristics (though not guaranteed) • Converge faster for small-scale problems • High efficiency in terms of range of techniques to use	• Computationally demanding and complex for large-scale problems • Limitations in handling non-linear problems

Reference: (Rodríguez et al., 2018)

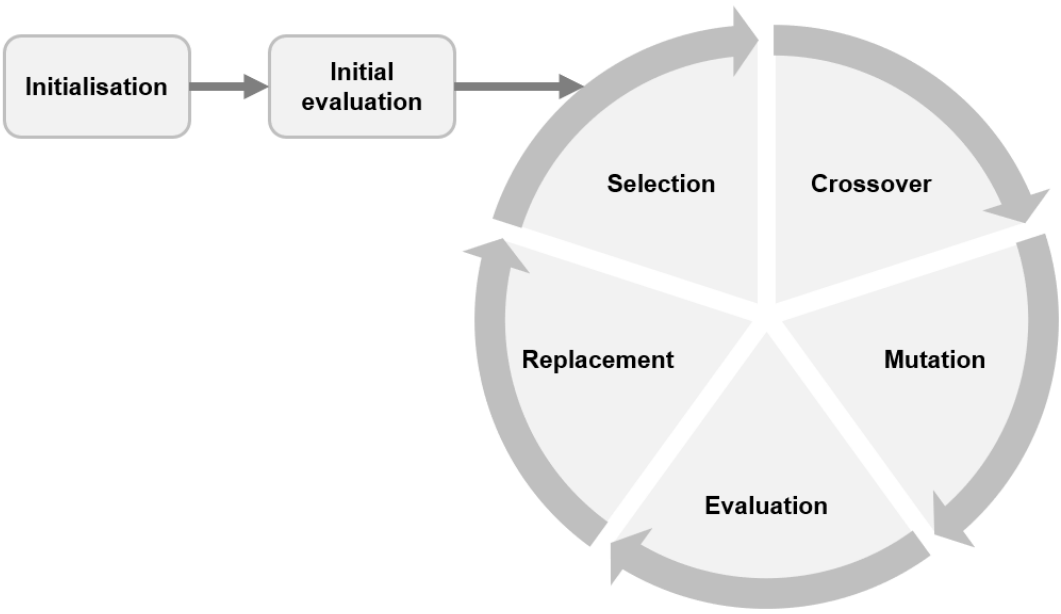

Figure 1.7 Graphic representation of the generalised procedure undertaken during a GA. As highlighted, those elements integrated within the cyclic portion of the diagram refer to steps that are repeated across the number of algorithm generations. Those tasks that appear outside of this are steps required to initialise the algorithm and are only repeated when multiple runs of the algorithm are carried out. More distinct definitions of the terms involved in a GA are outlined in Chapter 5.

Table 1.4 Glossary of key genetic algorithm terms.

Term	Definition
Gene	A single position within a chromosome. Represents a single piece of information in the solution
Locus	Specific position of a gene on a chromosome
Allele	The value given to a specific gene within a chromosome
Chromosome	A string of genes that represent one candidate solution
Population	A set of chromosomes
Parent	An individual chromosome that arises before any genetic operations are applied
Offspring	Chromosomes that result from the mating process between two parents and application of mutation
Selection	Process by which parents are chosen to undergo genetic operations (i.e. crossover and mutation)
Crossover	Mechanism by which parent genes are combined to create new chromosomes
Mutation	Random alterations made to one or more genes to create new chromosomes / solutions
Fitness	Measure of chromosome success with respect to the objective function(s)
Generation	A single iteration **within** the genetic algorithm e.g. selection, crossover, mutation, evaluation and replacement
Run	A single iteration **of** the genetic algorithm e.g. the whole procedure is conducted for the max generations. Used for reproducibility

1.5.3 Single and multi-objective optimisation

The purpose of any optimisation algorithm is the maximisation or minimisation of one or more objective functions. Problems which concern one objective function are therefore labelled as single-objective optimisation (SOO). In contrast, multi-objective optimisation (MOO) involves two or more objective functions (Zakaria et al., 2012).

1.5.3.1 Convergence

Another key point to consider is how convergence is assessed between either type of optimisation. For SOO, the average of the objective function across all runs and computation of the standard error have previously been employed. Jenkins (2018) reported the average fitness across generations of a genetic algorithm for bioprocess flowsheet optimisation. The standard error of the mean fitness was further utilised to quantify solution convergence, where smaller values were desirable. It is additionally possible to plot the change in fitness value across generations to identify improvements and ultimately a plateau. Evidence of this is shown in Webb et al. (2017), which used a genetic algorithm designed to minimise the volume of a plate structure. This presented the change in objective function over the algorithm generations, highlighting convergence. Furthermore, if a meta-heuristic technique like a GA is used, the output can be compared to the true optimal derived from e.g. a BFO to determine solution quality and convergence. This method is problem dependent and would be highly inefficient and time-consuming for large-scale applications.

Convergence checking is possible by eye when plotting the solutions across iterations. The graphical nature of this procedure will give general information regarding the evolution of the Pareto set over time, hence can be a good indicator of algorithm performance. However, visual inspection is not a robust way to assess convergence in general and for greater effectiveness, a quantitative metric is important to use for convergence checking. **Table 1.5** outlines some methods of doing this, particularly suited to multi-objective optimisation.

Of note, a popular metric, as highlighted in **Table 1.5**, is the hypervolume indicator. This relies on appropriate definition of a so-called reference point in order to derive the volume of the objective space covered by the non-dominated solutions. There are numerous approaches to defining an appropriate reference point. Some commonly selected methods include the ideal point, where both objective functions are minimised. Conversely, the Nadir point represents the maximum values for both objective functions. These techniques result in the reference point updating across generations to suit the solution set under consideration. A more flexible approach is a user-defined or random reference point. This is beneficial when there is prior knowledge regarding the bounds of the objective space and as such, ensures the point selected remains relevant to the problem. Defining a random point can also succeed in avoiding any bias, as the point will not be influenced by a particular point or weighted towards one objective in particular.

1.5.3.2 Constraint-handling strategies

In constrained optimisation, a number of constraints are typically applied to the problem in order to restrict the set of possible solutions (Rahimi et al., 2023). Any solutions that breach the imposed constraints are deemed infeasible and hence are not considered a viable option. Considering how the infeasible solutions are dealt with is a core part of how constraint-handling is defined. It is also the process of ensuring that these infeasible solutions are identified. Though it is possible to discard the constraint-breaching solutions, this can be problematic depending on the type of optimisation algorithm being used. For example, discarding solutions in an evolutionary algorithm (e.g. a GA) would interfere with the population size, a key parameter that generally should not be changed throughout the progression of the procedure. It must be noted that in general, selection of a constraint-handling strategies is highly problem dependent and often depends on the optimisation algorithm used. Furthermore, modifications to those techniques described in this section may often be made to best suit the problem in question.

Table 1.5 A selection of convergence metrics used in multi-objective optimisation.

Metric	Use	Benefits and limitations	Reference
Hypervolume	Measures the volume of the region that is dominated by the Pareto-optimal solutions that the MOO algorithm determines.	• Provides a scalar value • The true Pareto optimal is not needed to be known	(Wang & Sebag, 2013) (Jankauskas & Farid, 2019)
Generational distance	Measures the distance from each solution in the obtained Pareto front to the closest point in the true Pareto optimal	• Good for generality of the overall Pareto quality • Requires knowledge of the true Pareto optimal	(Santos & Xavier, 2018)
Inverted generational distance	Measures the distance from the closest point in the true Pareto optimal to each solution in the obtained Pareto front	• Good for generality of the overall Pareto quality • Requires knowledge of the true Pareto optimal	(Santos & Xavier, 2018) (Kouka et al., 2023)

There are several type of constraint handling strategy previously employed throughout the literature. By far one of the most widely used methods is the penalty function. In general however, the application of a penalty function involves penalising solutions which violate the constraints (Rahimi et al., 2023) by applying to the objective function a value which will ensure the solution will not be selected as optimal, e.g. if maximisation of the objective function is required, one may apply a value of 0. Penalty functions offer a simplistic method in dealing with constraints, however can be difficult in terms of deciding upon an appropriate penalty value to apply, particularly in minimisation problems. Another limitation with penalising solutions is that, when done correctly, infeasible solutions are disregarded from the selection process (Rahimi et al., 2023). Though intended, this may result in a loss of a solution that could be rearranged by crossover or mutation and inadvertently produce a better-quality solution, which can inadvertently diminish greater diversity in the population. Nonetheless, the penalty function method has been implemented and reported. Allmendinger et al. (2014) utilised a penalty value for research into the optimisation of chromatography sizing. This used a fixed (or static) penalty value regardless of how many constraints were violated or the degree of violation with respect to any one of the constraints. There has further been evidence of the use of a dynamic penalty function throughout the literature. These are concerned with assigning penalty values that change depending on the level of infeasibility the solution reaches. Yoo et al. (2021) described the implementation of a dynamic penalty function, which was systematically and gradually increased during a reinforcement learning task in approaching constrained control optimisation.

Another common method in handling constraints involves repairing solutions that are found to be infeasible. This may necessitate directly repairing the structure of an infeasible solution or generation a new one that satisfies the imposed constraints (Lagaros et al., 2023). In either case, conversion to a feasible solution is the desired goal. Repair functions can often be regarded as more robust than penalty functions, as instead of simplistically discarding infeasible solutions, repair methods leverage the existing genetic information to transform

violating solutions into feasible ones. However, the potentially iterative process by which a solution is repaired can lead to longer computational times and in some problem-dependent cases, may introduce additional bias and mutation like effects. Additionally, the specific procedure by which repair occurs is dependent on the algorithm selected and the structure of a candidate solution. Chootinan and Chen (2006) proposed the use of derived-gradient information to repair infeasible solutions. The gradient information was utilised to direct the infeasible solutions towards the region of the objective space where a population of feasible solutions were located. Moreover, Samanipour and Jelovica (2020) introduced an adaptive repair strategy within the non-dominated genetic algorithm-II (NSGA-II) (initially proposed by Deb et al. (2002)) for use in an engineering optimisation problem. This identified the variables driving constraint violation and ranked the importance so as to alter those that were most significantly influencing the violation.

It must be noted within a biopharmaceutical scheduling context, both Siganporia (2016) and Jankauskas (2018) rejected the use of repair strategies for candidate solution repair, deeming it too computationally expensive within the optimisation tools constructed. This further evidences that suitability of repair-based constraint-handling strategies is confined to the particular problem in question. Often, to circumvent any unnecessary complex implementations, it may be beneficial to initially run an algorithm with a more simplistic penalty function approach and assess the extent to which infeasible solutions could be repaired in a timely manner.

1.5.4 Use of computational methods in decision-support tools

Greater detail on the specific application of decisional tools within the biopharmaceutical industry is documented later, however this section provides an overview of the use of computational methods, in particular MILP and meta-heuristics, for biopharmaceutical portfolio management and capacity planning problems.

Concerning the use of mathematical programming, Lakhdar et al. produced a series of publications utilising MILP for biopharmaceutical manufacture planning and scheduling. This was initiated with the use of MILP in medium term capacity planning, which was concerned with identifying the optimal planning of production (Lakhdar et al., 2005, 2006). Lakhdar and Papageorgiou (2008) introduced a multi-objective model, where the medium-term planning of biopharmaceutical manufacture was considered in an uncertain environment. Mathematical programming was also implemented by Siganporia et al. (2014). This work described the use of a discrete-time MILP model for the optimisation of capacity plans when comparing fed-batch and perfusion manufacturing processes.

Meta-heuristics have been regularly used in biopharmaceutical portfolio management and capacity planning. George and Farid (2008) introduced a stochastic optimisation framework for the reconciliation of conflicting objectives; the maximisation of profitability as well as maximising the probability of achieving a profit. This study formulated a combinatorial problem, whereby a fixed number of products were to be chosen from a larger set. The structure of a candidate solution had three distinct components – drug selection, development timing and corporate manufacturing strategy (i.e. in-house, outsourced or partnered). Furthermore, a modified-GA was produced by Jankauskas and Farid (2019) for use in biopharmaceutical scheduling. Firstly, the GA parameters were optimised (referred to as meta-optimisation) using a Particle Swarm Optimisation (PSO) algorithm as a means of tuning. Furthermore, several unique elements were introduced into a traditional GA framework, such as the use of a variable-length and matrix-style chromosomes and hence modified crossover and mutation to handle the new structures. This also modelled multiple objectives, undertaking a ranking and selection process that reconciled objectives. As outlined in Section 1.5.3, multi-objective convergence metrics were employed in these studies, specifically the use of the hypervolume indicator.

1.6 Decisional tools

The lengthy process of drug development, combined with the significant budgets necessary to dedicate towards project activities, can inhibit the delivery of cost-effective therapeutics to patient populations. At the base level, biotechnology companies must therefore establish cost-effective and robust bioprocesses to manufacture products. Having access to tools that can carry out the rapid simulation, optimisation and ultimately economic appraisal is pertinent to achieving this. Additionally, at the portfolio level, as the biopharmaceutical industry has transformed, so has the pipeline of modality types developed by multiple companies. Given the characteristics of developing a therapeutic, a task which is both unique compared to other industries but also fraught with challenges, copious investment and severe risks, it is imperative that companies be advised on how best to handle a product portfolio mix, both from a resource allocation front, as well as a manufacturing stance.

Decisional tools refer to the techniques utilised to infer guidance on decisions that sit at the process-business interface (Farid, 2012), thereby typically integrate both operational and financial attributes. These support tools allow for rapid evaluation of varying bioprocessing strategies, both at the manufacturing and portfolio level. Furthermore, given that in reality, biotechnology companies receive a wealth of strict regulatory requirements, as well as facing company-related pressures in both budget and resources, decisional tools have the capacity to incorporate these real-life constraints in order to derive a feasible, and in many cases optimal solution to a problem.

1.6.1 Applications of decisional tools

Whilst the decisional tool itself typically involves an economic engine designed to generate financial metrics such as cost of goods (COG), fixed capital investment (FCI) or net present value (NPV), it can also integrate other tools or algorithms to give additional supporting information. This architecture is highlighted in **Figure 1.8.**

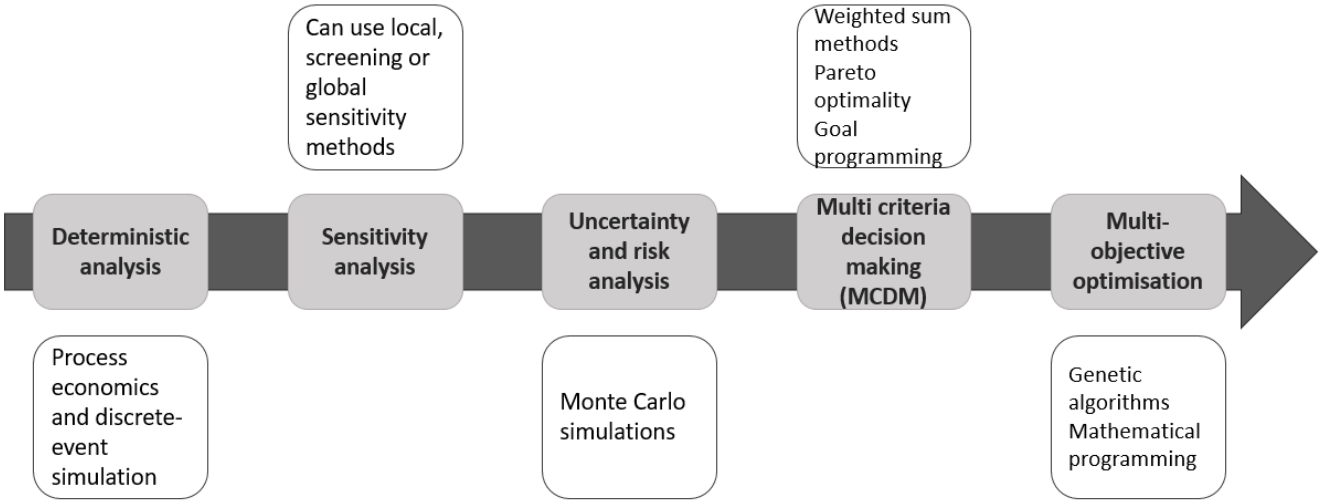

Figure 1.8 Adapted from Farid (2012). Typical analytical stages and techniques employed in decision making.

1.6.1.1 Deterministic analysis (base-case)

Case studies begin with a base case analysis, whereby no stochasticity in input parameters is introduced, thus scenarios output purely deterministic data, for example cost metrics such as COG, FCI or NPV. The deterministic approach is largely utilised as a way to better understand the mechanism of a particular process, thus is pivotal for capturing the high-level structure of a model. Several examples of this have been reported in the literature. A deterministic economic evaluation comparing process flowsheets pertaining to mode of operation has been evaluated by Lim et al. (2006) and Pollock et al. (2013). Moreover, Farid et al. (2000) developed a hierarchical framework, to evaluate a stainless steel plant versus a disposable plant as a means of manufacturing, incorporating both process and business-related variables into the model. This hierarchical structure has been employed also at the drug development level, whereby Rajapakse et al. (2005) used it to model the

biopharmaceutical drug development pathway, allowing for the formation of a decision-support tool to rapidly evaluate key profitability metrics such as NPV.

A further example of a deterministic analysis is the use of discrete-event simulation (DES), a technique widely applied in modelling the sequential progression (or change in state) of a system, at defined, discrete times (Stonier, 2013). This method is often utilised for the scheduling of activities and the allocation of resources within a biopharmaceutical facility, as it is characteristically both dynamic and discrete in nature (Sachidananda et al., 2016). Particularly when a company has multiple drugs in its portfolio, thus likely multiple processes occurring in the same facility, appropriate resource allocation is crucial, encouraging the use of DES. This, for example, allows for delays in certain processing steps to be highlighted due to a lack of resources. Notable work on DES for biopharmaceutical facility scheduling has been carried out by Stonier et al. (2009) and Stonier et al. (2012), where DES tools were utilised for use in identification of optimal purification sizing strategies, as well as incorporation of an optimisation element to monitor how the sizing strategy is affected by changing cell culture titre.

1.6.1.2 Uncertainty and sensitivity analysis

Whilst a deterministic analysis is useful for capturing the general picture, it characteristically fails to account for uncertainty in the inputs, thereby if relied upon alone, may result in an incomplete analysis and ultimately an inaccurate conclusion be drawn (Farid et al., 2007). The various uncertainties widely associated with drug development and manufacturing often necessitate the application of probabilistic variables to the inputs to generate model uncertainty (Coleman & Steele, 2009). Therefore, the next analytical stage to the base case often involves the generation of an uncertainty or sensitivity analysis. Particularly in bioprocessing, many inputs have exact values that are unknown, inferring inherent uncertainty in these parameters. However prior to this, a sensitivity analysis can be applied to ascertain the inputs that have the greatest impact on the output and therefore, those parameters that are likely to have the most uncertainty associated with them. In cases whereby a COG

evaluation is performed, sensitivity analyses can be used to determine those process or economics parameters that contribute to the greatest deviation from the base-case COG, as has been utilised in a number of publications (Jenkins & Farid, 2018; Lim et al., 2006).

Uncertainty analysis is utilised to identify how the uncertainty associated with the inputs propagates through the model and ultimately affects the output. This type of analysis is typically achieved through use of a Monte Carlo simulation. An abundance of researchers in the field have applied this technique to supplement the base-case analysis of bioprocessing related modelling, forming a more in-depth analysis (Farid et al., 2007; Lim et al., 2006; Pollock et al., 2013). Furthermore, the initial work from (Rajapakse et al., 2005) was extended to include a Monte Carlo simulation, thereby capturing some fundamental uncertainties associated with drug development (Rajapakse et al., 2006).

1.6.1.3 Multi-criteria decision making (MCDM)

Decisional tools integrate a wealth of both process and business related parameters in order to ease the decision-making process pertaining to some industrially relevant problem (Farid, 2012). Naturally, biotechnology companies must consider a range of financial and operational attributes when coming to a decision, whereby these often conflict with one another. Whilst the former are relatively simple to express quantitatively, the latter are not as easily quantifiable, thus prompting the use of a method within decision-making models to help resolve these conflicting attributes.

MCDM is a technique used to weigh up these conflicting criteria and ultimately search for the optimal solution from a pool of potential candidate solutions to a problem (Pavan & Todeschini, 2009). This has been applied to the comparison of fed batch versus perfusion cell culture by (Pollock et al., 2017), in order to weigh up financial metrics such as FCI and COG/dose and far more intangible metrics such as ease of validation and scale-up from an operational standpoint.

The use of MCDM has proved useful at a portfolio level, as highlighted by (George et al., 2007), where the technique was applied to create a framework for modelling from a process and business perspective, ultimately allowing for the identification of the most appropriate strategy for a company to acquire greater manufacturing capacity.

1.6.1.4 Optimisation

An in-depth analysis of the relevant optimisation techniques, along with their application throughout the literature was conducted in Section 1.5. However, the specific use of optimisation within a bioprocessing context is particularly relevant to the content of this thesis. Much of mathematical optimisation is concerned with the development of algorithms or methods that seek to either maximise or minimise some defined objective function, subject to several constraints. In the context of work in the decisional tools space, this objective function has often been attributed to a financial metric such as COG, FCI or NPV. In contrast to simulation, optimisation is utilised for broad decision spaces, whereby the number of candidate solutions is typically very large.

As discussed in Section 1.5, the field of optimisation can be broadly split into mathematical programming and heuristics/meta-heuristics. Heuristic approaches, given its name, utilise a commonplace approach to derive a feasible solution, however by nature does not seek to find the optimal solution; rather it merely satisfies the problem, but in a relatively short time in comparison to mathematical programming. Genetic algorithms (GA) are a frequently used heuristic algorithm; this type of algorithm has been applied to the identification of optimal manufacturing strategies, often pertaining to individual unit operations. A GA was utilised by Simaria et al. (2012) as a means of identifying the optimal purification strategy, with a focus placed upon the sequence of purification steps and sizing characteristics across a range of mAb products, testing multiple USP:DSP train ratios. Additionally, multiple evolutionary search algorithms have been considered and applied to finding the optimal chromatography sizing strategy in terms of cost-effectiveness, time and generation of product waste (Allmendinger et al., 2014). Moreover, multiple works have been produced related to the use of optimisation,

particularly GA-based algorithms, for capacity planning and biopharmaceutical scheduling (Jankauskas et al., 2019; Jankauskas & Farid, 2019) utilising genetic algorithms to address problems related to; significantly, with multiple objective functions under uncertainty and discrete-time optimisation problems respectively. These works featured use of a variable-length, matrix style chromosome to incorporate all scheduling decisions. The use of meta-heuristic algorithms has similarly expanded for use in portfolio management; (George & Farid, 2008a) utilised an estimation of distribution algorithm, inherently incorporating uncertainty, to determine optimal strategies relating to portfolio selection, acquiring capacity via a CMO or partner-company and the timing of drug candidates. Here, the model framework addressed a multi-objective optimisation problem, driven by a desire to maximise the NPV and the probability of attaining a positive NPV. The prospective pipeline was fixed at ten drugs and the case study evaluated combinations of choosing five from the set.

Conversely, mathematical programming algorithms are innately designed with the intent to guarantee the discovery of an optimal solution. One such example of this is MILP, involving decision variables that can either be integers or non-integers, with the additional condition that both the constraints and objective function(s) must be linear in nature. This has been frequently utilised in portfolio management and capacity planning. Lakhdar et al. presented a string of publications (Lakhdar et al., 2005, 2006; Lakhdar & Papageorgiou, 2008), all utilising MILP in a capacity planning context; supplementing the deterministic analysis presented in an earlier work by implementing MILP with uncertainty for management of a multi-product facility and identification of the optimal production planning strategies for manufacturing. Furthermore, the use of discrete-time MILP was similarly implemented by (Siganporia et al., 2014) in capacity planning, with a specific focus upon that of products manufactured via both fed-batch and perfusion cell cultures.

1.6.2 Decisional tools for novel modalities

In recent years, the use of decision-support tools has expanded from domination by mAb processes or facility simulations and optimisation to use for more novel therapeutics, such as cell and gene therapies. This work is summarised in **Table 1.6**.

Table 1.6 Summary table of the application of decision-support tools to novel therapeutics.

Author	Published work	Modalities studied	Summary of work
(Simaria et al., 2014)	Allogeneic Cell Therapy Bioprocess Economics and Optimisation: Single-Use Cell Expansion Technologies	Mesenchymal stem cells (MSC)	Evaluation of the most economical expansion / cell culture technologies. Also implemented is a brute force algorithm, to search through all options of cell culture technology and find the most economical.
(Hassan et al., 2015)	Allogeneic Cell Therapy Bioprocess Economics and Optimisation: Downstream processing decisions	MSC	Evaluation and subsequently identification of the optimal downstream processing and fill-finish strategies for MSCs. An optimisation algorithm was also incorporated to identify the optimal process in terms of COG/dose.
(Nie, 2015)	Cost Evaluation and Portfolio Management Optimisation for Biopharmaceutical Product Development	MSC*	Application of a drug development lifecycle cost model to cell therapies.
(Jenkins & Farid, 2018)	Cost-effective bioprocess design for the manufacturing of allogeneic CAR-T cell therapies using a decisional tool with multi-attribute decision-making analysis	CAR-T cells	Comparison of process flowsheets for allogeneic CAR-T cell production in terms of manufacturing costs. Stochastic MCDM is integrated as a way to reconcile conflicting financial and operational attributes.
(Pereira Chilima et al., 2018)	Impact of allogeneic stem cell manufacturing decisions on cost of goods, process robustness and reimbursement	MSC	Evaluation of cost of goods for cell culture technologies for allogeneic MSCs, supplemented with uncertainty analysis, MADM and optimisation (brute-force).
(Mizukami et al., 2018)	Technologies for large-scale umbilical cord-derived MSC expansion: Experimental performance and cost of goods analysis	MSC	Cost analysis across a range of MSC culture technologies with addition of stochastic analysis to identify output robustness

Note: *The work presented here was for a generic cell therapy product, however drew data from (Hassan et al., 2015; Simaria et al., 2014).

As outlined previously, whilst there have been studies capturing process and economic modelling of novel modalities, there are fewer studies that specifically focus on viral vectors as an *in-vivo* gene therapy product. Having said this, Masri et al. (2019) carried out an assessment of the suitability of manufacturing technologies for AAV and lentivirus production currently. This also gave an estimation of the market sizes for indications that are currently being addressed by viral vectors, either as an intermediate or as the final product. Specifically pertaining to AAVs, an upstream cost evaluation was conducted, comparing multiple cell culture technologies, including both adherent and suspension platforms, to identify which technology gave the minimum cost of goods per dose (Cameau et al., 2020). Summarised in **Table 1.6**, Comisel et al. (2021b) presented a decisional tool for the evaluation cost-effective lentiviral vector processes, particularly with a comparative focus on the upstream processing (USP) portion of the bioprocess. This tool highlighted the importance of moving to more scalable upstream options from a cost perspective, as suspension was shown to achieve a ~40% cost of goods (COG) reduction over more traditional technologies. This work was later extended to include a comparison between transient transfection and stable producer cell lines to generate viral vector products (Comisel et al., 2021a).

To date, there has not been an in-depth analysis of whole flowsheets with both upstream and downstream manufacturing strategies for AAV from both economic and purity perspectives. Particularly when considering the whole drug portfolio, whilst this chapter has outlined significant research into portfolio management and capacity planning for biopharmaceuticals, these have focused on mAb products and have not considered the implications when portfolio mixes of proteins and CGTs are encountered.

1.7 Aims and organisation of thesis

This review chapter has attempted to address both the complexities of biopharmaceutical drug development, with a specific focus upon how these are particularly pronounced with more novel modalities, such as cell and gene therapies. Details on AAV manufacturing and the scalability challenges encountered have also been provided. A focus on various computational methods relevant to addressing biopharmaceutical portfolio management and cost modelling case studies was also provided, particularly with a distinction between mathematical programming and meta-heuristic optimisation. Furthermore, an overview of decisional tools and their application to portfolio management, capacity planning and process economics has been detailed. As ascertained from the literature review, whilst work has been produced evaluating the economics of viruses as a gene therapy product, there has been very little scope into AAVs in particular, with no clear focus upon the downstream portion of the manufacturing process. Moreover, there is sufficient evidence of studies estimating R&D budgets for mAb products, delineating CMC contributions, however this has not yet been conducted for more novel therapeutic such as cell and gene therapies and hence no comparative analysis with more traditional mAbs. Building upon these elements, there is yet to be evidence of an integrated manufacturing, drug-development and portfolio tool that has optimisation and capacity planning capabilities for a range of modalities.

The aims and objectives of this thesis were to construct and utilise the aforementioned integrated portfolio management tool for biotherapeutic modalities, covering mAbs, ADCs, AAVs and CAR T cell products. Within this tool, further areas to focus on include the process economic evaluation of AAVs, for which no tool had yet been devised within the decisional tools space, for use as part of a drug development and cash-flow analysis for all modalities detailed. This integrated tool is hypothesised to cover case study questions from three distinct industrially relevant areas; manufacturing and COG analysis, drug development and CMC budgeting and dynamic portfolio optimisation and capacity planning. All three elements govern changes in one another, hence the necessity for the tool to be combined into one. As a result,

a series of case studies have been designed and implemented throughout this thesis, highlighting the incremental building of the tool into its fully-integrated state. Each results chapter refers to work conducted to address each significant part of this tool on industrially relevant scenarios.

Chapter 2 presents an overall description of the decisional tool requirements, dividing components appropriately and showing the interdependency between them. This highlighted the overall problem statement for the thesis, along with some of the individual contributions arising from each model within the tool, including the process economics work and R&D budget estimation.

Chapter 3 presents the construction of the first major elements of the tool; a process economics model for AAV manufacturing. A case study was devised where the process economics tools was used for assessment of cost-effectiveness of traditional AAV flowsheets versus more scalable alternatives. The impact of AAV dose size was also considered to highlight the variability across indications. Furthermore, the tool was supplemented with additional decision-making techniques such as uncertainty analysis via application of a Monte Carlo simulation, designed to capture the robustness of flowsheets investigated in the base-case scenario. A brute-force optimisation algorithm was implemented for rapid evaluation of the cost-effectiveness and purity potential of a range of AAV flowsheet options.

Chapter 4 described a tool and a study to compare and contrast the process development and manufacturing budgets for mAbs, ADCs, AAVs and CAR T cell therapeutics. This study also estimated the clinical trials cost by phase to be used in calculating the total out-of-pocket cost per success. The clinical success rates for each modality provided estimates of the number of projects required at each phase if one market success is to be achieved, which was supported by a sensitivity analysis across the range values. In addition to the AAV model built in Chapter 3, access to individual process economics models for proteins and CAR T cells was possible, through work carried out by Simaria et al. (2012) and Stamatis and Farid (2021) and Pereira Chilima et al. (2020) respectively. These could be used to derive the relevant

manufacturing costs across phases for use in line with process development and clinical trials assumptions to determine the out-of-pocket costs.

Furthermore, **Chapter 5** sought to integrate the previously defined elements and tools described in **Chapters 3** and **4** for use within portfolio management and capacity planning framework, thus presented the implementation of the fully-integrated decisional tool. The tool chiefly comprised a modified GA-based algorithm utilising a two-dimensional chromosome structure to characterise candidate portfolios and included bespoke constraint handling strategies. This further incorporated a success-failure algorithm based upon Bernoulli events to allow for the dynamic impact of drug failures to be expressed within the profitability analysis. The case study considered a large biotechnology company with a prospective pipeline of both protein therapeutics and CGTs. This firstly considered only mAbs and ADCs and comparing how a pipeline dominated by batch or products requiring continuous manufacture impacted profitability and capacity sourcing. This was extended to include CGTs, evaluating the risk: reward trade-off.

Chapter 6 summarised the conclusions drawn from the previous chapters, including key outcomes and contributions and **Chapter 7** highlighted the potential for commercialisation of the decisional tool described throughout the thesis, with discussion into current viability and alternatives software to be considered.

2 Decisional tool: Problem requirements and structure

2.1 Overview

The review chapter previously presented provided insights into the development and manufacturing of biotherapeutics. Additionally, a series of computational methods were outlined that have either been reported for use in portfolio management or capacity scheduling problems or were perceived to be options moving forward. Notably, the distinction between mathematical programming such as MILP-based models and meta-heuristic techniques such as genetic algorithms were previously specified, each with advantages and disadvantages in their implementation. This analysis evidenced the often-higher computational effort required for MILP-based algorithms, particularly when building a bespoke solution to a problem. In contrast, meta-heuristics offer users greater flexibility, facilitating efficient learning and implementation. In scenarios with non-linear decision variables and constraints, where reaching the true optimal solution is considered time-prohibitive (e.g. in stochastic environments), a GA-based approach was deemed to be a far more appropriate framework than mathematical programming.

As indicated in Section 1.7, the aim of Chapter 5 involved identifying the optimal portfolio composition in terms of drug selection and commercial capacity sourcing strategies when firstly considering batch versus continuous manufacture of mAbs and ADCs and later the impact of injecting CGTs. Whilst construction of the portfolio management tool used within this chapter was the end goal, several elements of the tool were necessary to define initially in order to generate the relevant costs for use within the profitability analysis (i.e. generation of the NPV). In particular, this necessitated the development of an AAV process economics engine and leveraging those currently available for the other therapeutic modalities under consideration (mAb, ADC and CAR T cell). In addition to manufacturing costs, calculation of

process development and clinical trials costs was also necessary, within a drug development lifecycle model that could account for the interdependencies between these activities, along with the impact of success rates on the overall R&D budgets. Therefore, the portfolio management tool utilised in Chapter 5, more specifically expressed as a stochastic multi-objective optimisation tool, extended the drug development lifecycle cost model with a cash-flow analysis to generate profitability, with the formation and evolution of solutions governed by a GA-based optimisation algorithm.

As such, due to the extent of techniques covered by the tool in its entirety, the specific materials and methods related to each individual model (i.e. AAV process economics, drug development lifecycle cost model and GA-based stochastic portfolio optimisation tool) have been outlined in their corresponding chapters within this thesis. Therefore, this chapter presents an overview of the whole decisional tool and the interactions between the models developed. Additionally, the motivations behind incorporating certain techniques have also been detailed within this chapter, along with the choice of building a custom tool over off-the-shelf software. To provide greater clarity and to summarise the tool components developed within this thesis and the case studies these addressed, the work in Chapters 3, 4 and 5 are labelled below as components of the whole decisional tool. The components are also numbered here for further granularity and are also expressed in **Figure 2.1**.

- **Component 1:** AAV process economics model (Chapter 3)
- **Component 2:** Drug development lifecycle cost model for mAb, ADC and CAR T (Chapter 4)
- **Component 3:** Cash-flow analysis and portfolio optimisation algorithm (Chapter 5)

The integration of the aforementioned components and hence the interaction between chapters is summarised in **Table 2.1**. This evidences the step-wise union of components, culminating in the portfolio optimisation tool and hence collation of all elements in Chapter 5.

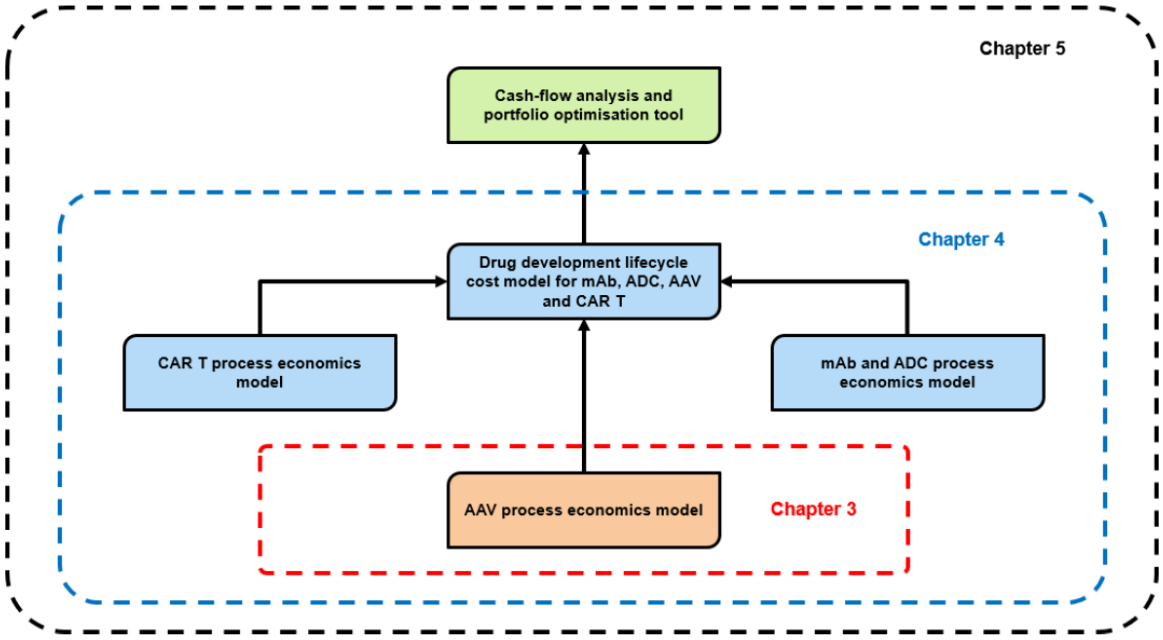

Figure 2.1 Schematic of the interaction between chapters within the thesis. The red contour indicates the tool component used in the AAV process economics work. The blue contour indicates those used within the drug development lifecycle cost model work. The black contour represents the overall decisional tool, incorporating the portfolio management and capacity sourcing elements also.

Table 2.1 Breakdown of results chapter by the model components used.

Chapter	Model components used
3	**Component 1**
4	Integration of **Components 1** and **2**
5	Integration of **Components 1, 2** and **3**

2.2 Problem definition

As summarised earlier, the overall goal within the thesis was the creation of a decisional tool for the optimisation of biopharmaceutical portfolios with respect to both the expected profitability (expected NPV) and the risk or volatility associated with the profit (quantitatively expressed as the standard deviation of the NPV). Candidate solutions were represented by the drugs selected and the capacity strategies used for each. The key components within the overall tool and their utilisation in each chapter were discussed in Section 2.1. This indicated the relationship between model components and thus interactions between the chapters. Whilst the overall portfolio management tool was employed in Chapter 5, the work conducted in Chapters 3 and 4 were necessary to build in the full capabilities of the decisional tool. As a result, the next section addresses the requirements and capabilities of the tool and follows a bottom-up approach; that is, the components are discussed in reverse order to highlight the overall goal and why it became necessary to build in the model elements utilised in Chapters 3 and 4.

2.2.1 Requirements and capabilities

The model was required to ultimately address a portfolio optimisation problem for a large biotechnology company. In terms of capabilities, the model had to consider an established starting portfolio, a pool of potential candidate drugs to inject into the portfolio annually and a series of capacity sourcing options to manufacture the drug candidates (i.e. in-house, outsourcing to a CMO or building a new facility). This would also require inclusion of constraints, namely those related to R&D budget and manufacturing capacity.

The goal of the study was portfolio optimisation, that is, ascertaining the portfolio composition of drugs and the corresponding capacity strategies that would maximise the expected profitability (eNPV). A secondary objective was to minimise the risk associated with this profit, which is quantitatively expressed as the standard deviation of the NPV (sdNPV). Derivation of these objective functions required a distribution of outputs be generated. This required

inputting distributions of parameters through an uncertainty analysis via Monte Carlo simulation, where larger standard deviations inferred riskier solutions. However, before integration of additional techniques such as an uncertainty analysis, the generation of the deterministic NPV was necessary. This required the integration of modality-specific process economics models and the drug development lifecycle model with a cash-flow analysis to determine annual revenues and expenses, before discounting cumulative costs to determine the NPV. As a result, components 1 and 2 defined in Section 2.1 were necessary to include within the overall portfolio tool.

The key expenses considered within the cash-flow for deriving the NPV were necessary to define. These in particular could be broadly categorised as those related to process development, manufacturing and clinical trial activities. This gave rise to the model developed and employed in Chapter 4, designed to outline these expenses, as well as introduce the impact of clinical success rates on overall R&D costs. Similar to that already reported in previous R&D budget studies, process development costs were calculated from considering an annual salary and the personnel required across phases to characterise and optimise the process prior to manufacturing. Clinical trial budgets were assessed through assumption on trial sizes (in terms of patient population) and the average cost per patient involved in the trial. On the manufacturing front however, as shown in Chapter 1, derivation of the cost of goods required construction of detailed process economics engines. At the time of formulating the problem statement, process economic models for mAbs, ADCs and CAR T cells were available to be used or built upon, however no such model was available for AAV manufacturing. This missing element, along with several of the challenges indicated in Chapter 1, provided motivation for the construction of an AAV process economics model.

As such, the work carried out in Chapter 3 focused on the generation of an economics model capable of providing AAV cost of goods values, whilst addressing a number of the USP and DSP challenges described in Chapter 1. In particular, it became significant to assess the feasibility of traditional versus scalable AAV manufacturing strategies. Additionally, the extent

of AAV flowsheet options available drove the implementation of a brute-force optimisation to evaluate technologies from both an economic and purity perspective.

2.3 Selection of software and overall model design

The previous section provided information on the computational methods that would be required for addressing each element of the problem statement. An important consideration for construction of the tool was the programming language utilised. The majority of the tools discussed in Chapter 1 were constructed with Microsoft Excel alone or in combination with Python, in particular those involving process economic or drug development case studies. More extensive tools such as those for portfolio management or capacity scheduling have been implemented using more powerful programming languages, including Python, C++ or C#. In particular, Python is an object-oriented programming (OOP) language, allowing for data and function organisation into “classes”, which are instantiated as “objects” for specific problems. The language as a whole provides a relatively intuitive syntax and access to an extensive range of open-source libraries for data manipulation, statistics and visualisation to name a few. Though it has been reported that other languages such as C++ and C# enable relatively improved performance over Python, attributes such as rapid learning and development of programming skills and use of existing libraries were considered more significant factors in choosing Python as the primary programming language. Furthermore, several of the existing process economics models available to use within the whole decisional tool had previously been constructed in Python, hence maintaining this uniformity was also a driver in utilising Python throughout.

Taking each tool component described in **Table 2.1** as a standalone model, the following section outlines the methods utilised on a chapter-by-chapter basis, including the motivations behind their inclusion.

2.3.1 AAV process economics

The following section outlines the key modelling elements from the AAV process economics model. The model was constructed in Python 3.8, with adjoining databases of assumptions stored in Microsoft Excel. Alternative process economic tools commercially available include BioSolve (Biopharm Services, UK), which allows for cost analysis of viral vector manufacturing. In this case, a software like BioSolve was not chosen due to the wider goal of the tool that was portfolio optimisation, which is not provided by this software. This would prove difficult in linking model components (as discussed in Section 2.1) if conflicting software was implemented on different tool elements. Other considerations for building an in-house process economics tool in Python 3.8 included the ability for customisation and incorporation of additional techniques (e.g. uncertainty analysis, brute-force optimisation) and particularly when compared to BioSolve, the perceived improved computational efficiency.

Furthermore, the object-oriented structure described earlier was used for the design of the AAV COG tool. General unit operations (e.g. centrifugation, filtration, chromatography) were designed as classes, with objects instantiated for specific variations, e.g. an affinity chromatography object can be instantiated from the general chromatography class. An example of this architecture is highlighted in **Figure 2.2**, using chromatography as an illustrative example. Object outputs instantiated from each unit operation class were grouped for any given flowsheet to calculate the overall cost of goods.

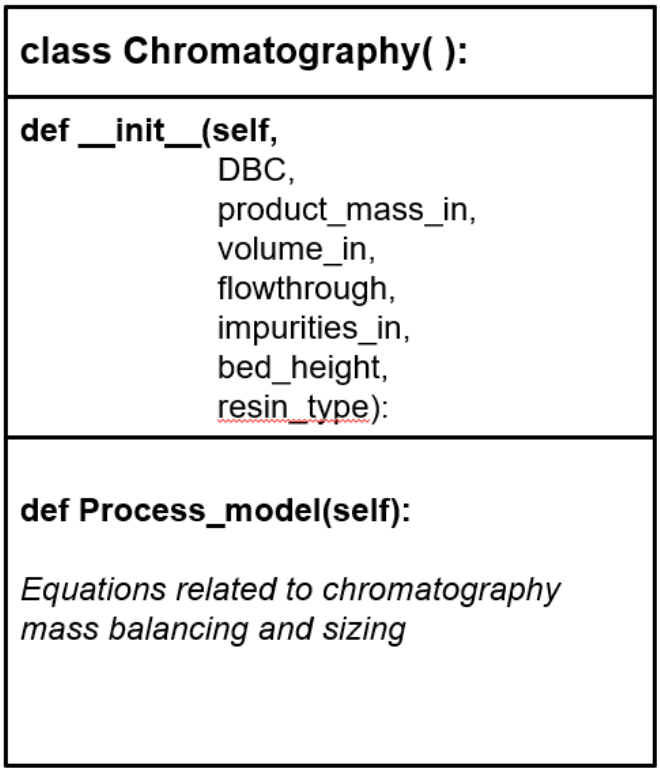

Figure 2.2 Example of class design in the AAV process economics model in Python 3.8, using chromatography as an example unit operation. All classes were coded in Spyder (IDE) and objects were instantiated in Jupyter Notebook (GUI). The structure of classes always took the following: class definition (e.g. chromatography), definition of relevant attributes (e.g. DBC, resin type) and the set of methods or calculations related to the class (e.g. mass balancing and sizing equations for chromatography).

The key elements within the AAV process economics tool are provided below. An overview is detailed within this section, with a more comprehensive discussion provided in materials and methods section of Chapter 3.

1. **Deterministic cost of goods:** This included the overall COG per dose, as well as a breakdown by relevant cost category, e.g. raw materials, labour, indirect. At the base-case, only a single COG was generated for any given scenario, as no sensitivity or stochasticity of input parameters was considered at this point. This provided the central model element

and therefore, any additional computational techniques built-in would utilise the deterministic model to derive COG outputs.

2. **Uncertainty analysis:** This linked to the process economics model and when provided with input distributions of uncertain input parameters, generated output distributions of COG/dose values. The inclusion of an uncertainty analysis is beneficial for assessment of the robustness or risk associated with any given AAV flowsheets. It also simulates the realistic uncertainty associated with several bioprocess-related parameters.
3. **Brute-force optimisation:** As with the uncertainty analysis, outputs relied on the deterministic model to generate COG values. Brute-force algorithms rapidly feed numerous potential solutions into the deterministic model to generate the objective functions associated with each. Outputs were also assessed for compliance with any imposed constraints. This technique is generally useful for a rapid evaluation of flowsheet options and circumvents much of the computational time and intensity associated with manually inputting each flowsheet into the deterministic COG model. Equally, for a case study such as identifying optimal flowsheets (i.e. finite number of combinations and a relatively small objective space), a brute-force algorithm is often an apt choice over a more powerful meta-heuristic or mathematical programming technique.

2.3.2 Derivation of R&D budgets for mAbs, ADCs, AAVs and CAR T

This chapter sought to estimate the R&D budgets for a range of biotherapeutic modalities and compare and contrast costs across phases and development activities. Each modality evaluated had specific process economics models associated with them (all constructed in Python 3.8) and as such, consistency in the programming language provided a driver in constructing the drug development lifecycle cost model also in Python 3.8.

The application of object-oriented programming within this model was particularly useful for instantiating phase-by-phase activities for a given modality, in calculating the cost breakdowns. An example of this architecture is highlighted in **Figure 2.3**.

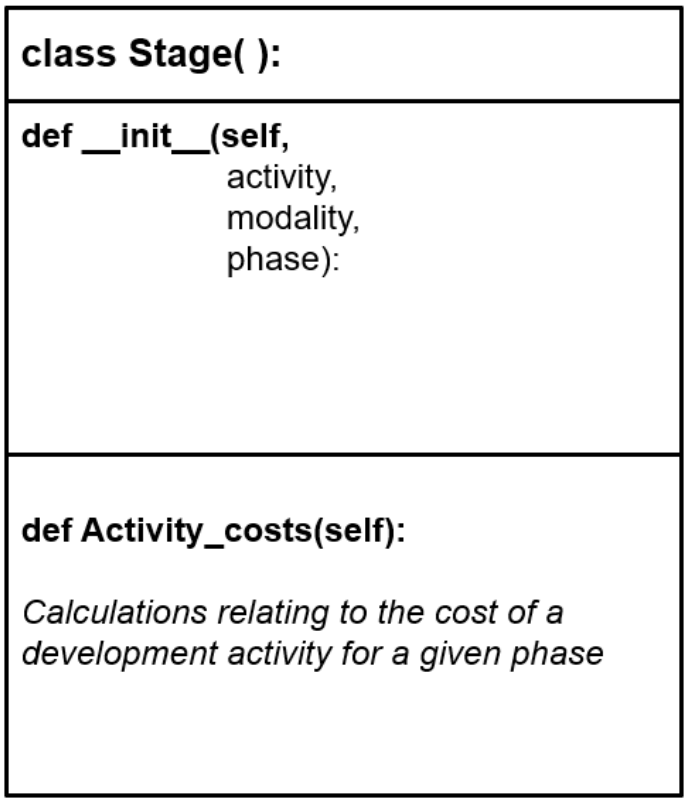

Figure 2.3 Example of class design in the drug development lifecycle model in Python 3.8, using the stage as an example. All classes were coded in Spyder (IDE) and objects were instantiated in Jupyter Notebook (GUI). The structure of classes always took the following: class definition (e.g. a given stage), definition of relevant attributes (e.g. activity type (process development, manufacturing or clinical trials), modality under consideration or phase (e.g. I, II, III, regulatory review) and the set of methods or calculations related to the class (calculation of the costs for the activity, phase and modality under consideration).

The major elements in the drug development lifecycle cost model are listed below. An overview is detailed within this section, with a more comprehensive discussion provided in a dedicated methodology section in Chapter 4.

1. **Deterministic total out-of-pocket cost per success:** This was an integrated tool for all modalities and provided links to all relevant process economics models (including that described in Section 2.3.1). In addition to manufacturing, process development and clinical trials calculations were conducted and the overall out-of-pocket costs (also termed budget) could be generated. This was derived on a per success basis, meaning the clinical success

rates were considered to calculate the theoretical number of project required at each phase to achieve a single market success.

2. **Sensitivity analysis:** This involved defining a best- and worst-case value alongside the base-case and inputting these into the deterministic out-of-pocket cost calculations. This targeted clinical success rates, due to their significance in influencing budgets and particularly, the distribution of costs across clinical phases.

2.3.3 Portfolio management and capacity planning for mAbs, ADCs, AAVs and CAR T

The building blocks of this section were described in Sections 2.3.1 and 2.3.2, however several additional computational elements were included here to address the problem statement more comprehensively. As described previously, the tool was designed in Python 3.8. In general, the language allows access to a range of libraries that expedite the implementation of various computational methods. Specific to optimisation, Python libraries such as PyGAD or PyMOO (for multi-objective problems) can effectively be regarded as off-the-shelf functions to implement optimisation. PyGAD provides tools for the implementation of genetic algorithms specifically, offering a framework for solution optimisation, parameter customisation and feature selection. Conversely, PyMOO is specifically designed for optimisation problems with two or more objective functions, where these often conflict with one another. This provides users with a range of multi-objective optimisation algorithms and tools for defining problem-specific objectives, constraints and decision variables.

Though these libraries were available, for the problem under consideration, several factors drove the implementation of a bespoke model in Python, coded without use of optimisation libraries or off-the-shelf tools. Chapter 5 provides more detail on the novelty of chromosome structure, however this motivated the construction of a bespoke tool, as typically off-the-shelf optimisation libraries come with a pre-defined chromosome structure. The use of highly specialised or unique chromosome structures would therefore be incompatible with the

aforementioned libraries. Furthermore, as discussed previously, the portfolio tool required integration with the existing model components, thus a custom tool can be beneficial in maintaining the overall tool architecture and data flow. It must also be noted that a driver behind the implementation of a custom portfolio optimisation tool was also to facilitate learning of the specific computational methods undertaken and to gain practical experience in building individual decision-making techniques.

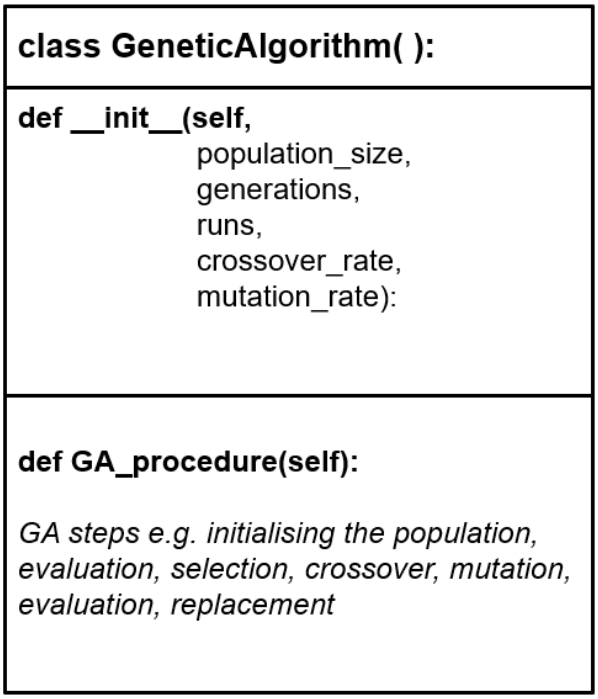

Figure 2.4 Example of class design in the portfolio optimisation tool in Python 3.8, using the genetic algorithm as an example. All classes were coded in Spyder (IDE) and objects were instantiated in Jupyter Notebook (GUI). The structure of classes always takes the following: class definition (e.g. genetic algorithm), definition of relevant attributes (e.g. GA parameters) and the set of methods or calculations related to the class (steps involved in evolving candidate solutions).

As displayed previously, the use of OOP in this section of the tool is outlined in **Figure 2.4**, utilising the genetic algorithm as an illustrative example. Furthermore, the key elements within

the optimisation tool are provided below. An overview is detailed within this section, with a more comprehensive discussion provided in the methodology section of Chapter 5.

1. **Discounted cash-flow:** This was fundamental to deriving the eNPV, which served as one of the objective functions. This allowed for multiple therapeutic products to be assessed and as such a combined cash-flow was considered based on the whole portfolio rather than just a single drug. The core of this was a profit and loss statement, with discounting of costs to account for the time value of money.
2. **Modified genetic algorithm:** This was an essential element to carry out the optimisation procedure. As previously discussed, GAs are a meta-heuristic algorithm and as such are not concerned with providing the true optimal of the set, but typically reduce computational time in comparison to mathematical programming. This allowed for rapid evaluation of populations of candidate portfolios and assessed their performance with respect to the outputs of the discounted cash-flow.
3. **Uncertainty analysis:** This was applied to entries into the cash-flow and resulted in a distribution of NPV values, ultimately generating the eNPV. This further allowed for the generation of the standard deviation of the NPV, which served as the second objective function.
4. **Multi-objective optimisation:** The incorporation of an uncertainty analysis yielded multiple objective functions and as a result, use of a modified-GA based algorithm that can cope with both objectives to be optimised was necessary. This introduced modified ranking and selection methods that considered the performance of both objective functions.
5. **Model validation:** Convergence metrics were defined to assess the performance of the algorithm, particularly ones suited to multi-objective optimisation as described in Chapter 1. Parameter selection was also conducted to confirm the appropriate selection of GA parameters.

6. **Dynamic risk simulation:** This was a necessary addition to assess the transition success rates in a dynamic environment. This considered the success or failure of products in each portfolio and how failure impacted the profitability and capacity considerations.

2.4 Conclusion

In summary, the overall decisional tool was shown to require three distinct components; that related to AAV process economics, drug development lifecycle cost modelling and portfolio optimisation and capacity strategies for a mix of modalities. Furthermore, the motivation behind the use of Python as a programming language and the building of a custom tool over off-the-shelf applications was also discussed, highlighting the benefits in tailoring the modelling procedure to the specific requirements of the problem. This also discussed the option for incorporating novel elements to the tool that may not be possible in off-the-self software programs. Furthermore, construction of a bespoke tool provides a unique learning element that allows for a better understanding of the algorithms, any caveats associated with their use and the intricacies of the problem domain.

3 Process economic evaluation and optimisation of adeno-associated virus manufacturing

3.1 Introduction

As outlined in Chapter 1, a key challenge identified in large-scale AAV processing is the scale-up of processes typically intended for lab-scale, a challenge present during both upstream processing (USP) and downstream processing (DSP). Cell culture has typically relied upon technologies that involve growing HEK293 cells adhered to a plastic surface, thus scale-out strategies are employed to increase the area required, rapidly increasing the number of incubators and ultimately facility footprint. Scalability issues are also encountered during purification as many traditional AAV protocols feature a non-scalable batch gradient density ultracentrifugation (UC) step, which similarly involves increasing the number of parallel ultracentrifuge units when a greater capacity is necessary. For annual demands characteristic of rare or orphan indications, scalability does not present a critical challenge. However, when targeting more prevalent disease areas or those with high dose sizes using AAVs, switching manufacturing strategies towards generation of a scalable platform is desired. As a result, there exists the need for the effective translation of the purification performance achieved with technologies such as ultracentrifugation at the lab scale, to more scalable technologies that are economically feasible in a commercial setting.

A significant and somewhat unique impurity issue that arises with AAV manufacturing is the generation of vector particles lacking fully packaged genetic material, referred to as empty or partially-filled capsids. The challenge industry faces is that empty capsids are structurally closely related to the full capsids (Qu et al., 2015), thereby making it difficult to utilise some chromatographic procedures and exploit molecular and structural differences between impurities. Steps such as ultracentrifugation have demonstrated success in removal of empty particles, independent of AAV serotype (Crosson et al., 2018) and allow for more stable yields

relative to IEX. This presents the trade-off between ultracentrifugation and IEX; that is a high yield and purity step against a scalable strategy respectively. Alternative scalable options include the use of continuous ultracentrifugation, which can allow for large product volumes to be processed (Chen et al., 2016; Wada et al., 2023). This provides a scalable, serotype-independent methodology for purifying AAV products, as well as linear scalability from the batch rotors during development to commercialisation (Merino & Brittle, 2023). In terms of purity, final product specifications lack definition with respect to empty capsids and hence there remains ambiguity around target removal levels. In contrast, information exists on AAV process-related impurities such as host cell proteins (HCP) and host cell DNA, where Wright (2014b) provided data on target levels for both.

As such, this chapter investigates the cost-effectiveness of AAV manufacturing strategies, evaluating both USP and DSP. Section 3.2 provides the materials and methods related to the process economics model. Section 3.3 gives the case study setup, detailing key scenario-related assumptions for the flowsheets under consideration. Significantly, Section 3.4 presents the results of the case study, firstly providing the deterministic analysis, focusing upon adherent cell factories (CF10) versus suspension stirred tank bioreactors for cell culture, and batch ultracentrifugation (UC) against anion-exchange chromatography (AEX) for polishing purification comparison. This is followed by study outlining how the dose size affects this base-case COG/dose ranking. Furthermore, an uncertainty analysis was carried out to compare the robustness of the different manufacturing strategies. Finally, an optimisation of AAV purification platform was then implemented to find the optimal capture and polishing options from an economic and purity perspective.

3.2 Materials and methods

3.2.1 Overview and description of decisional tool

The decisional tool in **Figure 3.1** was developed to allow for a comparison between AAV process flowsheets and ultimately determination of cost-effectiveness, whilst meeting any imposed purity constraints and targets. The tool comprised a process economics model, with an uncertainty analysis feature for assessment under stochastic conditions. Additionally, a brute-force optimisation algorithm fed information into the process economics model, where outputs were then fed back for identification of the optimal output. A hybrid modelling approach was undertaken, utilising both Python 3.8 (Python Software Foundation, DE, USA), and Microsoft Excel (Microsoft Corporation, WA, USA).

The tool itself was implemented in Python 3.8, with Spyder used as the main code editor of the model and Jupyter Notebook for the graphical user interface (GUI), to visualise key model outputs. Python 3.8 is well regarded as a relatively rapid programming software compared to using Microsoft Excel, with opportunities to leverage several shortcuts for data processing, analysis or visualisation through use of in-built libraries. Additionally, Python has often been used for object orient programming (OOP), a framework extensively followed when crafting bioprocessing economics models. Typically, any manufacturing flowsheet can be characterised as a series of unit operations, each with individual process models to determine sizing metrics and ultimately costs. Therefore, in this tool, model classes in Python were organised by general unit operation type (e.g. chromatography, filtration, cell culture) and specific objects were instantiated from a given class when calling the unit operation in the interface (e.g. affinity chromatography, depth filtration, chemical lysis). Whilst Python comprised the majority of the tool, Microsoft Excel was utilised as an adjoining database containing many of the inputs outlined in **Figure 3.**1. In particular, this included much of the mass balance, sizing cost and market data. As an additional impetus for the programming

language selected, the Pandas library in Python provides an intuitive means to load Excel-based assumptions as variables into the model.

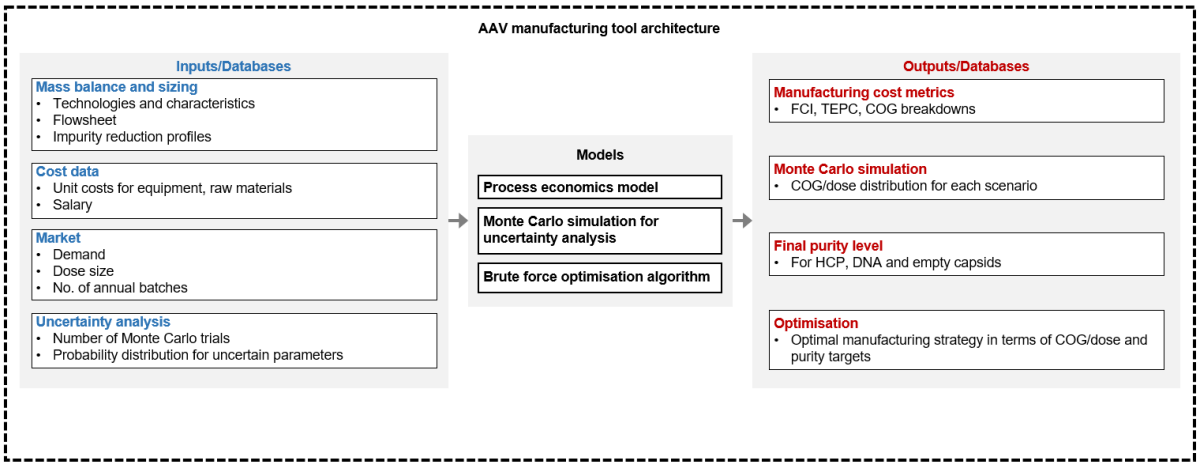

Figure 3.1 Decisional tool architecture for AAV process economics. Assumptions and process parameters feed into the deterministic model, where the COG/dose is calculated. Information is transferred between the stochastic model feature and the process economics model as part of the uncertainty analysis via Monte Carlo simulation. A brute-force optimisation component is also present to conduct rapid evaluation of AAV flowsheets.

3.2.2 Process models

The process models used throughout this chapter for mass balancing and sizing were largely derived and adapted from Simaria et al. (2012) and Stamatis & Farid (2021). Key viral vector process models, particularly fill-finish, were adapted from Comisel et al. (2021), but altered to represent AAV manufacturing over lentiviral vectors. Furthermore, new models were also incorporated (e.g. ultracentrifugation) for additional unit operations. The process models allowed for a whole flowsheet mass balance, as well as equipment sizing for each unit operation and ancillary equipment.

In general, the process models for AAVs track the vector genomes (vg) out of each stage. The models utilised for each flowsheet are dependent on the nature of the upstream process material; that is, whether the AAV is intracellularly or extracellularly expressed post-culture.

This often also goes hand-in-hand with the cell culture type, i.e. whether cells grown in adherent or in suspension mode.

The vg out of each step were, in the majority of cases (except where stated), calculated by assuming a step yield (Y_j) and applying it to the number of vg in.

$$vg_{out} = vg_{in} \times Y_j \quad (3.1)$$

3.2.2.1 Seed expansion

Seed expansion is characterised as a collection of stages designed to ensure the required seeding cell density for the production culture is achieved. The number of seed stages may vary between technology type, however in general, the seed vessels used also depend on whether cell culture is adherent or suspension. An adherent production cell culture means all adherent technologies are used throughout the seed and the same applies for suspension. In the work conducted in this chapter, each production cell culture technology was assigned a pre-defined seed train. Equations were then constructed to determine the number of units of each technology required at each seed stage based on the cells required for the following stage.

It has been reported that a single seed train can be used to feed multiple production batches in viral vector manufacturing, such that the seed is maintained for a fixed time to later feed the other production batches. For the purpose of this work, this was defined as a campaign, where each campaign may have a maximum of four production batches fed by one seed. Hence the number of campaigns could be used to define how many seed runs were required annually. In cases where the number of annual production batches (B) was not perfectly divisible by the maximum production batches per campaign (4), two varieties of campaign were defined. The equation for variety 1 is outlined below.

$$N_{campaigns,1} = FLOOR(\frac{B}{4}) \quad (3.2)$$

Campaign variety 2 was required if $\frac{B}{4}$ was found to be a non-integer value and as such the following equation was used.

$$N_{campaigns,2} = (\frac{B}{4} - N_{campaigns,1}) \times 4 \quad (3.3)$$

The assumption that one seed train could be used for multiple production batches governed the number of cells to be produced prior to seeding the first production batch and evidently meant an excess needed to be generated. In practice, this excess is further maintained in parallel seed stages as the first production batch is run, to ensure there are sufficient cells to seed the next production batch. As dictated previously, this calculation is further dependent on whether the cell culture is adherent or suspension.

3.2.2.1.1 Adherent cell culture

This type of cell culture involves the growth of cells on a surface, thereby densities are given in terms of cells per area of the technology. To seed one production batch, the following equation was utilised to determine the number of cells required.

$$N_{seed} = N_{units_n} \times A_n \times d_{s_a} \quad (3.4)$$

where N_{seed} = number of cells required to seed one production batch

N_{units_n} = units of the technology at production culture (denoted stage n)

A_n = surface area per unit of the technology (cm^2) at production cell culture

d_{s_a} = adherent seeding cell density ($cells/cm^2$)

The number of excess cells required to seed multiple production batches, in addition to N_{seed}, was ascertained by assuming a doubling time for the cells and the seed maintenance time. The following equation was formulated to do this.

$$N_{seed(total)} = N_{seed} \times \sum_{b=0}^{B_{campaign}-1} e^{-bkt} \quad (3.5)$$

where $B_{campaign}$ = number of production batches in a campaign

b = index of production batch and is in the range $(0 \ldots B_{campaign} - 1)$

$N_{seed(total)}$ = total cells required to cultivate

k = doubling time constant (see **Equation A1** in Appendix A)

t = time (days) that the seed is maintained for to seed the next production batch

The above equation only held true if $B_{campaign}$ exceeded 1. In cases where one seed train fed only one production batch, the only value *b* could take was 0, hence $N_{seed(total)}$ approximates to N_{seed}. This concurs with the theory that no excess of cells would be required if no seed maintenance was necessary. Furthermore, *t* relies on the assumption that the seed is maintained for the duration of USP and DSP (see **Figure A1** in Appendix A), thus incorporated the total time for which the cells must be maintained and further cultured in between two production batches.

The number of units of the cell culture technology required at seed stage $n-1$ was calculated based upon the ratio of the surface areas and seeding densities of the current and previous seed stage.

$$N_{units_{n-1}} = \frac{(d_{s_a} \times A_n \times N_{units_n}) + (N_{seed(total)} - N_{seed})}{d_{h_a} \times A_{n-1}} \quad (3.5)$$

where d_{h_a} = adherent harvest cell density (cells/cm^2)

A_{n-1} = surface area of technology at stage $n-1$ (cm^2)

The equation is similar, but slightly modified for the calculation of how many units of other seed stages are required $(n-2, \ldots n-m)$ where m is required number of seed stages.

$$N_{units_{n-k}} = \frac{\left(d_{s_a} \times A_{n-j} \times N_{units_{n-j}}\right)}{d_{h_a} \times A_{n-k}} \quad (3.6)$$

where $N_{units_{n-k}}$ = number of units of seed stage $n-k$, where $\mathrm{k} = 2, \ldots, m$

$N_{units_{n-j}}$ = number of units of seed stage $n-j$, where $j = 1, \ldots, m-1$

A_{n-k} = surface area of technology at stage $n-k$ (cm^2)

A_{n-j} = surface area of technology at stage $n-j$ (cm^2)

3.2.2.1.2 Suspension cell culture

In contrast to adherent cells, cells in suspension grow within the cell culture media. The seed equations for determining the number of units of each technology per stage required are similar to that of adherent, except volume is used instead of surface area (thus A_{n-1} becomes V_{n-1}). Additionally, the seeding and harvest cell densities differ for suspension and have the units of cells/mL and are represented by d_{s_s}or d_{h_s} *(*see **Equations A2** and **A3** in Appendix A).

3.2.2.2 Cell culture (expansion)

The production phase of AAV manufacturing involves the expansion of HEK293T cells. AAV production is induced by transfection of three plasmids into the cells, containing necessary genes for the formation of AAV particles. Calculations pertaining to the vg out or volume out per batch were determined from setting an annual demand (in terms of the number of doses). By also considering the required vg per dose (i.e. dose size), Equation 3.8 was then utilised to generate the annual vg requirement.

$$Annual\ target\ vg\ output\ (vg) = \frac{Dose\ size \times (1 + batch\ failure\ rate) \times Demand}{Overall\ yield} \qquad (3.7)$$

In calculating the vg output required per batch, the number of batches per year (N_{batch}*)* was applied.

$$vg_{out} = \frac{Annual\ target\ vg\ output\ (vg)}{N_{batch}} \qquad (3.8)$$

Harvest titre is often defined differently for adherent cell culture over suspension. Adherent generally reports titres in vg/cm^2 of cell growth area, whereas titre for suspension cell culture is typically expressed in terms of vg/L of media consumed. Therefore, for consistency with literature (see **Table 1.2**), these units are maintained throughout. As such, the output of

Equation 3.8 was used with the titre to ascertain either the growth surface area *($A_{n_{total}}$)* or working volume required per batch ($V_{harvest}$) (see Appendix A for titre determination).

$$A_{n_{total}} = \frac{vg_{out}}{Titre\ (adherent)} \quad (3.9)$$

$$V_{harvest} = \frac{vg_{out}}{Titre\ (suspension)} \quad (3.10)$$

The harvest volume per batch represents the volume that is removed from the cell culture vessel post-production. This value was utilised to generate the number of parallel units required to attain the volumetric capacity required (used for suspension only).

$$N_{units_n} = \left[\frac{V_{harvest}}{Maximum\ working\ volume\ of\ tech}\right] \quad (3.11)$$

Conversely, in the case of adherent technologies, the total area required per batch was used.

$$N_{units_n} = \left[\frac{A_{n_{total}}}{Maximum\ surface\ area\ of\ tech}\right] \quad (3.12)$$

The N_{units_n} from either Equations 3.12 or 3.13 was the value utilised in the seed equations shown in Equations 3.4 and 3.6.

3.2.2.2.1 Extracellular AAVs

The previous volumetric equations outlined were modelled differently depending on the AAV serotype under consideration, more specifically whether extracellularly or intracellularly expressed. For extracellular AAVs, V_{out} became equal to $V_{harvest}$, as all the vessel(s) contents were assumed to be transferred to harvest due to secretion of the product.

3.2.2.2.2 Intracellular AAVs

The intracellular case was further dependent on the type of cell culture used; adherent or suspension. For adherent cell culture, the volume out was a mixture of cells and the working volume of the technology that would be added back to re-suspend the cells following trypsinisation (i.e. detachment from the growth area). The assumption made is that all cells were successfully detached.

$$V_{out} = (V_{cells}) + (V_i \times N_{units_n}) \quad (3.13)$$

where V_{cells} = volume of cells (L)

V_i = working volume of technology i

3.2.2.3 Dead-end filtration

For an extracellular flowsheet, harvest features a depth filtration step operating in dead-end mode. For an adherent-extracellular scenario, the cells remain attached to the technology surface and as the product is secreted, only the broth is required. However, a subsequent filtration stage was incorporated due to the likelihood of a small percentage of cells having not adhered or lost adherence and if not removed, could be detrimental to later column steps.

In this work, clarifying depth filters and 0.2um filtration for sterility purposes were all conducted in dead-end mode with respect to the filter (flow is perpendicular), thus the design equations utilised to size the steps followed the same pattern.

$$V_{out} = V_{in} \times Y_{DEF} \quad (3.14)$$

where Y_{DEF} = yield of dead-end filtration stage

The key sizing metric used for filtration is the area. For dead-end filtration, the volume in (V_{in}) was divided by the filter capacity (V_{max}).

$$A_{DEF} = \frac{V_{in}}{V_{max}} \quad (3.15)$$

where V_{max} = filter capacity (L/m^2)

A safety factor is commonly applied to calculated filter areas as a precaution in the case of batch-to-batch variations (Lutz et al., 2015) thus the original A_{DEF} variable was updated.

$$A_{DEF} = A_{DEF} \times SF \quad (3.16)$$

where SF = filter safety factor

3.2.2.4 Lysis

This stage is only required if the AAV product under consideration is expressed intracellularly, thus cell breakage would be required to release the particles. Here, detergent treatment (i.e. chemical lysis) or microfluidisation were considered.

3.2.2.4.1 Chemical lysis

Chemical lysis involves the addition of detergent lysis buffer to the cells to disrupt their membranes and ultimately realise the intracellular product. An important consideration for this stage is how much lysis buffer must be added to enact the cell disruption process. The amount of buffer added was calculated on a volume basis.

$$V_{buffer} = V_{cells_{in}} \times f_{lysis} \times \left(1 + Overfill_{lysis}\right) \quad (3.17)$$

where $V_{cells_{in}}$ = cell volume into the step (L)

f_{lysis} = lysis buffer addition factor (L/L)

$Overfill_{lysis}$ = lysis buffer overfill (%)

Furthermore, in calculating the volume out of the stage, both the cell and broth volume were considered (whereby the broth volume included the lysis buffer added during the step as well as the product fluid).

$$V_{cells,out} = V_{cells,in} \times S \quad (3.18)$$

where S = cell carryover (%)

Assuming an even distribution of the product in the broth, the broth volume out was calculated via the following.

$$V_{broth,out} = V_{broth,in} \times Y_{lysis} \quad (3.19)$$

3.2.2.4.2 Microfluidisation

Microfluidisation is a mechanical means of lysis and operates similarly to high pressure homogenisation, where multiple cycles or passes are initiated to break open the cells. Due to the similarities between the two, namely that both operate in a high-pressure environment, similar design equations were assumed. Here, the yield was calculated as an output from the step, rather than an input.

$$vg_{out} = vg_{in} \times \left(1 - \frac{1}{Power\ factor}\right) \quad (3.20)$$

The power factor is determined by the following.

$$Power\ factor = e^{kN} \quad (3.21)$$

where N = number of passes through the microfluidiser

k = constant, determined by Equation 3.23

In calculating the constant (*k*), the pressure drop across the device was considered with how resistant to breakage the HEK293T cells are.

$$k = CP^{a} \quad (3.22)$$

where C = disruption constant (1/bar)

P = pressure drop (bar)

a = resistance to disruption

As previously discussed, yield was an output from this unit operation and was calculated via the equation outlined:

$$Y_{lysis} = \frac{vg_{out}}{vg_{in}} \quad (3.23)$$

Similar to that of chemical lysis, Equation 3.24 also applied for microfluidisation.

$$V_{out} = (V_{in} + V_{buffer}) \times Y_{lysis} \quad (3.24)$$

3.2.2.5 Nuclease treatment

This stage is utilised to degrade nucleic acid impurities that are contained within the broth. In general, Benzonase® is a frequently used reagent and as such, a key part of the process model was ascertaining the volume of such required to treat the broth.

The mass of Benzonase® required was calculated as a function of the total broth volume into the step, as well as the concentration of the reagent itself.

$$m_{benz} = V_{in} \times c_{benz} \quad (3.25)$$

where c_{benz} = concentration of Benzonase® required (units/mL)

Furthermore, as Benzonase® is an enzyme, it has a specific activity, which was utilised to find the volume from the mass.

$$V_{benz} = \frac{m_{benz}}{U} \quad (3.26)$$

where U = Benzonase® activity (units/uL)

$$V_{out} = (V_{in} \times Y_{benz}) + V_{benz} \quad (3.27)$$

3.2.2.6 Ultracentrifugation

3.2.2.6.1 Batch

This stage is conducted in batch mode, using a density gradient. The ultracentrifuge rotor contains slots for a small number of tubes to be placed within. In addition to the product, the tube contains n layers of reagent (usually either CsCl or Iodixanol), in differing concentrations. The ratios of each layer to the product volume were assumed from lab-based protocols. For simplicity, an overall ratio was determined for the calculations and was formulated as follows.

$$R_{total} = R_1 + \cdots + R_n \quad (3.28)$$

where R_1= ratio of product to product (as such will always be 1)

R_n= ratio of n^{th} layer of reagent to product, where n is the total number of layers

Whilst the rotor capacity is a common metric utilised when describing ultracentrifuges, a more relevant capacity measurement when tracking the product throughout the mass balance is the rotor capacity that is dedicated to housing the product stream, rather that that including the reagent, as outlined below.

$$V_{UC(feed)} = \frac{V_{UC(total)}}{R_{total}} \quad (3.29)$$

where $V_{UC(total)}$ = total rotor capacity

From this capacity metric, the number of ultracentrifuge parallel units required was calculated.

$$N_{units} = CEILING(\frac{V_{in}}{V_{UC(feed)}}) \quad (3.30)$$

The continuous process model is found in the Appendix A.

3.2.2.7 Chromatography

Due to the wide range of chromatography options employed for AAV purification, both bind-elute and flow-through type columns have been evaluated. Particularly applying to bind-elute columns, dynamic binding capacities are generally provided in units of vg/mL or vg/L for AAVs. Nevertheless, as with mAb bioprocessing, those chromatography columns operating in flow-through mode generally report dynamic binding capacities in g/L as they bind impurities such as host cell proteins (HCPs).

The sizing of the chromatography column must adhere to those column diameters that are commercially available. For bind-elute mode columns, the following was used to first ascertain the required column volume.

$$V_{column} = \frac{vg_{in}}{DBC \times N_{cycles} \times N_{column}} \quad (3.31)$$

where DBC = dynamic binding capacity of resin (vg/L)

N_{cycles} = number of cycles

N_{column} = number of columns

In the case of a flow-through mode operation, vg_{in} in Equation 3.32 was replaced with the mass in of a specific impurity.

For costing purposes, the column diameter (d) was necessary to calculate.

$$d = \sqrt{\frac{4 \times V_{column}}{\pi \times h}} \qquad (3.32)$$

where *h* = bed height (cm)

Whilst Equation 3.33 allows for determination of the required column diameter, this was compared with industrially available chromatography column diameters (d_{actual}), thus a larger size, that is closest to the calculated column diameter, was chosen. In doing this, the column volume was recalculated.

$$V_{column} = \frac{\pi \times {d_{actual}}^2}{4} \times h \qquad (3.33)$$

Furthermore, the actual volume out of the step also depends on the mode of operation. For bind-elute, Equation 3.35 was used.

$$V_{out} = CV_{elution} \times V_{column} \times N_{cycles} \times N_{column} \times Cutpoint \qquad (3.34)$$

where $CV_{elution}$ = elution column volumes

For flow-through, $CV_{elution}$ was replaced with CV_{chase}.

3.2.2.8 Ultrafiltration / diafiltration (UFDF)

At large, this step has a dual function, to both concentrate the product stream and also provide buffer exchange capabilities. UFDF operates in tangential flow mode, thereby the feed stream flows parallel to the surface of the filter. The two distinct phases during this step are concentration and buffer exchange (diafiltration).

Concentration involves reducing the volume into the step to a level which reaches the target concentration out (C_{target}). This was computed by the following.

$$V_{retentate} = \frac{V_{in}}{CF} \quad (3.35)$$

where CF is the concentration factor and can also be expressed as $\frac{C_{target}}{C_{in}}$

The required buffer volume to pass through the filter in diafiltration was then calculated and was proportional to the number of diavolumes selected to exchange through the filter.

$$V_{buffer} = V_{retentate} \times DV \quad (3.36)$$

where DV = number of diavolumes

Following diafiltration, the resulting concentration (C_{final}) may be lower than (C_{target}), thus if required, an additional concentration stage was employed as follows.

$$V_{retentate(final)} = \frac{V_{retentate}}{CF} \quad (3.37)$$

where CF = $\frac{C_{target}}{C_{final}}$

The filter sizing must consider the volume processed at both concentration and diafiltration. This gave rise to the following.

$$A_{UF} = \frac{\left(\left(\frac{V_{in}-V_{retentate}}{J_{UF}}\right)+\left(\frac{V_{buffer}}{J_{DF}}\right)\right)}{t_{UFDF}} \quad (3.38)$$

$$A_{UFDF} = (A_{UF} + A_{DF}) \times SF \quad (3.39)$$

where J_{UF} = ultrafiltration flux (LMH)

J_{DF} = diafiltration flux (LMH)

t_{UF} = time for ultrafiltration (hr)

t_{DF} = time for diafiltration (hr)

3.2.3 Process economics

The cost assumptions stored in the aforementioned Microsoft Excel database were used in parallel with the process models to calculate costs including raw materials (reagents, consumables, QCQA), labour and facility-related indirect costs for any given process flowsheet. These constituent costs were used to find the total cost of goods (COG) for both the drug substance and drug product stages. A breakdown of these costs can be found in **Table 3.1**. Here, the equations used have been adapted from Farid (2002) with the exception of the FCI calculation method, which has been adapted from Pereira Chilima et al. (2020).

3.2.3.1 Fixed capital investment (FCI)

Traditional methods of FCI calculation, namely utilisation of the Lang factor, have frequently been used for calculating the FCI, following consideration of the total equipment purchase cost (TEPC). However, the Lang factor method is arguably not well suited in the estimation of single-use facility costs and for modalities such as CGT products. Additionally, as outlined in Pereira Chilima et al. (2020), the manufacture of gene therapy products typically feature technologies that are relatively novel in comparison to traditional mAb processes, and costs for such can widely vary depending on the vendor. Therefore, it is for these reasons that the factorial method for FCI calculation outlined in Pereira Chilima et al. (2020) was implemented (see Appendix A for breakdown of cost calculations).

3.2.3.1.1 Equipment cost

The number of parallel units of any given piece of equipment was calculated via Equation 3.41. This allowed for the costing of equipment on a stage-by-stage basis (Equation 3.42).

$$N_{units_i} = \frac{Calculated\ size\ of\ equipment\ i}{Max\ size\ of\ equipment\ i\ available} \qquad (3.40)$$

$$C_{equip_j} = \sum_{i=1}^{n} (N_{units_i} \times C_{equip_i}) \qquad (3.41)$$

where N_{units_i}= number of units of equipment i, where $i = 1, \dots, n$ (n being the total number of equipment types used in single stage j)

C_{equip_i}= cost of a single unit of equipment i

Subsequently, the total cost of equipment was calculated.

$$C_{equip} = \sum_{j=1}^{k} C_{equip_j} \quad (3.42)$$

where C_{equip_j}= total equipment cost in unit operation j, where $j = 1, \dots, k$ (k is the total number of stages in the flowsheet).

3.2.3.1.2 Footprint

The footprint, i.e. area of the equipment in facility (A), was required in deriving the total facility area required. In this method of indirect cost calculation, project costs are contingent on the facility footprint (as detailed in Appendix A).

The method used for calculating equation footprint mirrors that of the costing of equipment, whereby the footprints of each piece of equipment used are totalled.

$$A_{equip_j} = \sum_{i=1}^{n} (N_{units_i} \times A_{equip_i}) \quad (3.43)$$

$$A_{equip} = \sum_{j=1}^{k} A_{equip_j} \quad (3.44)$$

The footprint was utilised with a series of ratios defined in Pereira Chilima et al. (2020) to calculate the total project cost and contingency costs, which make up the FCI.

Table 3.1 Cost of goods per year breakdown and equations utilised in model (Suzanne S. Farid, 2002).

Category	Cost type	Equations
Direct material costs (per year)	Reagents	$N_{units_{batch}} \times C_r \times N_{batch}$
	Consumables	$(N_{units_{batch}} \times C_c \times N_{batch} \times N_{cycles}) / N_{reuses}$
	QC/QA materials	$C_{QC,batch} \times N_{batch}$
Labour costs (per year)	Operating labour	$N_{op} \times C_{op}$
	Supervisors	0.2 x operating labour
	QC/QA labour	1 x operating labour
	General management	1 x operating labour
Other indirect costs (per year)	Maintenance	$0.1 \times \mathrm{FCI}$
	Local taxes	$0.2 \times \mathrm{FCI}$
	Insurance	$0.01 \times \mathrm{FCI}$
	Depreciation	FCI / t_{dep}
	General utilities	$C_{util} \times S_{fac}$
Cost of goods per year (COG/y)		Direct material costs per year + labour costs per year + other indirect costs per year
Cost of goods per dose (COG/dose)		COG/y / N_{doses}

Note: $N_{units_{batch}}$= units used per batch, N_{batch}= number of batches, C_r= unit cost of reagent, C_c= unit cost of consumable, N_{cycles}= number of cycles, N_{reuses}= number of reuses, $C_{QC,batch}$= cost of QC per batch, N_{op}= number of operators, C_{op}= annual salary of an operator, FCI = fixed capital investment, t_{dep}= depreciation period (years), C_{util} = general utilities cost per square metre of facility ($/m^2), S_{fac} = facility size (m^2), N_{doses} = number of doses

3.2.3.2 Direct costs

The cost of raw materials, as outlined in **Table 3.1**, was determined as a function of their utilisation in each process step. Consumables costs for each unit operation were calculated via the following.

$$C_{c_j} = \sum_{i=1}^{n}(N_{units,i} \times C_{c_i}) \qquad (3.45)$$

where $N_{units,i}$ = no. of units of consumable i

C_{c_i}= unit cost of a single consumable i

Reagent costs for each unit operation were calculated via the following general equation.

$$C_{r_j} = \sum_{i=1}^{n}(V_{r_i} \times C_{r_i}) \qquad (3.46)$$

where V_{r_i} = volume of reagent i. In certain cases, volume was replaced by mass of a certain reagent.

C_{r_i} = unit cost of a reagent i

Therefore, the total cost of raw materials was calculated by summing the total consumables and reagents cost for each unit operation, j.

$$C_{mat} = \sum_{j=1}^{k} C_{r_j} + \sum_{j=1}^{k} C_{c_j} \qquad (3.47)$$

As displayed in **Table 3.1**, QC/QA materials were ascertained from an assumed fixed cost per batch, such that the overall raw materials (RM) cost was calculated as follows:

$$C_{RM} = C_{mat} + (C_{QC,batch} \times N_{batch}) \qquad (3.48)$$

3.2.3.3 Indirect costs

3.2.3.3.1 Labour

Labour can be categorised as either a direct or indirect cost. As a direct cost, labour is based on the time for which the product in question is manufactured in the facility as a whole. If

indirect, labour is regarded as a fixed cost and thus an annual salary is assigned to each operator. Under the assumption that specialist operators are required for AAV manufacturing, labour was costed as an indirect cost throughout this case-study. A facility utilisation factor was also applied to capture the proportion of an operator's annual salary dedicated to the AAV product under consideration, as shown in Equation 3.50.

$$C_{lab} = N_{op} \times C_{op} \times f \qquad (3.49)$$

where C_{lab} = total labour cost ($)

N_{op} = number of operators required (#)

C_{op} = annual operator salary ($)

f = facility utilisation factor

The facility utilisation, f, was defined as follows.

$$f = \frac{t_{facility,AAV}}{t_{facility}} \qquad (3.50)$$

where $t_{facility,AAV}$ = time (days) that the specific AAV product manufacturing runs

$t_{facility}$ = time (days) that the facility is active

The time for which the facility is active was calculated by the following equation (see **Table A7** in Appendix A for more details).

$$t_{facility,AAV} = \left(t_{seed} + B_{campaigns(1)} \times (t_{USP} + t_{DSP}) + (t_{titration} + t_{fillfinish})\right) \times N_{campaigns(1)} + \left(t_{seed} + B_{campaigns(2)} \times (t_{USP} + t_{DSP}) + (t_{titration} + t_{fillfinish})\right) \times N_{campaigns(2)} \qquad (3.51)$$

USP labour cost was estimated by assuming the number of units of a particular technology that can be handled by a team of operators, as per cGMP requirements. The assumption for seed and USP was made that multiple shifts in a day were not required as the passage time

exceeded the need to be present regularly. It was also assumed cell culture could go unsupervised overnight.

$$N_{op_{USP}} = \frac{N_{op_{team}} \times N_{units_{USP}}}{Cap_{team}} \quad (3.52)$$

where $N_{\mathrm{op_{team}}}$ = no. of operators in a team

$N_{units_{\mathrm{USP}}}$ = no. of USP culture units

Cap_{team} = no. of units that can be handled by an operator team (denoted as capacity)

In contrast to USP, DSP labour was calculated by an assumed number of operators for the whole DSP per train, with multiple eight-hour shifts required due to variations in start and end times for unit operations (some of which may occur overnight). The labour requirement was further dependent upon the number of units operating in parallel for each unit operation. In the case of parallel units of a unit operation, the number of operators required specifically for this was added to the set number assigned for the whole of DSP. The underlying assumption made was that a maximum of four parallel units could be handled by a team of two operators.

$$N_{op_{DSP(total)}} = (N_{op_{DSP}} \times Shifts) + \sum_{j=1}^{k} \Big(CEILING(N_{units_j} \times 0.5) \Big) \quad (3.53)$$

where $N_{op_{DSP}}$= fixed number of operators for whole DSP

N_{units_j}= number of units of equipment used in unit operation j.

Note: the second part of the equation only applied if more than two units were utilised.

3.2.3.3.2 Other indirect costs

Other indirect costs accounted are outlined in **Table 3.1**, as are the equations associated with each. Depreciation costs use the FCI output outlined in Section 3.2.3.1 were divided by an assumed equipment lifetime or depreciation period. In the case of maintenance, local taxes and insurance, ratios adapted from Farid (2002) were used. Energy costs used an assumed cost per m^2 and the overall facility footprint. Similarly, monitoring costs require that the facility

be assigned various class environments (A, B, C, etc.). Using then assumed values for the classes per m^2 of facility, the total footprint for various process stages was used to calculate the monitoring cost per stage (see Appendix).

As with labour costs, when only a certain fraction of the facility is dedicated to the product under consideration, the facility utilisation factor (f) was applied to indirect costs to identify the specific contribution from the product in question.

3.2.4 Uncertainty analysis

Whilst those equations outlined in Sections 3.2.2 and 3.2.3 are the building blocks to establishing a deterministic COG output, they inherently fail to account for the realistic uncertainty that exists within any bioprocess and hence associated input parameters. The deterministic analysis tool was therefore linked to a Monte Carlo simulation to assess the robustness of the base-case scenario to changes in key parameters. The Monte Carlo method is a powerful analytical tool and can efficiently mimic the variability associated with several bioprocess parameters.

The uncertainty analysis via Monte Carlo simulation was applied to a selection of process parameters found to be the most variable in AAV bioprocessing. These were first evaluated in a sensitivity analysis to determine their impact upon the COG / dose. For each, an appropriate probability distribution function was assigned and a random value from each uncertainty distribution was drawn and replaced the base-case input value. This process was repeated numerous times, until the standard deviation of the output converged (this was plotted to identify the appropriate number of Monte Carlo trials required to reach such convergence). Following numerous Monte Carlo trials, a distribution of COGs was generated, thus allowing for the extraction of statistical data, such as the mean, standard deviation and the probability of achieving a target COG/dose. Moreover, the shape of the output distribution can give information about the robustness of the manufacturing scenario evaluated. A wider output

distribution has more risk associated with it and can be attributed to input parameters that generally are far more variable.

For the purpose of the work in this thesis, triangular distributions were assigned to all variables evaluated in the Monte Carlo simulation, thus for such inputs, the maximum, minimum and most likely values to be encountered were given.

3.2.5 Optimisation

As outlined in Chapter 1, optimisation refers to the process by which a set of candidate solutions are evaluated in terms of one or more objective functions, which is required to either maximise or minimise depending on the problem definition.

The optimisation problem in question within the model described in **Figure 3.2** can be mathematically formulated in the following way. Consider a bioprocess made up of k unit operations, where the unit operation index is j, such that j can take any value between 1 and k. Realistically, some unit operations within the AAV manufacturing process only have one possible option in terms of technology selection, thus in the context of this optimisation problem, some instances of j will only have one option. As a result, the possible values j can take can be reduced to encompass only those stages that have multiple possible options to choose from. This is illustrated in **Figure 3.2**, where arbitrary values of j have been allocated for visualisation purposes (case study specific values of j will be referred to in Chapter 3). Therefore, k can be updated to represent the number of unit operations in the bioprocess that have multiple options to be selected from.

At each instance of j, a particular technology can be assigned, defined by i_j, where i is an integer variable used to denote the technology. The number of possible options at each j is represented by n_j, such that $i_j = 1, \dots, n_j$. For example, for an instance of j where there are 5 options available, $n_j = 5$, thus $i_j = 1, \dots, 5$.

Unit operation index	1	2	3
Decision variables	i_1	i_2	i_3

Figure 3.1 Example generic string for optimisation algorithm.

The total number of candidate solutions to evaluate was calculated as the sum of all solutions from $x_1, \ldots, x_n$, n in this context being the number of solutions. However, whilst n represents the total solutions assessed, a portion of these will be deemed infeasible due to the constraints imposed. Equation 3.55 defines the total number of feasible solutions generated from the algorithm.

$$X = \sum_{m=1}^{n} x_m - X_{constraint} \qquad (3.54)$$

Tying the elements from Equation 3.55 and that described in **Figure 3.2,** the equation for the number of feasible solutions within the brute-force optimisation could alternatively be expressed by the following.

$$X = \prod_{j=1}^{k} n_j - X_{constraint} \qquad (3.55)$$

3.2.5.1 Brute-force optimisation

Brute-force optimisation, also termed exhaustive enumeration, allows for the evaluation of a given set of potential solutions by enumerating through each and identifying the extent to which their objective function values meet the requirements of the optimisation problem (e.g. maximisation or minimisation). For relatively small decision spaces, brute-force optimisation is an efficient optimisation algorithm, as it guarantees optimality due to the complete enumeration of the solution set. However, as the objective space increases in size, brute-force algorithms are rendered less effective due to the computational time required to evaluate every solution.

When used within the process economics model, the candidate solutions are AAV flowsheets. The brute-force algorithm is used to evaluate each flowsheet and compute the corresponding COG/doses. The algorithm functions by translating assigned integer variables to their corresponding unit operations to ultimately form a flowsheet and hence a possible candidate solution, which served as the input flowsheet into the process economics model. Each iteration provided the minimum COG/dose value of the set, thus was consistently updated based on how many iterations were carried out, alongside an index function to determine the flowsheet that gave the minimum COG. The set-up for this algorithm is shown in **Figure 3.3.**

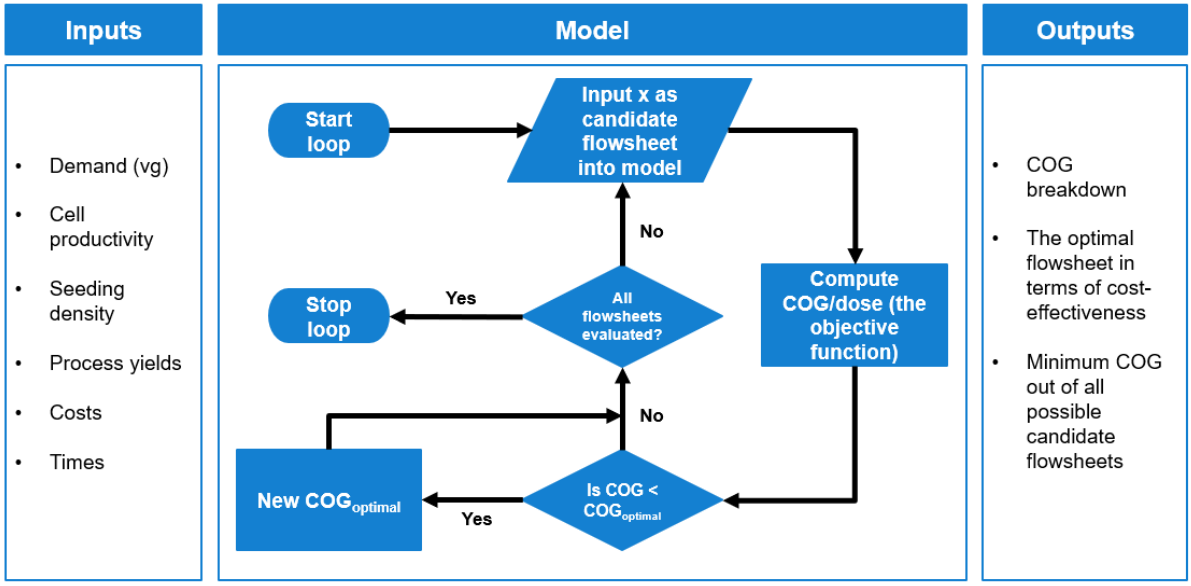

Figure 3.2 Architecture of brute force optimisation algorithm and the relationship with the base-case process economics model.

3.2.5.2 Constraint-handling

When conducting an optimisation procedure in a bioprocessing context, there often arise several strategies that realistically would not be employed as they do not satisfy one or more constraints. As such, whilst numerous solutions may be defined and subsequently simulated, only a fraction of these are deemed feasible based on pre-defined constraints. It is therefore vital that these solutions be appropriately handled in relation to those that do not violate constraints. A series of constraint-handling techniques were highlighted in Chapter 1, however

two of these incorporated within the optimisation work in this thesis – penalty functions and repair strategies.

For use with the brute-force optimisation, a static penalty function was implemented due to its simplicity and ease of execution. The brute-force algorithm was used with a relatively small solution space, where prior knowledge on the range of COG/dose values that would be achieved was available when running an unconstrained example. This helps in selection of a penalty value that is distinctly different enough from that contained in the range to distinguish between feasible and infeasible solutions. Structurally, constraints were considered prior to COG/dose evaluation of a particular flowsheet. Each constraint would be evaluated with respect to the solution and where a violation was found, the COG output for said scenario (the objective function) was set to the penalty value.

3.2.6 Data collection

The data utilised in Chapter 3 was collected from a variety of sources. Particularly the costs used in the adjoining model database were sourced from vendor information and often literature. This was also the case for many numerical assumptions, though some were gathered from industrial experts, namely AstraZeneca, UK. Yields for the study were drawn from literature studies, as highlighted in Table A1 in Appendix A. On the other hand, ultracentrifugation data was sourced from vendors (i.e. Alfa Wassermann), as well as industrial correspondence with the AstraZeneca process development team. Primarily, key industrial experts that provided data include Richard Turner, James Savery and Julia Thompson. Pertaining specifically to upstream processing of AAVs, key assumptions were gathered and sense-checked through discussions with Lekan Daramola (AstraZeneca, UK). Furthermore, regarding AAV DSP, data was collected through multiple discussions with Martyn Hulley and Ziyan Deng (AstraZeneca, UK).

3.3 Case study setup

3.3.1 Case study overview

The tool outlined in Section 3.2 was used to evaluate the economic and operational performance of various AAV flowsheets, initially from a small set of alternatives, before expanding the decision space to include a myriad of other processing options. The study began with exploring the impact of scalability during cell culture and at polishing purification, using a fixed demand of 1000 doses per year and a dose size of 1×10^{14} vg/dose (equivalent to ~1mg of AAV material in terms of mass). The range of dose sizes seen in marketed products and in late phase clinical trials across a range of indications were studied and the median of this range was used in the base case analysis. The base case demand was derived as the average of expected commercial patient populations (Masri et al., 2019). For cell culture, the trade-off between adherent and suspension culture was evaluated with adherent culture offering higher AAV productivities (vg/cell) and suspension culture offering better scalability. For polishing purification, batch UC was compared to AEX chromatography to assess the trade-off between UC delivering higher yield and purity (with respect to empty capsid removal) but being less scalable relative to AEX. The solution set was later expanded to include more purification platform options for evaluation in terms of cost and meeting increasing purity targets. This was further developed with the inclusion of USP and lysis options, to consider the whole AAV flowsheet.

The process economics model was used to generate the deterministic COG/dose across demands for the different scenarios, before a Monte Carlo simulation was used to capture the robustness of the scenarios. The optimization algorithm was later used to identify the most cost-effective flowsheet that met target purities.

3.3.2 Process outline

The various process flowsheets initially evaluated in this case study are shown in **Figure 3.4,** which includes a dendrogram to illustrate the key differences explored in the cell culture and

polishing stages. The preliminary case study investigated two alternatives for USP, adherent or suspension cell culture. For the adherent scenario, multi-layer cell factories (e.g. Cell Factory™) were used, specifically the 10-layer model (CF10), with a surface area totalling 6,360 cm^2 per unit. Moreover, the production culture vessel of choice in the suspension case was a stirred-tank single-use bioreactor (SUB), whereby the size was selected from the calculated working volume required.

The USP duration assumed was 5 days, whereby cells were seeded at the beginning of day 1 at a density of 25,000 cells/cm^2 for adherent and 125,000 cells/mL for suspension. Post-cell culture, harvest by TFF occurred, where the product stream was the cells as is the case with intracellular AAVs. Intracellular AAV flowsheets also contain a chemical lysis step, whereby cells are lysed by addition of detergent to rupture the plasma membranes, resulting in release of the product along with the generation of cell debris. This debris is removed by a clarifying depth filter stage post-lysis. For extracellular AAVs, a concentration stage of TFF was included to reduce the volume at the Benzonase stage.

Regarding purification, affinity chromatography featured as the capture stage in the first case study, supplemented by a traditional iodixanol gradient density ultracentrifugation polishing stage in some cases, or an AEX chromatography in others. For ultracentrifugation, one batch ultracentrifuge unit (e.g. Type 70Ti rotor, Beckman Coulter) was assumed to have a maximum rotor capacity of 312mL and was allowed to be operated for a maximum of two cycles per working day. As discussed in Section 1, ultracentrifugation has been shown to be successful at removing empty capsids generated in AAV processing, a product-related impurity known to be characteristically difficult to eliminate via other means. Due to slight pI differences between full and empty capsids, AEX has also been shown to give an adequate empty capsid removal - thus it was chosen as the scalable comparator against ultracentrifugation. Moreover, as also evidenced in **Table A1** in Appendix A, AEX yield can be variable and is often lower than what can be achieved by ultracentrifugation, thereby introducing the polishing purification trade-off of ultracentrifugation with higher purity and yield versus scalable chromatography.

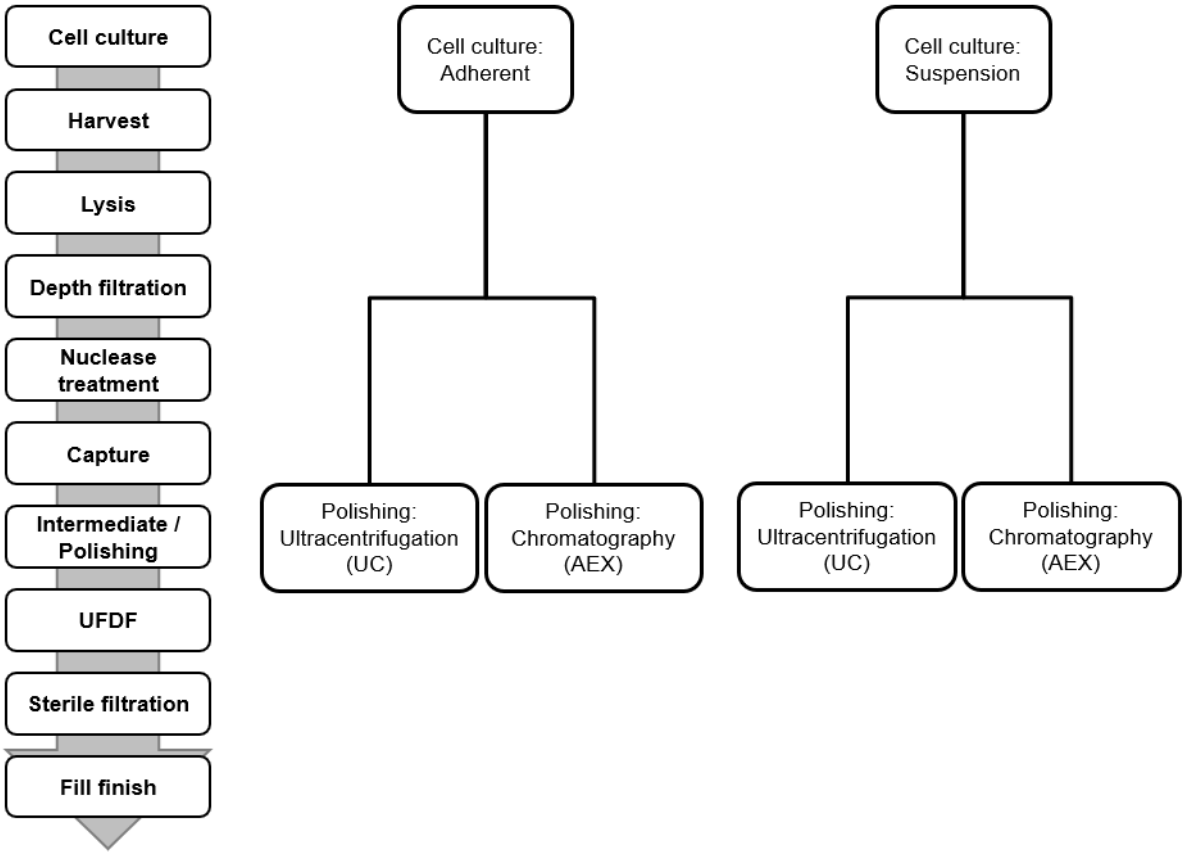

Figure 3.3 Viral vector process flowsheet for adeno-associated virus (AAV) vector product. The dendrograms illustrate the key differences between the four flowsheets initially evaluated in the cell culture (adherent versus suspension) and polishing (ultracentrifugation versus chromatography) stages. AEX, anion-exchange chromatography; UC, ultracentrifugation.

3.3.3 Key assumptions

Table 3.2 shows the scenario specific assumptions used. Due to the dependency on cell culture type to describe titres, the titres were expressed in vg/cm^2 and vg/L for adherent and suspension respectively. The cell productivity was used to calculate the titre and was chosen as the basis for comparison between scenarios. Furthermore, due to the differences in polishing purification between UC and AEX scenarios, the process yield differed between flowsheets, with UC assumed to result in a higher value. The key assumptions for the various unit operations employed across all scenarios can be found in **Tables 3.3** and **3.4.** Additionally, the active facility days was assumed to be 330. It was also assumed a maximum of 30 batches

could be carried out per year per train, where one train was defined as one single-use bioreactor through to fill-finish, with allowances for multiple units of certain DSP unit operations to run in parallel (e.g. ultracentrifugation).

Additionally, **Table 3.3** outlines the extra material required for QCQA purposes at both drug substance (DS) and drug product (DP), which was assumed to be a percentage in both cases. These values were sourced from Masri et al. (2019). Conversely, a fixed volume method for estimating QCQA demands has also been utilised in the literature, notably in Comisel et al. (2021). The model outputs from using either method differ depending on the dose size under consideration, where the fixed volume method results in a significant portion of product fluid being retained at smaller dose sizes. The impact of using either method is further discussed in Section 3.4.2.

3.3.4 Monte Carlo assumptions

The uncertain input parameters used in the Monte Carlo simulation, along with their corresponding probability distributions are displayed alongside the results (**Figure 3.7 c**). These include titres and the polishing purification yields, due to their characteristic variability in AAV manufacturing. The ranges set for each variable were selected from a review of the relevant literature, as well as industrial correspondence (see **Table A1**).

3.3.5 Optimisation assumptions

A series of options were identified and selected as part of determining the optimal AAV flowsheet from a cost and purity perspective (**Table 3.4**). Only capture and polishing purification unit operations were assessed (however, in three step purification cases, intermediate purification was also studied). Special conditions were assumed for a three-step purification process; a third step was only added where the two-step platform did not possess empty capsid removal capabilities, and, hence, a third step that did allow for such removal was added to bolster purification performance. Namely, this was only identified to occur for an affinity and multimodal combination and would only be followed by AEX.

Table 3.2 AAV flowsheet combinations considered in the deterministic analysis and the associated assumptions for each.

Flowsheet abbreviation	Cell culture technology	Polishing stage	Cell productivity (vg/cell)	Titre	Harvest cell density	Overall process yield
Ad-UC	Adherent	Ultracentrifugation	120,000	2.4×10^{10} vg/cm^2	2×10^5 cells/cm^2	29%
Ad-AEX	Adherent	AEX	120,000	2.4×10^{10} vg/cm^2	2×10^5 cells/cm^2	25%
Susp-UC	Suspension	Ultracentrifugation	60,000	6×10^{13} vg/L	1×10^6 cells/mL	29%
Susp-AEX	Suspension	AEX	60,000	6×10^{13} vg/L	1×10^6 cells/mL	25%

Table 3.3 Key AAV process assumptions for the case-study.

Category	Parameter	Value
General	Dose size (vg/dose)	1×10^{14}
	Max. batches per train	30
	Facility active days	330
	DSP shifts	3
Seed & production cell culture	Seeding cell density (adherent) (cells/cm^2)	2.5×10^4
	Seeding cell density (suspension) (cells/mL)	1.25×10^5
	Medium cost ($/L)	100
	Cell culture duration (days)	5
	Doubling time (days)	1
	Plasmid DNA requirement (µg/10^6 cells)	1
	Transfection mix cost (pDNA + PEI) ($/g)	190,000
Chemical lysis	Step yield	98%
	Lysis buffer requirement (L/L)	100
Depth filtration	Step yield	95%
	Filter capacity (L/m^2)	60
	Flux (LMH)	100
Nuclease treatment	Benzonase requirement (U/mL)	50
	Benzonase activity (U/µ L)	250
	Benzonase cost ($/25,000U)	230
UFDF / TFF	Step yield	95%
	Flux (LMH)	60
	Duration (concentration and diafiltration) (hrs)	6
Sterile filtration	Step yield	90%
	Flux (LMH)	40
Drug substance / drug product	DP concentration (vg/mL)	1×10^{13}
	Extra material produced for DS	10%
	Extra material produced for DP	10%

LMH = litres per square metre hour

Table 3.4 Purification assumptions utilised in the process economics model.

Technology	Abbreviation	Commercial equivalent	Step yield	DBC* (vg/mL**)	Resin cost ($/L)	HCP reduction (LRV)	DNA reduction (LRV)	EC reduction (%)	Ultracentrifuge cost ($)	Step
Affinity chromatography (high DBC)	AFFH	Poros AAVX, (Thermo Fisher)	70%	3×10^{13}	50,000	4	2.5	N/A	N/A	Capture
Affinity chromatography (low DBC)	AFFL	AVB Sepharose (Cytiva)	70%	3×10^{12}	25,000	4	2.5	N/A	N/A	Capture
Anion exchange chromatography	AEX	Poros 50HQ (Thermo Fisher)	60%	5×10^{13}	2,500	2.5	1.5	70%	N/A	Capture, Polishing
Cation exchange chromatography	CEX	Poros 50HS (Thermo Fisher)	55%	5×10^{13}	2,500	2.5	1.5	N/A	N/A	Capture, Polishing
Multimodal chromatography	MM	Capto Core 400, (Cytiva)	75%	13 (mg/ml)	4,500	2	0.5	N/A	N/A	Capture, Intermediate, Polishing
Batch ultracentrifugation	BatchUC	Type 70Ti (Beckman Coulter)	70%	N/A	N/A	3	3	95%	85,000	Capture, Polishing
Continuous ultracentrifugation	ContiUC	KII Model (Alfa Wassermann)	70%	N/A	N/A	3	3	95%	350,000	Capture, Polishing

Note: *DBC = dynamic binding capacity. ** unless otherwise stated.

For the purity aspect of the optimisation framework, empty capsids represent a product-related impurity unique to the AAV space and in a relatively nascent field, final targets are not well defined. In contrast, specifications for HCP and DNA are more clearly defined in literature, as these impurities have been well documented and tracked in other modality areas (derived from cell culture). For the case study, both HCP and DNA were assessed at two starting levels, termed low (L) and high (H). The target levels for HCP and DNA were assumed to be 100 ng/mg and 10 ng per dose respectively (Bracewell et al., 2015; Wright, 2020). The low starting levels for HCP and DNA were assumed to be $2x10^{-7}$ ng/vg and $6x10^{-10}$ ng/vg. For the high starting levels, the values were assumed to be $2x10^{-5}$ ng/vg for HCP and $6x10^{-8}$ ng/vg for DNA. For empty capsids, a single starting level was evaluated, however three potential targets were assessed, terms low (L), medium (M) and high (H).

This optimisation case study first evaluated the optimal strategy when one AEX yield was considered. The evaluation was then extended by illustrating how the optimal solution changes if varying AEX yields are encountered, as well as empty capsid reduction requirement. For this study, a suspension cell culture was assumed for each flowsheet option. In addition, the demand and number of annual batches were fixed throughout.

3.3.5.1 Constraint-handling

Within the optimisation algorithm, solutions that breached any imposed constraints were considered infeasible and disallowed as a viable solution. These constraints can be broadly categorised as those pertaining to manufacturing sequence, purity and equipment.

Sequence constraints were applied to capture, intermediate and / or polishing step, where it was defined that no duplicate stages were allowed. This requirement is characteristic of cGMP guidelines, where orthogonality in purification technologies is necessary. Secondly, breaching purity constraints referred to the manufacturing sequence under consideration failing to produce a final impurity profile that complied with the target end specification defined in the model, hence leading to exclusion from the feasible solution set. Finally, in the case of equipment constraints, limits upon the number of units that could be used in parallel for a given

unit operation were defined. For scenarios where scalability has historically been difficult, such as batch ultracentrifugation, employing multiple units in parallel has been typical. In this case study, it was assumed that any solution requiring over 12 units in parallel for a single unit operation was infeasible. A summary of these constraints can be found in **Table 3.5.**

Table 3.5 Constraints considered in the brute-force optimisation work.

Type	Constraint	Mathematical notation
Sequence	The purification train must feature orthogonal separation mechanisms, i.e. no duplicate unit operations utilised.	No unit operation, j, in a given flowsheet may appear more than once
Purity	HCP: must be reduced to below 100 ng/mg DNA: must be reduce to below 10ng per vector dose	$I_k = I_0 \times \prod_{j=1}^{k} R_j$ where I_0= initial impurity level of impurity I I_k= final impurity level of impurity I R_j= impurity reduction level for step *j* (%) where *j = 1…k* $I_k \leq I_T$ where I_T= target impurity level
Equipment	Any scenario requiring more than 12 units of equipment (for a single step) in parallel (particularly pertains to ultracentrifugation)	$N_{units_{ij}} \leq 12$ where $N_{units_{i,j}}$ =number of units of equipment type *i* in unit operation *j* (not including USP consumables)
USP	Applies particularly to batch-adherent scenarios e.g. roller bottles and cell factories. The number of culture units must not exceed 400 (for roller bottles) or 120 (for cell factories).	$N_{units_{USP}} \leq 400 \; or \; 120$ where $N_{units_{USP}}$ =number of USP units required

3.4 Results and discussion

The decisional tool introduced in Section 3.2 was utilised to evaluate the economic advantages that can be obtained from adapting to more scalable manufacturing strategies. This was initially addressed deterministically, before an uncertainty analysis was introduced to account for process variability and to assess the robustness of the base-case. Finally, the last part of the case study identifies the optimal manufacturing strategy in terms of both cost and purity targets from a broader set of alternatives.

3.4.1 What is the COG/dose breakdown for the traditional versus scalable AAV flowsheets?

The impact of the key traditional versus scalable USP and DSP choices for AAV flowsheets on the COG/dose was explored initially. **Figure 3.5** presents the COG/dose comparison between the initial four flowsheets studied at a demand of $1x10^{17}$ vg/year. These four flowsheets were adherent-ultracentrifugation (Ad-UC), adherent-AEX (Ad-AEX), suspension-ultracentrifugation (Susp-UC) and suspension-AEX. Overall, suspension-AEX (Susp-AEX) was shown to be the most cost-effective out of the set, offering a ~40% reduction over the most expensive flowsheet, which was adherent-UC (Ad-UC). This cost was driven by lower labour and equipment requirements associated with the use of one suspension bioreactor and one AEX column and skid versus multiple units in the competing flowsheets. The materials cost was not found to be a significant driver across scenarios. Furthermore, relative to the traditional flowsheet of Ad-UC, the competing manufacturing strategies were found to allow for a 17-41% reduction in COG/dose.

Figure 3.5 also provides insights on the COG drivers for each flowsheet. Comparing solely UC and AEX scenarios, DSP labour costs were higher for adherent-UC (Ad-UC) than adherent-AEX (Ad-AEX) due to the condition that one operator can handle a maximum of two ultracentrifuges per run. Twenty-three ultracentrifuges were required in parallel for Ad-UC, thus an additional 12 DSP operators were necessary for this flowsheet. This requirement

evidently also resulted in a greater DSP indirect cost than Ad-AEX, as a larger total equipment purchase cost (TEPC) and facility footprint were associated with numerous ultracentrifuges compared to a single AEX column and skid. This trend was similarly observed when comparing suspension-UC (Susp-UC) and Susp-AEX. Similarly, studying adherent versus suspension cell culture scenarios, cost differences were largely driven by labour costs. The Ad-UC and Ad-AEX required the use of 78 - 91 cell factory (CF10) units with 16 - 18 USP operators, in comparison to the 2 operators used in the suspension flowsheets with a 250L bioreactor (Susp-UC or Susp-AEX).

The trends observed can, to some extent, be described by examining the USP: DSP cost ratios. In general, it was shown that DSP costs dominated the COG, with the exception to this being Ad-AEX, where USP: DSP was found to be 54%: 46%. The impact of UC on the DSP costs was highlighted by the distinct shift in cost ratios from Ad-UC to Ad-AEX or Susp-UC to Susp-AEX. From a DSP perspective, this shift was from 64 - 77% to 46 - 65%. In terms of USP ratios, moving from an adherent to a suspension platform lowers the USP cost contribution from 36 - 54% to 23 - 35%, thus highlighting the significance of moving to more scalable platforms upon the cost of goods.

In summary, a suspension flowsheet coupled with AEX provided the most cost-effective strategy relative to other options explored, reinforcing the importance of moving to scalable strategies when in a commercial manufacturing environment. Having said this, the results here represent a single instance of demand and dose size, thus it became desirable to evaluate the cost-effectiveness of the flowsheets across dose size and demands.

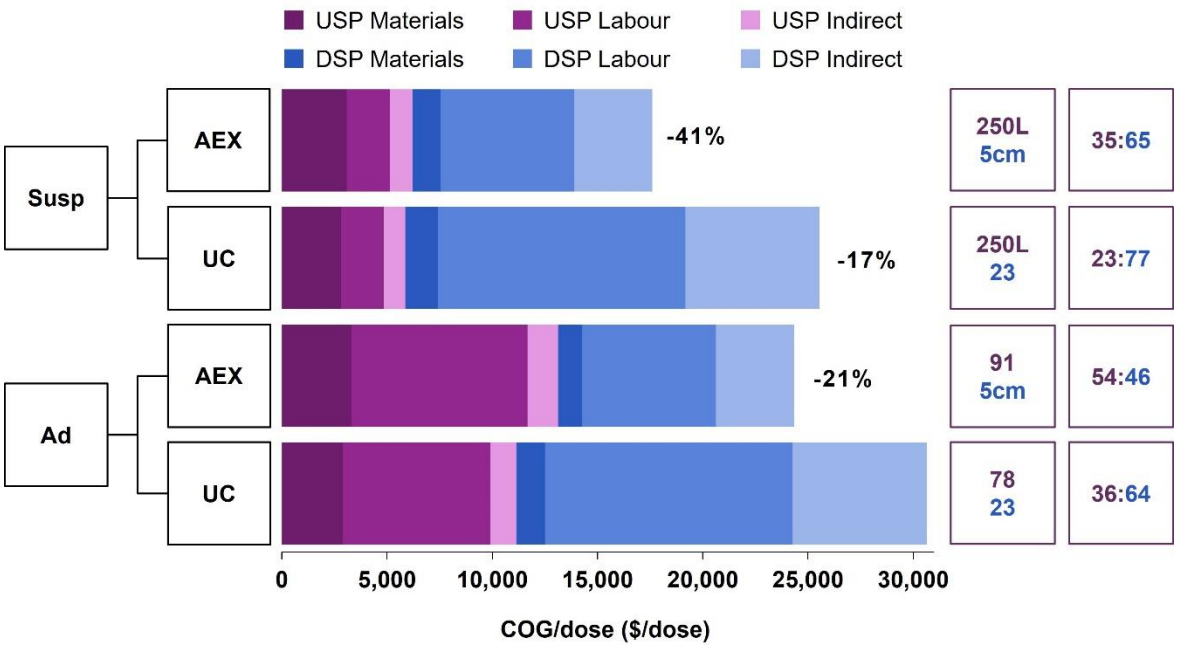

Figure 3.4 COG/dose breakdown by category within USP and DSP process stages for four AAV flowsheet options with adherent or suspension culture for USP and AEX or UC for polishing. The boxes on the right of each bar represent key sizing metrics; the top number highlights the number of cell culture units or the bioreactor volume (for adherent or suspension scenarios respectively). The bottom number represents the number of parallel ultracentrifuges used or the AEX column diameter (for UC or AEX scenarios respectively). The second set of boxes located to the right of the bars highlights the USP: DSP cost of goods ratios for each scenario. The percentages next to each bar represent the COG/dose reduction for each flowsheet relative to the traditional flowsheet of adherent-ultracentrifugation. The demand was assumed to be 1,000 doses/year, with a dose size of 1 x 10^{14} vg/dose. The facility was resized for each set of inputs. Ad, adherent culture; AAV, adeno-associated virus; AEX, anion-exchange chromatography; COG, cost of goods; DSP, downstream processing; Susp, suspension culture; UC, ultracentrifugation; USP, upstream processing.

3.4.2 How does dose size impact COG/dose?

The required dose of AAV varies significantly based on therapeutic indication, with ophthalmic indications at the lower end (e.g. 1x10^{12} vg/dose) through to neuromuscular and haemophilia indications at the higher end (e.g. 1x10^{15} vg/dose). Hence, scalability is a more significant

issue for those companies targeting diseases with characteristically high dose sizes. **Figure 3.6** displays the impact of dose size from $1x10^{12}$ - $1x10^{15}$ vg/dose upon flowsheet ranking. The optimal technology changes from AEX options in either adherent (Ad-AEX) or suspension (Susp-AEX) mode at the low doses to Susp-AEX being the clear winner at the higher doses. Little difference was found between Ad-AEX and Susp-AEX at dose sizes of $1x10^{13}$ vg/dose or lower, as Ad-AEX required 10 CF units per batch or less, needing only two USP operators as with the Susp-AEX scenario. This result suggests that for indications corresponding to these dose sizes, most notably ophthalmic genetic diseases, conducting adherent cell culture presents no extra financial burden to a company relative to suspension. Conversely, an increasing dose size accentuates the COG differences between suspension and adherent cultures. At $1x10^{15}$ vg/dose, the ranking alters such that Ad-AEX becomes less economically viable than either suspension scenarios, due to the increase in CF units and hence labour requirement. This suggests that for indications requiring a large dose size (e.g. neuromuscular and haemophilia), adherent is a less attractive cell culture option.

Further to the discussion of QCQA material in Section 3.3, the impact of using either a fixed volume or percentage approach is dose size dependent. For the base case dose size of $1x10^{14}$ vg/dose, the required equipment sizes and number of units (and ultimately COG/dose) do not differ significantly when using either material retention method. Quantitatively, the fixed volume method resulted in higher volumes for QCQA and hence more CF10 units or a higher working volume for suspension, with COG/dose differences of less than 3% with the percentage method (base case). At the lowest dose size evaluated in this study ($1x10^{12}$ vg/dose), the fixed volume method was shown to yield a higher COG/dose, due to the requirement for a higher working volume (and so CF10 units) than the percentage method.

It must also be noted that there are other adherent cell culture options (as outlined in Chapter 1) e.g. fixed bed reactors, which provide scalable alternatives to the cell factories considered in this study. As such, the innovations in adherent technologies may provide a more competitive ranking relative to suspension. Additionally, novel technologies such as CellRev

(Newcastle, UK), which employed continuous processing with adherent cell culture present opportunities for process improvement that would impact the results in **Figure 3.6** if considered here.

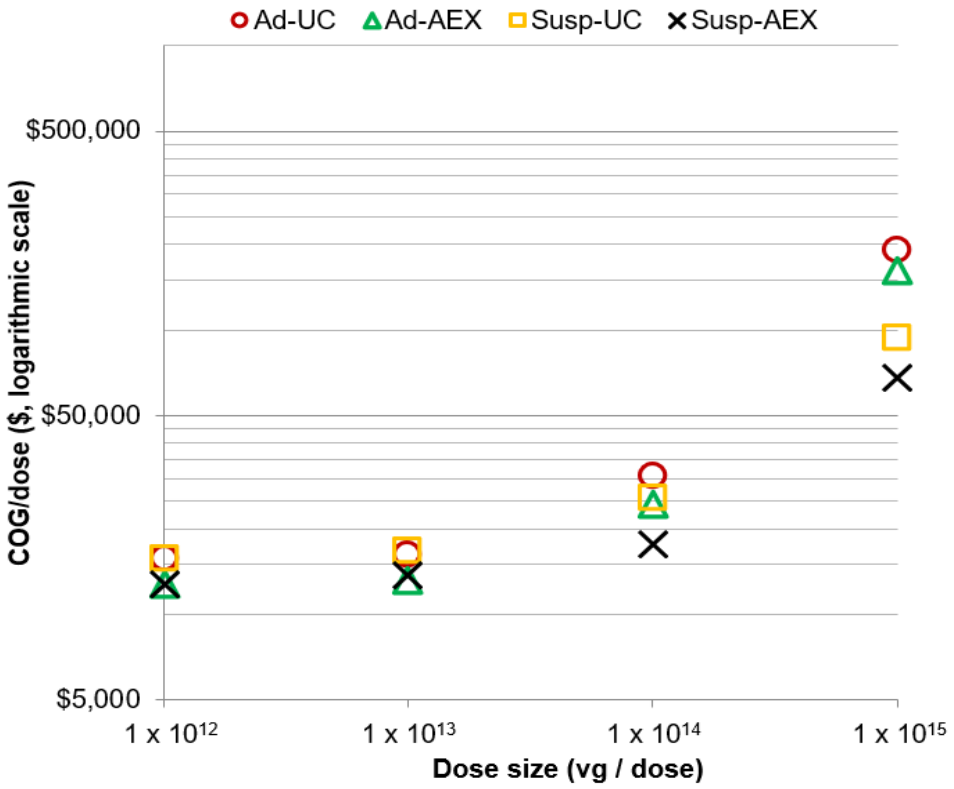

Figure 3.5 Scatter plots displaying the COG/dose change with increasing dose size. The demand was assumed to be 1,000 doses/year. The facility was resized for each set of inputs.

3.4.3 How does uncertainty impact the robustness of the strategies?

The initial deterministic cost comparison highlighted the economic competitiveness offered by Susp-AEX. The study was extended to capture the impact of the perceived greater uncertainties with suspension culture and AEX, reflected in wider distributions for the cell productivities in suspension culture relative to adherent and in the DSP step yields for AEX relative to UC (**Table 3.2**). The Monte Carlo simulation technique was used to characterise the impact of these uncertainties on the COG/dose values. The findings from this analysis were assessed in terms of robustness and risk associated with each strategy.

Figure 3.7 a) shows the results from the Monte Carlo simulation as COG/dose frequency distributions displayed as violin plots. This illustrates that the uncertainties do not change the ranking found in the deterministic analysis. Overall, the impact of uncertainty was more pronounced in strategies employing less scalable technologies, namely adherent cell culture and UC purification, despite the tighter input distributions upon these variables. Susp-AEX unequivocally achieved the lowest COG/dose and the tightest distribution, as well as the highest probability of meeting any COG/dose target. Furthermore, Ad-UC, Ad-AEX, Susp-UC all resulted in bimodal distributions, whilst Susp-AEX gave a trimodal distribution. Details into the key drivers for the shape of each distribution are outlined below.

In general, for UC-containing strategies, changes in the number of UCs required for purification was the key driving force in defining the shape of the distributions (shown in **Figures A3 a)** and **c)** in Appendix A). The distributions for both Ad-UC and Susp-UC show two distinct peaks, representing the change in the number of ultracentrifuges required in certain instances. As discussed in the base-case analysis and **Figure 3.5,** 23 ultracentrifuges were required in parallel, which is represented by the larger peak in **Figure 3.7 a)** for both Ad-UC and Susp-UC. In scenarios where it is possible to achieve higher UC yields or cell culture productivities, the number of UCs needed reduced to 9 (the smaller peak in the UC distributions). This distinct and relatively large drop highlights the sensitivity of UC sizing to changes in key input parameters.

Conversely, for AEX-containing scenarios, changes in USP were shown to be far more significant in driving the shape of the plots (as evidenced by **Figures A3 b)** and **d**). For Ad-AEX, shown in **Figure A3 b)**, the key factor in determining the distribution shape was found to be the number of incubators required for the many CF10 units used in both seeding and cell culture. Small differences in input parameters such as titres and yield resulted in changes in the number of CF10 units required. As this changes, so does the number of incubators used during USP. In contrast, Susp-AEX COG differences were primarily driven by bioreactor size, giving rise to three peaks as shown in **Figure A3 d).** At the base-case, a 250L bioreactor was

required, however instances where titre and yields fluctuated to lower levels resulted in larger processing volumes, prompting the use of bigger bioreactors, (e.g. 500L and 1,000L). Hence this ultimately gave rise to the trimodal distribution that is displayed.

a)

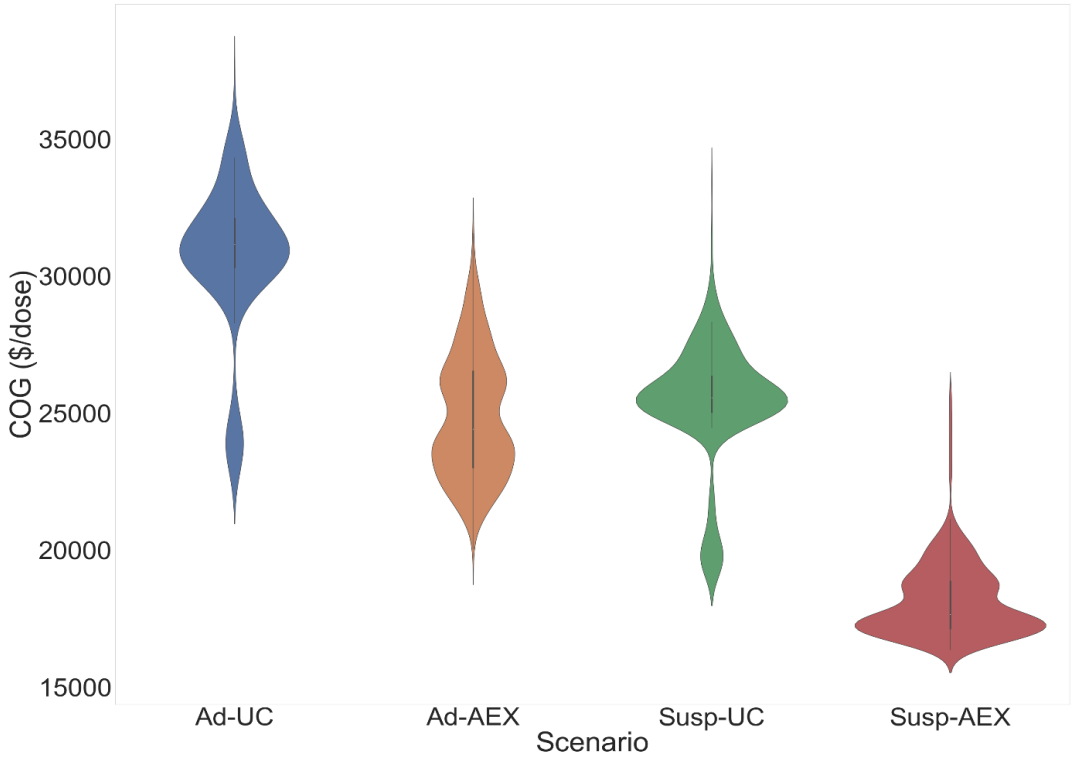

b)

Scenario	Mean ($/dose)	Standard deviation ($/dose)
Ad-UC	30,017	3,296
Ad-AEX	25,827	2,350
Susp-UC	24,058	2,951
Susp-AEX	18,214	1,537

c)

Flowsheet	Cell productivity (x10^5 vg/cell)	Adherent harvest cell density (x10^5 cells/cm^2)	Suspension harvest cell density (x10^6 cells/mL)	UC yield (%)	AEX yield (%)
Ad-UC	Tr(1, 1.2, 1.3)	Tr(1.6, 2, 2.4)	N/A	Tr(0.5, 0.7, 0.8)	N/A
Ad-AEX	Tr(1, 1.2, 1.3)	Tr(1.6, 2, 2.4)	N/A	N/A	Tr(0.4, 0.6, 0.8)
Susp-UC	Tr(0.2, 0.6, 1)	N/A	Tr(0.8, 1.0, 1.2)	Tr(0.5, 0.7, 0.8)	N/A
Susp-AEX	Tr(0.2, 0.6, 1)	N/A	Tr(0.8, 1.0, 1.2)	N/A	Tr(0.4, 0.6, 0.8)

Figure 3.6 Uncertainty analysis results from the Monte Carlo simulation showing (a) violin plots of the COG/dose distributions for each scenario under uncertainty, (b) key probabilistic output parameters for each scenario, (c) uncertain process input parameters and their distributions evaluated in the Monte Carlo simulations. The demand was assumed to be 1,000 doses/year, with a dose size of 1 x 10^{14} vg/dose. The facility was resized for each set of inputs.

3.4.4 What is the optimal purification strategy in terms of meeting cost and purity targets?

As discussed in Chapter 1, there are numerous unit operations available for purifying AAV vector products beyond batch ultracentrifugation (batchUC) and AEX; these include other chromatography options. In this study, the pool of purification options was expanded to include multi-modal chromatography (MM), cation exchange chromatography (CEX), continuous ultracentrifugation (ContiUC) and a range of affinity chromatography (AFF) resins, with different cost and capacity trade-offs (see **Table 3.4** for full list of options). DBCs reported for affinity resins range from 1 x 10^{12} to 1 x 10^{14} vg/mL, however more conservative values were selected to characterise the trade-off between affinity resins, e.g. lower DBC for the lower cost resins and a higher DBC for the higher cost resin. It must be noted that even if the upper end of the reported affinity DBC range was assumed, this would not significantly affect the outcomes, as typically the columns were oversized to reach a GMP size and to avoid longer column loading times. Furthermore, the oversizing was assumed not to impact column performance, for example yields or product quality.

Due to the breadth of flowsheets that could be constructed from such options, it is desirable to ascertain the most cost-effective of the set evaluated, which can simultaneously satisfy various purity targets. From a purity perspective, there is a lack of well-defined data published on various impurity starting and target removal levels in AAV manufacturing. Subsequently, three heat-maps were generated, one for each impurity investigated (empty capsids, HCPs

and DNA), evaluating a range of potential starting and target levels. **Figure 3.8** displays these heat-maps from assessing the COG/dose and purity of each DSP sequence. Red coloured boxes represent more expensive options relative to those that are blue. The grey coloured areas represent those options that breach the imposed constraints (see **Figure A4** for the specific constraint labelling on the grey-coloured areas). Moreover, solutions that fall within the purple contour represent feasible combinations at the given purity target or starting level.

Figure 3.8 a) evaluated three target empty capsid removal levels, with a distinct change in optimal solution shown at each. In scenarios where less than 75% empty capsid removal was achieved, the most economical and hence optimal purification strategy was “AFFH-MM”, using an affinity resin with high DBC (AFFH) and a mixed-mode resin. This can be primarily attributed to the high overall yield of the combination relative to other choices. This allowed for a lower overall processing volume at harvest and hence a lower raw materials cost. However, both AFFH and MM do not possess empty capsid removal capabilities since they cannot distinguish between full and empty particles. Thus, this train was not sufficient to meet either the 75% or 90% purity targets. The technologies assumed to be able to make the distinction between full and empty were AEX and UC techniques, thus the higher purity targets were shown to require inclusion of one of these steps. This was first observed for the 75% purity target, where AEX and UC options were sufficient to at least meet this goal. In satisfying both objectives of cost and purity, AEX was shown to be marginally more cost-effective than UC, driven by lower labour costs. Having said this, when moving to the 90% target, AEX became infeasible from a purity perspective and ContiUC was the operation that satisfied both the cost and impurity removal target. ContiUC sizing is based on flowrate, offering a more scalable alternative to the batch counterpart. In general, fully chromatographic platforms or those utilising ContiUC were shown to be more cost-effective than those using batchUC, reinforcing the importance of scalability. As shown in **Figure 3.8**, most purification trains containing batchUC as a capture step were omitted from the optimisation due to breaching the equipment constraint. BatchUC was shown to only be feasible as a polishing step coupled with a CEX or

AEX capture, due to their high dynamic binding capacities that translate into a lower volume to be processed by ultracentrifugation. Nevertheless, as evidenced by **Figure 3.8**, whilst feasible, these options are amongst the least cost-effective of the set, attributable to the requirement for 11 parallel ultracentrifugation units, thereby driving up labour and indirect costs.

When studying HCPs and DNA, the low level (L) for each resulted in AFFH-MM being optimal, (**Figures 3.8 b)** and **c)**). The AFF-MM flowsheet was assumed to be capable of reaching an overall HCP and DNA log reduction value (LRV) of ~7.5 and ~4.5, respectively, which did not meet the target specification. For high starting impurity levels, the optimal strategy that met the purity targets was found to be AFFH-ContiUC for HCPs and AFFH-AEX for DNA. AFFH-ContiUC yielded an HCP LRV of ~8.5, whilst AFFH-AEX was found to have a DNA LRV of ~6.

Also included in the analysis was the option for a three-step purification train, involving the addition of an AEX step after MM, to provide additional purification capabilities. Whilst the three-step using AEX met the higher purity targets (for HCP, DNA and empty capsids) in contrast to many of the two-step options alone, the three-step purification trains were found to be less cost-effective than AFFH-ContiUC. This observation highlights that three-step trains are only necessary if employing AFFH-ContiUC is not an available option, reinforcing its cost effectiveness and impurity removal capabilities.

Although, ContiUC was shown to be the optimal polishing choice when simultaneously considering cost and purity, it must be noted that there are still challenges surrounding its implementation and use in commercial AAV manufacturing. Though achieving scalability, ContiUC is relatively less understood than its non-scalable counterpart, batch ultracentrifugation. Additionally, unlike chromatography, ContiUC is not industrially established as a purification option and as a result, may require a larger process development effort initially when integrating into a manufacturing process. Furthermore, continuous flow ultracentrifugation generally requires establishment of a stable gradient at the large-scale to recreate the environment encountered in the batch ultracentrifuge, thus requiring additional

process optimisation and characterisation studies, to further prove compliance with cGMP requirements. Finally, the reliance on niche chemicals such as iodixanol may prove limiting in terms of throughput due to ongoing supply chain issues. As a result, further work is likely required to identify suitable materials and consistent supply for large-scale application and sourcing.

The potential of the technology is significant however, as it provides a level of linear process scalability when moving from the relatively well characterised batch ultracentrifugation. Furthermore, the ability for ContiUC to evade the same scalability issues as batch is advantageous for future commercial implementation, particularly as the product loading potential is up to 40 times the actual rotor volume.

3.4.5 How does the optimal polishing strategy change with AEX yield and empty capsid removal?

As alluded to in the uncertainty analysis section of the case study, there are several uncertain process parameters or targets associated with AAV processing. To capture this variability encountered in AAV manufacturing, the AEX yield was varied for different empty capsid removal targets. **Figure 3.9 a)** shows the resulting matrix of optimal solutions for different combinations. **Figure 3.9 a)** highlights that AEX yield has a significant impact on the choice of optimal solution. At the AEX yield of 60% (base-case) and 80%, AEX was preferred at the low and medium purity targets but was unable to compete at the high purity target with ContiUC. Nevertheless, at the 80% yield, a three-step chromatography-based alternative to ContiUC, featuring AEX, was shown to be competitive with ContiUC. Equivalence in this case was defined as two options having a COG/dose with less than 5% difference between them. However, if the AEX yield were to drop to 40% as some have reported (see **Table A1**), this would result in AEX being unable to compete at all, with it failing to feature across any of the purity targets. Such a drop pushes up the resin volume required and hence leads to a higher materials cost. As a result, the optimal solution shifts to either MM or ContiUC depending on the purity target required.

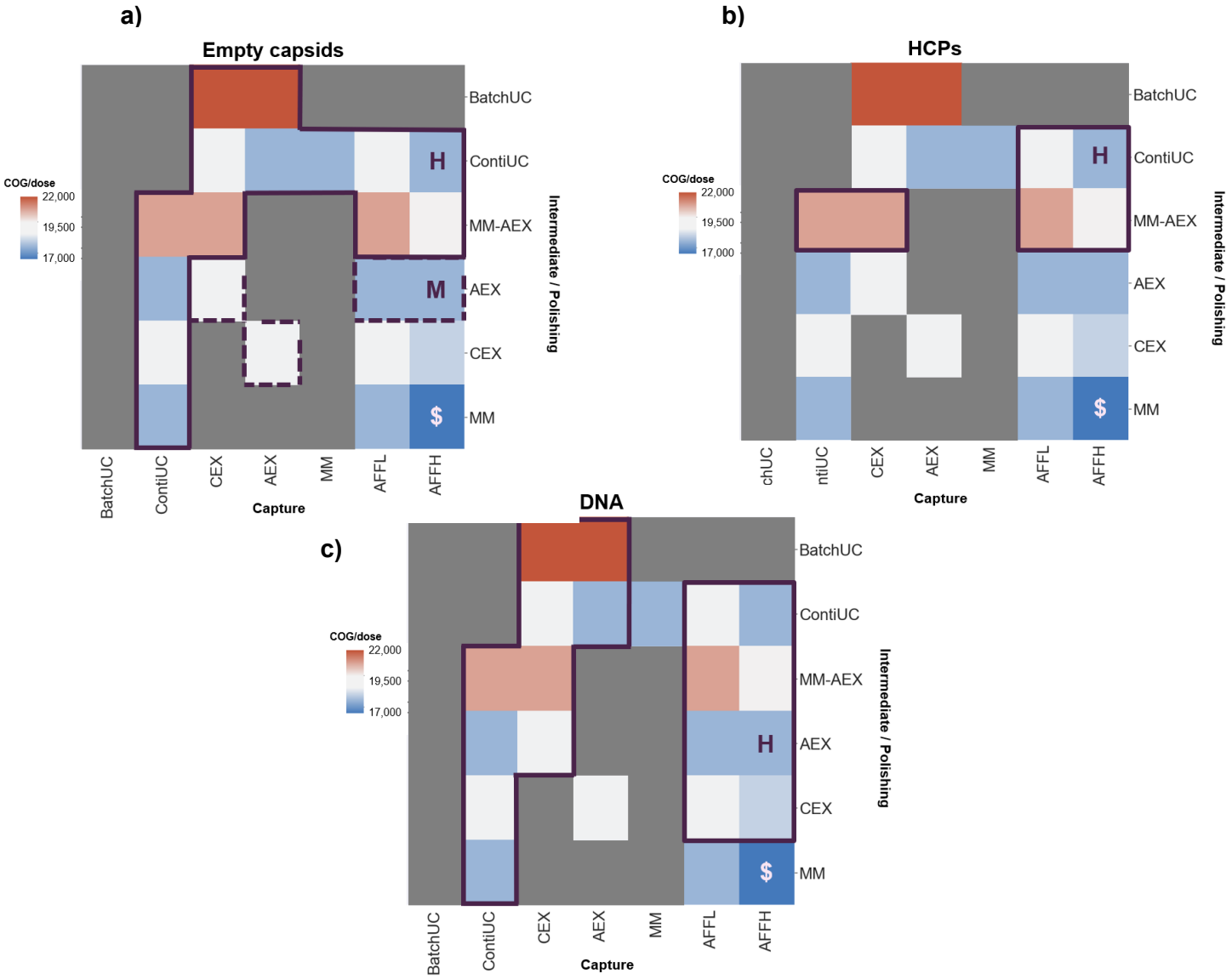

Figure 3.7 Brute-force outputs for AAV purification scenarios where **a)** differing target levels of empty capsid removal are encountered, **b)** different starting levels of host cell proteins (HCP) and **c)** different starting levels of DNA are defined. The $ symbols represent the most cost-effective option when less than 75% empty capsid removal is achieved or low starting levels of HCP or DNA ($2x10^{-7}$ ng/vg and $6x10^{-10}$ ng/vg) are assumed. For **a)**, M = optimal solution when at least 75% removal of empty capsids is required and H = optimal solution when at least 90% removal of empty capsids are required. For **b)** and **c),** H = optimal solution when a high impurity load is used ($2x10^{-5}$ ng/vg and $6x10^{-8}$ ng/vg). The contours represent the following; (- - -) meet target for a moderate impurity level, (——) meet target for a high impurity

level. Grey box = breach constraints (see **Figure A4** for details). The demand was assumed to be 1,000 doses/year, with a dose size of 1 x 10^{14} vg/dose.

Furthermore, as the purity target increases, the remaining feasible solution set reduces, as many platforms cannot meet the empty capsid removal requirement (**Figure 3.10 b)**). The effect of this can be observed when moving to the 75% target, where the key competitor to AEX, which was MM polishing, was removed as a feasible option. As outlined in **Figure 3.8**, AEX polishing (two-step) was not sufficient to meet the 90% removal target. As such, UC or three-step AEX was necessary to be included in the purification train due to their propensity for removing empty capsids. In this instance, as evidenced by **Figure 3.9 b)**, the feasible polishing steps remaining at this purity target were batch or continuous ultracentrifugation or three-step AEX. ContiUC was shown to be the most cost-effective across all AEX yields and additionally MM-AEX became more competitive at the higher AEX yield.

In summary, it was shown that where higher AEX yields were achievable, the optimal polishing solution shifted towards the inclusion of AEX, making it more attractive and competitive with other possible options. Nevertheless, the trade-off still exists between reaching higher purities with scalable technologies, whilst implementing robust unit operations that exhibit minimal yield variations between serotypes. Therefore, whilst AEX is known to be a scalable option, the wide range of yields that can be encountered may lead to reductions in cost-effectiveness relative to competing technologies and preference for more yield-stable polishing stages such as continuous ultracentrifugation in some instances.

a)

Increased chance of AEX as yield increases

AEX in optimal set

AEX not in optimal set

Increased need for ContiUC as purity target increases

Empty capsid removal target	AEX yield: 40%	AEX yield: 60%	AEX yield: 80%
90%	ContiUC	ContiUC	ContiUC / MM-AEX
75%	ContiUC	AEX / ContiUC	AEX
< 75%	MM	MM / AEX	AEX / MM

b)

Empty capsid removal target	Feasible polishing options: MM	CEX	AEX	ContiUC	BatchUC	MM-AEX
90%	N	N	N	Y	Y	Y
75%	N	N	Y	Y	Y	Y
< 75%	Y	Y	Y	Y	Y	Y

Figure 3.8 a) Optimal polishing purification choice in terms of COG/g across a matrix of scenarios with different combinations AEX yields and purity targets. A "/" sign in each box is used to represent solutions that fall within a 5% COG/dose difference from the optimal solution. Lighter shading represents solutions that do not contain AEX in the winning solution. Darker shading represents solutions that do contain AEX in the winning solution, **b)** Feasible solutions remaining in brute-force optimisation choices at each purity target. The demand was assumed to be 1,000 doses/year, with a dose size of 1×10^{14} vg/dose. The facility was resized for each set of inputs.

3.4.6 What is the optimal AAV flowsheet in terms of cost and purity targets?

As outlined in Chapter 1, AAV manufacturing can follow numerous possible flowsheets, beyond those already investigated in this chapter. Section 3.4.4 highlighted the results of the study pertaining to AAV purification, where the identified capture and polishing options were evaluated. This section expands upon this work, integrating USP and lysis options as part of the optimisation framework. In addition to the USP technologies already evaluated in the base case (i.e. cell factories and single-use stirred tank bioreactor), roller bottles were included as another adherent option and the rocking motion bioreactor as an additional suspension technology. Significantly, providing a more scalable adherent option, the fixed-bed reactor was investigated in this case study, with available sizes of 66m^2, 133m^2 or 333m^2.

As with the optimisation work in **Figure 3.8**, three distinct empty capsid removal levels were investigated (less than 75%, 75% and 90%). The resulting heatmap of COG/doses in **Figure 3.10** was ordered according to these purity levels. Red shaded boxes represent more expensive options relative to those that are blue. The grey coloured areas represent those options that breach the imposed constraints (the same constraints outlined in Section X). Contours were used to separate the regions by purity level achieved and the specific labelling is further detailed in the caption. In general, the change in colour occurs from left to right, highlighting the cost-effectiveness as the technologies move away from batch-adherent cell culture scenarios, driven by lower labour and equipment costs in the more scalable scenarios. Unsurprisingly, the least cost-effective option was shown to be a cell factory (CF) platform coupled with microfluidisation (MF), cation exchange (CEX) and batch ultracentrifugation (BatchUC), a result which further reinforces the conclusions drawn earlier in the chapter that coupling adherent cell culture with ultracentrifugation negatively impacts the COG/dose. Conversely, the most cost-effective option was shown to feature an AFFH-MM purification train, similarly shown in **Figure 3.8**. Suspension cell culture coupled with these options was shown to produce a set of the lowest COG/doses, independent of purity target.

Though slight, differences in cost were obtained in using CF versus roller bottles (RB). The benefit of RB from an economic perspective lies in the cost per unit. Whilst the size of a single roller bottle is approximately 3.5 times smaller than a cell factory, the cost difference does not follow the same trend; roller bottles were assumed to be $30 per unit and cell factories $500. This was the key impetus for the minor changes between scenarios shown in **Figure 3.10**. As a more scalable adherent alternative, the fixed-bed reactors yielded a far more cost-effective set of results than CF or RB. The three available sizes allowed for scalability in terms of sizing the process, particularly evading the need for multiple units used in parallel, as the largest available size was assumed to be 333m^2. Having said this, fixed-bed options were shown to be less favourable than the suspension cell culture options, the rocking motion (RM) and SUBs. This is attributable to the nature of fixed-bed sizing. In comparison to suspension cell culture, adherent production was assumed to require more rigid sizing to the full surface area of the vessel selected, e.g. if the calculated surface area was 210m^2, a 333m^2 FB model would be selected and the whole surface area was assumed to be covered. This results in overproduction of AAV product, hence a larger relative DSP process overall. Suspension cell culture has a greater sizing flexibility, where the working volume utilised can be anywhere between 20% utilisation of the reactor model and the maximum volume of the vessel. Nevertheless, FB was shown as a favourable alternative to other adherent options, highlighting its benefit for manufacturers who do not wish to adapt cell lines to suspension culture, but require production in a commercial environment.

From a lysis perspective, two options were investigated in this study - chemical lysis (CL) and microfluidisation (MF). Chemical lysis is generally regarded as a less invasive cell disruption method than microfluidisation, where the yield of the latter was assumed to be lower. This assumption, along with the capital requirement and consideration of SIP and CIP, drives the cost of flowsheet options that contain MF up in comparison to those with chemical lysis instead.

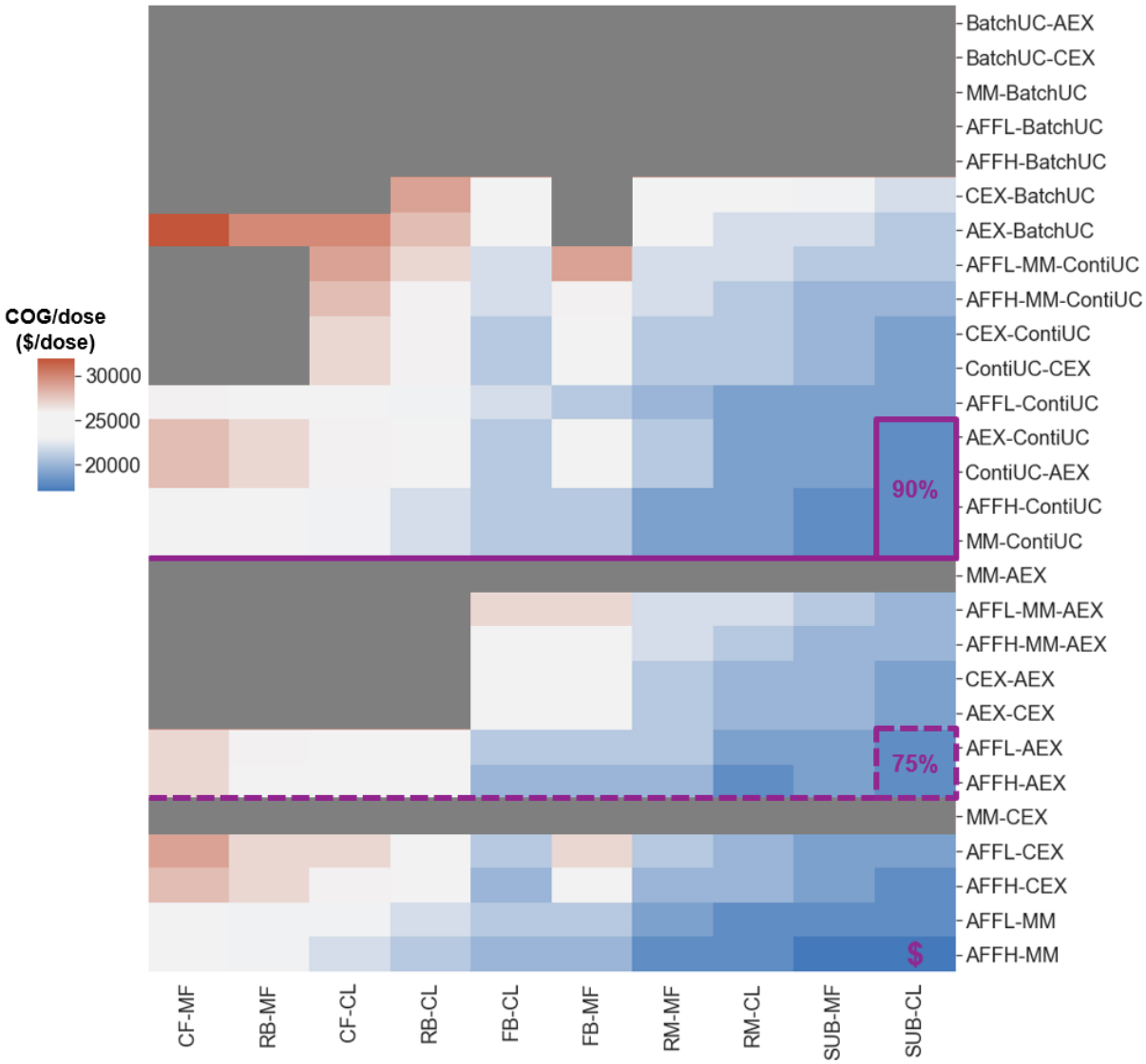

Figure 3.9 Brute-force optimisation outputs for full flowsheet scenarios. The $ symbol represents the most cost-effective option when less than 75% empty capsid removal is achieved. M = best performing solutions when at least 75% removal of empty capsids is required. H = best performing solutions when at least 90% removal of empty capsids are required. The contours represent the following; (- - -) meet the 75% target, (——) meet the 90% target. Grey coloured areas = breach constraints. The demand was assumed to be 1,000 doses/year, with a dose size of 1 x 10^{14} vg/dose. The facility was resized for each set of inputs.

3.4.7 How does the critical lysis point impact cost and impurity release?

AAV serotypes exhibit variable behaviour with respect to whether they are extra- or intracellularly expressed during cell culture. Oftentimes, those labelled extracellular AAVs are only partially secreted, with a certain percentage of material remaining within the cell post-culture. There has been industrial discussion around serotypes following this behaviour, particularly the question of whether it is economically significant to use lysis to collect the product that may be retained within the cell or instead discard the material. The compromise relates to the additional impurities that would be released when lysing the cells, thereby necessitating a greater purification effort.

Figure 3.11 investigates the aforementioned trade-off and provides information on the critical lysis point, across various extracellular: intracellular ratios. Each coloured block on the heat-map represents an extracellular AAV instance for a given number of doses and extent of secretion. This percentages are with respect to the amount secreted. For example in the 90% case, it was assumed 90% of the AAV product was secreted to the cell culture medium and 10% remained within the cell. As a result, the axis ranges only from 50 – 90%, as anything below 50% would be regarded as a primarily intracellular AAV product. Furthermore, the black dotted line in **Figure 3.11 a)** depicts the economic threshold (or critical lysis point). In any scenario situated to the left of the line, lysis is recommended as the product lost when the cells are discarded causes a >10% COG increase over the 100% extracellular AAV case.

Across all demands, it was found that discarding up to 20% of the product did not detrimentally impact the COG/dose relative to the 100% extracellular case, meaning lysis could be avoided. Scale was shown to impact the threshold trajectory, as it was found for the low demand of 500 doses, the COG/dose was not impacted by more than 10% even up to 50% product discarded. This is attributable to the sizing of the process primarily, where it can be concluded form **Figure 3.11 b)** that regardless of the product losses from avoiding lysis, the reactor was always sized

to a 250L model. This sizing trend was similarly observed for the 1,000 doses case, however the threshold was met past 80% secreted here. In this case, it must be noted that the 100% extracellular case featured the use of a 250L reactor used almost to its maximum capacity, thus even a 10% loss of product meant a resizing to a 500L model throughout. This gave rise to the initial and relatively large jump of 5% COG difference. Nevertheless, larger COG differences (%) between each percentage secretion are observed as the demand increases. This is because at higher demands and hence vg batch sizes, changes in product yield amplify the changes in working volume required.

An important trade-off to highlight is the cost-effectiveness versus meeting purity targets and thus to demonstrate this, a multimodal and anion exchange chromatography purification train was chosen in these figures, whilst assuming a high HCP starting level. This combination breached purity constraints by failing to meet the target HCP specifications, thus was regarded as an infeasible option for a high HCP starting level. However, this assumed an intracellular AAV and hence included a lysis step, after which it was assumed more impurities were released into the product fluid following cell breakage. Building upon that of **Figure 3.11 a)**, those solutions within the black dotted box represent instances where lysis can be avoided and less than 10% COG/dose difference is generated, however those outside this box recommend lysis in order to yield more product and hence reduce the resulting COG/dose**.** However, as discussed, if lysis is initiated, the level of impurities also increase as more are released from the cells, thereby impacting the overall LRV for the flowsheet. For this case study at least 6.5LRV reduction of HCP when a low starting level is encountered was required to meet the target of 100ng/mg, hence those solutions within the black box where no lysis is used allow for MM-AEX to meet the HCP targets. Upon lysing, a reduction to 6.1LRV is exhibited, meaning that as with the heat-map, MM-AEX fails to meet the specification.

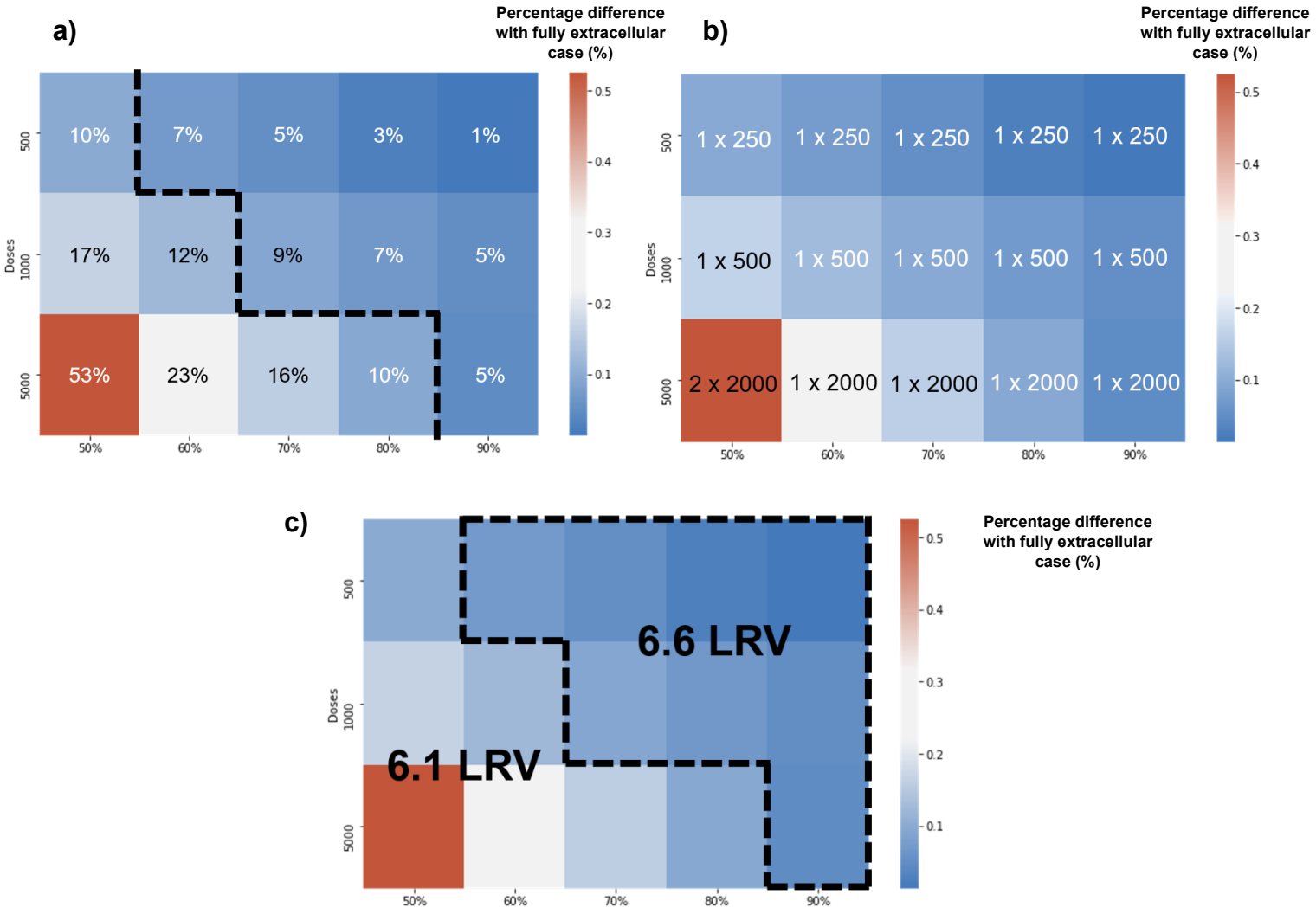

Figure 3.10 Heatmap generated for comparison of lysis point. Three demands (in doses) are presented, which are found on the y-axis. The x-axis refers to the extracellular scenario in question, e.g. 90% refers to a scenario where 90% of the AAV is secreted and 10% is retained in the cell. **a)** the percentages refer to the difference between the scenario under consideration and the case where a fully (100%) extracellular AAV was assumed (scale provided by the ladder on the right of the figure). The black dotted line is placed to give the critical lysis point, which is defined as the point beyond which a significant COG/dose difference is exhibited (significant being deemed 10%)**, b)** upstream sizing for each scenario, where the first number is how many bioreactors were required and the second is the bioreactor model used**, c)** for a multi-model and AEX purification platform, what the overall LRV would be in cases of lysis or no lysis.

3.5 Conclusion

This chapter presented the use of a decisional tool for the evaluation of AAV manufacturing processes, first evaluating a small decision space, before use of an optimisation algorithm to expand the solution set and find the optimal in terms of cost-effectiveness and meeting purity targets. The deterministic analysis focused upon comparison at key points in the process, namely addressing issues of scalability at USP and during purification. This analysis highlighted the economic superiority of a suspension cell culture strategy over an adherent one, as well as of AEX chromatography over iodixanol gradient ultracentrifugation, with the flowsheet combining suspension culture with AEX chromatography attaining a COG/dose below $20,000 at 1,000 doses per year. The impact of AAV dose (and hence chosen disease area) upon process economics illustrated that adherent and suspension culture offer similar costs at lower doses but, at higher doses, strategies utilising suspension culture are clearly cheaper.

The case study also incorporated an uncertainty analysis using Monte Carlo simulation to identify key risks associated with undertaking the various strategies. It was found that the strategy using adherent culture with AEX chromatography produced the widest distribution and hence was the least robust strategy. This was attributable to the wider input yield distribution associated with AEX and the impact this has on adherent process sizing. This would suggest that for manufacturers utilising the traditional AAV platform (adherent culture with ultracentrifugation), if a minimal process switch is initially desired, then efforts should be focussed upon a USP switch first over DSP, for a more cost-effective and robust initial outcome. However in general, it is important to note that whilst robustness of various strategies is significant as a decision criterion, manufacturers may have preferences in what to target for improvement based upon where their current process development experience is or their success to date.

The optimisation case study reinforced the cost-effectiveness of scalable purification platforms, however also revealed the distinct sensitivity that purification performance had on

the optimal choice. The purification sequence of affinity followed by multimodal chromatography was deemed the optimal solution at the low starting or target impurities levels, whereas affinity chromatography with continuous ultracentrifugation was found to be the best combination at high levels. This was similarly seen when varying AEX yield. The decisional tool therefore served as a strategy to rapidly assess a myriad of AAV manufacturing options, accounting for both economics and purity to derive optimal solutions.

4 Estimation of research & development budgets for novel modalities

4.1 Introduction

Chapter 3 introduced the perceived scalability challenges associated with traditional AAV manufacturing and provided cost estimates for a range of flowsheet alternatives. However, manufacturing activities represent just one component of the overall R&D cost that biotechnology companies must allocate towards development and commercialisation of a drug. In general, biopharmaceutical drug development is associated with lengthy timescales, high risk and substantial expense. From the initial discovery of a drug to its availability on the market, the entire process can span up to 15 years (Paul et al., 2010), with latest estimates on capitalised R&D costs amounting to ~$3.1bn in 2020 (Farid et al., 2020). Additionally, it is often necessary to initiate multiple projects at the start of the development lifecycle to ensure a single market success, given that the overall probability of drug success from Phase I to likelihood of approval (LOA) ranges from 12 – 17% for mAbs (see Appendix B). Consequently, estimating research and development costs for biological products is a complex task due to the unique characteristics of the drug development lifecycle, but is crucial to ensure the allocation of appropriate budgets across phases and ultimately projects.

In particular, it has become significant to define the contribution of process development and manufacturing (collectively described throughout this chapter as CMC activities) towards the total R&D budgets. Published studies to date have reported benchmark CMC contributions and costs specifically for mAb products, but have not addressed these elements for other modalities such as ADCs, AAVs and CAR T cells. More specifically, no comparison between these more novel modalities with mAb products in terms of clinical and non-clinical cost breakdowns has been presented. As a result, this chapter aims to provide estimations for the R&D budgets required to commercialise mAb, ADC, AAV and CAR T products, as well as

benchmark the contributions of CMC activities. In this chapter, the total R&D cost, also referred to as the out-of-pocket cost, is divided into three categories – process development, manufacturing and clinical trials. These stages share interdependencies, as each relies on the preceding activity to commence the next. For example, process development for a particular phase is necessary to establish and subsequently optimise the manufacturing process, which supplies a given clinical trial. Significantly, costs are sensitive to changes in the overall clinical success rates, which vary depending on modality type and target indication under consideration. As a result, this chapter also addresses the significance of success rates in influencing changes to the estimated R&D budgets. A drug development lifecycle cost model is presented, which considers process development, manufacturing and clinical trials costs for mAbs, ADCs, AAVs and CAR T cells. Additionally, the impact of varying the success rates was examined, particularly across modalities and indication, with the goal of identifying the modality requiring the smallest budget in each case.

The chapter is structured as follows. Section 4.2 outlines the structure of the drug development lifecycle. Subsequently, Section 4.3 describes the architecture of the drug development cost model constructed. Specific case study assumptions are highlighted in Section 4.4, that utilise the model previously highlighted. Finally, Sections 4.5 and 4.6 the analysis and discussion on estimating the CMC budgets required for a range of modalities is given, along with the conclusions drawn from the study.

4.2 Drug development lifecycle

The pathway taken by a biopharmaceutical typically follows a well-defined trajectory in the case of non-accelerated drugs. The product candidate under consideration first undergoes a pre-clinical trial stage, involving testing either *in-vitro* (usually in cells or tissue culture) or *in-vivo*, using animal models (Lo & Field, 2010). These studies aim to gather preliminary information regarding drug toxicity levels, pharmacokinetics, pharmacodynamics and the

safety of the dosing regimen (Mundae & Ostor, 2010; Schmidt & Grossmann, 1996). Upon successful completion of the pre-clinical phase and in order to enable the development process of a potential therapeutic to begin, an investigational new drug (IND) application must be submitted to the appropriate regulatory body, such as the FDA or EMA, depending on the region (Nitin Kashyap et al., 2013; Umscheid et al., 2011). If accepted, this allows companies to initiate clinical trials in human participants. A similar regulatory process exists with the European Medicines Agency (EMA), where instead of an IND, an investigational medicinal product dossier is filed (Nitin Kashyap et al., 2013).

The clinical trials progress through three distinct phases. Phase I focuses on assessing the drug's safety, tolerability and pharmacokinetics of the drug (Mundae & Ostor, 2010). The purpose of Phase II is proof of concept, through evaluating the drug's efficacy at specific dosing levels (Yuan et al., 2016). Phase III trials have a similar overall aim to Phase II, however the patient pool is far larger. More specific objectives of this phase include identification of side effects and therefore also forms the basis of the appropriate instructions and packaging corresponding to the therapy. Following the successful completion of clinical trials, a New Drug Application (NDA) is filed and submitted to the appropriate regulatory body. This application contains data collected from all trials and serves the primary purpose of providing sufficient evidence to obtain market approval for the therapy.

The work carried out in this chapter simulates the pathway of drugs from the pre-clinical phase to market approval. As outlined previously, there are several activities that occur before initiation of pre-clinical research and trials, such as drug discovery and target validation. The costs incurred during this period were not included within this study, as it is common for biopharmaceutical companies to evaluate multiple compounds simultaneously, leading to overlapping costs that are challenging to allocate appropriately. Therefore it is important to note that in reality, there are costs associated with the drug discovery portion of the development phase. However the work in this chapter focuses on the stages from pre-clinical process development and beyond.

Activities along the development timeline can be categorized into those relating to process development, manufacturing and clinical trials. Clinical trials are considered to be critical path stages, such that CMC (process development and manufacturing) activities take place to support them and occur in parallel with the critical path to ensure delays are avoided. In general, the process development refers to establishment and optimisation of the manufacturing process that is used to supply the clinical trials with material. The integrity of this order of activities (i.e. process development, manufacturing and trials) is maintained throughout. The interaction and any parallelisation of these activities is depicted in **Figure 4.1,** adapted from Nie (2015) and Farid et al. (2020). Of significance, **Figure 4.1** exemplifies the fact that many process development and manufacturing activities occur at risk with respect to critical stages (i.e. clinical trials), hence activities are often parallelised. In practice, this means the process development and manufacturing for clinical phase $n + 1$ may begin before the end of the trial for phase n, thus these activities would be costed "at risk", accounting for the potential failure of trial n.

Early process development studies involve optimisation and titre improvement, which can often result in disparity between early phase and late phase titres. This difference impacts the manufacturing activities, as titre is a key input within the process economics models. In terms of the manufacturing scale, Phase I and II were assumed to be equal. Phase III scales are assumed to be consistent with that used in commercial manufacturing, to avoid another scale up stage and further characterisation studies. Manufacture of material occurred across the clinical phases, with additional runs occurring during regulatory review to demonstrate process reproducibility and consistency, known as process performance qualification (PPQ) batches. The scale here is the same as Phase III and typically amounts to 3 to 5 batches.

Figure 4.2 provides both qualitative and quantitative definitions of each activity, divided into clinical phases. The typical manufacturing demands and trial sizes are also displayed. As this case study evaluates a range of modalities, the differences in demands and trial sizes are outlined between them. For brevity, these have been grouped into those that are protein

therapeutics and those that are cell and gene therapies (CGTs). mAbs and ADCs are classed as proteins, whereas AAVs and CAR T cell products are regarded as the CGTs. Protein therapeutics are generally characterised by large patient populations in each trial, relative to CGTs. The latter often target rarer disease in comparison to protein therapeutics, hence patient recruitment is relatively more difficult, leading to smaller trial sizes.

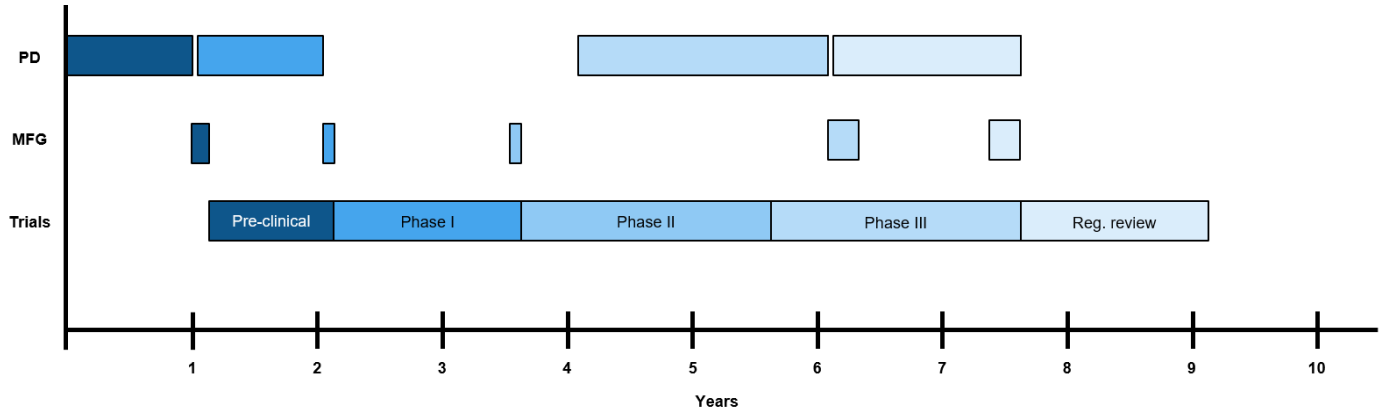

Figure 4.1 Representation of the dependencies between process development (PD), manufacturing (MFG) and clinical trials (Trials) activities. The example used here is the trajectory of a mAb product. Colours are used to distinguish between activities pertaining to a specific phase, e.g. the shade of blue used for Phase I is used for the corresponding PD and MFG activities.

a)

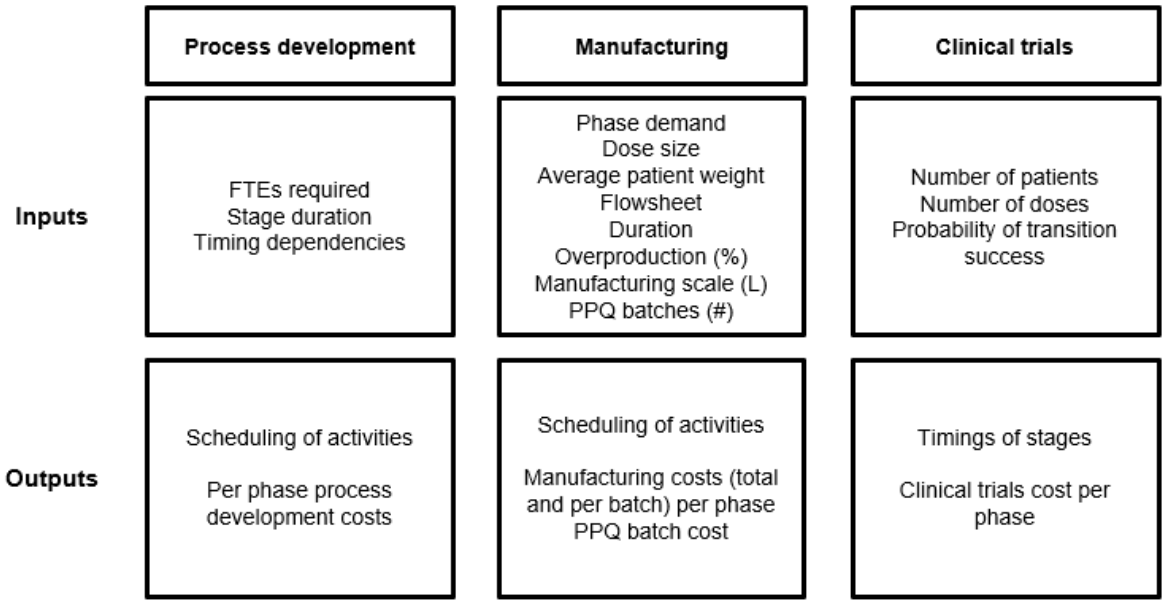

b)

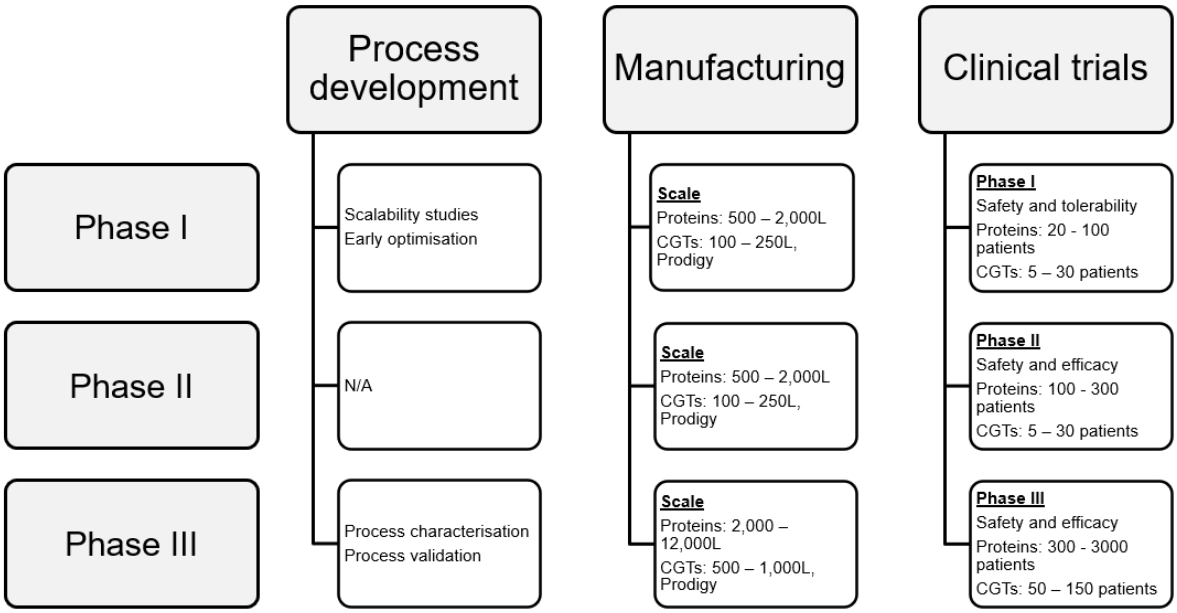

Figure 4.2 a) Key inputs and outputs into the decisional tool, divided by key cost category, including process development, manufacturing and clinical trial activities, **b)** specifics of each activity broken down by development phase. Included here is quantitative data related to the inputs outlined in **a).**

4.3 Methodology

4.3.1 Overview

Figure 4.2 a) depicts the schematic for the tool utilised. A Microsoft Excel-based cost model from Nie (2015) and Farid et al. (2020) was converted into Python 3.8 for further use. This Python model integrated the process economics models for each modality considered with calculations for process development and clinical trial activities. This constituted the overall drug development lifecycle cost model. The Python model drew upon process development, manufacturing and clinical trial assumptions stored in a Microsoft Excel database. As shown in **Figure 4.2,** key assumptions utilised included costs associated with each activity, stage durations and clinical success rates. In general, process development activities were assumed to include all bulk drug substance process and formulation development, as well as process characterisation and validation. Manufacturing activities included the manufacturing of the bulk drug substance material to supply each clinical trial and additionally process performance and quality (PPQ) batches necessary for regulatory purposes. For AAV and CAR T, drug product manufacturing steps (e.g. vialling) were also accounted for. Furthermore, clinical trials represented the actual clinical trial undertaken with patients and drug recipients.

The drug development model followed the specific product development pathway for a given modality, adjusting output costs for any activities assumed to be carried out “at risk” with respect to clinical trials, as described previously. Similarly, the phase-by-phase success rates were also considered throughout the lifecycle and were used to characterise the risk of drug failure. This generated the number of projects required to achieve a single market success for each modality. The number of projects was then used to determine the total out-of-pocket costs per phase, hence providing overall R&D budgets that accounted for the risk of clinical failure.

4.3.2 Process development

In general, process development activities preceded or occurred in parallel with each manufacturing activity. Such activities include process characterisation, product synthesis, comparability studies, validation, technology transfer and process optimisation. Process development is a pivotal activity, designed to develop and optimise the manufacturing process for a drug to ultimately supply the multiple clinical and commercial phases involved in bringing a product to market. Being able to plan these activities early on can reduce costs incurred throughout.

As displayed in **Figure 4.2,** when modelling process development activities, key attributes considered were the number of personnel and hence FTEs required, the salary per FTE year and the duration of the activity. These were used to calculate the number of FTE years and hence the overall process development cost on a per phase basis, for each modality under consideration. Process development personnel were categorised by job role before being estimated, (e.g. process scientists, tech transfer). A full list of the categorisations is provided later. Furthermore, the duration of each process development phase was estimated and used in conjunction with the number of personnel to calculate the FTE years. The hours worked by an employee functioned as the proportion of an FTE that was dedicated to a specific task. Assuming a typical 40-hour working week, one FTE was defined as an employee working all 40 hours. 0.5 FTEs represented the equivalent of one employee working 20 hours a week on the project under consideration. Subsequently, the FTE years were calculated based on the required personnel multiplied by the duration of the process development stage. The term FTE years denotes the personnel effort required if activities were restricted to completion within one year, hence 20 personnel used for two years is equivalent to 40 in one. The number of FTE years was then used to calculate the required cost of the stage. The key equations derived are shown below.

$$N_{FTE_y,i} = N_{personnel,i} \times t_i \quad (4.1)$$

where $N_{FTE_y,i}$ = number of FTE years required for process development for stage i, where i represents the phases considered across the development pathway, i.e. Phase I, II, III and regulatory review

$N_{personnel,i}$ = number of personnel required for process development for stage i

t_i = duration of process development stage i

$$C_{PD,i} = N_{FTE_y,i} \times C_{FTE} \quad (4.2)$$

where $C_{PD,i}$ = total cost of process development for stage i

C_{FTE} = FTE salary including overheads ($)

4.3.3 Manufacturing

Derivation of manufacturing contributions involved using modality-specific process economics models. For the protein therapeutics (specifically mAbs and ADCs) the model used was developed by Simaria et al. (2012) and was further optimised by Stamatis & Farid (2021). For viral vectors, the manufacturing cost models were based on versions described originally in by Comisel et al. (2021b) and Lyle et al. (2023), the latter of which was detailed more extensively in Chapter 3. Finally, the process economics model for CAR T cells was based on work by Pereira Chilima et al. (2020). Independent of modality type, each clinical and commercial phase required differing product demands, therefore each process economics model was required to run multiple times in order to obtain the cost of goods per phase. Additionally, PPQ was necessary for each modality post-phase III trials, requiring the process economics models to be run for around a 3 to 5 batch process depending on modality.

4.3.4 Clinical trials

The clinical trials costs was calculated using two key inputs; the trial cost per patient and the number of patients involved in the trial. Examples of these values were previously shown in **Figure 4.2.** This was computed for each clinical trial, as well as pre-clinical trial activities. Equations are outlined below for clinical trials costs.

$$C_{trials,i} = N_{patients,i} \times C_{trials,per\ patient} \quad (4.3)$$

where $C_{trials,i}$ = total clinical trial cost for stage i

$N_{patients,i}$ = number of patients involved in the trial for stage i

$C_{trials,per\ patient}$ = cost of clinical trial per patient

4.3.5 Transition success rates

As summarised in Section 4.2, the transition success rates were used to ascertain the number of projects required to achieve a market success per modality. Utilising these values provides a more realistic derivation of the total out-of-pocket cost on a per success basis for each modality. Success rates were assumed for each phase and were used to generate the number of projects required from the given phase to commercialisation. The overall number of projects from Phase I represented the inverse of the LOA from Phase I. A more comprehensive overview of the calculations is detailed below.

$$N_{projects,i} = \frac{1}{p(SR_i) \times p(SR_{i+1}) \times \dots\ p(SR_k)} \quad (4.4)$$

where i is an index for the phases in the development pathway, where $i = \{1, 2, \dots\ k\}$, k being the total number of phases considered.

$N_{projects,i}$= number of projects required to achieve a market success from phase i

$p(SR_i)$ = clinical success rate (probability) for phase i

4.3.6 Total budgets and capitalised equivalents

In summary, the information provided to this point was necessary in calculating the R&D budgets or out-of-pocket costs per phase ($C_{R\&D,i}$) and the following equation outlines its derivation.

$$C_{R\&D,i} = \sum_{i=1}^{k} \left(\left(C_{PD,i} + C_{MFG,i} + C_{trials,i} \right) \times N_{projects,i} \right) \qquad (4.5)$$

where $C_{MFG,i}$ = the total manufacturing cost for phase i.

It is often significant to consider the impact of the time value of money on costs and hence the capitalised equivalents of the total out-of-pocket costs. The equation outlined below details this calculation for a given phase i.

$$C_{R\&D_{cap},i} = C_{R\&D,i} \times (1 + Discount\ rate)^{(t_{total} - \sum_{n=1}^{i} t_{n-1})} \qquad (4.6)$$

where $C_{R\&D_{cap},i}$ = is the capitalised R&D cost for phase i

t_{total} = the total of all phase times

$\sum_{n=1}^{i} t_{n-1}$ = sum of phase times from $t_0 = 0$ to the time for phase i

4.4 Case study setup

The case study sought to simulate the typical trajectory a drug takes from entry into pre-clinical trials through to commercialisation and hence estimate the total out-of-pocket costs associated with each modality investigated, in this case mAbs, ADCs, AAVs and CAR T cells. As a result, the assumptions related to those activities detailed in Section 4.3 were crucial to define across the stages of the drug development lifecycle. In general, assumptions were derived from industrial correspondence or from previous values used within the UCL Decisional Tools group (Comisel et al., 2021a; Farid et al., 2020; Hassan et al., 2016). As

detailed previously, manufacturing assumptions were used in the relevant process economics models to generate COG values for the modalities under consideration in the case study.

4.4.1 Key assumptions

4.4.1.1 Process development costs

Process development costs were determined from estimations made on the number of FTEs needed for each phase and hence how many FTE years were required. This first involved the determination and definition of the relevant FTE categories, which has been outlined by **Table 4.1**. In particular, these categorisations and definitions were sourced that reported by Nie (2015) and Farid et al. (2020) and were further confirmed through industrial correspondence.

Table 4.1 Process development personnel breakdown by category and relevant definition.

Process development personnel classification	**Definition for case study**
CMC project manager	Team leader
Product development scientists	Involved in the process and analytical development
Tech-transfer	Involved in transfer of the process between PD and MFG or between MFG sites
Regulatory support	Examples may include assistance on scientific writing and regulatory procedure
QC/QA	Involved in product and process characterisation and testing
Site support	Preparation for commercial manufacturing, logistical and clinical supply

In **Table 4.1**, the term product development scientist was used to collectively describe those working on the development of the manufacturing process, such as cell culture, downstream

processing and formulation, as well as on analytical development. Estimations regarding the personnel required across modalities and for each phase were made and these values can be found in **Table 4.2** for protein therapeutics and **Table 4.3** for cell and gene therapy products. The number of personnel in **Tables 4.2** and **4.3** represented raw data on the actual number of employees assigned to each role across phases. One FTE was determined to represent an employee working an 8-hour day, ultimately totalling to a 40-hour working week. In instances where a non-integer value was used for the number of personnel, e.g. regulatory support and QC/QA for pre-clinical process development was assumed as 0.5 personnel, this represented situations where employees were drafted onto multiple projects at once, hence on average half their working day or week may be dedicated to the modality under consideration and the other half to a different project.

In addition to the number of FTEs estimated per phase, the process development duration was also assumed, which is displayed in **Tables 4.2** and **4.3**. As evidenced in Section 4.3, this was also used in the FTE year-based approach to process development cost calculations, in order to derive the workload required in terms of FTE years. Furthermore, the per unit cost of an FTE year workload was assumed to be $150,000, accounting for the FTE salary and overheads. These overheads included those that were employee-related, such as pension contributions or healthcare provisions, as well as support costs for management and infrastructure. This value had previously been estimated at around $250,000 (Nie, 2015), however through internal discussion with industry, was lowered.

An additional cost within the process development category related to product stability studies, involving the implementation of analytical tests and assays at various time points. This was assumed to be necessary for all modalities and across Phase I, III and during regulatory review process development activities. In parallel to that reported in Comisel et al. (2021b), Phase I and III product stability costs were fixed at $500,000 and $1,000,000 for the material produced in PPQ batches during regulatory review.

Table 4.2 Estimated FTE requirements for process development activities for mAbs and ADCs.

	mAbs					ADCs				
PD Personnel	***for* Pre-clinical**	***for* Phase I**	***for* Phase III**	***for* Reg. Review (PD)**	***for* Reg. Review (Comm)**	***for* Pre-clinical**	***for* Phase I**	***for* Phase III**	***for* Reg. Review (PD)**	***for* Reg. Review (Comm)**
CMC project manager	1	1	2	2	0	1	1	2	2	0
Product development scientists	3	6	10	12	0	3	7	12	12	0
Tech-transfer	1	2	4	4	0	1	3	6	4	0
Reg. support	0.5	1	2	7	0	0.5	1	2	7	0
QC/QA	0.5	2	2	4	20	0.5	3	3	4	20
Site support	0	0	0	0	20	0	0	0	0	20
Total personnel	6	12	20	29	40	6	15	25	29	40
Duration (year)	0.5	1	2	1.5	1.5	0.5	1.5	2	1.5	1.5
FTE year	3	12	40	43.5	60	3	22.5	50	43.5	60
Cost ($)	**450,000**	**1,800,000**	**6,000,000**	**6,525,000**	**9,000,000**	**450,000**	**3,375,000**	**7,500,000**	**7,200,000**	**9,000,000**

Table 4.3 Estimated FTE requirements for process development activities for viral vectors and CAR T.

	Viral vector [1]					CAR T [2]				
PD Personnel	***for* Pre-clinical**	***for* Phase I**	***for* Phase III**	***for* Reg. Review (PD)**	***for* Reg. Review (Comm)**	***for* Pre-clinical**	***for* Phase I**	***for* Phase III**	***for* Reg. Review (PD)**	***for* Reg. Review (Comm)**
CMC project manager	1	1	2	2	0	2	2	4	4	0
Product development scientists	3	9	10	12	0	6	18	20	24	0
Tech-transfer	1	2	4	4	0	2	4	8	8	0
Reg. support	0.5	2	2	7	0	1	4	4	10	0
QC/QA	0.5	2	2	4	20	1	4	4	8	40
Site support	0	0	0	0	20	0	0	0	0	40
Total personnel	6	16	20	29	40	12	32	40	54	80
Duration (year)	1	2	2	1.5	1.5	1	2	2	1.5	1.5
FTE year	6	32	40	48	60	12	64	80	81	120
Cost ($)	**900,000**	**4,800,000**	**6,000,000**	**7,200,000**	**9,000,000**	**1,800,000**	**9,600,000**	**12,000,000**	**12,150,000**	**18,000,000**

[1] Excluding pDNA process development as assumed it is outsourced

[2] Including both lentiviral and cell process development

As outlined previously, each process development team was assumed to be headed by a CMC project manager, designed to oversee operations. The numbers were assumed to be consistent across modalities, with double the number required at Phase III and beyond due to the large increase in overall team size. Of the total number of FTEs at each phase and for each modality, product development scientists made up the majority, as this FTE category served as an umbrella term for multiple different activities, defined in **Table 4.1**. Differences in the number of product development scientists were assumed between modalities. At Phase I, an additional process development scientist was required for ADCs over mAbs, due to the likelihood that process development effort may be higher for the drug-conjugate component of the ADC. Similarly, 9 process development scientists were assumed for viral vectors over the 6 for mAbs, coupled with a longer duration, reflecting the need for greater process development and optimisation effort early on to establish a scalable platform process for this relatively nascent modality. This difference is minimised at Phase III, with the experience gained in viral vector manufacturing, reflecting a situation similar to that of protein therapeutics. In the case of CAR T cells, the process development requirement was doubled in relation to viral vectors for each category, reflecting the process development effort needed for both the viral vector and CAR T cell component separately.

Moreover, tech transfer involved support in transferring the developed manufacturing process to clinical or commercial scale and as such, the number of FTEs increased with trial size and hence manufacturing scale. These values were assumed to be higher for ADCs, attributable to the complexities in transferring the conjugation process to larger scale.

For regulatory review, process development effort was split into two sub-categories. That which has been labelled *PD* in **Tables 4.2** and **4.3** refers to further process characterisation and validation activities, which saw an increase in the number of FTEs directed towards regulatory support compared to other phases, attributable to the need for extra effort in aiding regulatory writing and evidence gathering for the NDA submission. In contrast, the regulatory

review process development phase for commercial (*comm)* was assumed to be solely devoted to site support and QC/QA, to prepare for commercial launch, as outlined in **Table 4.1**.

4.4.1.2 Manufacturing

As discussed in Section 4.3, each modality considered in the case study was associated with specific process economics models, sourced from multiple locations. As such, the following section is organised by modality studied.

4.4.1.2.1 Protein model

For the purpose of this case study, the term protein was used to collectively describe mAb and ADC products. The cost of manufacturing for these were determined using an established techno-economic engine for proteins described in Section 4.3. In general, the manufacturing model utilised key assumptions such as demand, manufacturing scale, titre and annual number of batches.

Several manufacturing assumptions for mAbs were sourced from Farid et al. (2020) namely the number of participants in each clinical trial. The average patient weight and dose size were also gathered from the same sources, where the values were assumed to be 86kg and 7 mg/kg respectively. Furthermore, **Table 4.4** shows the flow of calculations required to calculate the demand input for the process economics model. This began with using the number of participants in each clinical trial, along with the average patient weight, dose size and the number of doses required by each patient.

An overproduction factor was also assumed, reflecting the necessity to overproduce material to account for manufacturing uncertainties and non-clinical uses (e.g. stability testing). To reflect the increase in manufacturing confidence and decrease in uncertainty as the drug moves along the development pathway, this overproduction factor was halved at Phase III manufacturing. Due to the small demands encountered at early phases, manufacturing for Phase I and II clinical trials was assumed to occur together. For example, the corrected demand for mAbs was calculated as 0.1kg for Phase I and 3.9kg for Phase II (as reflected in

Table 4.4), however as the manufacturing for both phases was combined, the overall manufacturing demand was assumed to be 4kg at a scale of 2,000L.

The data for pre-clinical or regulatory review manufacturing material has not been defined in **Table 4.4**, as they were not calculated in the same way as Phase I, II and III. As outlined by Nie (2015) through personal communication with industry, it was ascertained that 0.5kg is a typical target demand for pre-clinical manufacturing, hence this value was also used here, at a manufacturing scale of 250L. In the case of regulatory review material, manufacturing that took place at this phase served purpose for PPQ, featuring 3 engineering runs or batches to display reproducibility and compliance with cGMP manufacturing to the regulatory authorities. As it was assumed the same manufacturing scale and process is used for PPQ as for Phase III, the cost of a Phase III batch was used to generate the cost of PPQ runs.

Table 4.4 Key manufacturing inputs for the protein process economics model

Clinical phase	Trial duration (years)	Number of trial participants	Doses per patient	Manufacturing scale (L)	Demand (kg)		Corrected demand (kg)[1]	
Phase I	2	40	1	2,000	0.025	0.025	0.1	0.1
Phase II	2	200	13	2,000	1.6	0.6	3.9	1.6
Phase III	3	2,000	26	12,000	32	13.6	40	17

Note: the division in the demand and corrected demand columns represents the outputs for mAbs (first column) and ADCs (second column).

[1] Corrected demand includes an overproduction factor applied to the demand. 250% was used for Phase I and II, whilst 125% was used for Phase III.

4.4.1.2.2 Cell and gene therapy model

In the case of CGTs, the modalities under consideration were AAVs and CART cells. Assuming viral transduction of the CART, it was also necessary to consider the lentiviral vector component within the CAR T manufacturing cost models. The models described in Comisel et al. (2021) and Lyle et al. (2023) were used to generate COG values for both lentiviral vectors

and AAVs. Similarly, for CAR T cells, the economics models were sourced from Pereira Chilima (2019). In comparison to proteins, the number of trial participants for CGTs were assumed to be far smaller, characterised further by a smaller manufacturing scale at each phase. These relatively small trials are typical for CGTs as a whole. The demand was calculated by assuming a dose size for each modality. 7×10^{14} vg/dose was assumed for AAVs, reflecting that of marketed product Zolgensma, where the per kg dose is 1×10^{14}, however factors in an average patient weight of 7kg (this figure is small due to prevalence of SMA in infants). Similarly for CAR T products, the dose size was drawn from available market data and was placed at 2.5×10^{8} CAR T cells, the same as Yescarta (Kite Pharma, CA, US). In the case of the lentiviral vectors for transduction of the CAR, the dose size was not assumed and was instead calculated within the CAR T economics model. This allowed for an accurate determination of the required quantity of lentivirus in TUs, which was subsequently input into the lentiviral vector process economics model. AAV titres were assumed to be constant across phases, in comparison to mAbs and ADCs. This assumption was based upon that reported in Hassan et al. (2016) and Comisel et al. (2021b) and supported through industrial discussion. A value of 6×10^{13} vg/L was used, corresponding to that reported in Lyle et al. (2023).

For pre-clinical material, the equivalent of 5 patient doses of each modality were assumed to be necessary. Though no human volunteers are involved in pre-clinical trials, the number of doses was used as a means to express the demand for CGTs throughout this chapter and hence calculate the corresponding COG values. Additionally, the number of PPQ batches was assumed to be 3.

Table 4.5 Key manufacturing inputs for the viral vector and CAR T process economics models.

Clinical phase	Trial duration (years)	Trial participants (#)	Doses per patient	Manufacturing scale (L)	Demand (doses)	Corrected demand (doses)
Phase I	2	30	1	250 / Integrated USP and DSP	30	75
Phase II	2	50	1	250 / Integrated USP and DSP	50	125
Phase III	3	150	1	1,000 / Integrated USP and DSP	150	188

Note: the first entry in the manufacturing scale (L) column is the bioreactor volume for viral vectors and the second represents the manufacturing system used for CAR T products (integrated USP and DSP is commercially recognised as the Miltenyi Prodigy).

4.4.1.3 Clinical trials

It was reported in previous CMC budgeting work undertaken by Farid et al. (2020) and by knowledge of the increasingly larger participant pool required as drug development progresses, that mAb clinical trials represent the largest proportion of the overall out-of-pocket cost, with around 15 - 20% coming from CMC activities. Previously, the cost of clinical trials was estimated from an array of studies which published out-of-pocket costs for mAbs. In these cases, the process development and manufacturing costs were subtracted from the total R&D cost to ascertain the portion dedicated to clinical trial activities. In contrast, in this chapter, an approach more similar to that carried out in Hassan et al. (2016) and Comisel et al. (2021a) was employed, whilst using previously reported clinical trials costs as benchmarks. In these cases, the cost of clinical trials was estimated by using a trial cost per patient, along with the number of patients involved in each trial. However in contrast to Hassan et al. (2016) and Comisel et al. (2021a), an updated value for the trial cost per patient (specifically for oncology) was sourced from Mikulic (2021). This study placed the maximum value for oncology trials at around $150,000 per patient. Utilisation of this value with the perceived mAb patient populations resulted in similar trials costs to that reported in Farid et al. (2020), providing further motivation to selecting this cost per patient. In the case of CGTs, due to the numerous

uncertainties that still exist in comparison to protein therapeutics, including a lengthy patient follow-up period of up to 10 years, a trade-off was defined that the trial cost for CGTs would be higher than mAbs and ADCs. This value was placed at $1,000,000 per patient (C. Mason, UCL, UK, personal communication, 2022).

4.4.1.4 Transition success rates

The success rates associated with each clinical phase in the development lifecycle are displayed in **Table 4.6**. This provides a range for each phase, for the sensitivity analysis conducted in the case study, where the first number represents the worst-case scenario, the middle value the base-case and then the best-case scenario. The success rates in general are vital metrics in characterising the risk of drug failure and thus when applied to phase costs, provide an accurate representation of the excess that must be allocated to budgets to ensure market success. For mAbs, there is extensive published data for the success rates and these have been compiled in **Table B1** in Appendix B. When studying the more novel modalities relative to protein products, literature data is scarce, however the range in **Table 4.6** has similarly been assumed from a smaller selection of literature sources (outlined in **Table B1**). The data in **Table 4.6** evidenced the wider range of transition success rates for CGTs over mAbs, due to their relative infancy on the market.

To supplement the previously mentioned sensitivity analysis, the success rates by indication were also considered. Within this part of the case study, the indications were selected based upon their commercial relevance to the modalities being studied, i.e. common disease areas targeted or where market success has been shown. For this study, the indications selected were haematology, ophthalmology, oncology and neurology / central nervous system (CNS) (see **Table B2** in the Appendix B for data on success rates by indication).

Table 4.6 Clinical success rates for each modality by phase and the corresponding number of projects required overall.

Modality	Phase I	Phase II	Phase III	Reg. review	LOA from Phase I [a]	No. of projects
mAb	54%, 54%, 62%	34%, 34%, 36%	63%, 70%, 70%	91%, 91%, 91%	10.5%, 11.7%, 14.2%	13.8, 12.4, 10.2
ADC	54%, 54%, 57%	34%, 34%, 37%	54%, 63%, 63%	91%, 91%, 91%	9.0%, 10.5%, 12.1%	16.1, 13.8, 12.0
AAV	51%, 51%, 80%	34%, 34%, 66%,	21%, 64%, 75%	90%, 90%, 91%	3.3%, 10.0%, 36.0%	44.2, 14.5, 4.0
CAR T	51%, 68%, 80%	34%, 40%, 66%	21%, 70%, 75%	90%, 91%, 91%	3.3%, 17.3%, 36.0%	44.2, 8.4, 4.0

[a] LOA = likelihood of approval from Phase I

Note: Three numbers provided that represent the worst-case: base-case: best-case values

4.4.1.5 Durations

Each activity within the development timeline is associated with a duration, some assumed from that reported in previously published studied or through industrial discussion (particularly those associated with process development or clinical trial activities). Process development durations were previously defined in **Tables 4.2** and **4.3** and were significant in determining the FTE years required for these activities. Furthermore, manufacturing for each phase and modality were calculated within each process economics model based upon the number of batches in the year and hence the facility utilisation. Finally, clinical trial durations were assumed from multiple published sources (DiMasi et al., 2016; Farid et al., 2020; Paul et al., 2010), as well as through industrial discussion. For comparative purposes, these durations were set to be equal across modalities studied and have been presented in **Tables 4.4** and **4.5**. Pre-clinical and regulatory review durations were assumed to be 1 and 2 years respectively. The clinical trial durations were not directly used in estimating the total out-of-pocket costs, however played a significant role in determining the capitalised R&D cost. The capitalised cost represents the overall out-of-pocket cost adjusted for the cost of capital (assumed to be 11%) and to factor in discounting (time value of money). Generation of the capitalised equivalents was achieved through consideration of trial timings and the assumed cost of capital.

As is the nature of drug development, many activities are interdependent with one another, thus for a particular clinical trial to proceed, the process development and manufacturing must come first in order to supply said trial. In certain cases, there can be an activity overlap, such that one may finish after the next stage has started. This was previously defined as activities being conducted “at risk” and refers to the conductance of the $(n+1)^{th}$ process development or manufacturing stage before completion of the n^{th} clinical trial. This means the activities conducted in parallel to the clinical trial inherit the risk of failure and quantitatively results in the success rates associated with the n^{th} trial being used to amplify the budgets associated with the next activity.

4.5 Results and discussion

The framework described in Section 4.4 was used for an in-depth analysis of the process development, manufacturing and clinical trials costs for mAbs, ADCs, AAVs and CAR T cells. These were evaluated across development phases, ultimately deriving the total out-of-pocket costs for each modality to ensure a market success. The contribution of process development and manufacturing to the R&D costs was estimated from each modality. The impact of different clinical success rates on the budgets required for each modality was explored using a sensitivity analysis.

4.5.1 What is the CMC contribution towards the R&D cost?

It has become increasingly significant to define the contribution of process development and manufacturing activities (collectively referred to as CMC activities) to the total out-of-pocket cost (i.e. R&D cost). These activities underpin the supply of material to the clinical trials and as a result, estimating CMC budgets early on is critical to ensure appropriate allocation and to avoid delays. The drug development lifecycle model was used to determine the overall out-of-pocket cost per market success for companies focusing on a single modality type. The model outcomes are shown in **Figures 4.3** and **4.4** on a case-by-case basis for mAbs, ADCs, AAVs and CAR T cells, along with the cost breakdowns across the development pathway. This initially assumed an equal success rate from Phase I to approval for each modality under consideration of 12%. **Figures 4.3** and **4.4** highlighted the CMC cost as a percentage of the total R&D budget, ranging from 19 – 30% for mAbs and ADCs and 30 – 42% for AAVs. Overall, mAbs were shown to require the smallest R&D budget, offering a 7 – 23% out-of-pocket cost reduction over AAVs, ADCs and CAR T cell therapies. These cost differences were largely driven by both process development and manufacturing costs, highlighting a greater development effort and overall cost of goods required to commercialise ADCs, AAVs and CART cells over mAbs.

a)

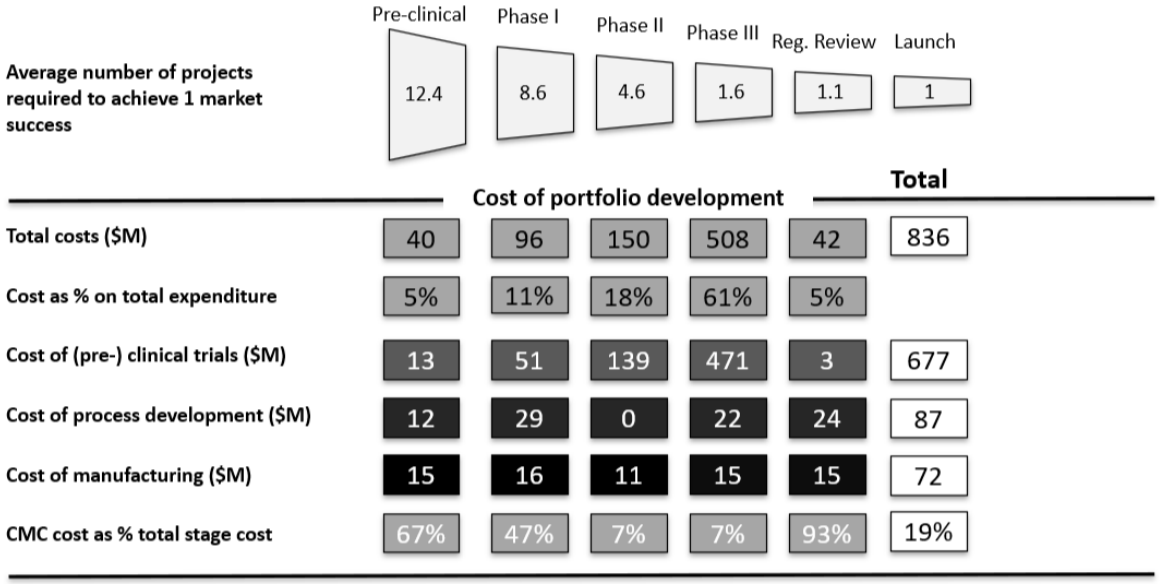

b)

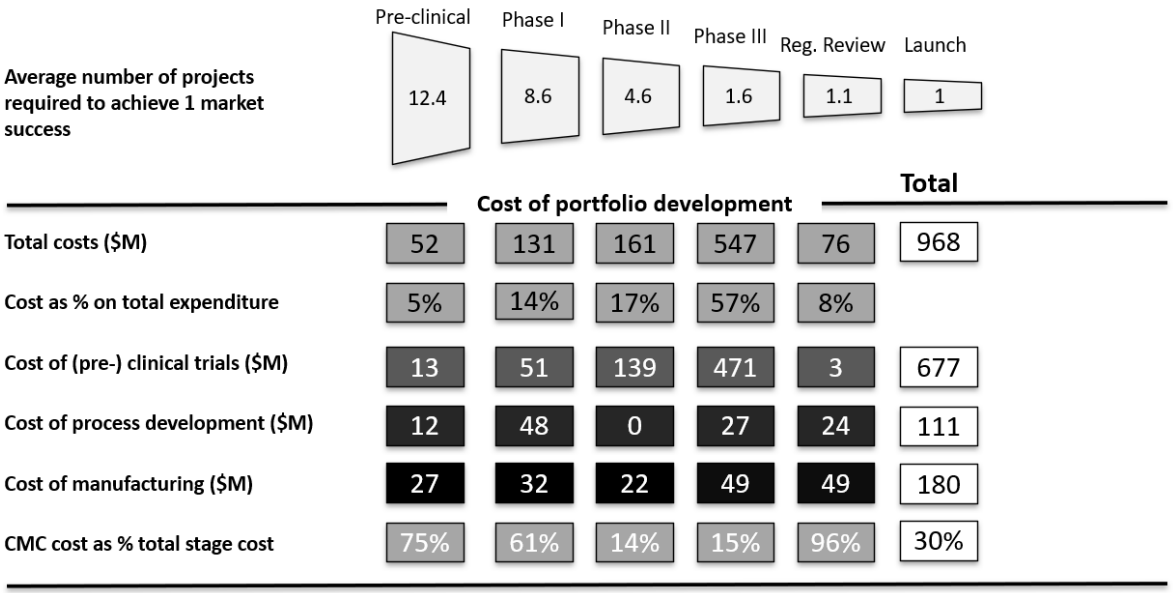

Figure 4.3 Out-of-pocket cost schematic depicting the development pathway and cost breakdown by development activity and phase for **a)** mAbs and **b)** ADCs. The clinical success rates (overall rate of 12% assumed for **a)** and **b)**) were used to calculate the number of projects required at each stage of the development pathway to achieve a market success. The process development and manufacturing activities were costed at-risk based on the number of projects. The number of projects at each phase are shown about the cost breakdowns. [Style of figure presentation adapted from Nie (2015) and Farid et al. (2020)].

a)

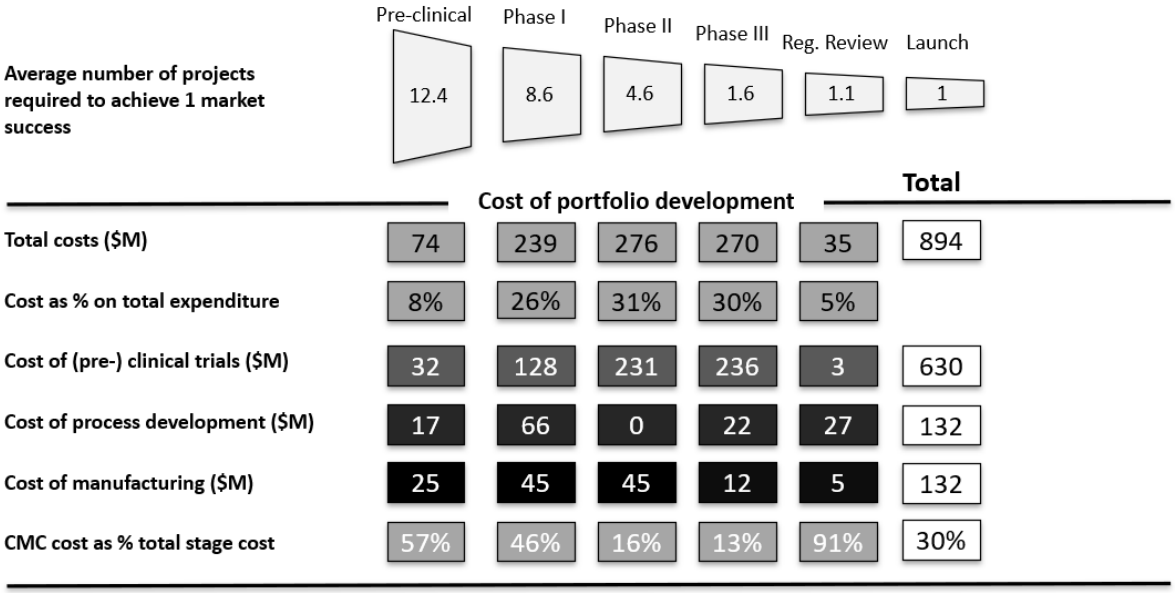

b)

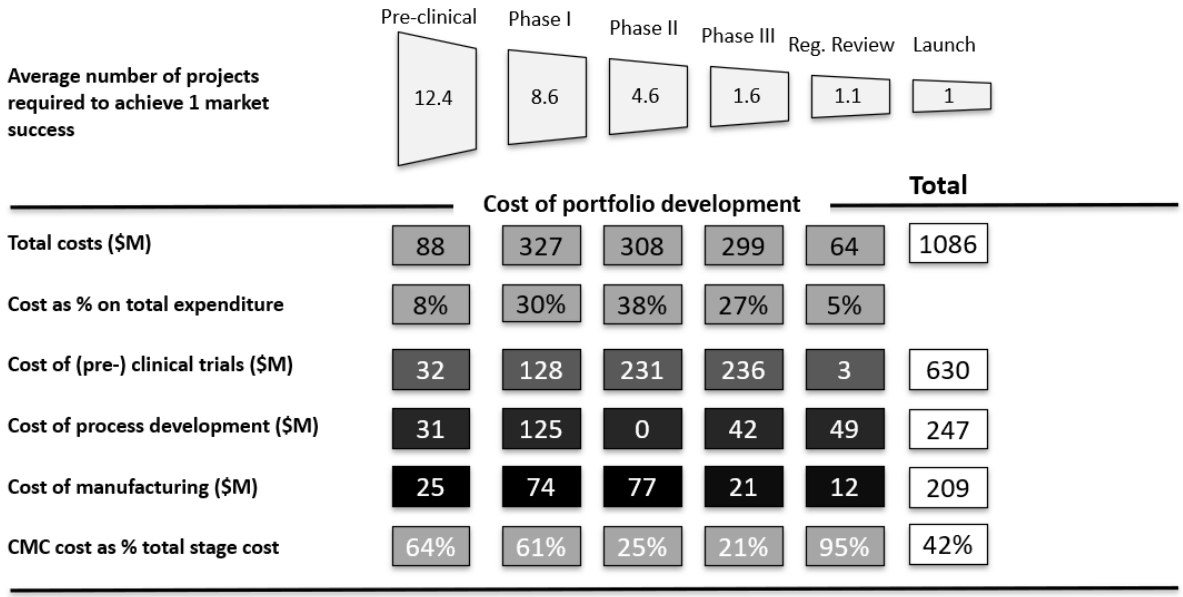

Figure 4.4 Out-of-pocket cost schematic depicting the development pathway and cost breakdown by development activity and phase for **a)** AAVs and **b)** CAR T cells. The clinical success rates (overall rate of 12% assumed for **a)** and **b)**) were used to calculate the number of projects required at each stage of the development pathway to achieve a market success. The process development and manufacturing activities were costed at-risk based on the number of projects. The number of projects at each phase are shown about the cost breakdowns. [Style of figure presentation adapted from Nie (2015) and Farid et al. (2020)].

Looking in greater detail, the total out-of-pocket cost per success was determined to be $836 million, $968 million, $894 million and $1,086 million for mAbs, ADCs, AAVs and CAR T products respectively for an overall clinical success rate of 12%. The capitalised equivalents were found to be $1,576m, $1,833m, $1,893m and $2,311m respectively. The trade-off between mAb and ADC trials sizes versus the higher clinical trial cost per patient assumed for CGTs resulted in a similar overall trial cost between modalities. As a result, CMC cost contributions was shown to be a key driver in mAbs achieving the smallest out-of-pocket costs. This is further explained in **Figure 4.5**, which delineates the CMC cost breakdown for each modality and the reduction in both process development and manufacturing costs for mAbs over other therapy areas. Process development budgets were shown to range from ~$90 – 250 million across modalities, whereas manufacturing costs were estimated between ~$70 – 210 million. For process development, early efforts were assumed to be higher for the novel therapies relative to the more standardised mAb, hence driving up process development costs for AAVs, ADCs and CART in earlier phases. This was particularly evidenced by the assumption regarding an increase in Phase I product development scientists over mAbs, as displayed in **Tables 4.2** and **4.3.** Across modalities and per project success, Phase I was shown to dominate overall process development costs, with a requirement for companies to allocate $29 million for mAbs, $48 million for ADCs, $66 million for AAVs and $125 million for CAR T, driven by the number of projects required in earlier phases. This exemplifies the near 5-fold difference in early-phase process development budget required to produce a CART over a mAb product. Per project costs for Phase I did not exceed that of the later phases, however they become dominant when considered on a per success basis, attributable to the higher number of theoretical projects required at Phase I. This is further evidenced by the “at-risk” nature of cost analysis conducted here, which as previously discussed involves costing CMC activities for a particular phase (e.g. phase $n+1$) based on the number of projects in the parallel trials for the previous phase (e.g. phase n). In the case of Phase I, the pre-clinical number of projects was therefore considered.

Regarding cost of goods, mAbs attained the smallest manufacturing budget overall compared to other modalities. The extent of manufacturing differences were evidenced during Phase I, where the patient populations across modalities did not differ significantly (40 patients for proteins and 30 for CGTs), yet the budgets exhibited variations. A breakdown of the cost of goods across modalities can be found in the **Figure B1** in Appendix B. This highlighted the key differences in the major COG categories. The higher manufacturing budgets for ADCs and AAVs compared to mAbs can be attributed to a higher materials cost (i.e. reagents and consumables). More specifically, the ADCs have a higher DSP material cost given the extra conjugation steps and the AAV have a higher USP material cost given the pDNA component required for transient transfection. On the other hand, the COG breakdowns for CAR T products highlighted a greater contribution from labour and indirect costs over materials. This can be attributed to the scaling-out process employed for autologous CAR T, requiring parallel equipment units and operators. Additionally, within the analysis, the manufacturing of biological components (e.g. lentivirus and associated pDNA) required as raw materials for CAR T production was assumed to be outsourced and hence, a premium was applied to costs due to the use of a CMO.

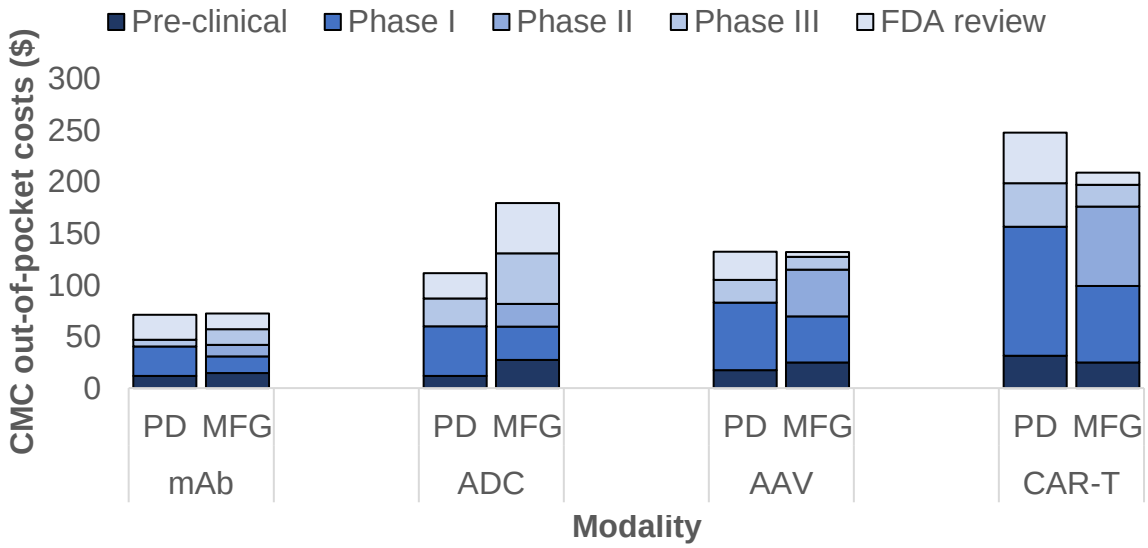

Figure 4.5 CMC out-of-pocket cost breakdown per success for each modality. The overall success rate was assumed to be equal across modalities (at 12% LOA from Phase I). PD = process development, MFG = manufacturing.

4.5.2 What is the impact of assuming different success rates between modalities?

The previous analysis fixed the clinical success rates across modalities. However, recent data has suggested differences between these values (QLS, 2021), with overall clinical success rates estimated as 12%, 10.5%, 10% and 17% for mAbs, ADCs, AAVs and CAR T respectively (also shown in **Table 4.6**). As a result, the impact of assuming different success rates across modalities was investigated and the cost breakdown plotted in **Figure 4.6**. This provided the categorisation of costs by activity (i.e. process development, manufacturing and clinical trials) for each modality and presented both transition success rate scenarios for comparative purposes. This highlighted the impact of success rates, shown by the change in modality ranking with respect to the overall budgets between **Figure 4.6 a)** and **b).** Additionally, **Figure 4.6** indicated the influence of clinical trials cost on the total budgets, which was found to have the greatest contribution in the case of each modality.

The trade-off between proteins and CGTs in terms of clinical trial cost per patient versus patient population yielded similar trial budgets overall. Larger clinical trials were assumed in the case of mAbs and ADCs, particularly evidenced during Phase III, where the number of trial participants was assumed to be 2,000 versus 150 in the case of AAV and CAR Nevertheless, despite this difference, overall clinical trials costs were shown to be similar between modalities, with the CGT cost only slighter smaller than the protein therapies ($630m for CGT and $677m for proteins). This was attributable to assumptions regarding the average per patient trial costs. Though trials were small, the CGTs per patient trial cost was estimated at $1,000,000 versus $150,000 for mAbs and ADCs. The near 7-fold difference in this value was a key driver in the ultimate similarities in clinical trials cost between modalities. The assumption of a higher trial cost per patient for CGTs arose due to the more stringent and time-consuming follow-up measures perceived necessary versus that of a mAb or ADC. In general, long-term effects of using CGTs are still yet to be fully addressed and as such, this follow-up period may be longer.

Generally, the half-life of a protein therapy is a matter of days, contrary to CGTs, which can persist longer in the patient. This results in a shorter follow-up time for protein therapeutics.

Furthermore, **Figures 4.6 a)** and **b)** characterised the effect of clinical success rates upon modality ranking in terms of R&D budget. **Figure 4.6 a)** assumed the same overall LOA from Phase I across modalities, whereas **4.6 b)** presented the case with differences, with values sourced from (QLS, 2021). This yielded a distinct change in modality ranking with respect to out-of-pocket cost. For example, the 17% overall success rate in **Figure 4.6 b)** for CAR T resulted in a similar budget to mAbs, thereby achieving the second smallest budget instead of the largest as shown in **4.6 a).** Additionally, assuming the same overall LOA from Phase I resulted in AAV products achieving the smallest budget behind mAbs. This was shown to change when assuming an overall success rate of 10% for AAVs, as it required a higher budget than both mAbs and CAR T in this case. The comparison made between the two success rate scenarios further emphasised the significance of clinical success rates in formulating the required budgets and served as an additional motivation to evaluate their impact further in the subsequent sensitivity analysis.

4.5.3 Sensitivity analysis

Typical clinical success rates are well-documented for mAb products, with numerous studies outlining estimations of the LOA from Phase I. Less information has been reported in terms of success rates for ADCs, AAVs and CAR T cells and as such, the range of values reported in the literature have a far wider distribution than that for mAbs.. Additionally, success rates are not only reported by modality group but frequently by indication, which is useful when considering modalities that may be commonly used in targeting certain disease areas. As a result, the sensitivity analysis conducted in this study evaluated how the cost of development changed when considering different success rate profiles, these driven by both modality type and indication.

a)

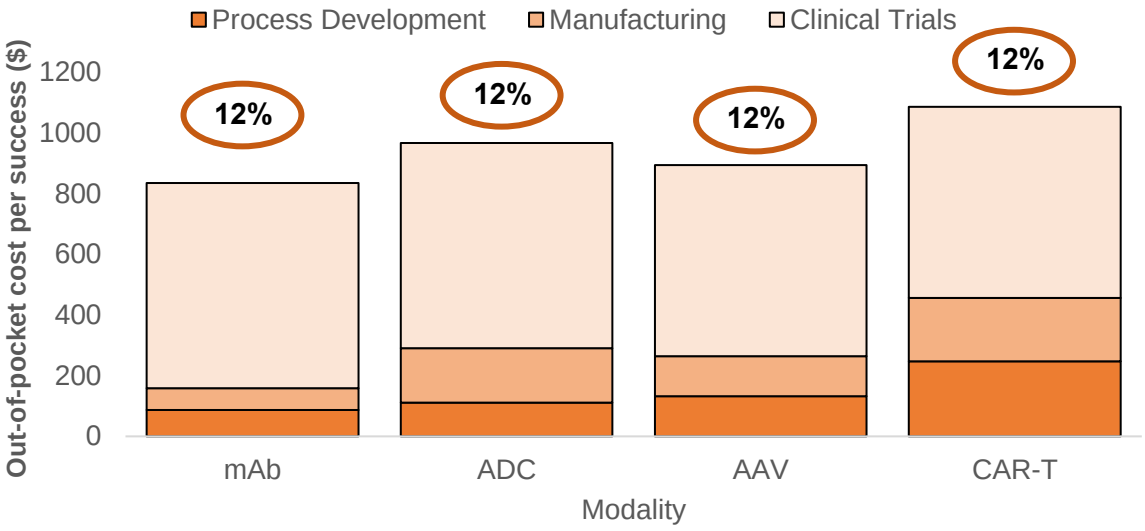

b)

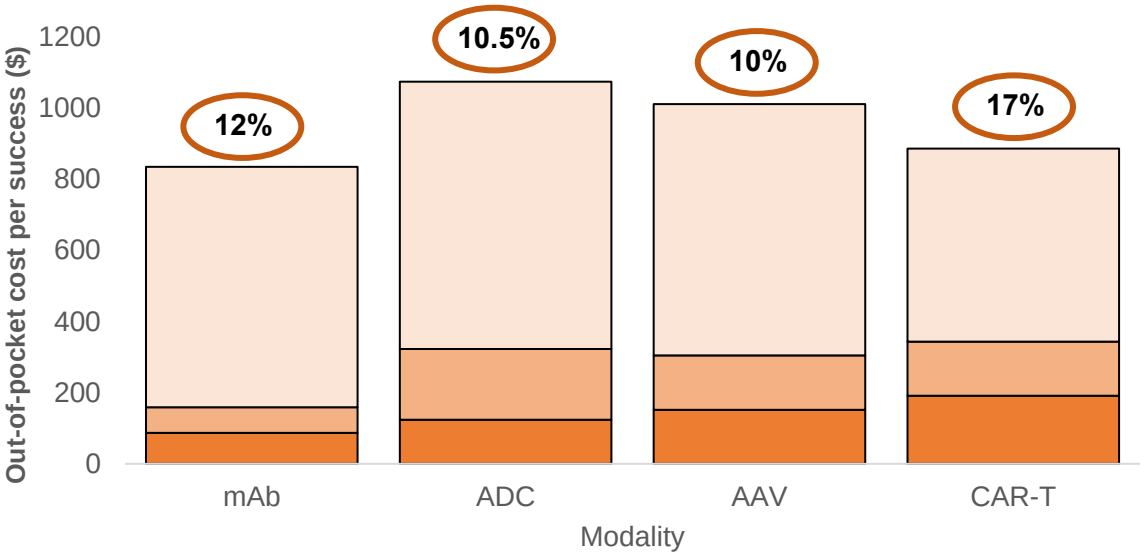

Figure 4.6 Out-of-pocket cost breakdowns per success when **a)** the same clinical success rates were assumed across modalities and **b)** different clinical success rates were assumed for each modality, sourced from (QLS, 2021).

4.5.3.1 How does the success rate by modality impact R&D budgets?

As dictated in previous sections, differences in the overall LOA from Phase I had a significant impact upon the budget ranking across modalities and as a result, their attractiveness in terms of development expense. A sensitivity analysis was first conducted assuming success rate values on a modality basis, with the distributions displayed in **Table 4.6**, highlighting the best, base and worst-case values. **Figure 4.7** presents the resulting heatmap from considering these three success rate scenarios for each modality. Furthermore, the row labelled base in the heatmap in **Figure 4.7** represents the case presented in **Figure 4.6 b)**. The results reflected the impact of the wide range of success rates associated with CGTs, with higher best case and lower worst-case values determined over mAbs and ADCs.

If the success rates dropped to the worst-case profile for each modality, AAV and CART would require a maximum of $3.2 – 4.2bn in R&D investment to bring a single product to market, whilst mAbs and ADCs would be of the order of approximately $1bn (**Figure 4.7a**). Additionally, the worst-case costs were 8% higher than the base case for mAbs and 20% higher for ADCs (**Figure 4.7b**). In relation to the CGTs, AAVs and CAR T out-of-pocket costs under the worst case profile were found to increase by 2.5- and 2.9-fold respectively over the base-case. Conversely, for best-case success rate profiles, mAbs and ADCs were subjected to a 7 – 9% reduction in budget as a result of the increased Phase I and II success rates. As described in **Table 4.6**, the best-case was assumed to be far more optimistic for CGTs, mirroring that reported in Hassan et al. (2016) and yielded a 42% cost reduction for AAVs and 40% for CAR T cell products.

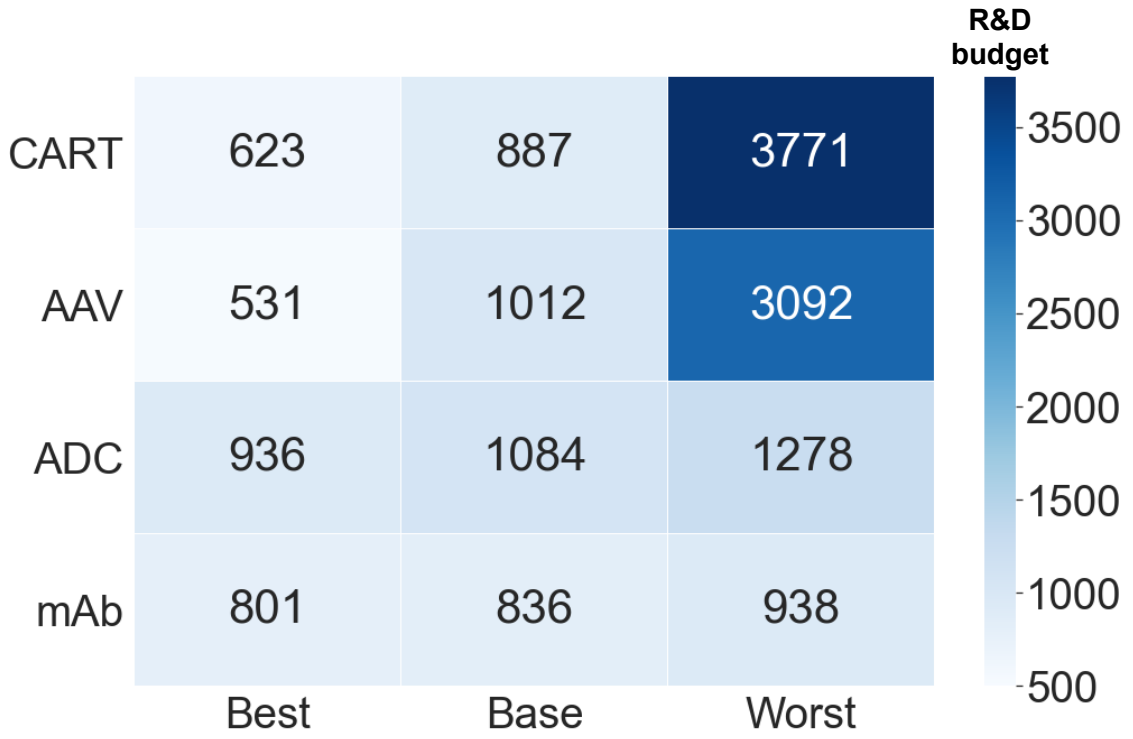

Figure 4.7 Sensitivity analysis output when considering success rate scenarios by modality type. The y-axis refers to the modality under consideration and the x-axis represents what success rate scenario was being considered. Each box corresponds to the total out-of-pocket cost per success for the given scenario. The ladder on the right-hand side is a Python 3.8 generated scale for the heatmap, where the darker shading relates to higher costs and lower costs for lighter shades. The best, base and worst scenarios reflect the data in **Table 4.6**, where the base case refers to the same used in **Figure 4.6 b).**

In summary, the analysis indicated the uncertainty in the success rates for each modality, reflecting the greater experience industry has in bringing mAb products to market over the more nascent CGT products. The wider success rate range reported for AAVs and CAR Ts reinforced the risk associated with estimating R&D costs, particularly highlighted by the 5 – 6-fold difference in budgets between the best- and worst-case scenarios. Particularly relative to mAbs, the magnitude of this range can be linked to the relative nascency of the CGT field, where a great deal of uncertainty exists. It is also important to note that some industrial players may have experience solely in CGT products, hence may achieve higher rates of success due to the experience gained and the ability to direct all process development efforts towards one modality group.

4.5.3.2 How does the success rate by indication impact R&D budgets?

In general, a breadth of disease areas are able to be targeted by the modalities under consideration in this study. These indications are also characterised by different overall success rates and as a result, **Figure 4.8 a)** presents the sensitivity analysis where success rate was considered on an indication basis. The indications were selected based on what was deemed most relevant to the modalities being studied. The indications were ordered by descending overall success rate.

Haematology had the highest overall LOA from Phase I rate, resulting in lower R&D budgets across modalities. The correlation between success rate and budget remained consistent across indications and modalities, with an exception to this shown for mAbs and ADCs between oncology and neurology (with success rates of 9.3% and 7.5% respectively). Despite a higher success rate for oncology, the neurology budgets for mAbs and ADCs were shown to be marginally smaller. This is attributable to the distribution of success rates across phases differing between indications. For example, the lower Phase III success rate in oncology results in 2.3 projects at this stage required over 2.1 for neurology/CNS. This difference results in the Phase III budgets for oncology being higher than neurology/CNS. This trend was only observed with mAbs and ADCs, however. This may be linked to the saturation of oncology drugs in either clinical trials or on the market, indicated by the large number of candidates assessed in **Table B1** in the Appendix. With a number of competitors, these drugs must highlight an improvement over existing products in order to progress.

The impact of cost distribution across phases is evidenced by **Figure 4.8 b)**. Phase III costs represent a significant portion of the total out-of-pocket cost, particularly for mAbs and ADCs. This suggests that a higher number of Phase III projects impacts the total cost more significantly than the lower success rates in Phases I and II particularly where protein therapeutics are concerned.

Significantly, the modality requiring the smallest R&D budget varied across indications. AAV yielded the smallest budget in both haematology and ophthalmology, however mAbs were

found to be optimal in the case of oncology and neurology. This change can also be traced to the varying individual phase success rates, as well as the cost breakdown by phase. To better explore these elements, the ratio of the number of projects required in Phase I to Phase III was computed for each indication and is presented in **Figure 4.8 a).** Here, the base case from earlier analysis was included for further evidence. This showed that in cases where the ratio of Phase I projects to Phase III was higher, mAbs required the smallest overall budget. At smaller ratios, AAV instead yielded the smallest costs. The significance of this derived ratio is explained by **Figure 4.8 b),** reflecting the distribution of out-of-pocket costs for each modality across phases. mAbs and ADCs were shown to be dominated by Phase III costs, whereas AAVs and CARTs had a more even distribution of costs across Phase I, II and III. Therefore, in cases where the Phase I: III ratio was higher (translating to a large project requirement in Phase I), AAVs were less favourable as they had a larger proportion of costs incurred in Phase I and II than mAbs. Similarly, when the ratio was smaller, Phase III projects became more significant and hence mAbs and ADCs were less favourable, with 61% of their out-of-pocket cost generated in Phase III.

Further granularity on the change in optimal modality (with respect to R&D budgets) across success rates was highlighted in **Figure 4.9.** This assessed the overall out-of-pocket cost for each modality in 1% increments of success rate to identify the critical point at which the modality with the smallest budget changed. It must be noted that the previously analysis demonstrated the impact of success rate distribution across phases, e.g. two indications may share the same LOA from Phase I success rate but yield different budgets if there are variations in how the rates were distributed. Thus, for the purpose of the data used in **Figure 4.9**, the distribution of success rates across phases for the base case (54%, 34%, 71%, 91% which resulted in a 12% LOA from Phase I) was used as a baseline in determining all other increments. As is the assumption for the sensitivity ranges defined in **Table 4.6,** in all cases of **Figure 4.9** where the LOA from Phase I was greater than 12%, higher success rates were equally assumed for Phase I and II and the Phase III value remained constant. Conversely,

for LOA from Phase I values in **Figure 4.9** that are lower than 12%, Phase I and II rates remained constant and Phase III rates were lowered accordingly.

At the lower end of the success rate range evaluated, the ranking of modalities in order of smallest budget was mAbs, AAVs, ADCs and CAR T. In parallel to the results generated in **Figure 4.8,** the optimal switched from mAbs to AAVs at a success rate of 16%. This similarly occurred for ADCs and CAR T cells at ~17.5%. This is significant in the context of the uncertainty associated with clinical success rates and provides a mapping of the various scenarios encountered along the development pathway. It may further govern the extent to which a company may favour the development of a protein therapeutic over a CGT. Having said this, additional factors must be considered when considering the development of a specific modality group. This analysis only sought to estimate the R&D budgets under varying risk scenarios and has not yet included the impact of revenues and profitability on the attractiveness of each modality or the consideration of portfolios where mixes of proteins and CGTs are encountered. These latter points are addressed in the next chapter.

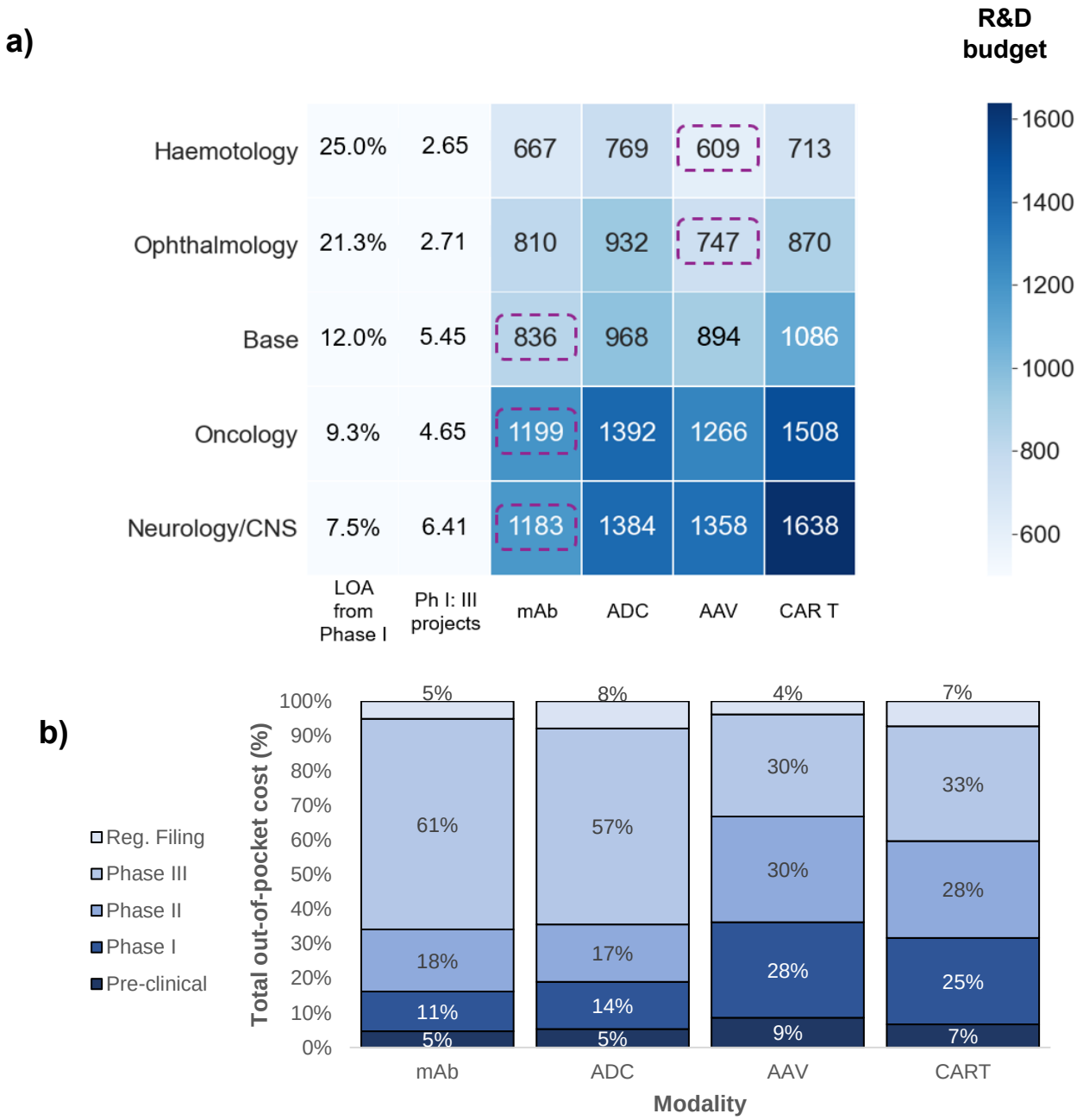

Figure 4.8 a) The sensitivity analysis output for each indication. The x-axis gives key inputs (LOA from Phase I and Ph I: III projects) and the modalities under consideration. The optimal modality in terms of budget is highlighted with the dotted contours around corresponding budget values. The y-axis represents the indication under consideration. The ladder on the right-hand side is a Python 3.8 generated scale for the heatmap, where the darker blue relates to higher costs and lower costs for lighter shades of blue. Each box corresponds to the total out-of-pocket cost per success for the given scenario. The base case from **Figure 4.4** was used as a reference point, **b)** total out-of-pocket cost distribution across all phases for each modality. The bars are annotated with the specific percentage contributions.

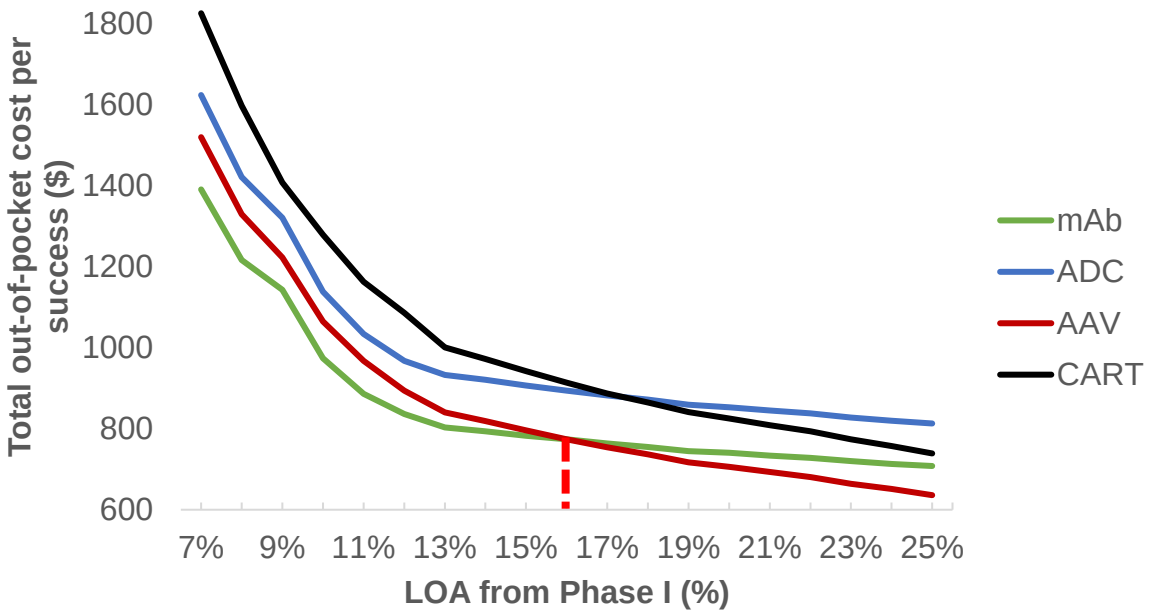

Figure 4.9 Change in total out-of-pocket cost with overall LOA from Phase I success rate across modalities. The red dotted line represents the critical overall success rate at which the optimal in terms of budget changes.

4.6 Conclusion

This chapter provided estimates for development budgets across modalities, in particular highlighting the portion represented by CMC activities. The drug development model outlined the division of activities into those concerning process development, manufacturing and clinical trials. The application of success rates and their impact on the budgets was also described. Modality specific assumptions were provided to highlight the trade-off between therapeutic groups, particularly with respect to manufacturing scale and trial size.

The results highlighted that for the base-case clinical success rates, mAb products achieved the smallest R&D budgets, driven by lower CMC costs compared to CGTs. This was shown in both cases where firstly the success rates were set to be equal for all modalities and in scenarios where they were assumed to be different. Significantly, the trade-off between a higher clinical trial cost per patient for CGTs with smaller patient pools versus a lower per

patient cost coupled with larger trials for protein products yielded similar trial budgets of $630m for AAVs and CAR T and $677m for mAbs and ADCs in the base case. Additionally, ADC, AAV and CAR T products were found to have CMC contributions towards the total out-of-pocket cost upwards of 30%, compared to the 19% found for mAbs.

Introduction of the sensitivity analysis on a modality basis highlighted the wider range of R&D budgets found for CGT products over protein therapeutics. In contrast, the sensitivity analysis by indication success rate suggested the optimal modality changed across disease area. Further analysis indicated the critical success rate at which the modality with the smallest required budget switched to AAVs over mAbs. This value was found to be 16%. This part of the study was significant in the context of current AAV market success. Higher success rates were shown to be associated with ophthalmology and haematology, which tend to be common disease areas commercially targeted with AAV products, emphasising the drive from industry.

In summary, this chapter provided estimates of the key expenses incurred across the development pathway. Risk was applied by adjusting stage costs based on the number of projects expected at each stage based on the clinical success rates; this was a static approach. As a result, the drug development model defined in this chapter underpinned the portfolio management and capacity sourcing work presented in the next chapter, where risk was further analysed in a more dynamic environment, such that drug failures were not only considered from a cost perspective, but also in terms of capacity planning.

5 Portfolio optimisation and capacity planning for mixed modality portfolios

5.1 Introduction

The previous chapter sought to integrate the process economics framework defined Chapter 3 with a drug development cost model to estimate R&D budgets for mAbs, ADCs, AAVs and CAR T products. This additionally provided benchmarks for the distribution of costs across development phases, in particular highlighting the contribution from CMC activities. Within these studies, biopharmaceutical development-related expenses were considered, namely process development, manufacturing and clinical trials costs, which realistically constitute the primary outgoings in a company's cash-flow. However, the work up to this point did not factor in revenues and ultimately the profitability (i.e. NPV) of each modality. Additionally, Chapter 4 considered each modality on an individual basis, without examination of the whole biopharmaceutical portfolio and a diversified pipeline to potentially be incorporated. The interaction between feasible portfolios and budget and capacity restrictions when bringing a prospective pipeline to market were also not considered to this point.

By nature, biopharmaceutical portfolios are often diversified in terms of modality type and capacity strategy employed for individual product candidates. The dynamic nature of a drug's trajectory throughout the development cycle and hence interaction with other candidates introduces greater uncertainties in addition to those described in Chapter 4. These included understanding the impact of budget constraints on drug selection and how capacity can be optimally allocated towards the overall portfolio. Significantly, Chapter 4 indicated the importance of success rates in governing overall R&D budgets and hence productivity and was used to characterise the risk of drug failure within the drug development lifecycle. These clinical success rates not only influence development expense, but also have dynamic implications upon drug selection, budget allocation and utilisation of capacity. To date,

published studies relating to portfolio management and capacity planning have focused primarily on drug selection or facility scheduling for protein therapeutics and have quantified risk (i.e. success rates) on solely an economic basis, i.e. to costs throughout the cash-flow, to generate a risk-adjusted profitability. As such, there has been no focus directed towards drug selection and capacity sourcing when mixed-modality portfolios are considered, in particular proteins and CGTs. Additionally, the work in this case study provides the first consideration of risk on a dynamic basis, by incorporation of a probabilistic simulation to determine drug success or failure, which is factored in to both the cash-flow and capacity decisions.

The case study presented in this chapter reconciles the multiple model frameworks outlined in Chapters 3 and 4 and integrates them with a discounted cash-flow model to evaluate the profitability of a range of biopharmaceutical portfolios. This was further extended to include a stochastic GA-based optimisation tool for assessing the most favourable portfolio mixes and capacity sourcing strategies (i.e., in-house, outsourcing or building a new facility), and considered the impact of drug failures within a dynamic environment by use of a Bernoulli-event based simulation. The significance of large-scale portfolio selection and capacity management served as the basis for the work outlined in this chapter. This was used to first evaluate batch versus next-generation continuously manufactured protein therapeutics, before considering the introduction of CGTs within the pipeline and hence the impact of portfolio mixes on reward and risk.

The following chapter outlines the portfolio management tool and the case studies arising from its implementation. An overview of the tool and its arrangement with the previously defined models in Chapters 3 and 4 is presented in Section 5.2. Section 5.3 outlines the problem statement and hence setup of the case study the tool was used to address. The results and subsequent analysis are presented in Section 5.4, which highlights both the non-risk and risk-adjusted outputs of the tool for illustrative purposes. Furthermore, the conclusions of the case study are outlined in Section 5.5.

5.2 Model formulation

5.2.1 Problem-specific notation

G number of generations in the optimisation procedure

g a single generation in the optimisation procedure $g \in G$

S_g a population of solutions from generation g

$s_{g,p}$ a candidate solution (chromosome) from the population in generation g, $S_g = \{s_{g,p=1}, \cdots, s_{g,p=P}\}$

N_{d_0} number of drugs in the current portfolio (when time, $t = 0$)

N_{d_f} number of drugs in the final (f) portfolio (when time, $t = f$)

$N_{d_{pipe}}$ number of drugs in the available pipeline

N_{pop} population size

5.2.2 Case study terminology

Table 5.1 Terms frequently used throughout the chapter and their specific definition.

Term	Case study definition
Starting portfolio	The drugs in the company's portfolio at time 0, i.e. before any drug injection is considered
Final portfolio	The drugs in the company's portfolio after the cash-flow duration, i.e. considers all successful drugs from the **starting portfolio**, as well as drugs that were injected and remained successful up until the end of the cash-flow
Pipeline	The pool of drug candidates that could potentially be injected into the portfolio from time 0 onwards. Not all drugs in the pipeline are necessarily injected into each candidate portfolio, hence the portfolio selection problem
Candidate portfolio / candidate solution / "the portfolio"	An example collection of drugs from the **pipeline** that is injected into the portfolio and with the **starting portfolio**, creates the final portfolio. A population of these are evaluated within the portfolio optimisation tool.

5.2.3 Overview

The portfolio optimisation tool can be broadly classified as a stochastic multi-objective optimisation framework and was developed to investigate portfolio-related decisions, namely drug selection and capacity sourcing. This framework can be divided into two parts; simulation and optimisation, which is better illustrated by **Figure 5.1**. The simulation component integrated the models described in Chapters 3 and 4 in order to generate relevant expenses for all drugs in both the starting portfolio and pipeline. These cost outputs were stored prior to initiating the optimisation component within the tool (detail provided in a later section). Stochasticity was introduced via a Monte Carlo simulation conducted on key inputs into the process economics and drug development models, and ultimately produced a distribution of NPVs for each candidate solution, yielding both the mean and standard deviation as objective functions. This Monte Carlo simulation was also conducted on transition success rates in a later part of the study, which served to highlight the risk associated with drug success or failure.

The model was constructed using Python 3.8 and Microsoft Excel. The simulation and optimisation were fully coded using Python, with Spyder being used as the integrated development environment (IDE) for class building and loading assumptions. Jupyter Notebook served as the graphical user interface (GUI) to instantiate objects from each class and run the optimisation algorithm. Its use as a GUI was leveraged to also create an intuitive and user-friendly experience by the addition of widgets, which enhanced interactivity with respect to setting assumptions and algorithm parameters. This feature is further explored later on when discussing the potential for commercialisation of the tool (Chapter 7). Utilising Python as a coding language was favourable in terms of computational time when considering the scope of the problem. As introduced in Chapter 2, the problem required incorporation of a number of complex features, as well as several algorithm runs. Python allowed access to a range of existing libraries with tools for more rapid evaluation. Additionally, Python was used initially in this work (i.e. for the process economics and drug development models) due to its simplified syntax and relatively intuitive nature, hence maintaining this continuity in coding language was

an important factor driving its use in the portfolio optimisation framework, particularly over other languages. Microsoft Excel was used to store all modality specific assumptions, including those required in the process economics and drug development cost models, as well as any general inputs relating to the portfolio. A separate Microsoft Excel database containing characteristics for all drugs considered in the case study (both starting portfolio and pipeline) was also used. These databases were loaded into the portfolio tool through use of a Spyder function that harnessed the capabilities of the Pandas inbuilt Python library and converted the data into a format for use in the GUI.

As previously alluded to, calculations involved in the generation cost data for each drug were computed outside of the optimisation loop (contained within the red contours in **Figure 5.1**). Cost data such as development related expenses (e.g. process development, manufacturing and clinical trials costs) were calculated from the integrated process economic and drug development models outlined in Chapter 3 and 4. These were stored in a dictionary (see Section 5.2.6 for the details), with keys indicating the corresponding product ID. Incorporating the process economics and drug development cost models within the GA loop was found to impair efficiency and timeliness of algorithm completion, increasing the run time by ~120-fold compared to when keeping the components separate. Having said this, the calculation of the combined NPV (i.e. evaluating candidate solution fitness) for any given portfolio was conducted within the optimisation loop, as this depended upon the drug portfolio that was under consideration.

As depicted in **Figure 5.1**, also included within the tool was a success-failure algorithm to model the progression of drugs throughout the development pathway, labelled as a Bernoulli-event based simulation. This was utilised to generate the likelihood of success and its impact upon the NPV when realistic biopharmaceutical risk is considered on a dynamic basis. The algorithm was modelled as a series of constituent and independent Bernoulli trials, where only two outcomes were possible; success or failure of the given drug. These trials occurred outside of the bulk of the simulation and optimisation modelling, which is highlighted by **Figure**

5.1, however the outcomes were subsequently used within the optimisation framework to adjust for failures within candidate portfolios (see Section 5.2.9).

The optimisation process was implemented by a stochastic, multi-objective GA-based tool that utilised bespoke constraint-handling strategies to ensure populations of infeasible portfolio solutions were not consistently produced. Chromosomes adopted a two-dimensional encoding strategy to accommodate both drug selection and capacity decisions in the candidate solutions, i.e. the first row represented the drugs included and the second was dedicated towards choice of capacity for said drug. The multiple decisions to be made as part of the portfolio problem prompted the use of this two-dimensional representation, which further drove modifications to the function of the traditional genetic operators such as crossover and mutation. Furthermore, the representation of a candidate portfolio took various forms, depending on the different stages of the simulation or optimisation framework, however the model ensured integrity of the candidate solution was maintained throughout. Specifically, binary or ternary value representation was utilised for crossover and mutation, as representation of the genes in binary format has been reported to be the most appropriate method when concerning genetic operations, detailed in Chapter 1. In contrast, the full drug names corresponding to each binary or ternary value and index within the chromosome were used when it was necessary to reference the product IDs, required for sourcing relevant cost data.

At a glance, the optimisation procedure was initialised through the random generation of a population of candidate portfolios. These were evaluated with respect to the expected profitability and risk or volatility associated with the profitability indicator (quantitatively expressed as the eNPV and standard deviation of the NPV respectively), across Monte Carlo trials, and those deemed superior, subject to constraints, were selected for genetic manipulation through selection, crossover and mutation. This process was repeated across several generations of the GA. Due to the stochastic nature of the problem, a series of uncertain input parameters were generated prior to the initialisation of the algorithm, hence a

distribution of NPVs were calculated for each candidate portfolio. This distribution resulted in the expected NPV being used as an objective function and the standard deviation serving as a secondary objective. Therefore, the structure of a traditional, single-objective GA was modified to address the multiple-objectives through implementation of a NSGA-II (Deb, 2000; Deb et al., 2002). This is a multi-objective evolutionary algorithm approach that considers the impact of both objective functions to assess Pareto optimality.

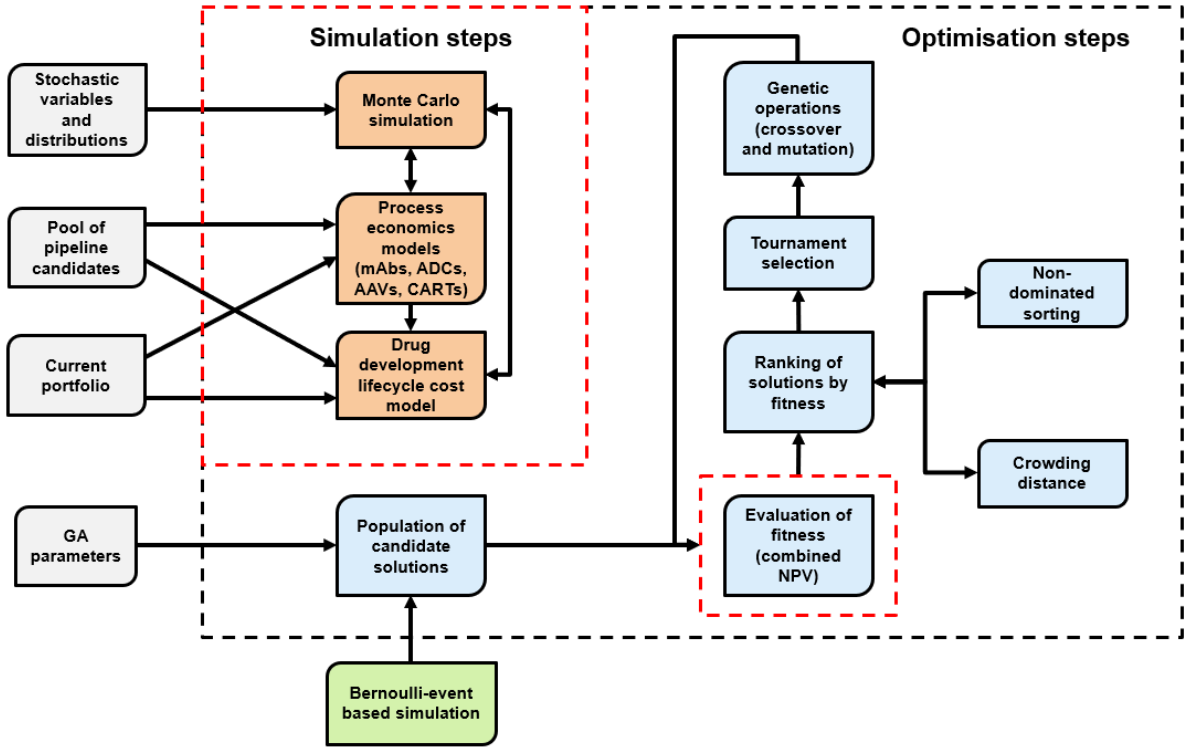

Figure 5.1 Overall tool architecture for the portfolio management and capacity planning case study. Grey shaded boxes located outside the dotted contours relate to assumptions or key model inputs. Simulation-based steps (i.e. generating cost data from process economics and drug development cost models) are contained within the red dotted contours or are shaded orange. Optimisation-based (i.e. use of the modified GA) are contained within the black dotted contours or are shaded blue. The step labelled “Evaluation of fitness” is contained within the optimisation procedure, but draws upon the outputs from the simulation part of the model, hence lies within a red contour. The green shaded box represents the success-failure simulation, which is an independent part of the tool.

5.2.4 GA theory

The following section provides further granularity on that discussed in Chapter 1, outlining the range of techniques available for GA attributes or methods. This provided a more in-depth analysis of that employed in the literature to drive the most appropriate choice of techniques. The remainder of Section 5.2 focuses upon that selected, drawing on the information discussed here.

5.2.4.1 Chromosome-encoding

In the context of a GA, a chromosome is the name given to a single solution, made up of a number of genes. Each gene confers a level of information, and when strung together, form the whole chromosome which represents uniquely encoded candidate solution. The strategy by which chromosomes are encoded is an integral part to structuring any GA. Several methods for chromosome-encoding have been reported and are used selected due to problem-specific dependencies.

One of the most commonly employed encoding methods is binary representation. In this case, genes within the chromosomes are restricted to taking values of 0 or 1, hence chromosomes resemble binary strings of information (Katoch et al., 2021). An individual binary-encoded gene represents a piece of information within the candidate solution as a whole. The encoding strategy selected is generally problem dependent and in certain scenarios, binary encoding may not be possible. It is fairly inherent strategy when considering binary decisions, e.g. yes or no, true or false, but in cases where decision variables are integer or decimal values chromosomes must be converted to binary through use of bit-string representation (that is, if binary-representation is desired). The implementation of genetic operators, namely mutation, is arguably less computationally demanding when opting for binary encoding (Koziel & Michalewicz, 1999). Mutating a binary-represented gene simply means the only alternative value is taken during the procedure (e.g. if the allele was originally 0, then the mutated alternative can only be 1).

An alternative encoding mechanism is permutation encoding, which is typically driven by integer representation. In contrast to binary, this technique allow a wider set of values to be assigned to genes, where the range of values used is based upon the problem definition. Permutation encoding using integer representation is particularly useful in problems where the order of the genes in the chromosome is essential to the characteristics of the solution. A common problem this type of encoding has been applied to is the Travelling Salesman Problem, further highlighting its benefit within logistics and transport scheduling. The application of permutation encoding to this problem was reported by Kaabi and Harrath (2019), where specific permutation rules were devised for the algorithm to solve the traditional problem.

Furthermore, value encoding is useful when decision variables can take any user defined value (Fox & McMahon, 1991). From this definition, strictly speaking, integer representation can be categorised as value encoding, but does not consider the permutation element to defining the candidate solution. More significantly, decimals or string may be used in value encoding, as highlighted in **Figure 5.2 c).** This format is particularly useful for use in the optimisation of neural network weights or hyperparameters, which take decimal values (Katoch et al., 2021). In general, conversion to more traditional binary-encoding format from decimal values adds greater complexity to the algorithm. Having said this, if value encoding is selected, it often requires modification to the traditional crossover and mutation approaches, as discussed earlier in this section. The range of values that each gene can take is restricted based on the specific problem in question so that violations within the encoding do not occur.

Converting decision variables to binary representation promotes greater genetic diversity within GA-based algorithms, explained by how conversion takes place to binary strings. Based on the range of values within the chromosome, a number of bits (greater than one) is selected which remains fixed across all genes. This effectively translates to the number of binary variables used to represent the original value of the gene. This is illustrated in greater detail in **Figure 5.3,** where the number of bits was chosen to be three. As a result, each gene is

expressed as multiple variables, thus crossover and mutation are able to operate upon a bigger chromosome, enhancing diversity and the chance for exploring untapped regions of the decision space. A caveat to the conversion to binary is that chromosome length is increased, thus for large-scale applications, is not beneficial to computational time. Carvalho et al. (2011) reported conversion of both integer and decimal decision variables to binary format. This study used metaheuristics in line with an artificial neural network.

a)

0	**1**	**1**	**1**	**0**	**0**	**1**	**0**	**1**	**1**

b)

2	**6**	**3**	**1**	**4**	**5**	**10**	**7**	**9**	**8**

c)

0.32	**0.11**	**0.87**	**0.45**	**0.65**	**0.44**	**0.32**	**0.78**	**0.54**	**0.22**

Figure 5.2 Examples of chromosome-encoding strategies employed when using GA-based algorithms, where **a)** is binary-encoding, **b)** permutation-encoding / integer representation and **c)** value-encoding.

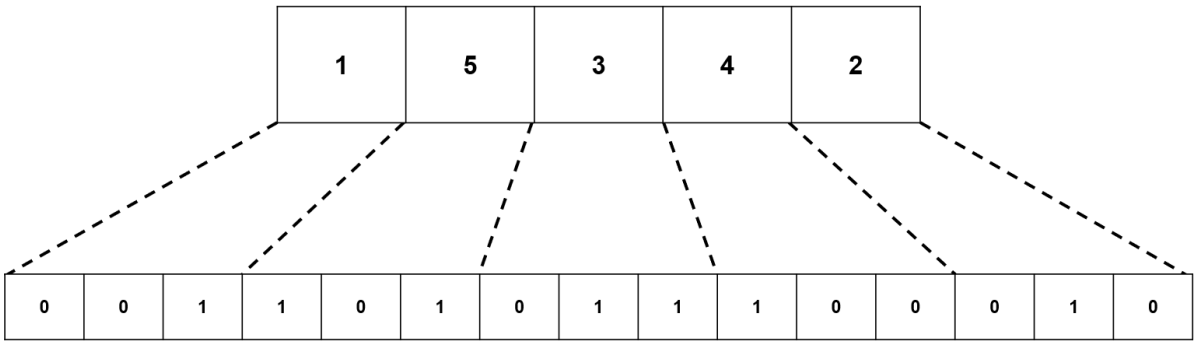

Figure 5.3 Illustration of how value encoding can be converted to binary. The number of bits was assumed to be 3, hence each gene is represented in triplets, shown by the contour lines drawn.

5.2.4.2 Selection methods

Selection is a critical component in the progression of a GA-based algorithm, whereby individuals from the population are chosen for reproduction in order to generate members of the next generation. In general, the goal of the procedure is to ensure fitter individuals advance, so that their genetic information can be passed on to offspring. In general, individuals in the population are ranked with respect to their objective function(s), which aids in several of the selection methods that will be discussed in further detail.

One of the most commonly employed selection methods is tournament selection. As the name suggests, individuals are typically selected in pairs (e.g. a tournament size of two) (Fiandaca et al., 2009) from the population and compete against one another in terms of fitness (i.e. the extent to they perform with respect to maximising or minimising the objective function). The individual with a better fitness (or rank) is selected for reproduction. Nevertheless, due to the random nature of the process in selecting two chromosomes to compete, prior ranking in terms of fitness is not necessarily required for tournament selection. The method can therefore be considered as beneficial from an efficiency perspective. However, it must be noted that for large population sizes, tournament selection may give unwanted attention to weaker performing solutions, as it is more likely through the random selection of individuals in large

sets (Goldberg & Deb, 1991). Having said this, occasional selection of weaker performing individuals can confer greater genetic diversity to the resulting population, as these chromosomes may have desired characteristics that can be inherited through later operations such as crossover and mutation.

A technique referred to as Roulette Wheel selection has also been implemented in the literature (Behera, 2020). Selection here has a stochastic nature, whereby the probability of selection for each chromosome is derived from its proportionality to its fitness (Hu et al., 2022). For example, the probability would be higher for fitness individuals, increasing the likelihood of selection. The wheel is effectively spun, which in practice relates to the generation of a random number between 1 and the population size. Limitations to using this method have been reported, such that errors often arise introduced by the stochastic nature of the selection process (Katoch et al., 2021).

5.2.4.3 Crossover and mutation methods

Crossover is a fundamental genetic procedure occurring within a GA, aimed at introducing diversity into the population. It mirrors the natural process of gene exchange between two parent chromosomes designed to create offspring.

Perhaps the most traditional crossover method is single-point. In this approach, a random, single crossover point within the chromosomes is selected (Burkowski, 2001). Genes beyond this point are exchanged with those before the point in the second chromosome and vice versa. As a result, offspring inherit a significant portion of parent genes, hence the algorithm can often converge quickly due to lack of genetic diversity promoted throughout (Katoch et al., 2021). Conversely, two-point crossover has also been implemented, which involves generation of two crossover points randomly. The process is similar to single-point, except that genes within the two points are swapped with those either side in the second chromosome. This is not limited to two points and has also been referred to as *k*-point crossover, as multiple crossover points may be defined (Soon et al., 2013). This has been reported for use in the literature, with Fiandaca et al. (2009) presented the use of a multi-point crossover

methodology within a multi-objective optimisation framework for use in designing pressure swing adsorption processes.

Furthermore, uniform crossover does not define crossover points but instead treats each gene on an individual basis. Each gene has an equal probability of being swapped or not, thus generally promoting more genetic diversity and opportunities for crossover to occur. Soon et al. (2013) provided a comprehensive comparison of the aforementioned crossover techniques, for use in video game design. Moreover, Hu and Di Paolo (2009) highlighted the benefits of uniform crossover, depicting its ability to encourage greater exploration of the objective space and often diversity.

Regarding mutation, two methods have been widely used to perform the genetic operation. Arguably the simplest of the two is bit-point mutation, which operates similarly to single-point crossover. A mutation rate is defined representing the probability that mutation will occur on any given chromosome. If a chromosome is selected for mutation, a single gene is probabilistically chosen to be mutated. For binary-encoded chromosomes, the selected gene is flipped to the other available value (e.g. 0 would become 1 and vice versa). On the other hand, uniform mutation treats each gene on an individual basis. The mutation rate governs which chromosomes participate in the mutation, however an additional measure of mutation probability must be adopted to identify which genes will be mutated within the chromosomes. If binary-encoding is used, genes are flipped to the only alternative value, as before. However if integer representation is adopted, genes are randomly changed to any values between the specified lower and upper bounds.

5.2.5 Chromosome-encoding strategy

Before outlining the structure of a candidate portfolio, it is important to discuss the strategy by which chromosomes and hence solutions were encoded. Candidate solutions encoded the drugs selected from the pipeline for injection into the portfolio and ultimately the nature of capacity sourcing associated with each, i.e. whether commercial manufacturing operations

were kept in-house, outsourced to a CMO, or if a future facility was used. Due to the multiple layers associated with decision-making, chromosomes were structured as an m by n array, where n represented the string length (number of columns) and also equated to the number of drugs available for selection in the pipeline ($N_{d_{pipe}}$) and m denoted the number of rows in each chromosome. The number of rows was fixed at two, the first for drug selection and the second for the commercial manufacturing strategy (i.e. capacity) used for a given drug. The chromosome structure is further described by **Figure 5.4**.

Traditional GAs are characterised by the use of one-dimensional chromosomes, thus the matrix structure employed within this tool represented a more novel encoding strategy. As a general heuristic in programming, two-dimensional arrays are often more computationally expensive than one-dimensional, however this notion does not hold true in cases where the column length differs between each array type being compared. For example, if the two-dimensional structure outlined in **Figure 5.4** were transformed into an array, where each couplet of genes referenced one drug, the chromosome length would equivalently double. Particularly for a GA-based method, where genetic operations rely on scanning the length of the whole chromosome, a reduction in chromosome length was deemed desirable. The matrix structure was additionally useful for indexing the position of genes, allowing for ease of translation to the corresponding product IDs. Within the pipeline, each drug was assigned an index value translating to its position within the chromosome (which remained constant throughout as chromosome length was fixed). This offered a simplistic method for identifying which drugs were included within any given candidate portfolio and as a result, using a one-dimensional array risked interfering with the chronology of indexing. It must be noted that whilst matrix-style chromosome structures are relatively more novel than traditional encoding strategies, their use has been previously reported in scheduling optimisation problems. Tsai et al. (2015) introduced a two-dimensional chromosome structure for use in aircraft scheduling and as delineated in Chapter 1, Jankauskas and Farid (2019) also adopted a matrix-style structure for biopharmaceutical capacity planning. Both of these studies introduced

modifications to the genetic operators (i.e. crossover and mutation) that adapted to the multiple chromosome layers.

Furthermore, a hybrid binary and ternary chromosome-encoding strategy was used. As depicted in **Figure 5.4,** the first row of the chromosome represented drug selection decisions and was coded using binary variables. Specifically, 1 was assigned to those drugs included within a candidate portfolio and 0 to those excluded. For the second row concerning capacity decisions, a ternary-encoding system was utilised, meaning genes could take only one of three distinct values, i.e. {0, 1, 2}. This decision was indicative of the three strategies available for commercial manufacturing, those being in-house manufacturing, outsourcing to a CMO and a future facility build.

$d_{s,1}$	$d_{s,2}$	…	$d_{s,N_{d_{pipe}}}$
$m_{s,1}$	$m_{s,2}$	…	$m_{s,N_{d_{pipe}}}$

Figure 5.4 Generic chromosome structure for the case study. Notation: $d_{s,i}$ = candidate drug i from candidate solution (s), $i \in N_{d_{pipe}}$, $m_{s,i}$ = commercial manufacturing strategy for drug i (in-house, CMO or future facility), $i \in N_{d_{pipe}}$, $s \in N_{pop}$.

5.2.6 Candidate portfolio structure

In each generation of the modified-GA, g, a population of solutions was denoted by S_g. Individual solutions were represented by $s_{g,p}$, where $p = \{1, 2, \ldots N_{pop}\}$ and N_{pop} was the parent and offspring population size. As a result, p was used as an index for each candidate solution in the population. Bringing all these elements into coherence, a population of candidate solutions from a single generation could be expressed by the following notation.

$$S_g = \{s_{g,p=1}, s_{g,p=2} \ \dots \ s_{g,p=N_{pop}}\} \qquad \forall g \in G, p \in N_{pop} \qquad (5.1)$$

Any given candidate portfolio, $s_{g,p}$, was divided into drug selection and capacity sourcing decisions. These were denoted with different mathematical representations within the optimisation setup and as such, $s_{g,p}$ could be further expressed as (d_s, m_s). This meant that for a given instance of $s_{g,p}$, the set of drugs available for injection was denoted by d_s, the size of which was fixed and previously defined as $N_{d_{pipe}}$. The following equation was used to represent d_s.

$$d_s = \{d_{s,i=1}, d_{s,i=2} \ \dots \ d_{s,i=N_{d_{pipe}}}\} \qquad \forall s \in S_g, i \in N_{d_{pipe}} \qquad (5.2)$$

It was necessary to distinguish between the number of drugs available in the pipeline for selection ($N_{d_{pipe}}$) and the actual number of drugs selected for a given portfolio (denoted by N_{d_s} in this case). Outlined in the case study notation and terminology in Section 5.2.2, $N_{d_{pipe}}$ referred to the total number of drugs in the pipeline (available for injection into the portfolio). Whilst this was the total number available, not all of these drugs were necessarily injected and hence included within each candidate solution, governed in reality by budget and capacity constraints. Thus in comparison, N_{d_s} was randomly generated value by the algorithm and could be less than or equal to $N_{d_{pipe}}$. In practice and highlighted by Equation 5.2, each instance of d_s had an equal length of $N_{d_{pipe}}$, which did not vary between candidate solutions so to maintain the chromosome length. Instead, the distribution of binary variables within each d_s was varied, based upon which drugs were included or excluded. Therefore, the number of drugs with a 1 assigned to them within d_s (i.e. those selected in the portfolio) summed to N_{d_s}, whilst $N_{d_{pipe}}$ remained constant throughout. The binary encoding and thus restriction of any $d_{s,i}$ to either of the two possible values is shown below.

$$d_{s,i} \in \{0, 1\} \qquad \forall s \in S_g, i \in N_{d_{pipe}} \qquad (5.3)$$

The second part of a candidate solution involved the commercial manufacturing strategies used for each drug in d_s as part of any $s_{g,p}$ and was denoted by m_s. The overall structure of the set is represented by the following.

$$m_s = \{m_{s,i=1}, m_{s,i=2} \dots m_{s,i=N_{d_{pipe}}}\} \qquad \forall s \in S_g, i \in N_{d_{pipe}} \qquad (5.4)$$

As discussed previously, a ternary representation was used for the capacity strategies, where 0 represented in-house manufacturing, 1 related to using a CMO and 2 for building a new facility and conducting operations within this.

$$m_{s,i} \in \{0, 1, 2\} \qquad \forall s \in S_g, i \in N_{d_{pipe}} \qquad (5.5)$$

The constraints considered within the tool and the strategies employed to handle them are discussed in detail later in a dedicated section. However to briefly summarise, a basic repair strategy was employed to deal with any instances of an infeasible capacity strategy being assigned to certain modality types (following crossover or mutation). For example, if an AAV were assigned in-house manufacturing by a genetic operation, when the assumption is this was not possible for CGT products, the repair method employed by the model would switch the gene to a feasible capacity strategy.

5.2.7 Objective functions

The optimisation tool addressed both the expected profitability (eNPV) and the standard deviation of the profitability (sdNPV) as objective functions. The deterministic NPV was calculated through a discounted cash-flow, which for a given product, considered the income and outgoings from its development and ultimately commercialisation, before applying a discount factor to consider the time value of money (as the cash flow is forecasted over a fixed period of time). In comparison, the eNPV can be defined as the average of a given set of NPVs. In this case study, the uncertainty analysis generated a distribution of NPVs and hence, the eNPV was calculated as the average of these outputs.

Independent of the Monte Carlo simulation, the workflow employed to calculate a single NPV for a candidate portfolio has been presented in **Figure 5.5**. At any given iteration of the algorithm (i.e. a generation, g), the population was represented by a Python list, which contained a number of sub-lists within designed to characterise the candidate portfolios in the population. These candidate portfolio lists were assessed in the modified-GA, in terms of their objective functions, as shown in **Figure 5.5**. Furthermore, each drug element in a given candidate portfolio list, as previously described, could be represented by $d_{s,i}$. Denoted by the grey shaded boxes in **Figure 5.5**, a dictionary of the cash-flow elements was constructed outside of the GA loop. In using Python dictionaries, keys must be defined for referencing and drawing out values when necessary. Keys and their values are separated by a colon, such that 'calling' the key yields the associated value. An illustrative example of the dictionary structure is outlined below, along with a list, to give clarity to the terminology utilised.

$$dictionary \quad = \quad \begin{Bmatrix} key_1 : value_1, \\ key_2 : value_2, \\ key_3 : value_3 \end{Bmatrix} \quad \rightarrow \quad \begin{Bmatrix} mAb1 : [0, 1, 2], \\ AAV1 : [3, 4, 5], \\ ADC1 : [6, 7, 8] \end{Bmatrix} \qquad (5.6)$$

$$list \quad = \quad \begin{bmatrix} [value_{1,1}, value_{1,2}, value_{1,3}], \\ [value_{2,1}, value_{2,2}, value_{2,3}], \\ [value_{3,1}, value_{3,2}, value_{3,3}] \end{bmatrix} \rightarrow \begin{bmatrix} [0, \ 1, \ 2], \\ [3, \ 4, \ 5], \\ [6, \ 7, \ 8] \end{bmatrix} \qquad (5.7)$$

Each drug in both the starting portfolio and pipeline was used as a key to reference its individual set of expenses and revenues (these served as the values shown above). All drugs assessed in the case study were included in these dictionaries. Furthermore, expenses and revenues were ordered and indexed by their cash flow year, which allowed for correct entry and hence discounting in the combined cash-flow for each portfolio assessed. Independent of the grey-shaded dictionaries in **Figure 5.5**, separate expenses and revenue lists were generated during each generation of the optimisation algorithm to store the relevant cash-flow entries for each drug within all candidate portfolios assessed, which are enclosed within the solid purple contour. This can be cross-referenced with that detailed in **Figure 5.1**, where the evaluation of fitness for a candidate portfolio was shown to be independent from the initial

generation of expenses and revenues for each drug. Revenue for each drug was calculated using the annual selling price and the total number of patients treated in a year. This is summarised in the following equation.

$$Revenue = SP \times N_{doses/year} \quad (5.8)$$

In contrast, the dotted contours represent the adjusted expenses and revenues list when risk was considered within the scenario. This accounted for the original lists within the solid contours alongside the output of the Bernoulli event-based simulation. The output of the Bernoulli event-based simulation was used to highlight, for each drug, whether it succeeded along its ideal trajectory or if not, the position within the pathway where failure occurred. The index of the failure position was a vital part of determining the adjusted costs for a given drug, as it was used in parallel with the cash-flow years to determine the position where costs were no longer considered (as the drug had failed). Numerically, values in both the expenses and revenues list beyond the failure point were set to 0 to ensure that any theoretical cash-flow contributions from the failed drug were not included in the NPV calculation.

The specific calculations used within the cash-flow to generate the NPV can be found in **Figure C1** in Appendix C. This provides a step-by-step procedure of handling income and outgoings.

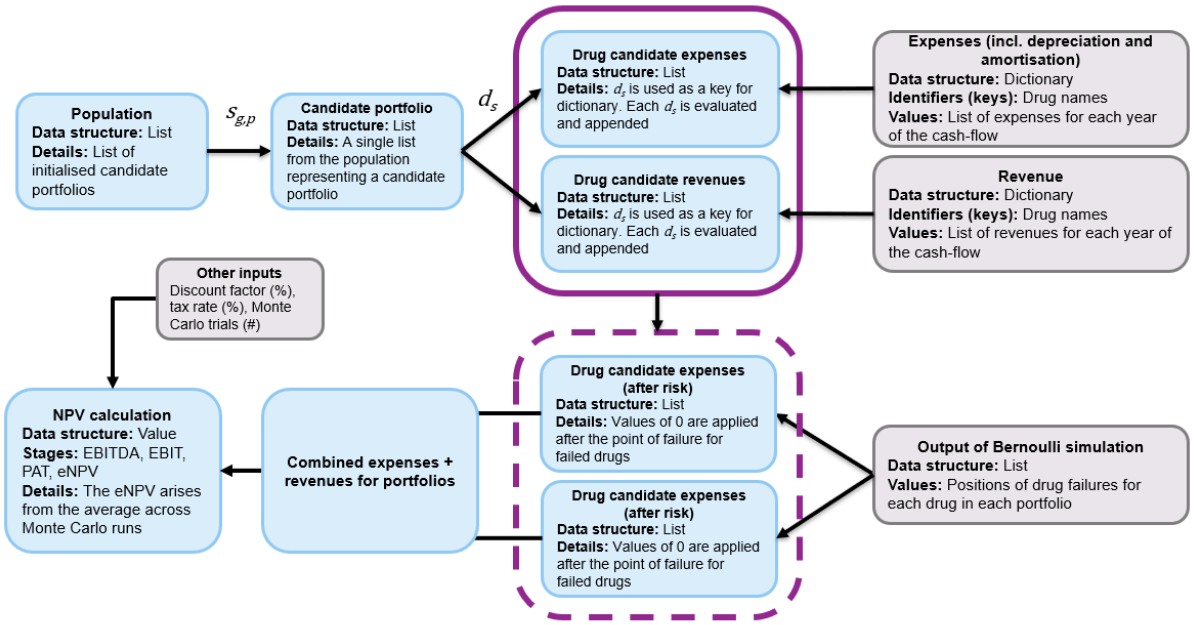

Figure 5.5 Derivation of the objective functions within the tool. Within each box, an indication of the Python data structure used for coding the datasets, e.g. list or dictionary, is provided. Boxes shaded in grey represent datasets that are constructed outside of the optimisation algorithm loop, thus were not confined to any form of time complexity that arose from running over multiple iterations. Boxes shaded light blue represent datasets that vary across each iteration or generation within the algorithm, hence were re-generated during each loop. The solid contour (——) was used to highlight the grouping of the expenses and revenues for any given candidate solution, though values were expressed in separate lists (income versus outgoings). The dotted contour (- - -) was used to group the income and outgoings after the impact of drug failures were applied, if the Bernoulli event-based simulation was conducted.

5.2.8 Optimisation algorithm

5.2.8.1 Overview of modified genetic algorithm

The optimisation portion of the tool incorporated several elements of a traditional genetic algorithm and the non-dominated sorting and crowding distance features from the NSGA-II, as outlined in Chapter 1. Crucially however, several modifications were made in adapting the more traditional GA methods to the chromosome-encoding strategy described in Section 5.2.5. As highlighted in the tool architecture in **Figure 5.1**, the optimisation framework featured GA functions such as population initialisation, evaluation of fitness, crossover, mutation, offspring evaluation of fitness and population replacement. During population initialisation, a set of size N_{pop} candidate portfolios (chromosomes) were generated, with varying sizes (N_{d_s}) as described previously. These candidate portfolios were expressed as both a binary string and by their corresponding drug names to source relevant cost data. Portfolios were then evaluated through the calculation of the combined NPV for each portfolio, using a whole portfolio cash-flow function within the optimisation loop. This was conducted across Monte Carlo trials and the mean and standard deviation of the NPV were derived to determine the objective functions.

Deviation from the traditional structure of a GA occurred following the evaluation of the objective functions. The presence of multiple objective functions required alternate strategies be introduced to accurately rank solutions, by considering the contribution of both. Ranking with respect to only one objective would disregard the impact of the second objective and hence fail to capture any trade-offs in the results. In this work, the NSGA-II was employed. In contrast to traditional ranking methods for fitness evaluation, which are inherently designed for single-objective problems, NSGA-II reconciles both objective functions when ranking solutions. The specific protocol by which the NSGA-II was employed is discussed further within this chapter, as well as the additional modifications made to tournament selection for handling two objective functions.

Figure 5.6 depicts the flow of the modified-GA used within the optimisation tool. Crossover and mutation were both implemented to enhance genetic diversity within the population, but were both refined to suit the manipulation of two-dimensional chromosomes. A uniform method for both was selected over the more conventional single-point (or bit-point), which probabilistically treated each gene in chromosomes individually, rather than selecting only a single gene to perform genetic changes on. As discussed in Chapter 1, uniform approaches to both crossover and mutation have been shown to enhance diversity and coverage within the objective space.

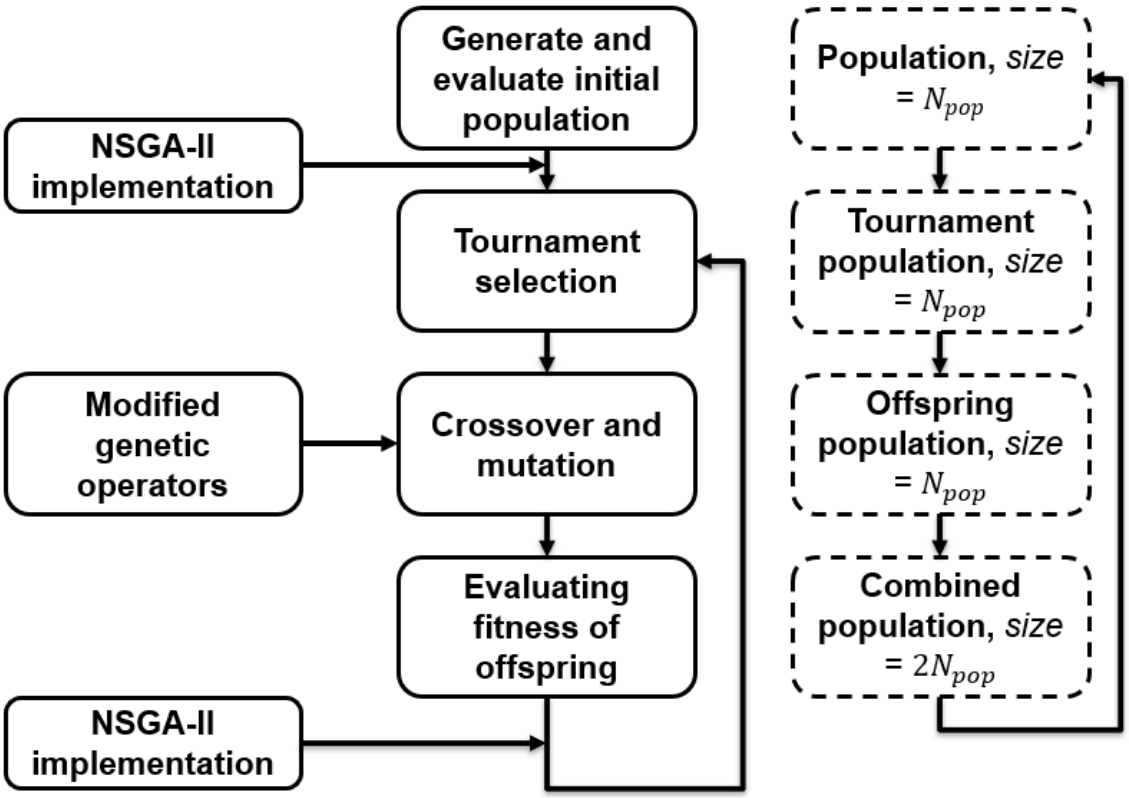

Figure 5.6 General tool architecture for the modified genetic algorithm. The dotted boxes further highlight the changes occurring to the population size throughout the procedure.

5.2.8.2 Multi-objective optimisation

The nature of multi-objective optimisation centres on evaluating and optimising for two or more objective functions. Due to the often-conflicting nature of multiple objectives, there regularly arises cases where some solutions may perform well in relation to one, but poorly for the second. To this end, the sorting and selection mechanisms used in single-objective optimisation cannot be efficiently transferred into a multi-objective environment. Instead, all solutions can be plotted with the objective functions as axes and a schematic known as the Pareto frontier can be constructed, representing the non-dominated and hence optimal solutions within the objective space. It must be noted that the Pareto front is not constituted by a plot of the entire objective space but is instead a specific subset of the objective space representing the optimal trade-offs between the multiple, conflicting objectives. Throughout this chapter, the algorithm utilised for MOO was the NSGA-II, selected for its robustness in handling problems with large numbers of variables and non-linear constraints. Hence, for an application in biopharmaceutical portfolio management and capacity planning, this algorithm is well-suited, with evidence of its implementation in similar fields being outlined in Chapter 1.

The placement of the NSGA-II components of the algorithm is highlighted in both **Figures 5.1** and **5.6**. Its use was primarily in population ranking and selection. This ranking occurred post-fitness evaluation and facilitated the process of tournament selection. For further clarity, the pseudocode in **Algorithm 5.1** outlines the procedure. This process sought to identify the non-dominated set of candidate solutions. Within the procedure of non-dominated sorting, when comparing two solutions x and y, x is said to dominate y if the following holds true:

- Solution x is no worse than y in all objective functions
- Solution x is strictly better than y in at least one objective function

Each candidate solution was compared to another with respect to the performance of both objective functions and the number of solutions that dominated or were dominated by the candidate under consideration were recorded. This looped procedure is referred to as non-

dominated sorting, which governs the categorisation of solutions into ranks and therefore, leads to the formation of the Pareto front. These ranks are referred to as Pareto fronts or ranks, e.g. rank 1 would be considered superior in comparison to rank 2. Upon this basis, Pareto rank 1 represented the non-dominated solutions within the population and therefore the optimal set, such that no other solutions dominated them in terms of all objectives simultaneously. Nonetheless, all solutions were assigned Pareto ranks based on their dominance relationships with other solutions, not the top performing set alone. Illustration of this procedure is displayed in **Figure 5.7**.

With reference to the concept of Pareto optimality and in the context of the NSGA-II, the goal of the algorithm is often more accurately aligned with achieving convergence toward higher Pareto ranks rather than specifically toward the Pareto front. The NSGA-II is designed to attain a diverse set of solutions across all prescribed Pareto ranks. By exploring solutions across ranks, the NSGA-II promotes genetic diversity in the final set of solutions, ensuring the algorithm does not converge to a limited portion of the Pareto front, but instead provides a more comprehensive representation of the trade-offs.

Evaluation of the fitness involved combining the offspring and parent populations (see **Figure 5.6**) and then ranking the integrated set. However, only half of this combined population were selected for the next generation of the process, which evoked scenarios where certain Pareto ranks required division to achieve a population size of N_{pop} for advancement. As a result, operations to divide the front were necessary to define. This was achieved through non-dominated sorting (discussed previously) and crowding distance sorting. The procedure has been displayed in **Figure 5.7** for clarity. Crowding distance is a measure of how close a candidate is to its neighbouring solutions in the population. The procedure here, which utilised the Manhattan distance calculation, is outlined in Appendix C1. The aim is maximisation, where the greater the crowding distance, the higher the ranking of the solution, as this has been found to promote a greater population diversity, by encouraging exploration of less dense areas of the objective space that have yet to be covered. The calculated crowding distance

also served as a relevant criterion during tournament selection. When comparing two competing chromosomes with the same Pareto rank, the solution that achieved the higher crowding distance would be selected for reproduction. In contrast, binary tournament selection during a single-objective optimisation problem simply involves comparing the objective functions of two randomly selected chromosomes from the population and selecting the one that better meets the problem conditions, i.e. minimisation or maximisation of the objective function.

For model validation purposes, an important consideration was how to assess algorithm convergence and solution quality within a multi-objective environment. A far more simplistic approach can be taken when only one objective function is considered, typically involving how the fitness changes over successive generations and identifying the threshold where no significant improvement takes place. For MOO, this methodology does not translate as effectively, particular where problems often yield conflicting objective function values. As outlined in Chapter 1, the hypervolume indicator is a well-established performance metric widely used in MOO problems, particularly NSGA-II based algorithms. This particularly prompted the use of it throughout this work. Additional points governing its suitability include its relatively simplistic computation for two-objective problems and that it does not add additional computational complexities in terms of time. The hypervolume is often driven by selection of a reference point, which confers flexibility to the user as it can be randomly selected. Other derivations of reference point have been highlighted in Chapter 1, however a user-defined reference point was utilised in this chapter due to the flexibility it allows, as well as its benefits when knowledge of the breadth in the objective space has been acquired. In this case, the decision space was evaluated in terms of the minimum and maximum values found for each objective (i.e. the boundaries). For an objective requiring maximisation, the reference coordinate was set to be smaller than the minimum value of that objective in the space. The converse was then true for an objective function to be minimised, i.e. a reference coordinate value greater than the maximum value obtained in the objective space.

Furthermore, in comparison to other indicators outlined in Chapter 1, the hypervolume is the only metric that strictly satisfies the mathematical definition of Pareto dominance, a concept highlighted throughout this work.

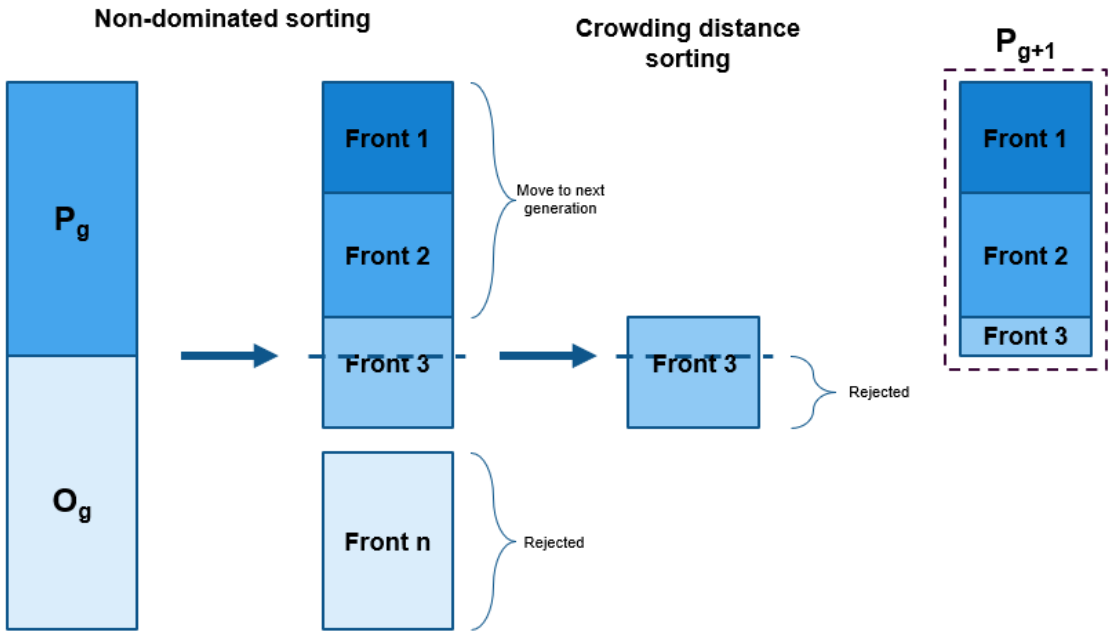

Figure 5.7 Creation of new population at each generation in the optimisation algorithm. P_g and O_g together depict the combined parent and offspring population. The next stage highlights the procedure of non-dominated sorting, where the combined population are divided into a series of Pareto ranks or fronts (front 1 is the optimal set). The next parent population is half of the combined population in the previous generation and therefore, any relevant splitting of a particular Pareto front / rank is handled by crowding distance sorting, which seeks to reject a portion of the front which is considered more crowded. Furthermore, P_{g+1} reflects the new population created for the next generation.

Algorithm 5.1 Pseudocode for NSGA-II Pareto ranking and crowding distance is calculated.

Require: R $(Pareto\ rank\ dictionary)$, Dom_x $(set\ of\ solutions\ that\ are\ dominated\ by\ x)$, $n_{dom,x}$ $(number\ of\ solutions\ that\ dominate\ x)$, S_g $(population\ of\ solutions\ from\ a\ given\ generation, g)$, $f_1(objective\ function\ 1\ values\ for\ all\ solutions)$, $f_2(objective\ function\ 2\ values\ for\ all\ solutions)$

1 R is an empty dictionary with Pareto front ranks as keys and empty lists ([ ]) as values

2 **for** r in R

3 $Dom_x = \{\}$, $n_{dom,x} = 0$

4 **for** x in S_g

5 **for** y in S_g

6 **if** x dominates y

7 y is added to set Dom_x # y is dominated by x

8 **else**

9 $n_{dom,x}$ = $n_{dom,x}$ + 1 # add one to the number of solutions dominating x

10 append solutions which have $n_{dom,x} = 0$ to whatever r is being considered

11 remove from S_g the solutions which have $n_{dom,x} = 0$

12 **repeat**

12 Create new dictionaries to rank solutions by f_1 and f_2

13 **for** r in R

14 Calculate the crowding distance (see Algorithm C1 in Appendix C)

The hypervolume is a measure of the volume of the objective space taken up by the Pareto solutions evaluated. In general, larger hypervolume values are indicative of a better-quality set that is close to approximating the true Pareto optimal. Additionally, convergence can be monitored by assessing the change in hypervolume over time. As this change lessens, the process of convergence is likely to be occurring. The hypervolume calculated in this study was the area under the Pareto curve, utilising a rectangular method for computational simplicity (highlighted in **Figure 5.8**). It must be noted that whilst used here, the terminology of

hypervolume is more aptly used in optimisation problems with 3 or more objectives. Furthermore, though division of the objective space into rectangular segments provided a rapid means to calculate the indicator, it would be more accurate to adopt a triangular or trapezoidal methods, as this would ensure greater coverage of the area in the objective space (as highlighted in the results section).

The formation of these rectangles are contingent on defining a set of coordinates (the reference point) in the objective space. The arrangement of the reference point and the rectangles formed in the objective space is illustrated by **Figure 5.8**. Additionally, the pseudo-code for the hypervolume calculation is outlined in **Algorithm 5.2**.

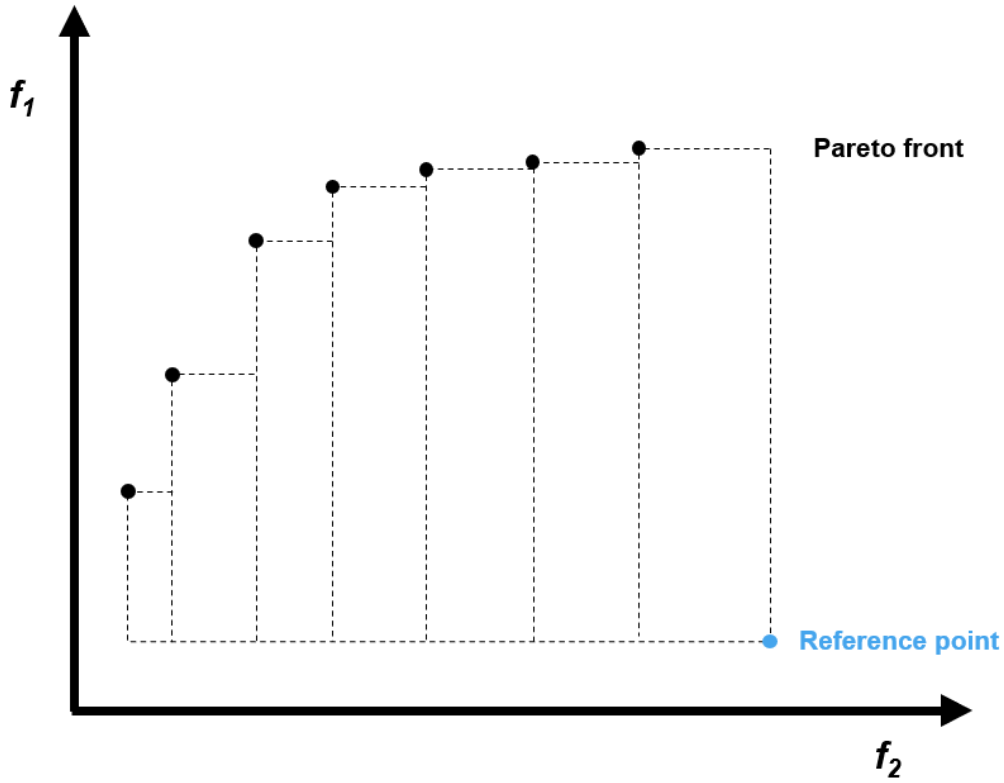

Figure 5.8 Illustrative example of the hypervolume calculation. The axes represent an illustrative example of an objective function 1 (f_1) and objective function 2 (f_2), where it is desirable to maximise f_1 and minimise f_2. The dotted lines show how the rectangles are formed for the calculation of the overall hypervolume. The reference point is highlighted in blue.

Algorithm 5.2 Pseudocode for hypervolume calculation as part of the NSGA-II algorithm.

Require: $RP\ (Reference\ point), f_1\ (objective\ function\ 1\ values\ for\ all\ non-dominated\ solutions)\ f_2\ (objective\ function\ 2\ values\ for\ all\ non-dominated\ solutions), G\ (number\ of\ generations), HV(hypervolume\ indicator)$

1 $HV,\ HV\_list = 0, [\,]$ # Initialise a hypervolume list to store the value across generations

Hypervolume loop for each generation

2 **for** g in G

3 **for** y, x in (f_1, f_2)

4 **if** index of $f = 0$ # If it's the first entry in the list

5 $HV = HV + (x - RP_1) \times (y - RP_2)$

6 $RP = (x, RP_2)$ # x coordinate of RP updated

7 **else**

8 $HV = HV + (x - RP_1) \times (y - RP_2)$

9 $RP = (x, RP_2)$

10 append HV to HV_list

11 **return** HV_list

5.2.8.3 Crossover and mutation

A modified methodology for both crossover and mutation was proposed by Tsai et al. (2015) to perform genetic operations upon two-dimensional chromosomes. This presented techniques similar to single-point crossover and bit-point mutation, but adapted for two-dimensional chromosomes, where the crossover and mutation points were defined as a row and column index, instead of a single gene position. In general, single-point based genetic operations are widely regarded to lack in promoting genetic diversity throughout the algorithm, risking instances of premature convergence towards local optima. A single-point swap or mutation often leads to similar patterns of gene inheritance in offspring to that of the parent chromosomes, and over generations, leads to minimal genetic variations as parents tend toward having similar characteristics with one another (i.e. convergence).

In contrast to these methods, uniform crossover and mutation treats each gene in the chromosome on an individual probabilistic basis, resulting in greater diversity in the offspring population and offers the chance to explore regions of the decision space where there may be better performing solutions. As a result, the work in this chapter introduced the use of a bespoke uniform crossover and mutation method tailored specifically to two-dimensional chromosomes. Illustration of the differences between the traditional single-point or bit-point crossover and mutation methods and the uniform approach is provided in **Figure 5.9**. Highlighted in **Figure 5.9 a),** the modifications to the methods are shown in the definition of a row and column index to define where crossover or mutation takes place. Selection of these indices was random and the probability of either genetic operation taking place was subject to the defined crossover and mutation rate respectively.

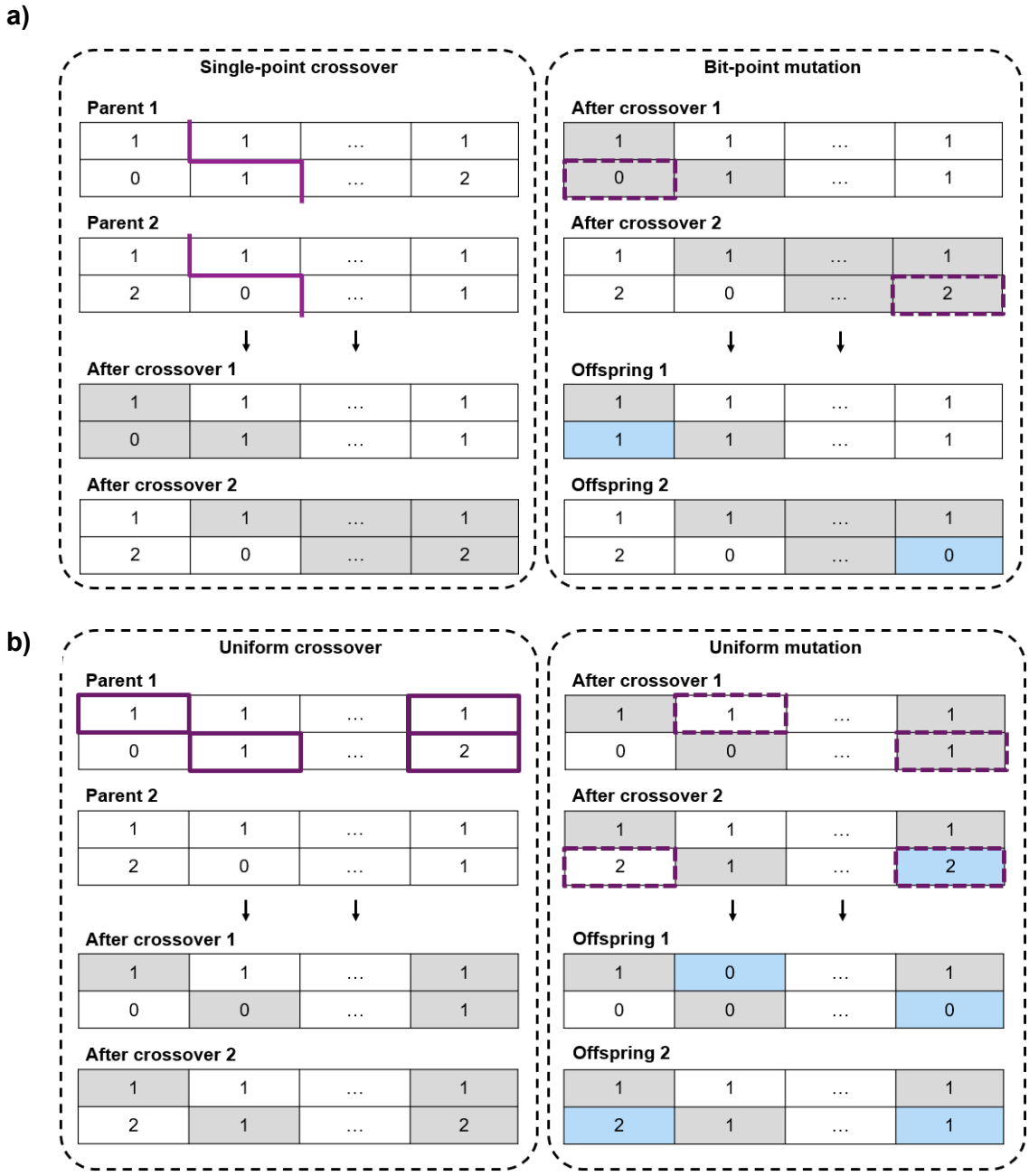

Figure 5.9 Examples of the crossover and mutation procedures followed in the tool (**b**) and their differences between single-point and bit-point crossover and mutation, **a)** single-point crossover and bit-point mutation procedure for matrix-style chromosomes and **b)** uniform crossover and mutation for matrix-style chromosomes. In both **a)** and **b),** the split between crossover and mutation is defined. The solid contours in the parent chromosomes represent the crossover point(s) and the impact is shown in the “after crossover” chromosomes, shaded grey to depict the swapping of genes. The dashed contours highlight the mutation points(s), where the blue shading in the offspring highlighted the result of a gene mutation.

5.2.8.4 Parameter selection

Balancing the trade-off between computational efficiency and solution quality is an important task when selecting GA parameters and is generally problem dependent. It may also require some form of prior knowledge or iterative experimentation. The population size and number of generations are two key parameters that greatly impact algorithm performance. Throughout the literature, these values vary greatly depending on the type and size of the problem. Allmendinger et al. (2014) presented a GA structure for the optimisation of chromatography sizing and utilised a population size of 80, along with 25 generations. In portfolio and capacity planning problems, where typically the objective space is larger, Jankauskas et al. (2019) reported using upwards of 100 generations with a population size of 100. However, defining the problem broadly as related to portfolio management or capacity planning does not necessarily govern the selection of GA parameters, as shown by George and Farid (2008). This study imposed a maximum of 17 generations on the algorithm. Therefore, particularly where population size and generation number were concerned, arbitrary selection of these parameters based on comparison with those reported in literature for similar sized problems was deemed an unsuitable selection method. Another consideration and potential driver for selecting GA parameters related to a balance between reducing computational speed and maintaining solution quality. For many problems in portfolio optimisation, smaller GA parameters may be sufficient to provide a set of optimal solutions and would ensure the computational time does not exceed any potential user-defined constraints.

These considerations prompted the use of a parameter selection study, to ensure appropriate values were opted for throughout the work conducted. Ranges of population size and number of generations were explored and the optimal solution achieved from each scenario was recorded, along with the computational time. The specifics of the procedure undertaken is outlined below.

1. The population size was fixed at the median of the defined range, then the number of generations was varied. The GA was run multiple times for reproducibility and the optimal solution, hypervolume indicator and computational time was recorded and averaged across runs.
2. The number of generations was fixed at the median of the defined range, then the population size was varied. The GA was run multiple times for reproducibility and the optimal solution, hypervolume indicator and computational time was recorded and averaged across runs.
3. The results from both experiments were plotted and the optimal solution was analysed with respect to how it changed with the GA parameters. The same was done for any changes in hypervolume indicator.

Of note, in the population size study specifically, a large pool of potential candidate solutions (greater than the upper bound of the range evaluated) were first generated as part of the population initialisation phase of the GA-based procedure. Utilising the same possible candidates throughout the study ensured sampling was conducted on the same pool for every population size tested. This was thought to minimise the bias introduced by random efforts, such as the consistent reinitialization of the population in every population size run, which may influence the results. The Python library “random” was harnessed to sample the desired number of chromosomes each time, before running the GA as normal.

Additionally, to consider the impact of both objective functions, a weighted value between the two was also expressed and the following calculation was used.

$$Weighted\ objective\ function = f_1 \times 0.5 + f_2 \times 0.5 \qquad (5.9)$$

5.2.8.5 Constraints and handling strategies

The portfolio optimisation problem under consideration was constrained, thus by definition, feasible solutions needed to adhere to various constraints imposed. As is the nature of constrained optimisation, often a portion of solutions generated violate the constraints and are deemed infeasible. Specifically for the portfolio optimisation tool used in this chapter, budgetary and capacity constraints were defined.

Budgetary constraints related to the expenses injected into the cash-flow over a defined period of time. An R&D budget was assumed over a fixed duration and in cases where expenses required for a candidate portfolio for the same time period exceeded the defined budget, the solution became infeasible. On the other hand, capacity constraints required a more in-depth calculation to assess solution feasibility. In general, capacity considerations introduced a dynamic element to the portfolio problem, as it considered the position of a given drug within the cash-flow timeline and hence if and when they occupy manufacturing capacity. The specific constraints were handled by calculating the number of batches required to manufacture the drug and considering the maximum batches that could be carried out from the trains available in the facility. The procedure for determining capacity violation is found in **Algorithm 5.3**.

Algorithm 5.3 Pseudocode for determining solutions which breach capacity constraints.

Require: d_0 $(set\ of\ drugs\ in\ the\ starting\ portfolio)$, d_s $(set\ of\ drugs\ in\ candidate\ portfolio\ from\ solution\ s)$, $N_{batches}$ $(no.\ of\ batches\ required\ to\ manufacture\ each\ drug\ in\ d_0)$, STG_idx $(the\ index\ of\ the\ development\ stage\ that\ each\ drug\ in\ d_0\ is\ at\ time\ 0)$ $years$ $(list\ of\ years\ in\ the\ cashflow)$, C_{max} $(in\ house\ capacity\ annually)$, T $(trains)$

Create an empty dictionary. Each drug in d_0 represents a separate key
$C, C_{combined} = [\,], [\,]$ # Initialise lists for capacity
for d in d_0 # Each drug in the starting portfolio
    append $N_{batches,d}$ and STG_idx_d # Tabulate the batches required and the position the drug is at in development
for d in d_s # Each drug in candidate solution d_s
    append $N_{batches,d}$ # Tabulate the batches required
for $d_{s,i}$ in $(d_0 + d_s)$ # Combined portfolio to assess capacity
    for y in $years$
        for d in $d_{s,i}$ # for each drug in candidate portfolio
            consider position of d in the development timeline
            if d is in a manufacturing phase
                append $N_{batches,d}$ to C
            $STG\_idx_d = STG\_idx_d + 1$ # Move the drug on in the development timeline
C is indexed by the candidate portfolio and year under consideration
for $d_{s,i}$ in $(d_0 + d_s)$
    for y in $years$
        $No.drugs = len(C_{i,y})$ # How many drugs share the manufacturing suite at the same time (in a given year)
        if $No.drugs > T$ # Drugs at one time exceed the number of trains
            call Algorithm C2 (see Appendix C)
        else
            append $N_{batches,d}$ to $C_{combined}$ # Assign each drug to a train
for y in $years$
    if $C_{combined,y} > C_{max}$
        d_s is deemed infeasible
    else d_s is considered feasible

In the pseudocode shown in **Algorithm 5.3**, the starting portfolio refers to drugs already in the portfolio before the cash-flow was instigated and the d_s refers to an example chromosome in the population (made up of prospective drugs to inject into the portfolio).

Constraint-handling involves dealing with solutions that violate the constraints defined in the problem. A violation renders the solution infeasible. Chapter 1 detailed several constraint handling techniques reported in the literature, including application of penalty functions and repair mechanisms. As a summary, penalty functions are notably simple to implement and can be useful when prior knowledge is available on the range of objective function values in the decision space. Repair-based mechanisms are often problem dependent and offer flexibility in building bespoke handling strategies for the specific population. In the work conducted in this chapter, a hybrid constraint handling methodology was undertaken, with elements of a penalty and a repair function implemented, depending on the specific constraint being violated. A repair mechanism was implemented following crossover and mutation on any chromosomes that did not follow the logic of the structure, e.g. instances where a drug was not included in the portfolio (and so the gene labelled a 0), but CMO decisions were still present (a 1 or 2 used for genes pertaining to CMO vs in-house for that specific drug). Here, repair ensured that if a gene in the first row was 0, then all other genes in the same column also had to be 0. Similarly, a chromosomal repair took place if crossover and mutation yielded chromosomes where some violating capacity strategies were assigned to drugs, e.g. if in-house was assigned to a continuously manufactured drug (there is no available in-house continuous manufacturing).

A simplistic penalty function was used for budget and capacity constraint violations, which involved setting the NPV to 0 for infeasible solutions and the standard deviation as 1×10^{10}, so as to penalise these strategies for ongoing ranking and genetic operations. Nevertheless, as will be discussed later in the chapter, a bespoke repair strategy was also incorporated within the model for capacity violations. Practical implementation of constraint-handling is often dependent on the problem in question and as a result, may require some initial running

to identify any intrinsic biases or caveats to consider. Therefore, the capacity-repair method was implemented in cases where the penalty function introduced any algorithmic biases or impeded the genetic operators and further details are discussed later in the chapter. In summary, a more simplistic penalty function was opted for initially and a repair only if needed. Penalty functions provided a simpler method to implement, particularly amidst an algorithm that contains many computationally demanding additions. From a contextual perspective, the prior knowledge on the specific objective functions used also favoured its use, which aids in selecting appropriate penalty values.

5.2.9 Uncertainty

Stochasticity was introduced in the form of uncertain parameters related to process economics, CMC activities or market characteristics. For each parameter, a distribution of values was generated. Each value replaced the base-case value, such that a corresponding output distribution was generated. In the case of the portfolio tool, a distribution of NPVs were ultimately generated, as well as the standard deviation of the NPV.

5.2.10 Bernoulli event-based simulation

The simulation of drug success throughout the portfolio architecture was one of a stochastic nature, where each development phase had an associated transition success rate. As a result, the journey of a given drug through the development pathway could be modelled as a series of consecutive stochastic events, where the outcome of each was either drug success (1) or failure (0). In instances where a drug under consideration failed, its development pathway was prematurely cut short as failure represented its removal from consideration within the portfolio. As such, the binary nature of the simulation enabled the use of a Bernoulli distribution to represent the two possible outcomes of success or failure. Each critical phase (clinical trial) had a probability of transition success attributed to them (defined in Chapter 4) and as such, all phases could be independently modelled using a Bernoulli distribution with probability of drug success p and failure $1 - p$.

The simulation was conducted as follows. A random variable U was generated from a pseudo-random number generator, following a uniform distribution. For any given drug and clinical trial phase, if U exceeded the probability of transition success, p, then X was equal to 0 and hence the drug failed. Conversely, if U was less than or equal to the probability of transition success, the drug was assumed to succeed in transitioning from that clinical phase to the next. This can be better highlighted by the following representation:

$$X = \begin{cases} 1, & if\ 0 \leq U < p \\ 0, & if\ p \leq U \leq 1 \end{cases}$$

The event simulation did not consider the individual reasons for drug success or failure; it solely described the progression of drugs on a quantitative basis. Any interdependencies between trial outcomes or drugs were also not considered within the simulation e.g. if a drug targeting one indication fails, does this make another more or less likely to succeed. Placement of the Bernoulli event-based simulation was also investigated. Introduction of the algorithm before the optimisation loop and within the final generation of the procedure were compared in terms of quality of solution, as well as how the resulting populations illustrated risk in a realistic environment. Nevertheless, regardless of where the simulation was introduced, the pseudo-code for the procedure can be found in **Algorithm 5.4**. Of note, the operation in line 5 loops through each element within two input lists (must be of equal size), whilst also producing a third list containing the indices associated with the list elements. The indices range from 1 to the length of the lists. As highlighted here, *positions* represented the output of the Bernoulli event-based simulation, which gave the dynamic pathways for each drug within the candidate portfolios comprising the whole population. Lines 6 to 12 represent the key Bernoulli events taking place within the algorithm. For instances where the uniformly generated random variable U was less than the probability of transition success for the particular drug and phase in question, a 1 was added to the *positions* list, indexed by the drug and the candidate solution within the population. Conversely, a 0 was added to the list to highlight that the drug had failed to progress into the next development phase. Furthermore,

lines 11 and 12 were used to deal with the presence of any 0 values within *positions.* In a practical context, this related to handling drug failures that were simulated. As shown in these lines, no further additions were made to *positions* if the drug under consideration has failed.

Within the wider context of the model, the *positions* output was used in parallel to the functions described in **Figure 5.5**, where expenses and revenues were compiled for drugs under consideration. By design, *positions* was structured such that 0 values were paired with the stage index where failure occurred (shown in line 8). For example, if the failure occurred in Phase 2, the couplet [0, 2] was appended to *positions.* The code break in line 12 meant that the couplet signifying failure would consistently be the last element in the given sub-list within *positions* (sub-lists were indexed by drug and candidate portfolio). The stage index could then be sourced within the cash-flow model in order to define the phase where failure occurred and in practice, the position from which revenues and expenses were no longer considered for the given drug.

Algorithm 5.4 Pseudocode for Bernoulli event-based simulation for characterising risk.

Require: N_{pop} $(population\ size), S_g(population),\ TSR$ $(probabilities\ of\ transition\ success), is\_current$ $(boolean\ variable\ to\ determine\ if\ the\ simulation\ is\ for\ the\ current\ portfolio\ or\ injected\ drugs), STG(stages\ in\ the\ development\ pathway)$ $Crit\_STG(the\ critical\ stages\ in\ the\ development\ pathway)$

Create an empty list $positions = [\,]$
for s in S_g
  for $drug$ in s
    generate a uniformly distributed random variable x
    for i, j, k in enumerate(zip$(STG, Crit_STG))$
      if $i = k$ and $STG_{drug} < i$
        if $x > TSR_{drug,j}$
          append 0 and j to $positions$
        else
          append 1 to $positions$
      else append 1 to $positions$
      if $positions_{s,drug,i}$ is 0 # if drug has failed stop the simulation and
        break # move to the next drug

Note: if drug is part of the pipeline, it will always start at position 0 in the development pathway. However, if the drug is in the starting portfolio, STG concerns the index of the stage it is at from time 0, e.g. Ph II clinical trials is represented by an index of 4. Additionally, critical stages in the development pathway were defined as those where transition probabilities need to be considered (in practice critical stages were clinical trials)

5.3 Case study setup

5.3.1 Case study definition

The integrated optimisation tool introduced in Section 5.2 was used in evaluating a series of portfolio-related questions, with a particular aim to optimise drug selection and capacity sourcing for protein therapeutics (i.e. mAbs and ADCs) initially, before the injection of AAV and

CAR T products were also considered. The study first explored the impact of changing the proportion of future protein therapeutics that were manufactured continuously. This compared scenarios of 20% versus 80% continuous: batch in the pipeline. A key trade-off existing between the batch and continuous manufacturing options was that the biotechnology company being modelled did not have existing in-house continuous manufacturing capabilities, hence only outsourcing or facility build options were available for capacity sourcing. In comparison, batch could be conducted in-house, outsourced or built. A further distinction between the manufacturing options related to the cost of goods, where it was assumed that the continuous flowsheet would allow for a 35% reduction in COG over the batch, as reported in Mahal et al. (2021). A further trade-off was defined that early phase process development effort was 50% greater in terms of FTE requirement for the continuous platform, due to its nascency relative to batch configurations.

The case study was later expanded to include CGT options. For each modality under consideration, the transition success probabilities outlined in Chapter 4 were used to address the impact of risk in a dynamic environment, highlighting how drug success and failure influenced the objective functions. Similarly, the sensitivity analysis using success rates presented in Chapter 4 was also reinforced, giving insight into how the portfolio structure in terms of protein to CGT ratio changed across each risk profile evaluated. The model produced both a non-risk and risk adjusted output to illustrate the economic impact of risk, as well as how it logistically affects capacity.

The optimisation framework involved using a stochastic, modified-GA based structure to generate populations of candidate portfolios and the capacity strategies associated with each. Additional techniques were built-in to bolster the overall analysis, including a Monte Carlo simulation and a Bernoulli-event based algorithm for simulating drug success and failure. Due to the complexities that can often arise relating to GA parameter selection, an additional study was included to investigate the impact of the selected inputs (i.e. population size and number of generations) on the resulting Pareto front and the hypervolume indicator. Optimisation with

respect to drug selection and capacity sourcing was constrained, with constraints placed upon annual budget allowance and the manufacturing capacity both internally and in facility build options. Section 5.2 outlined the key notation and terminology associated with the case study. To add further clarity to this, the following problem definition was constructed, alongside key assumptions used throughout.

5.3.1.1 Problem statement

The objective of the whole study was to assess a large biopharmaceutical company with an established array of drugs in their starting portfolio. Management has a prospective pool of candidates in the pipeline available to inject into the portfolio, in addition to the set already in development. The starting portfolio can be expressed in the following format.

$d_0 = \left\{d'_1, d'_2 \dots d'_{N_{d_0}}\right\}$ representing the drugs in the portfolio at time $t = 0$, where N_{d_0} is the total number of drugs in the starting portfolio (at time 0). The d' was used to highlight drugs in the starting portfolio over the future pipeline. The pipeline of prospective drug candidates can be represented by the following set.

$d_{pipe} = \left\{d_1, d_2 \dots d_{N_{d_{pipe}}}\right\}$ where $N_{d_{pipe}}$ was the total number of drug candidates in the pipeline. Candidate drugs were indexed independent from those in the starting portfolio, hence the distinction between d' and d. In defining the problem statement further, the key scenario attributes and inputs were outlined in the following section.

Given:

- Large biotechnology company
- $N_{d_0} = 15$
- $N_{d_{pipe}} = 50$
    - The injection rate of $N_{d_{pipe}}$ is 10 per year across a period of 5 years
    - When only protein therapeutics were considered, a ratio of 80: 20 of mAbs: ADCs was assumed in the pipeline

- When CGT products were also considered, injection initially occurred at a rate of one per year (alternating AAV and CAR T). As described in detail in later sections, the injection rate was varied, considering three and then five per year.

Determine:

- The optimal portfolio composition and capacity strategies when batch v continuously manufactured proteins are considered
- The impact of injecting CGT products into the portfolio
- The dynamic impact of risk on the optimal portfolios

To:

- Maximise the expected NPV (eNPV), also referred to as the reward or profitability
- Minimise the standard deviation of the NPV (sdNPV), also referred to as the risk or volatility associated with the profitability.

Subject to:

- **Budget constraints –** $3bn each 5-year period
- **Capacity constraints –** placed on in-house and future facility (i.e. build) manufacturing, not CMO
    - **In-house –** available only for mAbs and ADCs (not drug-conjugate component) and was constrained to 4 x 12,000L USP trains and 4 DSP trains.
    - **Future facility –** available for all product candidates and was constrained. Details of facility configurations and capacities are discussed later.

5.3.2 Portfolio outline

A case study was formulated to represent a large biotechnology company specialising in mAb and ADC production, with growing interest in developing CGTs such as AAVs and CAR T cell products. Referring to the biotechnology company as large indicated the presence of an established portfolio of products (i.e. starting portfolio) in conjunction with the pipeline of

potential drugs that could be injected. With specific reference to the notation defined in Section 5.2, N_{d_0}, i.e. the number of drugs in the starting portfolio when $t = 0$, was assumed to be 15. The pool of potential drugs that could be injected from the pipeline (i.e. $N_{d_{pipe}}$) was assumed to be 50, with an equal number injected per year considered. The entry year of any given drug in the pipeline was fixed and hence was not considered as part of the optimisation string (details on the entry years for each drug are found in **Tables C1, C2** and **C3** in Appendix C).

The nature of the optimisation problem was constrained, therefore biotechnology-specific constraints were defined previously to frame realistic portfolio management and capacity planning questions. Further detail on the constraints relating to budget and capacity, as well as strategies to handle violations is discussed later. In any case, it was vital that quantitative measures for assessing these constraints were defined. In terms of budget, characterisation of the biotechnology company in question as large referenced not only the size of the portfolio, but also the annual profits and ultimately R&D budgets available. As such, the budget was assumed to be $3bn for each five-year increment (to be split over these years not necessarily equally). In terms of capacity, an in-house facility for commercial mAb manufacture was assumed to be available, with 4 processing trains, each with a bioreactor size of 12,000L. This was also capable of manufacturing the mAb component of ADC products, with conjugation and further purification requiring outsourcing to a CMO.

Another facility was assumed to be available for clinical mAb, ADC and AAV manufacture. The bioreactor sizes in this smaller facility were set at 100L, 250L, 500L and 2,000L. This facility was only able to support up to Phase II clinical trials for AAV products, hence outsourcing was required beyond this point. Furthermore, CAR T manufacture for only Phase I trials was assumed to be possible in a separate facility utilising an integrated USP and DSP processing platform. Greater clarity on these constraints and any additional caveats is provided in a dedicated section later in the chapter.

5.3.3 Key portfolio assumptions

Table 5.1 shows the key assumptions for the starting portfolio (referred to as d_0). Titre, demand and scale were used within the process economics model to generate the associated COG values. Also defined was the stage of development, which related to the assumed position of the drug within the development pathway at the start of the cash-flow. Taking mAb1 as an example, **Table 5.1** shows that when the cash-flow was initiated, the drug had entered into manufacturing for Phase III trials. This position was important in understanding the correct annual allocation of costs when considering the combined portfolio. It was also significant in considering capacity and specifically the accurate tracking of when drugs were utilising the manufacturing facility.

For drugs in the pipeline, **Table 5.2** outlines the key ranges of assumptions. Due to the quantity of drugs in the potential pipeline, ranges were provided for brevity, however the more detailed database with specific product IDs can be found in Appendix C. In contrast to the stage of development column in **Table 5.1**, the equivalent metric defined for future drugs was the entry year into the portfolio, which particularly influenced capacity scheduling and the discounting of costs in the cash-flow. Process development and clinical trial assumptions remained consistent from those described in Chapter 4, and for drugs in the same modality group, no variations were assumed. The exception to this were mAbs or ADCs requiring continuous manufacture versus their batch alternatives, where a 50% increase in Phase I process development personnel was assumed.

Also significant to capacity sourcing considerations was the assumed premium on COG values when outsourcing manufacturing to a CMO. A factor of 1.5 was applied to COGs for mAbs and ADCs and for AAV and CAR T cell products, manufacturing costs were amplified by a factor of 2. A difference in these premiums was defined through industrial correspondence.

Table 5.1 Characteristics of the drugs in the starting portfolio.

Product ID	Stage of development	Titre (g/L)	Commercial demand (kg)	Patient population	Selling price ($/patient/annum)
mAb1	P3 MFG	9	484	30250	29791
mAb2	P2 MFG	9	185	11563	34240
mAb3	P1 PD	7	537	33563	33145
mAb4	P3 MFG	8	257	16063	80839
mAb5	P2 MFG	8	600	37500	96240
mAb6	P1 CT	7	140	8750	101353
mAb7	P4 PD	7	536	33500	122489
mAb8	P3 MFG	5	191	11938	183484
mAb9	P2 MFG	8	207	12938	102274
mAb10	P1 CT	8	449	28063	48381
mAb11	P4 PD	7	447	27938	184426
mAb12	P3 MFG	7	482	30125	27141
mAb13	P3 MFG	5	357	22313	151076
mAb14	P1 MFG	9	307	19188	83616
mAb15	P2 CT	12	481	30063	192256

Note: P1, P2, P3, P4 = Phase I, II, III and regulatory review

Table 5.2 Ranges of assumptions used for drugs in the pipeline.

Product	Titre	Commercial demand	Patient population	Selling price ($/patient/annum)
mAb	5 – 15 g/L	150 – 1,000 kg	5,000 – 100,000	20,000 – 180,000
ADC	5 – 15 g/L	150 – 1,000 kg	5,000 – 100,000	20,000 – 180,000
AAV	6×10^{13} – 1×10^{14} vg/L	500 – 5,000 doses	500 – 5,000	800,000 – 2,000,000
CAR T	N/A	500 – 5,000 doses	500 – 5,000	400,000 – 800,000

5.3.4 Optimisation structure and assumptions

As discussed in Section 5.2, chromosomes followed a two-dimensional structure, where the first row corresponded to drug selection and the second dealt with commercial capacity decisions. Mathematically, drug selection was regarded as a binary activity, where 1 represented a given drug's inclusion in the candidate portfolio and 0 denoted exclusion. This binary representation allowed for a fixed chromosome length across all candidate solutions, as drugs excluded from the portfolio were still considered in the string, but were assigned a 0. Example chromosomes and their translation to the corresponding product IDs were formulated and shown in **Figure 5.10**, to highlight their setup. For brevity in illustrating this, a set of only ten drugs was considered in this example. This indicates the fixed chromosome length and the translation of binary encoding to different examples of portfolio selection. Maintaining the length of the chromosome enabled it to be consistently expressed as $N_{d_{pipe}}$.

Though binary representation was used for chromosome-encoding, the algorithm required conversion to the corresponding product names for use in referencing costs from associated Python dictionaries. Generation of the product names from each chromosome was achieved by considering the position of a given gene and its index with respect to the string length. An example of how these are used is provided in **Figure 5.10.**

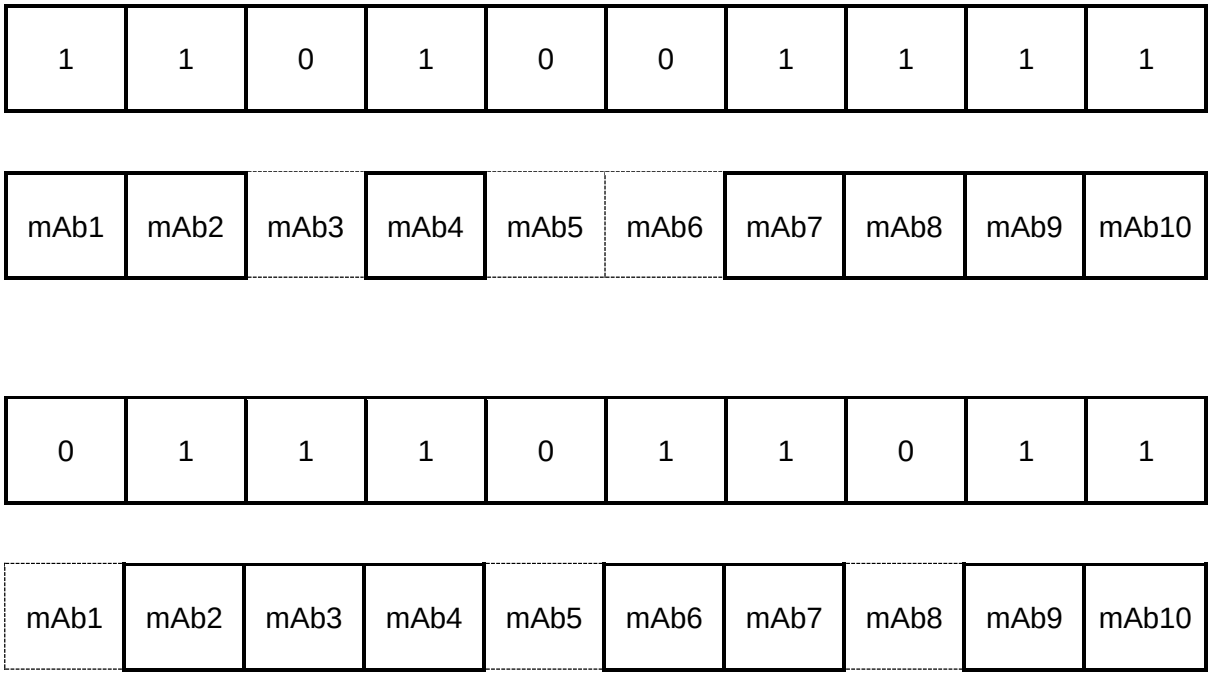

Figure 5.10 Illustrative examples of chromosome encoding and the translation to the corresponding product IDs. The dotted contours around certain drugs highlight their exclusion and hence a 0-value assigned during binary encoding.

Additionally, the assumptions related specifically to the optimisation process are found in **Table 5.3.** The number of generations and population size were expressed as ranges, as these were evaluated in a parameter selection study. Section 5.2 outlined the procedure for this, intended for ensuring the selection of the appropriate GA parameters (i.e. population size and generations). As a result, ranges were necessary to define to conduct this study.

Due to the number of algorithm runs employed, an array of high-performing solutions were generated across all conducted. Reporting of the results was carried out differently depending on the nature of the case study under consideration. More specifically, when the desirable outcome of the case study was assessing the structure of candidate portfolios (i.e. gene by gene), the algorithm selected the top performer across all algorithm runs to analyse. However, when the more general characteristics of the portfolios became the significant output, average values of the objective functions and portfolio weightings across runs were taken to include in the analysis. The summarised difference here is that in the first case, a single result was

considered, i.e. the best of the set. In the second method, an average of all top performers across runs was considered.

Table 5.3 Key inputs used for the GA-based optimisation work and corresponding values.

Parameter	Value
Number of generations	1 – 40
Selection method	Binary tournament selection
Mutation probability	0.05
Crossover probability	0.55
Population size (parent and offspring)	20 - 180
Monte Carlo trials	25
Bernoulli simulation runs	100
Number of runs*	10

Note: * Runs refer to the whole algorithm

5.3.5 Constraints

5.3.5.1 Capacity

As discussed in the problem statement, in-house commercial manufacturing capacity was considered an option for mAb products, which also allowed for production of the mAb component in ADCs. The linker and drug component were assumed to always be outsourced. The in-house capacity was constrained to four 12,000L stainless steel bioreactors, with four downstream processing trains. Both starting portfolio mAbs and ADCs, as well as those injected from the pipeline could utilise the existing in-house capacity. In-house clinical manufacturing was available for each modality under consideration. mAbs, ADCs and AAVs were assumed to share a smaller facility, with bioreactor sizes of 100L, 250L, 500L and 2,000L available. All clinical phases for mAb and ADC products were able to be supported in-house, however for AAVs, the facility was assumed to only support Phase I and II trials. As a result, Phase III manufacturing for AAVs required outsourcing. Furthermore, another in-house clinical

site for CAR T was available, supporting only Phase I manufacturing. This featured an integrated USP and DSP system, utilising a single CliniMACS Prodigy (Miltenyi Biotech, Germany).

Assumptions around the capacities of the facilities that could be built are found in **Table 5.4**. This highlights the available manufacturing trains, as well as the fixed capital investment required for building. The facility to build for mAbs and ADCs was dependent on the pipeline scenario under consideration, i.e. whether drugs requiring continuous manufacture made up 20% or 80% of the pool. For the 20% continuous scenario, future facility manufacturing would need to prioritise batch, hence 4 of the 6 possible USP trains were 12,000L stainless steel reactors for fed-batch culture. Conversely, for the 80% continuous scenario, the weighting of USP trains switched to 2 out of 6 for fed-batch.

The capital investments outlined in **Table 5.4** were calculated from the corresponding process economics models for each modality for facilities having the manufacturing capabilities listed in the table. These were further benchmarked against studies reporting FCI values for the modalities in question. Specifically, Pollock (2015) presented a comparison of batch and continuous (perfusion cell culture) FCI values. This study determined a 40% FCI reduction for perfusion-based manufacturing facilities over batch. Additionally, Mahal et al. (2021) suggested for multi-train continuous facilities, the indirect cost reduction over stainless-steel batch was between 20 – 30%. Therefore, the data generated in **Table 5.4** aligns with this, where a ~30% FCI difference was found between the majority batch over continuous facility.

Furthermore, for autologous CAR T products, Pereira Chilima et al. (2020) produced a correlation between FCI and annual demands (in doses) for different manufacturing platforms, suggesting an FCI between ~$110 – 125M for 5,000 doses per year. It was further assumed that the CAR T facility would be a centralised site, hence product transportation costs were necessary to consider in the cash-flow. Overall product transportation costs were assumed to amount to $3,000 per dose produced (Pereira Chilima, 2019). **Table 5.5** summarises the capacity availability and options across modalities. These provided additional constraints

within the optimisation algorithm, such that breaching any rules would require the repair mechanism (detailed in Section 5.2) be implemented.

Table 5.4 Future facility options and manufacturing capacities.

Modalities in facility	Manufacturing trains	FCI ($M)
mAb, ADC (20% continuous pipeline)	**Batch mAb and ADC:** 4 x 12,000L SS and associated DSP for each **Continuous mAb and ADC:** 2 x 2,000L SU and associated DSP for each	230
mAb, ADC (80% continuous pipeline)	**Batch mAb and ADC:** 2 x 12,000L SS and associated DSP for each **Continuous mAb and ADC:** 4 x 2,000L SU and associated DSP for each	160
AAV	4 x 2,000L SU and associated DSP for each	100
CAR T	Integrated USP / DSP platform with capacity for up to 5,000 doses 100 CliniMACS Prodigy units	120

Table 5.5 Summary of capacity options available for each modality.

Capacity option	mAb	ADC	AAV	CART
In-house (commercial)	Yes	Yes (mAb component) No (drug / linker)	No	No
In-house (clinical)	Yes	Yes	Yes (to Phase II)	Yes (to Phase I)
CMO	Yes	Yes	Yes	Yes
Future facility (Build)	Yes	Yes (mAb component) No (drug / linker)	Yes	Yes

5.3.6 Uncertainty assumptions

The uncertain input parameters used in the portfolio model are displayed in **Table 5.6,** along with the deviation applied to the base-case value to generate the minimum and maximum values for the triangular distribution. These parameters included those related to the process economics (such as those from Chapter 3), drug-development and within the combined portfolio profitability analyses. Triangular distributions were assumed for each parameter and the number of Monte Carlo trials utilised was 25 given that this was sufficient following convergence tests. A weighted value was computed that considered an equal contribution of objective functions 1 and 2. The standard deviation of this weighted value was then considered across Monte Carlo trials. The objective here was stabilisation of this standard deviation across trials, confirming an appropriate level of convergence for the problem in question.

Table 5.6 Uncertain parameters utilised in the portfolio management tool.

Parameter	Upper and lower bounds
Cell culture titre*	± 30%
Process yield (%)	± 10% (mAb, ADC), ± 30% (AAV, CAR T)
Selling price ($)	± 15%
Clinical trials cost per patient ($ / patient)	± 10%
Probabilities of transition success rates	See later Section 5.3.7

5.3.7 Bernoulli-event based simulation

This simulation was devised as a method to characterising the dynamic impact of risk upon drugs in the portfolio. This primarily relied on the probabilities of transition success for each modality, first outlined in Chapter 4. However, these have been again expressed in **Table 5.7**. The ranges provided here similarly served as the triangular distributions utilised in the uncertainty analysis, as dictated by **Table 5.6**.

The procedure for the algorithm was outlined in Section 5.2, where it was shown that uniformly distributed random variables were generated in each trial for comparison with the transition success rates. These random variables were generated by the Python 3.8 library “random”,

which uses the Mersenne Twister as its core pseudo-random number generator. The overall simulation was run multiple times to aid in reproducibility, with 100 runs selected as a preliminary value. The final non-risk adjusted population of portfolios from the modified-GA were collated and remained consistent throughout all runs of the Bernoulli-event simulation. This meant that each run of the risk simulation operated on the same final population, to avoid any bias introduced (i.e. 100 risk-adjusted variations of the final population were generated).

For further clarity on the definition of a run within the tool as a whole, run as listed in **Table 5.6** referred to the whole algorithm, including the modified-GA and the Bernoulli simulation (across all 100 runs). This whole procedure was run 10 times, therefore, the mean output across all Bernoulli runs and then whole algorithm runs was utilised in the portfolio weightings and objective function values displayed in the results section.

Table 5.7 Probabilities of transition success for each modality by phase and the corresponding number of projects required overall.

Modality	Phase I	Phase II	Phase III	Reg. review	LOA from Phase I [a]	No. of projects
mAb	54%, 54%, 62%	34%, 34%, 36%	63%, 70%, 70%	91%, 91%, 91%	10.5%, 11.7%, 14.2%	13.8, 12.4, 10.2
ADC	54%, 54%, 57%	34%, 34%, 37%	54%, 63%, 63%	91%, 91%, 91%	9.0%, 10.5%, 12.1%	16.1, 13.8, 12.0
AAV	51%, 51%, 80%	34%, 34%, 66%,	21%, 64%, 75%	90%, 90%, 91%	3.3%, 10.0%, 36.0%	44.2, 14.5, 4.0
CAR T	51%, 68%, 80%	34%, 40%, 66%	21%, 70%, 75%	90%, 91%, 91%	3.3%, 17.3%, 36.0%	44.2, 8.4, 4.0

[a] LOA = likelihood of approval

Note: Three numbers provided that represent the worst-case: base-case: best-case values

5.4 Results and Discussion

The tool described previously was used to address the problem statement defined in Section 5.3. The results presented in this section detail the optimal portfolio compositions and capacity strategies initially considering mAbs and ADCs, before later including AAV and CAR T cells into the pipeline, across a range of success rate scenarios and objective weightings. Portfolios were evaluated in terms of their expected NPV (eNPV) and the standard deviation of the NPV (sdNPV). Transition success rates were investigated on a dynamic basis to produce a set of risk-adjusted candidate solutions. The study was extended to include a sensitivity analysis where the transition success rates were varied and the resulting weightings of protein to CGT products were generated. The objective function weightings were then adjusted to present the potentially different business goals for the company. Initially however, a parameter selection study was conducted to verify the choice of GA parameters, specifically the number of generations and population size.

5.4.1 What is the appropriate choice of GA parameters?

When using GA-based algorithms, the choice of hyperparameters govern the trade-off between the algorithm's ability to discover fitter solutions across the entire procedure and the computational time expended. As a result, a parameter selection study is often important in defining the optimal parameters to balance the trade-off between solution quality and computational efficiency. The progression of the algorithm in exploring the objective space and forming the Pareto front was firstly evaluated across generations, using a fixed population size (100), crossover rate and mutation rate. The results are shown in **Figure 5.11**. Discovery of the objective space is incrementally highlighted from **Figures 5.11 a)** to **i)**. The range of figures presented evidence the convergence of solutions toward the non-dominated, Pareto front and in general, towards higher Pareto ranks. Convergence towards the Pareto front occurred relatively early in the process and evidence of this was observed from the 5th generation onwards. Though this convergence process began early, increasing the number of

generations further was shown to generate higher eNPV values, evidencing the improvement in solution quality and shift towards the Pareto frontier.

For the first generation displayed in **Figure 5.11 a)**, a random dispersion of candidate solutions and hence objective function values was observed. This relates to the random initialisation of the population in GA-based algorithms, which promotes the initial exploration of the objective space. The ranking and selection steps, as well as the genetic operations (i.e. crossover and mutation) lead to convergence over time towards the Pareto front and higher ranks, as fitter solutions are preferred in each generation. This trend was observed from **Figures 5.11 a)** to **i).** In many cases of multi-objective optimisation, it can be expected for the Pareto to change in terms of distribution, even after the shape has formed and convergence is taking place. In earlier generations, solutions tended towards a specific portion of the Pareto, particularly in **b)** and **c)**. Moving towards **d)** and **e)** highlighted the tendency for the algorithm to approximate the entire Pareto front, with a greater distribution across the entire ideal curve. This reflects the trade-off between the two objectives and indicates the diversity in the algorithm, hence it being the idealistic outcome. From a decision-making perspective, converging towards the whole Pareto evenly rather than an individual region of it allows for a more comprehensive understanding of which solution can best fit a company's goals. Nonetheless, no significant progression of the Pareto front was displayed between **Figures 5.11 e)** and **i)**.

Independent of the type of optimisation problem (whether single- or multi-objective), visualising how the objective function(s) changes with key parameters such as population size or number of generations is useful to gain a general understanding of solution convergence and quality. As a result, this was plotted in **Figure 5.12**. To capture the impact of both objective functions, regardless of whether they conflict with one another, a weighted value was derived from both (the equation for this is detailed in Section 5.2.8). This value accounted for both the eNPV and the sdNPV, with an equal weighting of 50% for each taken. As with any weighting-based procedure, different weights could be assigned to either objective function, to confer any level of importance if necessary, which was investigated later.

Figure 5.12 was plotted to determine the ideal number of generations to use in the GA-based procedure and to support the conclusions drawn from examining the plots of the objective space. This outlined the increase in both solution quality and computational time with the number of generations. Increasing the number of generations allowed access to areas of the objective space where fitter solutions were located, however required a greater level of computational power and time, hence the trade-off between time and solution quality. The weighted value was shown to increase with generations, before maintaining solution quality at around 22 generations or higher. Also shown in **Figure 5.12** was an upper and lower boundary around the optimal weighted value obtained, placed 5% either side. GA-based algorithms inherently are meta-heuristic and are not intended to reach the true optimal solution during an algorithm run. As such, it can be useful to learn the generation number beyond which no significant variation in the optimal solution was exhibited. A range of ±5% was selected to give flexibility that may be realistically encountered in an industrial setting. This range similarly confirmed the lack of variation in the weighted value from 22 generations.

To bolster the visual conclusions derived from **Figures 5.11** and **5.12**, the hypervolume was introduced as a quantitative metric for analysis. This takes into consideration both objective functions whilst providing a numerical indicator for assessing solution quality and convergence. The normalised hypervolume values calculated at each generation, as well as the corresponding objective function values are displayed in **Table 5.8.** The hypervolume increased with the number of generations, confirming the convergence found in **Figures 5.11** and **5.12.** Beyond 20 generations, whilst the optimal solution did not differ and quality was maintained throughout, the hypervolume began to decrease slightly despite the increase in solution quality. Nevertheless, it must be noted that the hypervolume provides information on the quality of the objective space as a whole, rather than just the optimal solution. As a result, it was important to balance the trade-off between maximising hypervolume and generation of high-quality solutions.

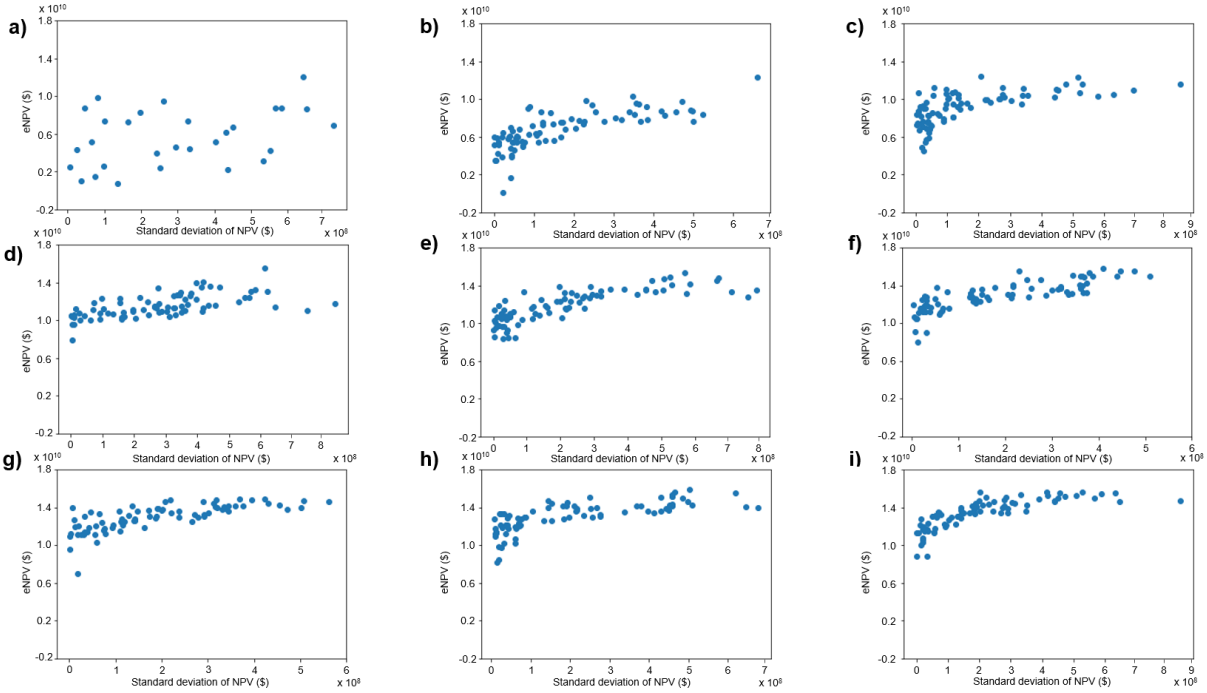

Figure 5.11 Progression of the objective space over generations, **a)** generation number 1**, b)** generation number 5**, c)** generation number 10**, d)** generation number 15**, e)** generation number 20, **f)** generation number 25, **g)** generation number 30, **h)** generation number 35, **i)** generation number 40.

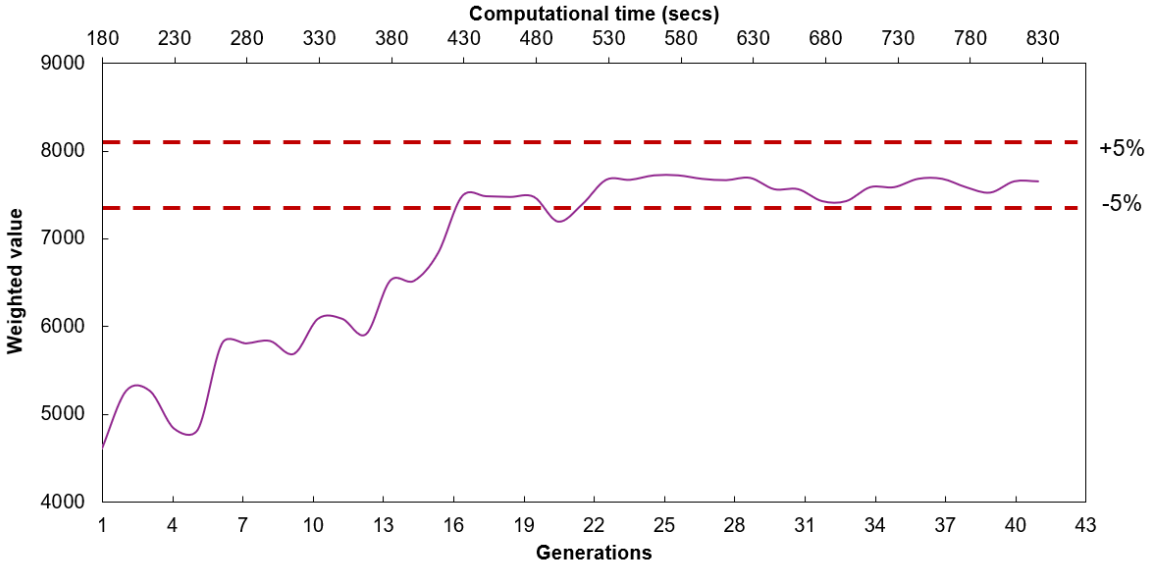

Figure 5.12 Change in the weighted objective functions with the number of algorithm generations. A secondary axis of computational time is provided to show the increased computational intensity required to achieve fitter solutions. Red dotted line = boundary defined where the optimal solution is +/-5% of the maximum value achieved in the study.

Table 5.8 Key model results across algorithm generations.

Generation number	Optimal solution (a, b)	Weighted value	Hypervolume (normalised)	Computational time (secs)
1	a: 9,866 b: 642	4,612	0.000	180
5	a: 9,877 b: 214	4,832	0.906	246
10	a: 12,393 b: 207	6,093	0.963	329
15	a: 14,104 b: 418	6,843	0.991	412
20	a: 14,929 b: 527	7,201	1.000	495
25	a: 15,865 b: 407	7,729	0.989	578
30	a: 15,754 b: 612	7,571	0.991	661
35	a: 15,883 b: 504	7,690	0.985	744
40	a: 15,729 b: 408	7,661	0.975	827

a = eNPV ($M), **b =** sdNPV ($M)

The second algorithm parameter to be investigated was the population size. In this case, the number of generations was fixed at 20. As discussed in Section 5.2, a population of 500 chromosomes were generated for sampling purposes, in order to minimise potential bias that may occur from consistently reinstating the population during each run. The change in distribution of the objective space was plotted across population sizes and the results are highlighted in **Figure 5.13**.

The shape of the Pareto front was shown to become more defined as the population size increased, driven largely by the increased saturation of points within the objective space. It must be noted that the Pareto did not significantly change in terms of the range of objective function values obtained across **Figures 5.13 a)** to **i)**, despite the smaller set of candidates evaluated (population size of 20). This was driven by the fixed number of generations used, where it was previously shown in **Figure 5.13** that the Pareto had taken shape around 20 generations, independent of population size. Therefore, the population size was shown to influence the coverage of the objective space more significantly over convergence and Pareto

distribution. A larger population resulted in a more evenly distributed Pareto front, which can be beneficial for the promotion of diversity and exploration of the decision space. It is worth noting that the number of non-dominated solutions found across the study was relatively small. This can be traced to the relatively strict budget and capacity constraints imposed, which was found to significantly reduced the number of feasible solutions (~40% breached these constraints).

Figure 5.14 derived the weighted objective function across population sizes and computational time exceeded. As denoted previously, equal weightings of 50 : 50 were given to each objective function and the weighted value was plotted with a ±5% threshold to assess convergence. This indicated that a population size of ~60 or greater could be considered to have attained convergence, where the data did not deviate outside the 5% boundary. Additionally, higher population sizes increased the computational intensity of the algorithm, with 100 solutions running for approximately 8 minutes. Balancing the time and population size was important considering the complexity of the algorithm moving forward. Furthermore, the specific data on the objective function values and hypervolume indicator are shown in **Table 5.9.** In the case of population size selection, hypervolume was considered to be a less important metric in defining the appropriate value. This is attributable to the larger hypervolume values found as population size increases, suggesting the method of portioning the objective space into rectangles was not suitable for the calculation of hypervolume when used as a solution quality indicator. Instead, computational time and satisfying the trade-off between exploration and exploitation were considered to be more significant metrics for selecting the population size for the case study.

Accommodating both exploration and exploitation when using meta-heuristic algorithms is an important trade-off to consider. Evidenced particularly in **Figure 5.13 i)**, a larger population size encouraged greater exploration of the objective space. However, focusing solely on this aspect can inadvertently place less significance on convergence towards higher Pareto ranks and hence the exploitation of fitter solutions. Therefore, selecting a population size that

promotes a balance between exploration and exploitation is beneficial. In particular, **Figures 5.13 d)** and **e),** which indicated adequate convergence, whilst sustaining a well populated objective space.

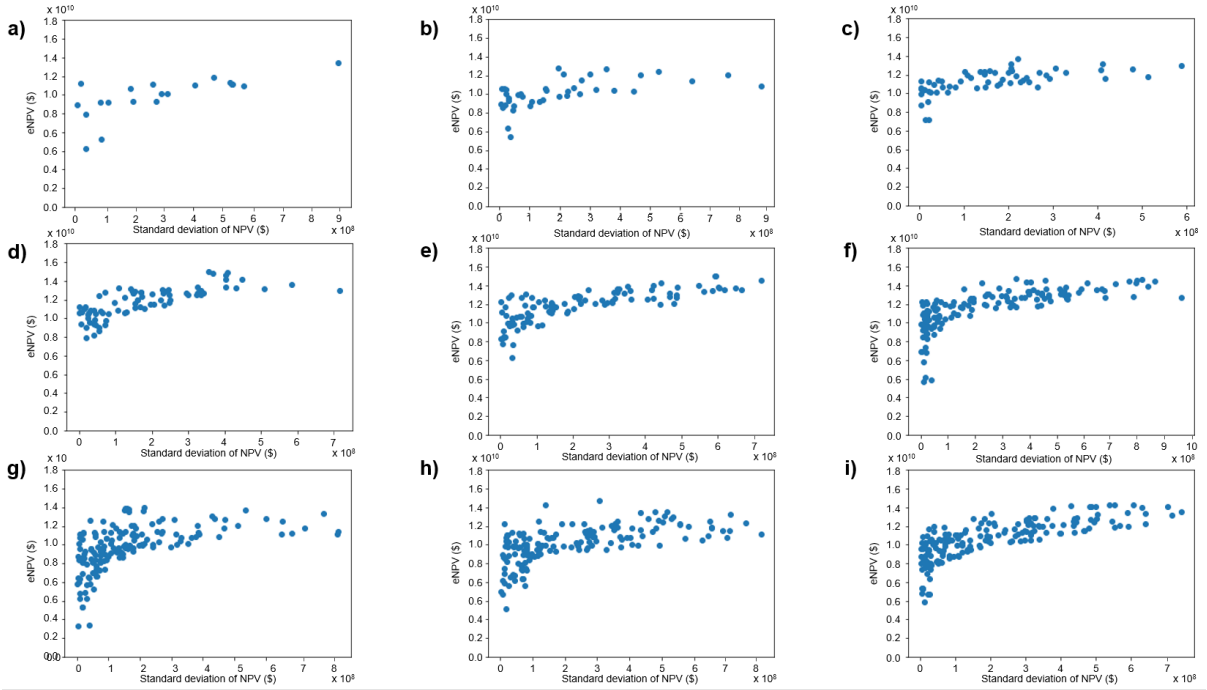

Figure 5.13 Progression of the objective space across population sizes, **a)** population size = 20**, b)** population size = 40**, c)** population size = 60**, d)** population size = 80**, e)** population size = 100, **f)** population size = 120, **g)** population size = 140, **h)** population size = 160, **i)** population size = 180.

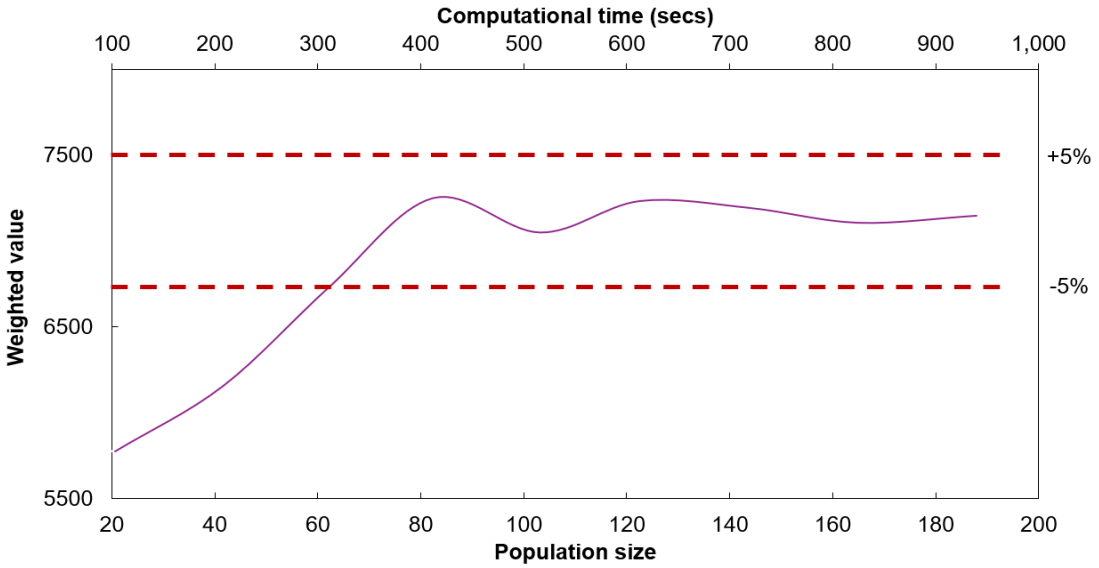

Figure 5.14 Change in weighted objective value with the population size. A secondary axis of computational time is provided to show the increased computational intensity required to achieve fitter solutions. The optimal line represents the fittest solution achieved after successive algorithm iterations. Red dotted line = boundary defined where the optimal solution is +/-5% of the maximum value achieved in the study.

Table 5.9 Key model results across population sizes evaluated.

Population size	Optimal solution (a, b)	Weighted value	Hypervolume (normalised)	Computational time (secs)
20	a: 11,905 b: 353	5776	0.000	103
40	a: 12,669 b: 356	6157	0.161	208
60	a: 13,797 b: 334	6732	0.377	311
80	a: 14,717 b: 778	6970	0.414	412
100	a: 14,708 b: 949	6880	0.632	516
120	a: 14,768 b: 304	7232	0.721	613
140	a: 14,733 b: 350	7192	0.808	720
160	a: 14,657 b: 626	7016	0.923	825
180	a: 14,351 b: 703	6824	1.000	940

5.4.2 What is the optimal portfolio structure when different batch: continuous ratios are assumed?

It is widely perceived that implementation of continuous manufacturing for mAb and ADC products can lead to a reduction in overall cost of goods compared to batch, with figures ranging from 10 – 35% depending on the kg demand of product (Mahal et al., 2021). As described in the problem statement in Section 5.3, the biotechnology company under consideration in this case study was assumed to run in-house batch processing capability, thus sourcing continuous capacity would require outsourcing or construction of a new facility. To investigate the impact of implementing next-generation continuously manufacturing mAbs or ADCs, on portfolio selection and capacity sourcing, two scenarios were evaluated relating to pipeline composition. The first case assumed that 20% of the potential pipeline of mAbs and ADCs requiring continuous manufacture. The second scenario increased this percentage to 80% of the prospective mAb and ADC pipeline. The results are outlined in the following section, providing both non-risk and risk-adjusted runs.

5.4.2.1 Non-risk adjusted approach

Though accounting for risk provides a more comprehensive and realistic output, a non-risk adjusted comparison was first presented to convey information on the underlying structure of the algorithm and how it may influence the choices made. Introduction of the Bernoulli-event simulation immediately, which is inherently stochastic, may neglect some significant trends in the progression of the algorithm, particularly with respect to drug and capacity selection. As such, **Figure 5.15** presents the objective space and resulting Pareto front from the final generation of algorithm, with specific reference made to the five of the top performing candidate solutions. The progression of the objective space and discovery of the Pareto can be found in **Figure C2** in Appendix C. Furthermore, the portfolios associated with the circled solutions can be found in **Figure 5.16**. Overall, the these exhibited structural similarities concerning portfolio selection and capacity strategies. Particularly relevant to the case study comparison, the top-performing solutions consistently opted for more than 90% of the

available products requiring continuous manufacture in the pipeline, which were shaded grey in **Figure 5.16**. Additionally, there was shown to be benefits in facility building occurring slightly later in terms of timing, as in all cases, the first instance of “F” occurred in Year 1.

Despite the lack of representation in the pipeline, drugs requiring continuous manufacture were shown to be preferentially selected, as over 90% of those available were selected in the top performers (details are provided in **Table 5.10**). This equated to selecting at least nine out of the ten continuously manufactured products available in the pipeline. The inclusion of a substantial percentage of mAbs or ADCs requiring continuous manufacture in the optimal portfolios was noteworthy, given that these products accounted for only 20% of the overall pipeline. Additional insights could be gained by comparing this 20% figure to the proportion of continuous products in each winning portfolio. The ratios of continuously manufactured products to batch in each winning portfolio ranged from 36%: 64% to 43%: 57%, indicating a preference for selecting continuous products, particularly relevant to the pipeline ratio of 20%: 80% continuous to batch. For the sake of contextual comparison, it is worth noting that the proportion of products requiring continuous manufacture in a lower-performing portfolio was significantly lower. For instance, a solution selected from Pareto rank 8 for analysis contained only 40% (four out of ten) of the available continuous options, which represented 21% of the entire portfolio. This comparison further reinforces the inclination towards incorporating proteins requiring continuous manufacture, leveraging the lower cost of goods.

In terms of capacity sourcing, the ratios of in-house: CMO: future facility are displayed in **Table 5.10**. The percentage of drugs in the winning portfolios occupying in-house capacity ranged from 21 – 36%, providing benchmarks to compare with the 80% pipeline scenario later. Moreover, the solutions depicted in **Figure 5.16** were the result of a constrained optimisation problem, in terms of both budget and capacity. The capacity ratios defined in **Table 5.10** evidence the influence of constraints upon the composition of the portfolio, specifically the distribution of in-house and future facility options, as indicated by the orange and green shading. Given the stricter limitations on in-house capacity (four manufacturing trains

available), large groupings of these options were not observed. This is attributable to the dynamic nature of the capacity constraint, where selection of in-house manufacturing for multiple products each year created significant pressure upon capacity, particularly when considering the products already utilising in-house capacity in the starting portfolio. As will be highlighted in the risk-adjusted simulation provided later in the section, drug failures were indirectly beneficial in adhering to capacity constraints. Products that failed before commercialisation represented opportunities for capacity to be directed toward a successful drug to be manufactured in-house.

Figure 5.16 also provided insights into the importance of the facility build timing in relation to the cash-flow. When assessing any given candidate portfolio, the algorithm considered the index of the first instance of “F” or 2 in ternary representation. Where “F” first occurred related to the position in the cash-flow at which building was initiated (i.e. building occurred in parallel to development of the given drug). Other drugs associated with an “F” for a capacity strategy could then occupy commercial capacity. It must also be noted that the entry years defined for each drug were indexed in different terms to that described for the discounting in the cash-flow. For example, entry years of 1 and 2 into the portfolio were equivalent to Years 0 and 1 respectively, with respect to the cash-flow and hence discounting of costs. To this end, across the winning portfolios, the first instance of “F” occurred in drugs with a portfolio entry year of 2, equivalent to Year 1 in the cash-flow. As a result, the capital investment to build was injected later within the cash-flow and was discounted by a factor of $\frac{1}{(1+0.11)^n}$, where n represented the year index in the cash-flow. In practical terms, this decreases the initial facility investment by a factor of 1.11, proving advantageous to the eNPV. The capital investment was assumed to be spread evenly over the course of the build time of three years, thus further discounting occurred in Years 2 and 3, by factors of 1.23 and 1.37 respectively, driving slightly later build positions from a profitability perspective.

Table 5.10 Key outputs for top performing candidate portfolios in the 20% study.

Candidate portfolio	eNPV ($bn)	SdNPV ($bn)	% of portfolio which is continuously manufactured	% of continuous options selected from pipeline	Capacity strategies (IH:CMO:FF)
1	16.1	0.20	40%	100%	24%: 64%: 12%
2	16.1	0.21	36%	90%	36%: 44%: 20%
3	15.5	0.13	43%	90%	29%: 52%: 19%
4	15.1	0.02	38%	90%	24%: 52%: 24%
5	14.6	0.01	42%	100%	21%: 58%: 21%

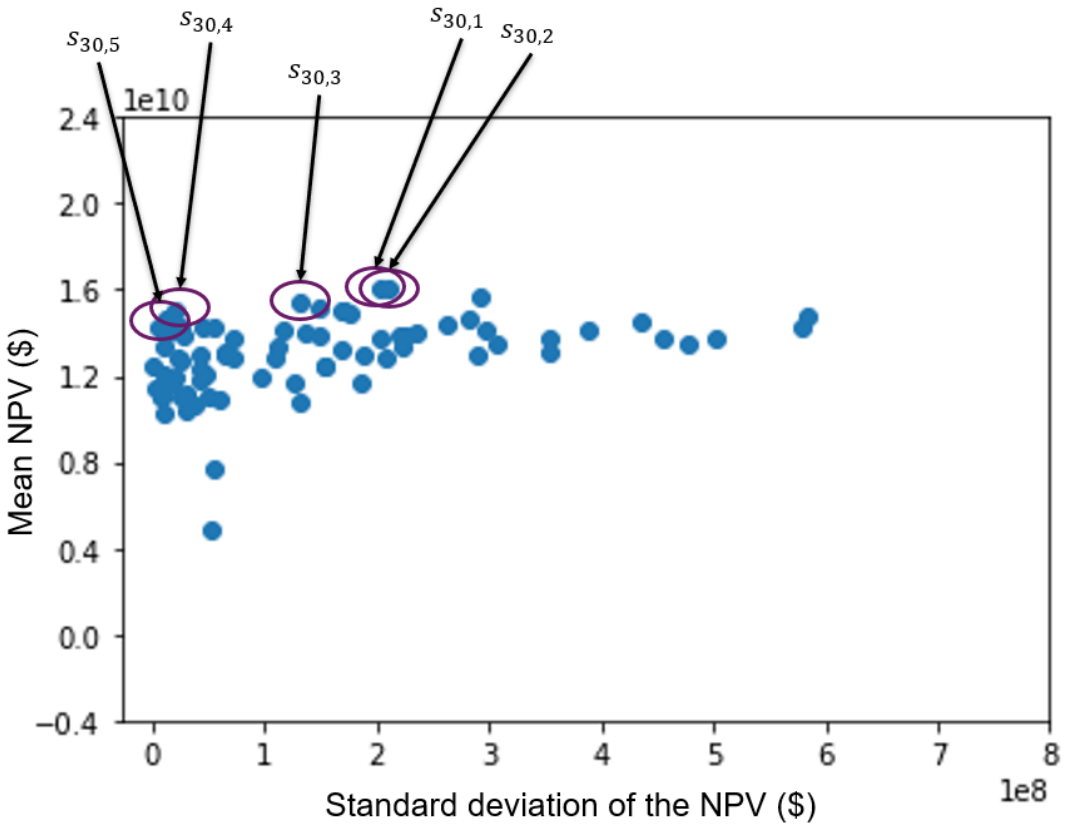

Figure 5.15 Plot of the objective space from generation 30. Circled solutions are part of the non-dominated frontier or Pareto rank 1 and were hence selected to further analyse on a drug-by-drug basis. As discussed in Section 5.2, candidate solutions are generally represented by $s_{g,p}$, where g = generation number and p = solution index in the population.

Solution 1 - $s_{30,1}$

M3	M4	M8	A1	A2	M11	M12	M13	M14	M16	M17	M18	M19	M23	M24	A5	A6	M25	M27	M29	M32	A7	M34	M35	M40
C	C	C	I	I	C	I	C	I	F	I	C	F	C	C	C	C	F	C	C	C	I	C	C	C

Solution 2 - $s_{30,2}$

M2	M3	M4	M8	A1	M11	M12	M13	M14	M17	M18	M19	M20	M23	M24	A6	M27	M28	M29	M30	M32	A7	M34	M35	M40
I	C	I	C	I	F	C	C	I	I	C	C	C	I	C	F	F	I	I	F	C	I	C	C	F

Solution 3 - $s_{30,3}$

M9	M11	M12	M13	M15	M16	M18	M19	M20	M22	M23	M24	A6	M27	M30	M32	A7	A8	M35	M36	M40
C	C	F	I	I	C	I	C	C	I	C	F	C	F	C	F	I	I	C	C	C

Solution 4 - $s_{30,4}$

M4	M8	A1	A2	M9	M11	M12	M16	M17	M18	M19	M20	M23	M24	A6	M25	M27	M30	M32	A7	A8	M34	M35	M36	M40
I	C	C	I	C	C	C	F	C	C	C	I	C	C	C	F	F	C	F	I	I	C	F	I	F

Solution 5 - $s_{30,5}$

M3	M8	A1	A2	M11	M13	M16	M18	M19	M20	M23	M24	A6	M25	M27	M29	M30	M31	M32	A7	M35	M38	M39	M40
C	C	I	I	F	C	I	I	C	C	C	C	C	I	C	C	F	C	F	F	C	F	C	C

Figure 5.16 Structure of the candidate portfolios highlighted in **Figure 5.14**. Each set of two rows represents a single candidate portfolio, as denoted in the figure. M = mAb product and A = ADC product. I = in-house, C = CMO and F = future facility. Orange shading = internal capacity options selected (in-house), blue shading = outsourcing to CMO and green shading = future facility. Grey shading = products that are manufactured continuously and white shading = products that are manufactured in batch mode.

The second scenario evaluated the case where 80% of the pipeline were continuously manufactured, with the remaining product options produced in batch mode. As with the 20% continuous case study, the objective space was plotted across a number of generations (see **Figure C3** in Appendix C) and the final iteration was was selected for further analysis, shown in **Figure 5.17**. The top five strategies chosen for analysis are depicted in **Figure 5.18**. Overall, selection of continuous options was more likely due to their prevalence within the pipeline, coupled with a distinct decrease in in-house capacity selected. Additionally, the range of eNPV values generated across top performers was significantly higher than those found in the 20% pipeline scenario.

As with the 20% scenario, **Table 5.11** evidenced the continued preference for including continuous products relative to their weighting in the pipeline, where the ratio of continuous to batch in the winning portfolios ranged from 80: 20 to 88: 12, thereby greater than or equal to the ratio in the pipeline. The economic benefits of including more continuous proteins is exhibited by the distribution of eNPVs within **Table 5.11** compared to **Table 5.10**. Here, the average of top performing eNPV values in the 80% scenario was found to be 21% higher than that in the 20% scenario. This was driven by the lower overall COG values for continuously manufactured products, along with the smaller capital investment required for a future facility focusing primarily on smaller, continuous trains compared to fed-batch. This was shown to override the differences in a higher early phase process development effort for continuous products over batch or the premium set on CMO activities, as defined in the trade-off in Section 5.3. Furthermore, in terms of capacity sourcing, **Figure 5.18** indicated the preference for build and buy manufacturing options (future facility and CMO) when including more continuous options in the pipeline. This is particularly evidenced by the reduction in orange-shading comparing **Figures 5.17** and **5.18**, thus a reduction in the use of available in-house manufacturing capacity, which decreased on average across solutions from 27% to 8%. This is attributable to the feature within the model that continuous manufacturing was not permitted by the in-house facility available, hence only CMO and future facility options could be selected.

To this end, position of the facility build was shown to be less significant than in **Figure 5.17**, as less capacity options were available for the portfolios weighted towards products requiring continuous manufacture over batch.

Whilst the economic benefits from both a cost of goods and profitability perspective are noteworthy, it is also important to consider the qualitative attributes that support the decision-making process. In general, continuous manufacturing is evidenced to achieve higher productivities than fed-batch, which allow for smaller downstream facility footprints due to smaller upstream volumes to process. Moreover, with particularly reference to perfusion cell culture, the periodic removal of product results in shorter residence times in the reactor and is often linked to lower rates of product degradation (Khanal & Lenhoff, 2021). It is however, a less established platform for the manufacturing of biologics than a batch flowsheet and so it is important to consider the company's current level of expertise and therefore the potentially additional process development effort required when recommending the integration of continuous manufacturing.

Table 5.11 Key outputs for top performing candidate portfolios in the 80% study.

Candidate portfolio	eNPV ($bn)	sdNPV ($bn)	% of portfolio which is continuously manufactured	% of continuous options selected from the pipeline	Capacity strategies (IH:CMO:FF)
1	19.9	0.23	88%	73%	6%: 55%: 39%
2	19.2	0.03	80%	60%	4%: 53%: 43%
3	18.6	0.03	88%	70%	13%: 53%: 34%
4	18.4	0.03	84%	68%	6%: 66%: 28%
5	17.7	0.01	84%	68%	9%: 56%: 35%

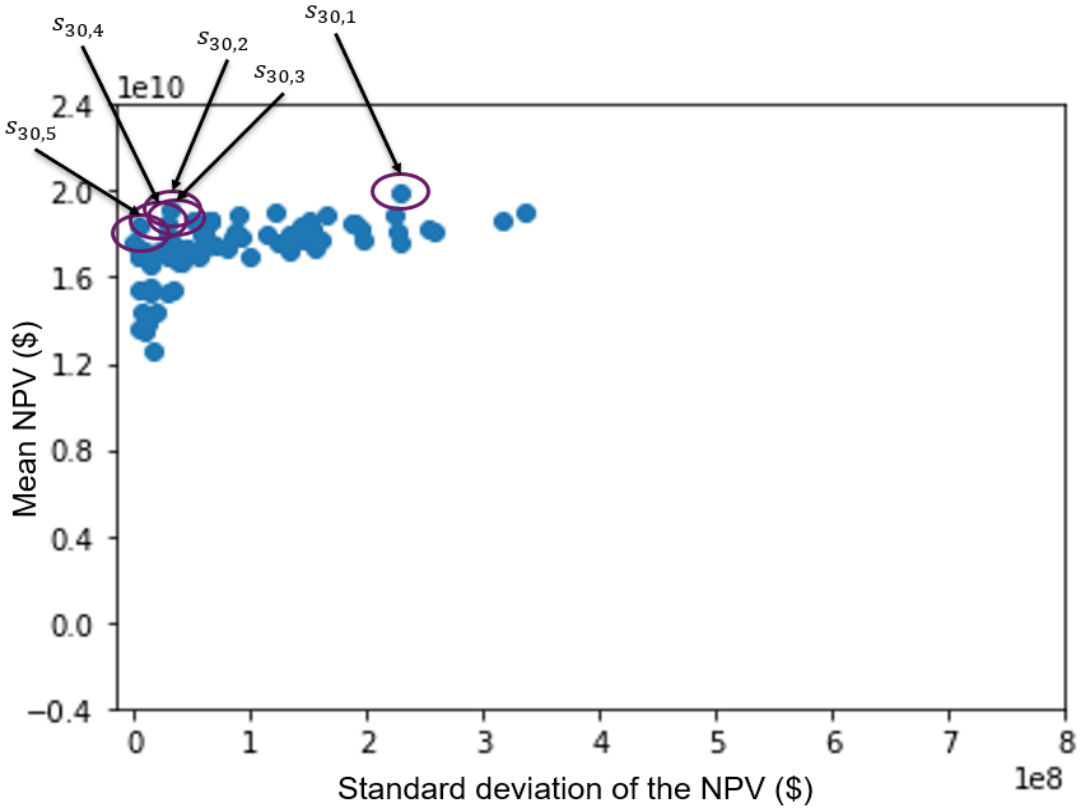

Figure 5.17 Plot of the objective space from generation 30. Circled solutions are part of the non-dominated frontier (or Pareto rank 1) and were hence selected to further analyse on a drug-by-drug basis. As discussed in Section 5.2, candidate solutions are generally represented by $s_{g,p}$, where g = generation number and p = solution index in the population.

Solution 1 - $s_{30,1}$

M2	M3	M4	M7	M8	A2	M9	M11	M13	M15	M16	M17	M18	M19	M20	M22	M23	M24	M28	A6	M25	M26	M28	M30	M31	M32	M33	M34	M35	M36	M37	M39	M40
F	C	I	F	C	F	F	F	C	C	C	F	C	F	I	F	C	F	C	C	C	C	C	F	C	C	F	F	F	C	C	C	C

Solution 2 - $s_{30,2}$

M1	M3	M4	M7	M8	M11	M12	M13	M14	M17	M19	M20	M21	M22	M23	M24	A5	A6	M27	M28	M30	M31	M32	A7	A8	M34	M35	M38	M40	A10
C	F	F	F	C	C	C	C	F	F	F	C	C	F	F	C	C	C	F	C	C	F	C	I	F	F	C	C	F	C

Solution 3 - $s_{30,3}$

M1	M2	M3	M5	M8	M9	M11	M13	M14	M15	M16	M17	M18	M19	M20	M21	M23	M24	A5	A6	M25	M27	M28	M30	M32	A7	A8	M34	M35	M39	M40	A10
C	F	F	F	C	C	C	C	F	C	F	C	C	C	I	C	C	F	I	C	F	F	I	F	C	I	F	F	C	C	C	C

Solution 4 - $s_{30,4}$

M3	M4	M7	M8	A2	M11	M15	M16	A4	M17	M18	M19	M20	M21	M23	M24	A6	M25	M26	M27	M28	M30	M31	M32	A8	M33	M34	M35	M36	M39	A9	A10
F	C	C	C	C	F	F	F	C	C	F	C	I	C	C	C	C	C	C	C	I	C	F	C	F	C	C	C	C	F	C	F

Solution 5 - $s_{30,5}$

M2	M3	M5	M7	M8	M9	M11	M12	M13	M15	M16	M18	M19	M20	M21	M22	M24	A5	A6	M25	M26	M28	M29	M30	M31	A7	A8	M34	M35	M37	M38	A10
C	F	C	C	C	C	F	I	F	F	F	C	C	I	C	C	F	C	F	C	C	I	C	F	C	C	F	C	C	F	F	C

Figure 5.18 Structure of the candidate portfolios highlighted in **Figure 5.16**. Each set of two rows represents a single candidate portfolio, as denoted in the figure. M = mAb product and A = ADC product. I = in-house, C = CMO and F = future facility. Orange shading = internal capacity options selected (in-house), blue shading = outsourcing to CMO and green shading = future facility. Grey shading = products that are manufactured continuously and white shading = products that are manufactured in batch mode.

Most notably, **Figures 5.17** and **5.18** evidence the differences in portfolio size generated between the case studies, where the average size was found to be 24 drugs and 32 drugs respectively. This revealed a significant structural driver within the algorithm and can be directly traced to the nature of constraint-handling employed throughout, which as described in Section 5.2, was a penalty function method. Initially, penalty values of 0 for the eNPV and 1×10^{10} for the sdNPV were assigned to the objective functions of violating solutions to penalise their rankings in the population, thereby favouring the selection of superior strategies that comply with budget and capacity constraints. However, this approach may inadvertently exclude from consideration solutions with favourable attributes that are worth inheriting in subsequent generations. Notably, in this case, larger portfolios may be disproportionately penalised as they breach capacity constraints, rather than switch the violating genes to CMO or FF options that would be deemed feasible. Over the course of the algorithm run, this can cause populations to converge towards smaller portfolios. Therefore, to ensure that differences in fitness between scenarios were truly attributable to portfolio characteristics and not influenced by size biases, a repair strategy was implemented in cases where in-house capacity was exceeded. This concerned switching in-house strategies to CMO (i.e. 0 to 1) in solutions where a capacity violation was flagged.

The 20% continuous pipeline was compared with and without the repair with respect to the eNPV, portfolio size and the number of constraint violations. Detailed results of this analysis is presented in **Table 5.12**, with the drug selection and capacity characteristics for the scenario using the repair strategy provided in **Figures C4** and **C5**. This confirmed the unintentional bias introduced when opting for a penalty function for in-house capacity constraints, indicated by the increase in both average eNPV and portfolio size, along with the decrease in in-house constraint violations after implementation of the repair strategy. Utilising the repair strategy yielded a 12% increase in average eNPV over the 20% scenario when using a penalty function method. This highlighted the benefits to inclusion of a repair strategy for the 20% scenario to allow for an equitable assessment between the pipeline case studies. Nonetheless, the 80%

scenario still achieved a ~9% higher average eNPV than the improved 20% scenario, reinforcing the benefits of the continuously weighted pipeline over batch when similar sizes portfolios are assessed.

Table 5.12 Change in eNPV and portfolio size when repair strategy is implemented.

Pipeline scenario	Average eNPV ($bn)	Average portfolio size (# drugs)	Budget constraints violated	Capacity constraints violated (IH)	Capacity constraints violated (FF)
20% (without repair)	15.5	24	7	24	0
20% (with repair)	17.3	32	9	0	0
80%	18.8	32	7	0	9

5.4.3 How does risk dynamically impact the portfolio?

Whilst the previous section uncovered significant underlying trends within the algorithm, in terms of both constraint-handling and performance, it did not yet integrate the realistic impact of the drug failure risk. As outlined in Chapter 4, accounting for success probabilities is crucial due to the inherently high levels of uncertainty and risk associated with drug development and commercialisation. Additionally, the work conducted in Chapter 4 highlighted the impact of these success rates upon budgets within a static environment, with no investigation into how failures impact capacity planning or profitability.

In order to simulate the realistic trajectory of drug portfolios, the addition of dynamic risk was achieved through use of a Bernoulli event-based simulation for all drugs at each development phase (outlined in Section 5.2.9). The application of the simulation upon the population of solutions generated in both the 20% and 80% continuous pipeline generated the results in **Table 5.13**. In line with that generated in the non-risk adjusted case, the 80% continuous pipeline achieved a higher average NPV than the 20%. From the data in **Table 5.13**, the average NPV for the 80% continuous pipeline was shown to be 16% higher than the 20% scenario. Significantly, no constraints were violated across scenarios in comparison to the

non-risk adjusted scenarios. This highlighted some of the unintentional capacity benefits that arose when drug failure occurred, where failures represented opportunities for capacity or remaining budget to be directed towards another project. As a result, the repair strategy previously detailed was not necessary in the risk-adjusted case.

Table 5.13 Risk-adjusted results for both continuous pipeline scenarios.

Scenarios	eNPV ($bn)	sdNPV ($bn)	Percentage of portfolio that is continuously manufactured (%)	Capacity sourcing ratios (IH:CMO:FF)
20% continuous pipeline	6.32	0.5	40%	23%: 50%: 27%
	5.67	0.3	34%	50%: 40%: 10%
	6.12	0.4	33%	33%: 59%: 8%
	5.12	0.3	33%	0%: 57%: 43%
	4.83	0.1	38%	15%: 40%: 45%
80% continuous pipeline	7.55	0.5	100%	0%: 63%: 37%
	5.29	0.3	87%	0%: 50%: 50%
	6.97	0.4	90%	10%: 60%: 30%
	6.28	0.4	90%	0%: 50%: 50%
	6.41	0.2	82%	9%: 55%: 36%

A major driver governing solution performance after application of the Bernoulli event-based simulation was the distribution of failures across the development phases, as well as the actual average LOA from Phase I (how many drugs were commercialised from the total injected before the application of risk). **Figure 5.19 a)** highlighted these characteristics in both top performers and for illustrative purposes, a subset of lower performing solutions. This was conducted on the 80% continuous pipeline due to its performance earlier in the case study. Top performing solutions yielded an average 3-fold higher eNPV over lower performers. **Figure 5.19 a)** indicated the correlation between high profitability and higher achieved LOA from Phase I rates. In practice, portfolios achieving higher overall success rates (a greater conversion of injected drugs to commercial success) correspond to a smaller proportion of failures and hence less expense incurred within the portfolio for no revenue gain. On a similar track, the data split in **Figure 5.19 a)** indicated that earlier failures also drove higher eNPV values. The raw data in **Figure 5.19 b)** evidenced that in top performers, over 90% of failures

occurred in Phase I. Comparatively, 69 – 83% of failures occurred in Phase I for the example lower performing solutions. For similar reasons to lower achieved LOA from Phase I rates, portfolios where the majority of failures occurred later into the development pathway (i.e. Phase II and in particular Phase III) resulted in greater expense injected into the cash-flow for no return for the failed drug, which reduced overall profitability. In general, Phase I clinical trials were characterised by relatively small patient pools and as a result, the process development and manufacturing activities that support the trial equivalently required either less personnel effort or smaller product demands. As a result, failure landscapes weighted greatly towards Phase I are associated with smaller injections of expense for no revenue return than those with failures also in Phase II and III (when comparing similar sized portfolios).

From an algorithm perspective, consideration of the optimal placement of the Bernoulli-event based simulation within the optimisation tool was accounted for. As a means of validation, two scenarios were evaluated with respect to the placement. The first of these initiated the simulation prior to running the optimisation loop across generations, hence occurred immediately post-initialisation of the population. This effectively meant that genetic operations such as selection, crossover and mutation took place on risk-adjusted chromosomes (where failed drugs had been removed from the candidate solutions). The second scenario introduced the simulation at the end of the algorithm, specifically after the last generation.

Application of the risk simulation before any genetic procedures were undertaken was found to unintentionally bias the outputs, with results paralleling that of non-risk adjusted scenario. Conversely, placement of the simulation after algorithm completion produced a far more realistic set of risk-adjusted results. The issues with the first scenario are associated with the tendency for the algorithm to optimise the objective functions, hence over time and with the use of genetic operators such as crossover and mutation, larger portfolios were produced that were preferentially selected for their typically higher associated profitability values. As such, the second placement scenario for the Bernoulli event-based simulation was applied within each case study, to characteristic the risk of failure on a more realistic basis.

a)

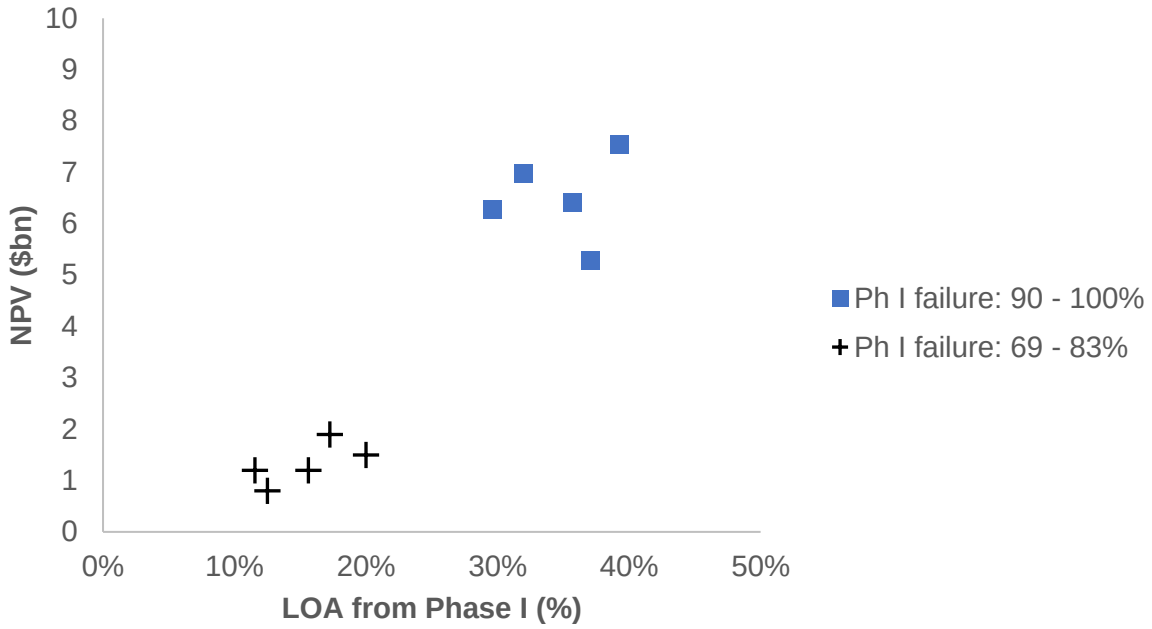

b)

Solutions	NPV ($bn)	Successful drugs	Total injected drugs	Failed in Phase I (%)	Calculated LOA from Phase I (%)
Top performers (rank 1)	7.55	11	28	94%	39%
	5.29	10	27	90%	37%
	6.97	8	25	100%	32%
	6.28	8	27	90%	30%
	6.41	10	28	94%	36%
Lower performers (rank 8)	1.9	5	29	83%	17%
	1.5	6	30	77%	20%
	1.2	5	32	74%	16%
	1.2	3	26	69%	12%
	0.8	4	32	79%	13%

Figure 5.19 a) Profitability of selected candidate solutions compared with the overall LOA from Phase I (%). The data is split corresponding to the percentage of failures that occur early, i.e. in Phase I, **b)** raw data corresponding to that plotted in **a).**

5.4.4 How does the injection of CGTs impact the portfolio characteristics?

The previous sections outlined the impact of different manufacturing strategies upon portfolio selection and capacity sourcing for protein therapeutics, specifically mAbs and ADCs. However, as described in the problem statement in Section 5.3, the biotechnology company being modelled also considered the injection of CGT products (i.e. AAVs and CAR T cells) into the portfolio, at an initial rate of one product per year. As such, the impact of CGT injection was evaluated on the optimal portfolio characteristics. Significantly, this was investigated initially through a sensitivity analysis utilising the same risk profiles introduced in Chapter 4. Within that case study, worst-, base- and best-case success rates were defined for all modalities under consideration (also restated in **Table 5.7**) and their influence on CMC budgets within a static environment were outlined. The worst-case success rates for CGTs were assumed to be significantly lower than for protein therapeutics and the best-case higher, linked to that reported to date within the literature and also in line with the relative nascency of CGTs in comparison to protein therapeutics. Having said this, evaluating a range of success rates for CGTs is important given the nascent nature of the field. Success rates can vary depending on the level of experience with new modalities ranging from an understanding of the link between the manufacturing process and product quality through to how best to demonstrate clinical safety and efficacy with evolving regulatory frameworks. Values typically range from 3 – 36% depending on these experience levels.

Consequently, the sensitivity analysis conducted within this chapter utilised the success rates from Chapter 4, but determined the dynamic implications of injecting a modality mix into portfolios and the influence of drug failure across various risk profiles. Across scenarios, the Bernoulli event-based simulation was conducted and the resulting top performing portfolios recorded. Key structural characteristics emphasised from the resulting solutions included the ratios of mAbs, ADCs, AAVs and CART and how this changed across the risk profile employed. The results are highlighted in **Figure 5.20**. On average, the eNPV was shown to increase with

success rate, shown in its descent from the red shading towards the blue. Significantly, the worst-case profile included CGTs in only one out of five of the winning solutions, however upon an increase in success rate, a more even modality distribution within the portfolio was shown.

In a strictly deterministic environment, the base-case risk scenario underlined the profitability benefits in sporadic injection of CGT products. Compared to the same scenario in **Table 5.13**, where only mAbs and ADCs were evaluated, the average eNPV was shown to increase from $6.5bn to $7.3bn in **Figure 5.20.** This was driven by the significantly higher selling prices assumed for CGTs, ranging from $450,000 to $2,000,000. Though the patient populations were assumed to be smaller than for mAbs and ADCs, the revenues generated from these selling prices were shown to override the impact of the smaller market demands.

In contrast, the worst-case risk scenario generated lower eNPVs on average than those in the base- and best-cases, attributable to the greater number of failures occurring. Due to the relatively wide success rate distribution for CGT therapeutics, they are not generally featured within the winning portfolios, evidenced by the change in product distribution compared to the base-case and best-case. For CGTs, the worst-case LOA from Phase I was assumed to be 3.5%, roughly translating to a probability of 1 in 30 CGT products achieving success. Interestingly, the worst-case risk scenario resembles that of the data in **Table 5.13**, where only mAbs and ADCs were considered in the portfolio.

Overall, the increase in average eNPV from the worst-case to best-case scenario was found to be 34%. Furthermore, the analysis demonstrated the high risk, high reward nature of CGT commercialisation. This trade-off was particularly shown in the deviation in portfolio composition across risk profiles, but a significantly higher base-case and best-case NPV compared to the protein-only scenario previously shown. As such, a more in-depth analysis of this trade-off was conducted to assess the impact of varying CGT injection ratios, as well as risk : reward weightings.

Worst-case risk profile

Candidate portfolio	NPV ($bn)	Product ratios (mAb: ADC: AAV: CART)
1	7.24	90%: 10%: 0%: 0%
2	6.68	75%: 0%: 25%: 0%
3	6.25	86%: 14%: 0%: 0%
4	6.20	80%: 20%: 0%: 0%
5	5.81	72%: 28%: 0%: 0%

Base-case risk profile

Candidate portfolio	NPV ($bn)	Product ratios (mAb: ADC: AAV: CART)
1	8.14	73%: 9%: 9%: 9%
2	7.66	64%: 29%: 7%: 0%
3	7.25	91%: 9%: 0%: 0%
4	7.14	84%: 8%: 0%: 8%
5	6.31	70%: 20%: 10%: 0%

Best-case risk profile

Candidate portfolio	NPV ($bn)	Product ratios (mAb: ADC: AAV: CART)
1	9.71	70%: 12%: 6%: 12%
2	9.54	73%: 7%: 7%: 13%
3	8.24	100%: 0%: 0%: 0%
4	7.80	67%: 8%: 17%: 8%
5	7.76	60%: 20%: 10%: 10%

Figure 5.20 Sensitivity analysis results when three risk profiles are considered in the portfolio optimisation framework. The probabilities of transition success used across scenarios are found in **Table 5.7**. The red shading represents the worst-case. The white shading is the base-case. The blue shading is the best-case.

5.4.5 How does the portfolio structure change if CGTs are injected at the same rate as mAbs?

Up to this point, CGT products were injected at a rate of one per year, alternating between AAVs and CAR Ts. This translated to 10% of the pipeline being CGT products, with the remainder protein therapeutics. To indicate the impact of developing mixed-modality portfolios on portfolio structure, an additional two scenarios were evaluated, where the percentage of CGTs in the pipeline was increased. Of the ten drugs to potentially be injected per year, scenarios where 3 (30%) and 5 (50%) of these were CGTs were investigated relative to the 10% case, across the same three probability of transition success profiles – worst, base and best. The results are presented in **Figure 5.21**, indicating the significance of risk profile upon the resulting portfolio composition and capacity sourcing structure. As success rate increased, the inclusion of more CGTs in the winning portfolios was observed, chiefly driven by the higher

LOA from Phase I associated with AAV and CAR T products versus the proteins in the best-case risk profile (36% versus 12 - 14% respectively). This trend was observed across each CGT ratio in the pipeline. Similarly, increasing the percentage of CGTs injected into the portfolio (i.e. from left to right in the matrix) also increased the likelihood of their appearance in the final portfolios, independent of success rate.

Even when a worst-case risk profile was assumed, injecting a higher percentage of CGTs into the pipeline resulted in an increasing quantity within the resulting portfolios, moving from 0% towards 29% in the case of the 50% CGT scenario. This is attributable to the quantity of CGTs available in the pipeline. More significantly, the 30% and 50% CGT scenarios highlighted the profitability benefits arising from including an increased number of CGTs within the portfolio, indicated by shading in **Figure 5.21**. Particularly at the base and best-cases, the winning portfolios were shown to exceed the eNPV threshold set, in comparison to lower percentages of CGTs in the pipeline.

Scenarios where an increased proportion of CGTs were found in the winning portfolios highlighted the preference for building capacity and hence manufacturing within these future facilities. As described in Section 5.3, both AAV and CAR T cell products required a separate facility to mAbs and ADCs. In part, this preference for future facility options in **Figure 5.21** was driven by a lower competition, as separate facilities were assumed, however the key driver related to the CMO premium required for AAV and CAR T products. A higher premium was assumed for CGTs over proteins (2 versus 1.5), therefore effectively inflating commercial COGs by a factor of 2, driving the utilisation of the build-capacity for CGT weighted portfolios.

In summary, the results presented in this section emphasise the realistic nature of the risk: reward trade-off associated with CGT commercialisation, where high selling prices allow for large returns and hence eNPVs, however there is a greater uncertainty associated with their development, given the perceived wider probabilistic range of success reported. As only the eNPV as an objective function was studied within this particular section, it was also necessary to consider the quantitative impact of including CGTs upon the sdNPV, further expressed as

the risk associated with the profitability. Therefore, the next section examined variations in the weighting of the objective functions and its influence upon the choice of optimal portfolios.

NPV > $8bn / NPV < $8bn		CGTs in pipeline (%)		
		10%	**30%**	**50%**
Risk scenario	**Worst**	100 : 0 14: 42: 44	80 : 20 7: 40: 53	71 : 29 3: 33: 64
	Base	82 : 18 9: 40: 51	64 : 36 1: 31: 68	57 : 43 0: 32: 68
	Best	75 : 25 4: 35: 61	59 : 41 0: 34: 66	46 : 54 0: 30: 70

Figure 5.21 Optimal portfolio composition across different CGT injection rates when success rate (risk scenario) is also varied. Within each box, the top value represents the ratio of protein products to CGT products within the final portfolio and the bottom value highlights the ratio of in-house to CMO to future facility capacity selected. The shading (key in the top-left) represents those solutions that fall below or above a set NPV threshold, defined here as $8bn. The risk scenarios represent those presented in **Table 5.7**.

5.4.6 How does the portfolio structure change if risk is favoured over reward?

The NSGA-II elements of the algorithm introduced in Section 5.2 were primarily intended for the ranking of the population, by giving equal consideration to each objective function. However, in practice, decision-makers may find it beneficial to assign different priorities to objectives depending on their business goals. This prioritisation can be achieved by weighting either objective, which typically involves multiplication or division of the objective function value by a fixed factor or coefficient. This process plays a crucial role in achieving optimal solutions that address problem-specific goals and particularly in this context, where profitability and risk

are the objectives, satisfy companies adopting either a more risk-averse or risk-tolerant approach.

To capture these weightings, three scenarios were generated and presented in **Figure 5.22**. As a control, the equally weighted series was presented alongside those where the priority was placed upon both the reward and risk. In each case, a weighting factor of 2 was applied. When prioritising the reward, the factor of 2 amplified the eNPV as the goal was to maximise the profitability. Conversely, the sdNPV was divided by the factor to minimise the risk. Of additional note, the sensitivity scenarios (i.e. worst, base, best) were not conducted here, thus to consider the uncertainty and variations in the success rates across modalities, these were instead considered within the Monte Carlo simulation as an uncertain input parameter, utilising the inputs distributions from **Table 5.7**.

As depicted in **Figure 5.22 a)**, a shift towards lower eNPVs was shown when favouring risk. Significantly, **Figure 5.22 b)** applied the same colour-coding as in **a)**, which highlighted the change in portfolio composition across weighting scenarios. This evidenced the propensity for protein-dominated portfolios when the minimisation of risk is favoured and above all, the high risk, high reward nature of CGT directed portfolios.

When a higher weighting was assigned to the eNPV, the curve was shown to have greater y-values due to the priority given to the profitability. In contrast, the sdNPV values were shown to have a relatively wide distribution, but in general were clustered towards the higher end of the axis. This was attributable to the cumulatively higher risk associated with solutions that favoured reward. This also correlated with favouring a portfolio composition that included up to ~55% CGTs, as depicted in **Figure 5.22 b).** As a result, the benefits of including AAV and CAR T products when reward is favoured became apparent, attributable to the higher selling prices of CGTs relative to mAbs and ADCs. As risk was considered a less significant objective in this weighting scenario, the uncertainty associated with CGT commercialisation did not heavily impact the optimisation algorithm, emphasising the risk: reward trade-off. Conversely, when prioritising the risk, winning portfolios contained less than 15% of CGT products. The

risk-averse approach favoured the injection of mAbs and ADCs, which had a tighter distribution of transition success rates, hence a relatively more robust set of products within the pipeline. An indication of the smaller range of standard deviations generated is evidenced in **Figure 5.22 a)** with the grey-shaded line. Despite the overall lower profitability, these values fell between $0.5bn and $1bn.

In summary, this study provided a more diverse set of user-tailored scenarios, as in practice, decision-making may be weighted towards curtailing risk or bolstering profitability depending on the overall business goals. As shown, the drug ratios in resulting portfolios were found to be significantly dependent on the weighting of either objective function, with protein-dominated considered to be a less risky approach over a generally more profitable CGT and protein equal portfolio ratio. The scenarios provide benchmarks on optimal portfolio weightings for an array of company-specific aims.

a)

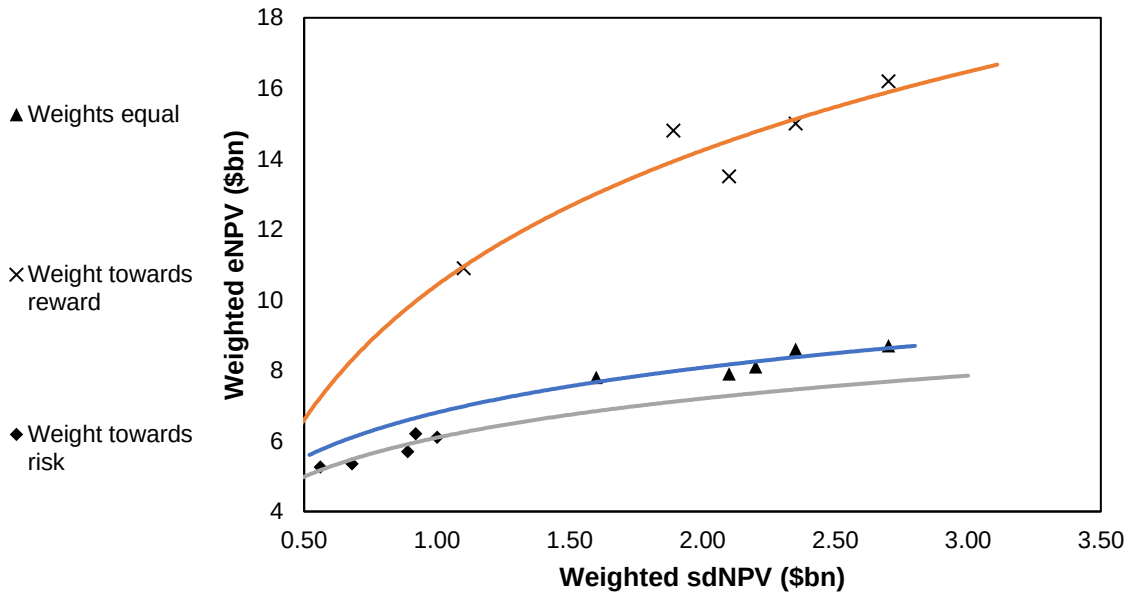

b)

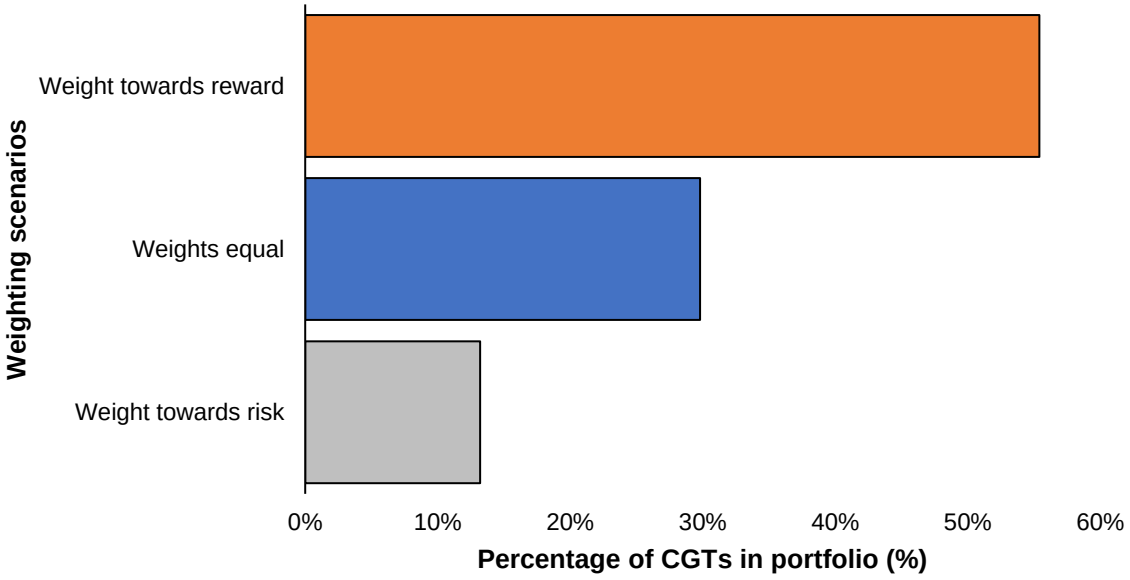

Figure 5.22 a) Top ranking solutions plotted by each objective when different weightings were assigned to each objective function and **b)** the percentage of CGTs that appeared in the top performing portfolios in each weighting scenario. The bar colour in **b)** correspond to the lines in **a).**

5.5 Conclusion

This chapter sought to address a series of portfolio management and capacity planning case studies utilising the decisional tool described in Section 5.2. This first evaluated the impact of batch versus continuous manufacturing for mAb and ADC pipelines on portfolio selection and capacity decisions, considering both the impact of a non-risk and risk simulated environment. Providing both scenarios with and without the presence of the risk simulation gave insights into the algorithm performance structurally, which further motivated the use of a repair strategy for constraint-handling. The analysis indicated the benefits of including drugs requiring continuous manufacture within portfolios, with up to a 16% increase in eNPV over the predominantly batch pipeline. Particularly for a large biopharmaceutical company, already with some experience in the continuous manufacturing space, this highlighted the benefits to incorporating a greater proportion of continuously manufactured products in the portfolio. This further evidenced the requirement for sourcing external capacity or building in capabilities when favouring continuous products, where the average utilisation of existing in-house capacity decreased from 27% to 8% between the 20% and 80% continuous scenarios.

The addition of the dynamic impact of success probabilities revealed the significance relating to the timing of drug failure in the optimal portfolios. The case study supported the general heuristic that failing early is preferable, particularly when comparing optimal portfolios with lower performing solutions. Between 90 – 100% of drug failures occurred early (i.e. Phase I) in better performing portfolios, concurrent with the earlier conclusions regarding the smaller expense injected for no return, versus the 69 – 83% of failures in Phase I for lower performers. This was attributable to the greater expense required for later failures without revenue, which were characterised by larger trials and equivalently more PD effort and manufacturing demands.

The consideration of AAV and CAR T products within the pipeline reflected the extent of the risk: reward trade-off associated with their development. Lower transition success rate scenarios tended to exclude CGTs from the top candidate portfolios, however larger eNPV

values were exhibited through their inclusion in either the base or best-case scenarios. Furthermore, introducing weighting to each objective function provided a realistic spread of scenarios to address the potential for various business goals. This further emphasised the risk: reward trade-off, where 15% of CGTs were selected in portfolios during the risk-averse scenario, versus 55% in the risk-tolerant approach. This indicated the quantitative impact of the wider success rate distributions that have been reported in the literature for CGTs, namely linked to their nascency and the mixed success achieved across a range of industry players. As such, it is important to note that whilst the risk: reward trade-off for CGT inclusion highlighted in this work is certainly relevant to companies looking to increase activity in the space, there would be variation in the case of companies that solely target CGT products and that already have facility infrastructure to support in-house manufacturing of AAVs and CAR-Ts.

6 Conclusions and future work

6.1 Introduction

The work carried out in this thesis presented three distinct applications of a decisional tool, addressing industrially relevant case studies in areas of AAV process economics, drug development budget estimation and ultimately portfolio management and capacity sourcing. There was an initial focus upon AAV manufacturing, with a comparison between traditional and scalable flowsheets alternatives. This included an optimisation algorithm that investigated a variety of flowsheet options in terms of cost-effectiveness and meeting purity targets. The focus was then shifted towards investigating mAb, ADC, AAV and CAR T products in Chapters 4 and 5. These were initially evaluated statically, outlining the R&D budgets per product success across phases. The final chapter sought to integrate the previous elements of the tool, to be used for portfolio management and capacity sourcing purposes and approached the study with a consideration for the dynamics of drug success or failure. The results presented throughout this thesis are summarised within this chapter and are supported by suggestions for how the work could be extended in the future.

6.2 Process economic evaluation and optimisation of AAV manufacturing

6.2.1 Summary of findings

The work in Chapter 3 provided a cost comparison between traditional versus more scalable AAV manufacturing strategies. This constituted an initial evaluation of adherent versus suspension cell culture, as well as batch ultracentrifugation and anion exchange chromatography as a polishing purification option. Additionally, to capture the variability arising in AAV serotype behaviour, a comparison between intracellularly and extracellularly expressed AAV products was presented. The tool allowed for slightly different flowsheets for either case, which varied the product stream accordingly (i.e. cells for intracellular AAVs and the culture

broth for extracellular AAVs). The deterministic element of the tool described in Chapter 3 was utilised to calculate the COG/dose for any given AAV manufacturing scenario. The tool also featured a Monte Carlo simulation to assess the robustness or risk associated with each base-case scenario, considering the impact of uncertain process parameters and inputs. Moreover, the study was further extended to capture a larger set of AAV processing options, which were rapidly evaluated through use of a brute-force optimisation algorithm within the tool.

The results highlighted the potential for up to 40% COG/dose savings in utilising more scalable flowsheet alternatives in AAV manufacturing. Furthermore, COG/dose differences were shown to be minimal at smaller dose sizes, particularly when comparing suspension and adherent cell culture. This supported some of the industrial trends observed that companies targeting indications with lower dose sizes have not implemented suspension cell culture. The uncertainty analysis feature of the decisional tool indicated the relative robustness of implementing suspension and AEX-based flowsheets. For the competing flowsheets, the uncertain input parameters had a more significant impact upon the adherent and ultracentrifugation sizing and ultimately the COG/dose distributions generated, highlighting the greater relative risk associated with these strategies. Moreover, upon expansion of the set of flowsheet options available, the optimisation framework indicated the benefits of continuous ultracentrifugation as a polishing purification option. Continuous ultracentrifugation offered a cost-effective alternative to chromatography, coupled with a high purity performance. Nevertheless, further process development effort was concluded to be likely for continuous ultracentrifugation to be implemented in a commercial environment.

6.2.2 Future work

Though the brute-force optimisation portion of the work in Chapter 3 evaluated a plethora of AAV manufacturing options, there is a more novel subset of purification options available commercially that were excluded from analysis, driven by a lack of assumptions available, particularly on a comparative basis with packed-bed chromatography. Therefore, future research could feature the inclusion and hence evaluation of more novel purification

approaches. In particular, this could include nanofibres, which introduce advantages over packed-bed chromatography by offering higher surface areas and porosity, avoiding some of the diffusion and pressure drop limitations encountered in the packed-bed strategies. Additionally, nanofibres show the potential for a large reduction in residence time, which may reduce the overall purification time. Other options include membrane chromatography or monoliths, which provide similar advantages to nanofibers in terms of reducing bottlenecks in processing time. Monoliths additionally have been perceived to provide higher purification capacities than traditional packed-bed. Studying these novel purification techniques in comparison to traditional options may highlight the purification benefits with respect to HCP, DNA and empty capsids, potentially allowing for a one-step purification in some cases. The reduction in the number of processing steps would lead to improvements in overall yield and circumvent any bottlenecks in terms of step durations.

In terms of scheduling, assumptions were made throughout the case study that a single seed train, through culture maintenance, could be used to seed four production batches. This allowed for the overall number of production batches performed annually to be increased, as running a new seed for each batch creates scheduling bottlenecks unless activities are parallelised. It may therefore be beneficial to investigate the impact of this upon the COG/dose, by varying the number of production batches seeded by one seed train. This would present a mapping of various production scenarios and would likely lead to multiple production trains required in parallel to meet annual demands. There could also be qualitative considerations given to the study, such as any caveats related to the cell viability or any deterioration through seed maintenance. Therefore, future work could seek to address this trade-off between economic and operational attributes, potentially through implementation of a MCDM analysis.

6.3 Estimation of CMC budgets for novel modalities

6.3.1 Summary of findings

Chapter 4 outlined the budgets required for the development of mAbs, ADCs, AAVs and CAR T cell products. This evaluated the contribution of process development, manufacturing and clinical trials costs on a phase-by-phase basis, as well as the impact of transition success rates on the number of projects required to produce a market success. In addition, the process development and manufacturing activities were collectively described as the CMC component of the total out-of-pocket cost. This grouping was used to define the contribution of clinical versus non-clinical activities towards the total cost. Furthermore, the tool also incorporated a sensitivity analysis to strengthen the conclusions drawn on the optimal budgets under varying transition success rate scenarios. These evaluated success rates on both a modality basis, as well as by disease area.

In the initial study, mAbs were found to require the smallest overall out-of-pocket costs per success, driven by lower CMC costs, which represented 19% of the whole budget. In comparison, between 30 – 42% of the budgets for ADCs, AAVs and CAR T were related to CMC activities. Furthermore, clinical trials costs across modalities did not vary significantly, despite the trade-off between trial cost per patient and patient population employed for CGTs versus proteins. The introduction of the sensitivity analysis indicated the relative risk associated with CGTs over proteins, evidenced by the wider distributions of total out-of-pocket cost determined when evaluating success rate by modality group. Conversely, the sensitivity on success rate by indication highlighted a change in optimal modality across disease areas. This drove an additional case study on determining the critical success rate at which this change in optimal modality occurs, which was found to be 16%. Below this value, mAbs were found to provide the smallest budget and if over, AAV was optimal.

6.3.2 Future work

At present, the study assumed all modalities took non-accelerated development or regulatory pathways to commercialisation. However, particularly in the case of CGT products, regulatory agencies typically grant access to at least one accelerated pathway, which was discussed in-depth in Chapter 1. In this case, the durations along the pathway would be reduced or in some situations, certain phases may be circumvented altogether. Therefore, future research could direct efforts towards evaluating the impact of accelerated regulatory pathways on the budgets. The speed at which the field evolves would necessitate regular model updates as part of future research, namely relating to development timelines and cost assumptions. This may be particularly relevant for AAVs and CAR T cell products, as existing products on the market, e.g. Luxturna, Kymriah, were reported to have taken an expedited pathway. This would introduce alternative scenarios to compare with the more traditional protein therapeutics, potentially highlighting some of the additional regulatory benefits that can be leveraged when developing and commercialising novel therapies.

Moreover, the work in Chapter 4 assumed a trade-off between the clinical trial cost per patient for proteins and CGTs, which remained constant throughout each scenario evaluated. Particularly relevant to the sensitivity analysis on success rate by indication, further work could bolster the conclusions drawn by including variations in trial cost per patient for each indication in parallel with the transition success rates. This addition would allude to any additional factors that govern changes in the optimal modality with respect to budget.

Furthermore, the CMC development cost framework produced enables process change decisions to be evaluated from a COG versus cost of development (COD) perspective. Further research on this would involve evaluating each modality on a switch in manufacturing procedure along the development pathway, particularly investigating the impact on COG and COD when early versus late phase-switching is undertaken. In general, a process change necessitates a bridging study take place to confirm comparability in terms of product quality and stability, thus incurring greater development costs. Conversely, a manufacturing change

is often implemented to drive down COG values through enhanced scalability or process optimisation, thus the trade-off between COG and COD.

6.4 Portfolio management and capacity planning for mixed modality portfolios

6.4.1 Summary of findings

Chapter 5 presented an integrated model framework to perform portfolio optimisation and capacity planning for mixed modality portfolios (proteins versus CGTs as with Chapter 4). The goal of the optimisation process was maximisation of the expected profitability, generated through a discounted cash flow to calculate the NPV, as well as minimisation of the standard deviation of the NPV, which qualitatively translated to the volatility or risk associated with the profitability. Candidate solutions (or portfolios) within the algorithm concerned drug selection from the available pipeline and the commercial capacity sourcing strategy utilised for each. The algorithm itself comprised a GA basis, with modifications to traditional crossover and mutation to operate on a two-dimensional chromosome structure. The algorithm also featured components of an NSGA-II for handling the presence of multiple objectives, bespoke constraint handling strategies and a Bernoulli-event based simulation for emulating biopharmaceutical risk of failure.

The initial study focused on a pipeline with only protein products (mAbs and ADCs) available. This evaluated the impact of batch versus continuously manufactured proteins, comparing a batch-dominant pipeline to a continuous-dominant and how this influenced the resulting final portfolios selected by the algorithm. The results indicated the preference for selecting continuously manufactured products, regardless of whether they were dominant in the pipeline, driven by the lower COGs that could be achieved relative to batch. Furthermore, consideration of risk via the Bernoulli simulation highlighted the profitability benefits in portfolios where the majority of failures occur early (i.e. in Phase I). Significantly, the impact of injecting CGT products into the portfolio was investigated, highlighting the risk : reward trade-

off associated with their addition. It was found that favouring profitability (i.e. reward) as an objective function yielded winning portfolios with a greater proportion of CGTs injected compared to the case where risk (standard deviation of NPV) was favoured.

6.4.2 Future work

Firstly, when considering the specifics of the algorithm and computational methods employed, unique crossover and mutation techniques were implemented. This built upon the principles of uniform crossover and mutation, however adapted their execution to suit a two-dimensional chromosome structure. Due to the novelty of these techniques, there is potential for further research to be conducted on comparing these with other methods of crossover and mutation. Soon et al. (2013) highlighted a study which compared single-point, k-point and uniform crossover and mutation in terms of performance with respect to the objective function. A similar study may be beneficial for two-dimensional chromosomes and equally for a multi-objective optimisation problem.

Furthermore, on the case study side, capacity was a fundamental part of the optimisation string, where each drug selected within the portfolio had a capacity strategy associated with it. In-house and future facility capacity was constrained and as outlined in Chapter 5, solution feasibility was assessed by considering the batches required to manufacture each product and the years when manufacturing took place. If the number of available batches and then manufacturing trains were exceeded for a particular year, a constraint violation arose. Further research could involve modelling capacity not only as a constraint, but perhaps also as an additional objective function in the optimisation process. This may involve derivation of the optimal production schedule for the drugs in the portfolio, which can be framed as a combinatorial optimisation problem.

Finally, consideration of the realistic impact of portfolio diversification would be a beneficial additional to future drug selection problems. Specifically, it is possible that success for one product may adversely impact another if they target the same indication. Having multiple drugs

in the portfolio that are within the same disease area can introduce competition and hence limit returns for one drug over the other. In previous studies, this has been quantified with a series of factors to be applied to the revenue (revenue dependencies).

6.5 Summary

In summary, the work in this thesis demonstrated the importance of decisional tools in providing insights on a range of industrially relevant case studies, including those related to process design, allocating development budgets and portfolio and capacity decisions. This also highlighted the benefits of mathematical modelling techniques and computational methods in satisfying these process-business trade-offs. This chapter outlined the potential to build upon the work carried out in this thesis, with suggestions for novel integrations at both the modelling and case study levels.

7 Commercialisation

7.1 Introduction

The tool described throughout this thesis gave rise to a potential plan for its commercialisation as a biopharmaceutical decision-support tool. As a result, this chapter provides details on how commercialisation could be achieved, including key considerations required. The current state of the tool is discussed, to ascertain the extent to which current components can be leveraged in a commercialisation environment. Similarly, any software or framework alternatives that can aid interactivity are also outlined. Logistical considerations are also made, including data sourcing, security measures, pricing strategy and ongoing performance reviews (and code amendments if necessary).

7.2 Tool appraisal for industrial practices

At present, the model described throughout this thesis was developed in Python 3.8, using Spyder as an IDE and Jupyter notebook as a GUI. To aid the simplicity of using the tool internally within industry, several software additions were made to the Jupyter framework to enhance its applicability commercially. This firstly involved a library addition to Jupyter notebook to allow parts of the code to be selectively hidden or not. From a practical perspective, this would allow users unfamiliar with Python programming to be concerned only with inputting data, rather than scanning through the bulk of code. Similarly, Python allowed accessed to a variety of measures to improve interactivity of assumption definition, particularly through the use of ipywidgets. Specifically, this is a library within Python that enables assumptions to be displayed in different ways, e.g. sliding scales, check-boxes, dropdown boxes. The specific details of these additions are outlined in the following sections.

7.2.1 Hiding Jupyter code

When used in the biopharmaceutical industry, it is often the case that users may not possess the specialist programming knowledge to handle extensive sections of complex code

displayed on a Jupyter notebook GUI. Particularly in cases where code is often very long and outputs can be generated sporadically throughout, displaying all code can decrease the effectiveness and efficiency of using the tool in industry. As a result, a Jupyter notebook extension was sought to enable the option of code hiding, leaving only inputs cells or outputs on the GUI. This was achieved through use of an extension called “NbExtensions”, where this contained an option for hiding code as a checkbox. This is practically highlighted in **Figure 7.1**. The resulting output from triggering the hide code command is displayed in **Figure 7.2**.

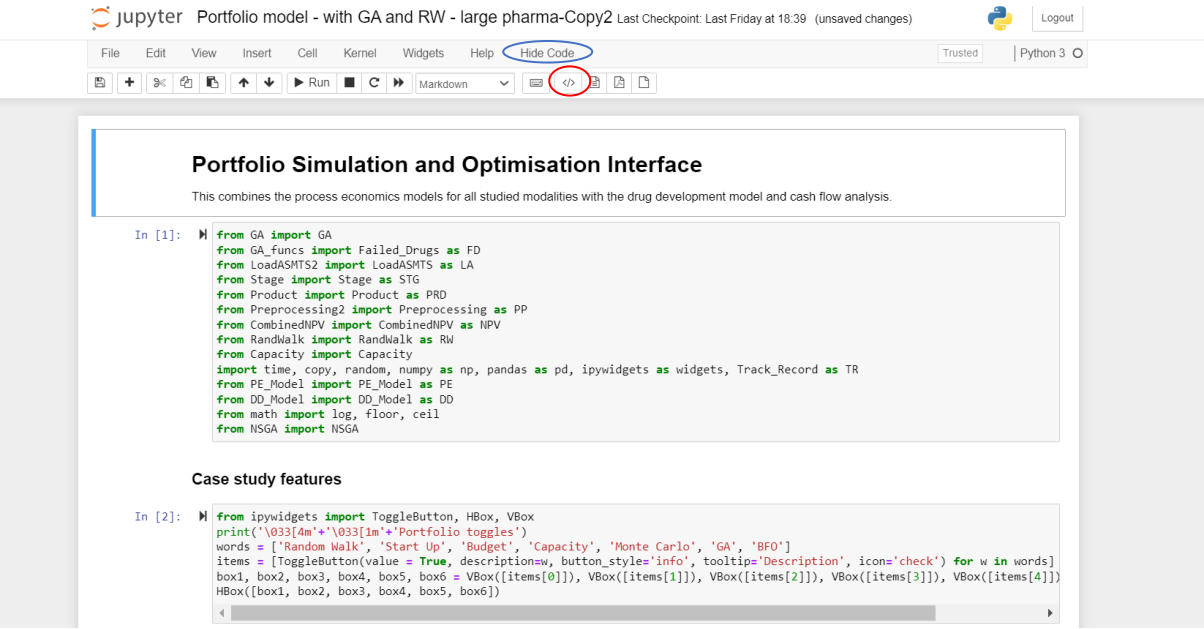

Figure 7.1 Snapshot of the GUI for the decisional tool on Jupyter notebook. The blue circle highlights the hide code tab installed through “NbExtensions” and the red circle highlights a shortcut to access this hide code feature.

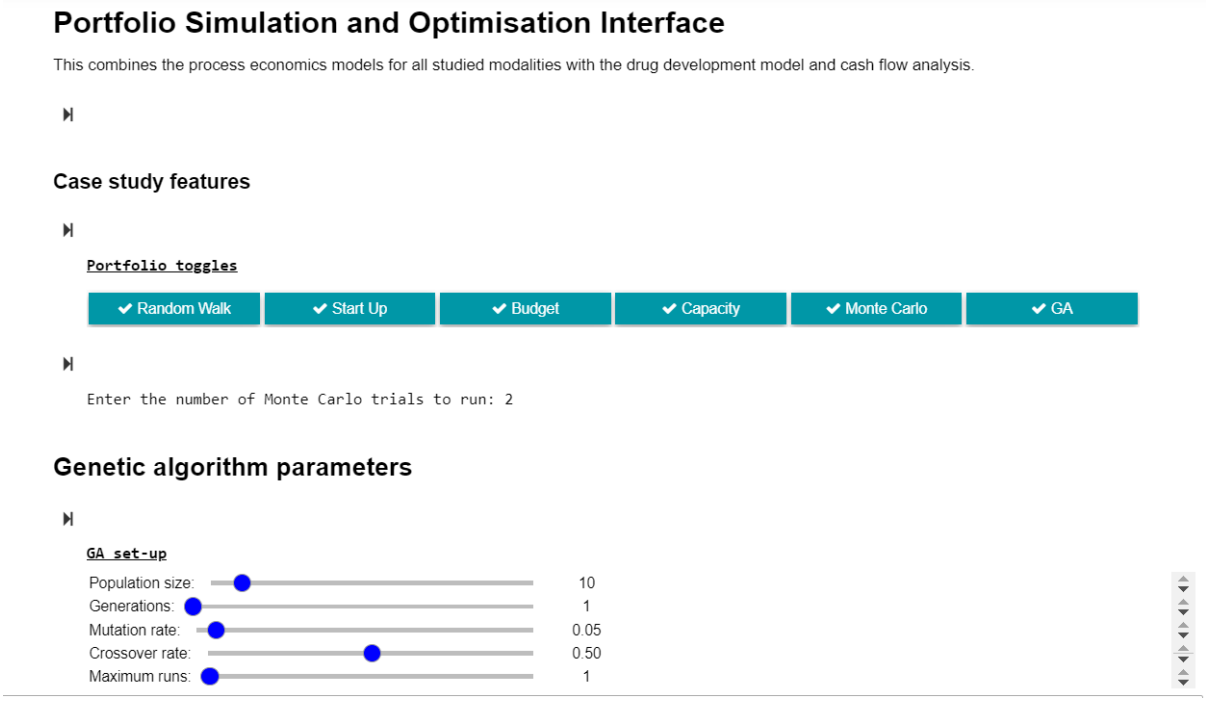

Figure 7.2 Resulting GUI from enabling the hide code feature. The only remaining displays are any input widgets or outputs from the functioning of the hidden code.

Though the previous elements described improved the overall experience and interactivity of the decisional tool, there are alternatives means to create a GUI using Python-related libraries or software, or by leveraging the capabilities of a different program. Development of an intuitive and user-friendly GUI is essential to allow for non-programming users within the biopharmaceutical industry opportunities to understand the tool better. Python itself has several alternative libraries, such as Tkinter or PyQt. In contrast, building an interface that is web-based may evoke the need for a framework such as Flask or Django.

Tkinter is a standard library for GUI implementation in Python. Running the library from the command line triggers a separate window to open, which highlights the most basic example of a Tkinter-generated GUI. This also utilises widgets to display any inputs. However, in all of the aforementioned software or libraries, companies may benefit from having access to a specialist programmer, to aid in any troubleshooting when issues arise.

7.2.2 Implementation of widgets

In general, widgets refer to a component of the GUI that confers a level of interactivity to performing some function. In Jupyter notebook, this is commonly achieved through importing the library “ipywidgets”. This enables addition of widgets such as sliding scales, checkboxes, dropdown boxes or buttons for toggling various assumptions.

Implementation of widgets improves interactivity, particularly for users with little coding experience. The default alternative to expressing assumptions as widgets is changing the assumptions within the code itself, which can be more tedious to edit. Furthermore, rerunning certain cells of code is not necessary when using widgets, allowing for increased productivity.

Some examples of this can be seen in **Figures 7.1** and **7.2**. As highlighted, the GA specific parameters were controlled by a sliding scale. Elements pertaining to the case study setup, such as whether optimisation was to be constraint or not, or the risk simulation was run were controlled by toggle buttons. Alternatively, numerical inputs such as the number of Monte Carlo trials were not strictly controlled by a instance from the ipywidgets library, but rather an input cell. The syntax corresponding to this is highlighted in **Figure 7.3**.

```
risk_MC = int(input("Enter the number of risk trials to run: "))
```

Figure 7.3 Syntax relating to the input of the number of Monte Carlo trials. Input is an in-built Python 3.8 function for entering numerical data if paired with int().

7.2.3 Performance

Throughout the model construction process, performance testing was routinely conducted to ensure outputs were generated in a timely manner. As discussed in Chapter 5, the overall model speed was increased by ~120-fold over its previous state. Initially, generation of expenses and revenue required running the integrated process economics and drug development model within the modified-GA for each drug in each portfolio evaluated. This was

found to impair efficiency of the tool, particularly when full-scale datasets and other additions, such as the Monte Carlo or Bernoulli-event based simulation, were included. This was circumvented through introduction of data structures such as dictionaries and lists as a means to store costs outside the modified-GA loop. Other means of code optimisation were performed, such as avoiding large library imports and instead only calling the specific functions required.

Furthermore, the tool currently communicates with Microsoft Excel for loading assumptions related to process economics, drug development and portfolio attributes across modalities. At present, this functioned effectively and Excel is regarded as a relatively user-friendly database software within the biopharmaceutical industry. However, in cases where the scalability of the datasets increase, Microsoft Excel can be limiting in terms of time and hence may evoke performance issues within the tool as a whole. Alternatively, structured query language (SQL) databases provide a scalable alternative to Excel, particularly where datasets are likely to expand. Furthermore, considering the use of this tool by multiple users within a company, SQL is beneficial for maintaining the integrity of databases across versions. The drawbacks lie in the relative complexity of SQL over Excel, which may hinder tool use for non-technical users.

7.2.4 Supporting documentation for usage

One of the fundamental elements when considering commercial deployment of the decisional tool is provision of a user-guide or supporting documentation for its implementation. At the most basic level, both Spyder and Jupyter notebook allow for commentary throughout, which was leveraged for this decisional tool to provide indications of why certain functions or equations were included. Jupyter notebook enabled more extensive commentary, where cells could be changed to markdown over code to add text (see **Figures 6.1** and **6.2**).

However, for large-scale use, a separate supporting document could be beneficial to construct for use in industry. This would provide a comprehensive tutorial, including installation of Python and additional Jupyter extensions required for full interactive accessibility. A user guide would

be included that defines relevant tool functions and features and any particular caveats that a user would find helpful.

Understanding the simplicity of using the tool, or lack-thereof, there has been an opportunity to distribute the tool for use in a student project. This provided opportunities to understand where extra explanation or notes would be beneficial in a real commercial environment. Therefore, in accessing the commercial feasibility of the tool in its current state, this documentation requires writing.

7.2.5 Revenue

Looking beyond internal use, full commercialisation of the tool would require consideration of a revenue model or pricing structure. The choice of scheme depends on a number of factors and in practice may require a deeper valuation of the product and market characteristics, however there are a number of common revenue models used for computational tools.

A one-time purchase-based license is often implemented, where a fee is paid once and the tool is free to use perpetually. Alternatively, a subscription-based revenue scheme is also often opted for, where users pay on a fixed term to access the tool. From a cash-flow perspective, this provides a more consistent revenue stream and could be useful in defining tiers of access, e.g. certain subscription levels to access more features of the tool. It also provides greater simplicity in implementing version updates and troubleshooting. Ultimately, from a contextual perspective a subscription-based model would provide the flexibility required in the biopharmaceutical industry, where differing model tiers can accommodate the varying needs of individual industry users. From a consumer perspective, a model that allows users to stop paying when they no longer require the tool is also attractive and serves as a marketing benefit.

Bibliography

Abozaid, G. M., Kerr, K., McKnight, A., & Al-Omar, H. A. (2022). Criteria to define rare diseases and orphan drugs: a systematic review protocol. *British Medical Journal Open*, *12*(7), e062126. https://doi.org/10.1136/BMJOPEN-2022-062126

Allay, J. A., Sleep, S., Long, S., Tillman, D. M., Clark, R., Carney, G., Fagone, P., McIntosh, J. H., Nienhuis, A. W., Davidoff, A. M., Nathwani, A. C., & Gray, J. T. (2011). Good manufacturing practice production of self-complementary serotype 8 adeno-associated viral vector for a hemophilia B clinical trial. *Human Gene Therapy*, *22*(5), 595–604. https://doi.org/10.1089/hum.2010.202

Allmendinger, R., Simaria, A. S., Turner, R., & Farid, S. S. (2014). Closed-loop optimization of chromatography column sizing strategies in biopharmaceutical manufacture. *Journal of Chemical Technology and Biotechnology*, *89*(10), 1481–1490. https://doi.org/10.1002/jctb.4267

Arnett, A. L. H., Ramos, J. N., & Chamberlain, J. S. (2012). Gene therapy of skeletal muscle disorders using viral vectors. *Muscle, 2*, 1045–1051. https://doi.org/10.1016/B978-0-12-381510-1.00076-4

Aslanidi, G., Lamb, K., & Zolotukhin, S. (2009). An inducible system for highly efficient production of recombinant adeno-associated virus (rAAV) vectors in insect Sf9 cells. *Proceedings of the National Academy of Sciences of the United States of America*, *106*(13), 5059–5064. https://doi.org/10.1073/pnas.0810614106

Ayuso, E., Mingozzi, F., & Bosch, F. (2010). Production, Purification and Characterization of Adeno-Associated Vectors. *Current Gene Therapy*, *10*(6), 423–436. https://doi.org/10.2174/156652310793797685

Basu, S. B., Liebman, R. S., & Saponjian, Y. (2017). *Decoding Phase II Clinical Trial*

Terminations. Converge Advisory Group. http://www.convergeadvisory.com/app/download/13807055/20170908+Phase+II+Terminations+WP+vF.pdf

Behera, N. (2020). Analysis of microarray gene expression data using information theory and stochastic algorithm. In *Handbook of Statistics* (pp. 349–378). https://doi.org/10.1016/bs.host.2020.02.002

Bennicelli, J., Wright, J. F., Komaromy, A., Jacobs, J. B., Hauck, B., Zelenaia, O., Mingozzi, F., Hui, D., Chung, D., Rex, T. S., Wei, Z., Qu, G., Zhou, S., Zeiss, C., Arruda, V. R., Acland, G. M., Dell'Osso, L. F., High, K. A., Maguire, A. M., & Bennett, J. (2008). Reversal of blindness in animal models of leber congenital amaurosis using optimized AAV2-mediated gene transfer. *Molecular Therapy*, *16*(3), 458–465. https://doi.org/10.1038/sj.mt.6300389

Bioprocess International. (2019). *Zolgensma: We all know the price, but how is it made?* Bioprocess International. https://bioprocessintl.com/bioprocess-insider/therapeutic-class/zolgensma-we-all-know-the-price-but-how-is-it-made/

Booth, M. J., Mistry, A., Li, X., Thrasher, A., & Coffin, R. S. (2004). Transfection-free and scalable recombinant AAV vector production using HSV/AAV hybrids. *Gene Therapy*, *11*(10), 829–837. https://doi.org/10.1038/sj.gt.3302226

Bracewell, D. G., Francis, R., & Smales, C. M. (2015). The future of host cell protein (HCP) identification during process development and manufacturing linked to a risk-based management for their control. *Biotechnology and Bioengineering*, *112*(9), 1727. https://doi.org/10.1002/BIT.25628

Burkowski, F. J. (2001). Evolutionary Optimization Through PAC Learning. *Foundations of Genetic Algorithms 6*, 185–207. https://doi.org/10.1016/B978-155860734-7/50093-7

Burova, E., & Ioffe, E. (2005). Chromatographic purification of recombinant adenoviral and adeno-associated viral vectors: Methods and implications. *Gene Therapy*, *12*, 5–17. https://doi.org/10.1038/sj.gt.3302611

Cameau, E., Pedregal, A., & Glover, C. (2020). Cost modelling comparison of adherent multi-trays with suspension and fixed-bed bioreactors for the manufacturing of gene therapy products. *Cell and Gene Therapy Insights*, *5*(11), 1663–1675. https://doi.org/10.18609/cgti.2019.175

Carvalho, A. R., Ramos, F. M., & Chaves, A. A. (2011). Metaheuristics for the feedforward artificial neural network (ANN) architecture optimization problem. *Neural Computing and Applications*, *20*(8), 1273–1284. https://doi.org/10.1007/s00521-010-0504-3

Cell and Gene Therapy Catapult. (2022). *ATMP Clinical Trials Database 2022*. Catapult. https://ct.catapult.org.uk/resources/clinical-trials-database

Chen, H., Marino, S., & Ho, C. Y. (2016). 97. Large Scale Purification of AAV with Continuous Flow Ultracentrifugation. *Molecular Therapy*, *24*(1), 1. https://doi.org/10.1016/s1525-0016(16)32906-9

Choong, C. J., Baba, K., & Mochizuki, H. (2016). Gene therapy for neurological disorders. In *Expert Opinion on Biological Therapy, 16(2)* .https://doi.org/10.1517/14712598.2016.1114096

Chootinan, P., & Chen, A. (2006). Constraint handling in genetic algorithms using a gradient-based repair method. *Computers & Operations Research*, *33*(8), 2263–2281. https://doi.org/10.1016/J.COR.2005.02.002

Chorghade, M. S. (2006). Drug Discovery and Development. *Drug Discovery and Development*, *1*, 1–456. https://doi.org/10.1002/0471780103

Clark, K. R. (2002). Recent advances in recombinant adeno-associated virus vector

production. *Kidney International*, *61*(1). https://doi.org/10.1046/j.1523-1755.2002.0610s1009.x

Clément, N., & Grieger, J. C. (2016). Manufacturing of recombinant adeno-associated viral vectors for clinical trials. *Molecular Therapy - Methods & Clinical Development*, *3*, 16002. https://doi.org/10.1038/mtm.2016.2

Coleman, H. W., & Steele, W. G. (2009). Experimentation, Validation, and Uncertainty Analysis for Engineers: Third Edition. In *Experimentation, Validation, and Uncertainty Analysis for Engineers: Third Edition*. John Wiley and Sons. https://doi.org/10.1002/9780470485682

Collard, F. (2021). *Transfection scaling challenges for viral vector manufacturing*. Cytiva. https://www.cytivalifesciences.com/en/us/news-center/transfection-scaling-challenges-for-viral-vector-manufacturing-10001

Comisel, R. M., Kara, B., Fiesser, F. H., & Farid, S. S. (2021a). Gene therapy process change evaluation framework: Transient transfection and stable producer cell line comparison. *Biochemical Engineering Journal*, *176*, 108202. https://doi.org/10.1016/j.bej.2021.108202

Comisel, R. M., Kara, B., Fiesser, F. H., & Farid, S. S. (2021b). Lentiviral vector bioprocess economics for cell and gene therapy commercialization. *Biochemical Engineering Journal*, *167*, 107868. https://doi.org/10.1016/j.bej.2020.107868

Crosson, S. M., Dib, P., Smith, J. K., & Zolotukhin, S. (2018). Helper-free Production of Laboratory Grade AAV and Purification by Iodixanol Density Gradient Centrifugation. *Molecular Therapy - Methods and Clinical Development*, *10*, 1–7. https://doi.org/10.1016/j.omtm.2018.05.001

Daya, S., & Berns, K. I. (2008). Gene therapy using adeno-associated virus vectors. In

Clinical Microbiology Reviews, 21(4), 583–593. https://doi.org/10.1128/CMR.00008-08

Deb, K. (2000). An efficient constraint handling method for genetic algorithms. *Computer Methods in Applied Mechanics and Engineering*, *186*(2–4), 311–338. https://doi.org/10.1016/S0045-7825(99)00389-8

Deb, K., Pratap, A., Agarwal, S., & Meyarivan, T. (2002). A Fast and Elitist Multiobjective Genetic Algorithm: NSGA-II. *IEEE Transactions on Evolutionary Computation*, *6*(2). https://doi.org/10.1109/4235.996017

DiMasi, J. A., & Grabowski, H. G. (2007). Economics of new oncology drug development. *Journal of Clinical Oncology*, *25*(2), 209–216. https://doi.org/10.1200/JCO.2006.09.0803

DiMasi, J. A., Grabowski, H. G., & Hansen, R. W. (2016). Innovation in the pharmaceutical industry: New estimates of R&D costs. *Journal of Health Economics*, *47*, 20–33. https://doi.org/10.1016/j.jhealeco.2016.01.012

Du, Y., Walsh, A., Ehrick, R., Xu, W., May, K., & Liu, H. (2012). Chromatographic analysis of the acidic and basic species of recombinant monoclonal antibodies. *MAbs*, *4*(5), 578. https://doi.org/10.4161/MABS.21328

Emmerling, V. V., Pegel, A., Milian, E. G., Venereo-Sanchez, A., Kunz, M., Wegele, J., Kamen, A. A., Kochanek, S., & Hoerer, M. (2016). Rational plasmid design and bioprocess optimization to enhance recombinant adeno-associated virus (AAV) productivity in mammalian cells. *Biotechnology Journal*, *11*(2), 290–297. https://doi.org/10.1002/biot.201500176

Farid, S. S., Novais, J. L., Karri, S., Washbrook, J., & Titchener-Hooker, N. J. (2000). A tool for modeling strategic decisions in cell culture manufacturing. *Biotechnology Progress*, *16*(5), 829–836. https://doi.org/10.1021/bp0001056

Farid, Suzanne S. (2002). A decision-support tool for simulating the process and business perspectives of biopharmaceutical manufacture. *Doctoral Thesis, UCL (University College London).* https://discovery.ucl.ac.uk/id/eprint/170944/

Farid, Suzanne S. (2012). Evaluating and Visualizing the Cost-Effectiveness and Robustness of Biopharmaceutical Manufacturing Strategies. In *Biopharmaceutical Production Technology* (717–741). Wiley. https://doi.org/10.1002/9783527653096.ch22

Farid, Suzanne S., Baron, M., Stamatis, C., Nie, W., & Coffman, J. (2020). Benchmarking biopharmaceutical process development and manufacturing cost contributions to R&D. *MAbs*, *12*(1), 1754999. https://doi.org/10.1080/19420862.2020.1754999

Farid, Suzanne S., Washbrook, J., & Titchener-Hooker, N. J. (2007). Modelling biopharmaceutical manufacture: Design and implementation of SimBiopharma. *Computers and Chemical Engineering*, *31*(9), 1141–1158. https://doi.org/10.1016/j.compchemeng.2006.10.020

Faust, N. (2023). *Establishing an end-to-end vector manufacturing solution for the gene therapy industry*. Cell and Gene Therapy Insights. https://insights.bio/cell-and-gene-therapy-insights/journal/article/2760/Establishing-an-end-to-end-vector-manufacturing-solution-for-the-gene-therapy-industry

FDA. (2014). *Guidance for Industry -Expedited Programs for Serious Conditions*. https://www.fda.gov/regulatory-information/search-fda-guidance-documents/expedited-programs-serious-conditions-drugs-and-biologics

Fiandaca, G., Fraga, E. S., & Brandani, S. (2009). A multi-objective genetic algorithm for the design of pressure swing adsorption. *Engineering Optimization*, *41*(9), 833–854. https://doi.org/10.1080/03052150903074189

Florea, M., Nicolaou, F., Pacouret, S., Zinn, E. M., Sanmiguel, J., Andres-Mateos, E., Unzu,

C., Wagers, A. J., & Vandenberghe, L. H. (2023). High-efficiency purification of divergent AAV serotypes using AAVX affinity chromatography. *Molecular Therapy. Methods & Clinical Development*, *28*, 146. https://doi.org/10.1016/J.OMTM.2022.12.009

Fox, B. R., & McMahon, M. B. (1991). Genetic Operators for Sequencing Problems. *Foundations of Genetic Algorithms*, *1*, 284–300. https://doi.org/10.1016/B978-0-08-050684-5.50021-5

Fraser Wright, J., Wellman, J., & High, K. (2010). Manufacturing and Regulatory Strategies for Clinical AAV2-hRPE65. *Current Gene Therapy*, *10*(5), 341–349. https://doi.org/10.2174/156652310793180715

Fu, Z., Li, S., Han, S., Shi, C., & Zhang, Y. (2022). Antibody drug conjugate: the “biological missile” for targeted cancer therapy. *Signal Transduction and Targeted Therapy*, *7*(1), 1–25. https://doi.org/10.1038/s41392-022-00947-7

George, E. D., & Farid, S. S. (2008a). Stochastic combinatorial optimization approach to biopharmaceutical portfolio management. *Industrial and Engineering Chemistry Research*, *47*(22), 8762–8774. https://doi.org/10.1021/ie8003144

George, E. D., & Farid, S. S. (2008b). Strategic biopharmaceutical portfolio development: An analysis of constraint-induced implications. *Biotechnology Progress*, *24*(3), 698–713. https://doi.org/10.1021/bp070410s

George, E., Titchener-Hooker, N. J., & Farid, S. S. (2007). A multi-criteria decision-making framework for the selection of strategies for acquiring biopharmaceutical manufacturing capacity. *Computers and Chemical Engineering*, *31*(8), 889–901. https://doi.org/10.1016/j.compchemeng.2006.12.009

Glover, C., Smith, D., & Marshall, D. (2019). Room for improvement: tackling suboptimal downstream process unit operations for viral vectors. *Cell and Gene Therapy Insights*,

5(2), 165–176. https://doi.org/10.18609/cgti.2019.024

Goldberg, D. E., & Deb, K. (1991). A Comparative Analysis of Selection Schemes Used in Genetic Algorithms. *Foundations of Genetic Algorithms*, *1*, 69–93. https://doi.org/10.1016/B978-0-08-050684-5.50008-2

Gomis-Fons, J., Andersson, N., & Nilsson, B. (2020). Optimization study on periodic counter-current chromatography integrated in a monoclonal antibody downstream process. *Journal of Chromatography A*, *1621*, 461055. https://doi.org/10.1016/J.CHROMA.2020.461055

Gonçalves, G. A. R., & Paiva, R. de M. A. (2017). Gene therapy: advances, challenges and perspectives. *Einstein*, *15*(3), 369. https://doi.org/10.1590/S1679-45082017RB4024

Grand View Research. (2022). *Monoclonal Antibodies Market Size & Share Report, 2030*. https://www.grandviewresearch.com/industry-analysis/monoclonal-antibodies-market

Grieger, J. C., Soltys, S. M., & Samulski, R. J. (2016a). Production of Recombinant Adeno-associated Virus Vectors Using Suspension HEK293 Cells and Continuous Harvest of Vector From the Culture Media for GMP FIX and FLT1 Clinical Vector. *Molecular Therapy*, *24*(2), 287–297. https://doi.org/10.1038/mt.2015.187

Grieger, J. C., Soltys, S. M., & Samulski, R. J. (2016b). Production of recombinant adeno-associated virus vectors using suspension HEK293 cells and continuous harvest of vector from the culture media for GMP FIX and FLT1 clinical vector. *Molecular Therapy*, *24*(2), 287–297. https://doi.org/10.1038/mt.2015.187

Hassan, S., Huang, H., Warren, K., Mahdavi, B., Smith, D., Jong, S., & Farid, S. S. (2016). Process change evaluation framework for allogeneic cell therapies: Impact on drug development and commercialization. *Regenerative Medicine*, *11*(3), 287–305. https://doi.org/10.2217/rme-2015-0034

Hassan, S., Simaria, A. S., Varadaraju, H., Gupta, S., Warren, K., & Farid, S. S. (2015). Allogeneic cell therapy bioprocess economics and optimization: Downstream processing decisions. *Regenerative Medicine*, *10*(5), 591–609. https://doi.org/10.2217/rme.15.29

Hay, M., Thomas, D. W., Craighead, J. L., Economides, C., & Rosenthal, J. (2014). Clinical development success rates for investigational drugs. *Nature Biotechnology*, *32*(1), 40–51. https://doi.org/10.1038/nbt.2786

Hebben, M. (2018). Downstream bioprocessing of AAV vectors: industrial challenges & regulatory requirements. *Cell and Gene Therapy Insights*, *4*(2), 131–146. https://doi.org/10.18609/cgti.2018.016

Holland, J. H. (1975). *Adaptation in Natural and Artificial Systems* (1st ed.). University of Michigan Press. https://doi.org/https://doi.org/10.7551/mitpress/1090.001.0001

Hu, B., Xiao, H., Yang, N., Jin, H., & Wang, L. (2022). A hybrid approach based on double roulette wheel selection and quadratic programming for cardinality constrained portfolio optimization. *Concurrency and Computation: Practice and Experience*, *34*(10), e6818. https://doi.org/10.1002/CPE.6818

Hu, X.-B., & Di Paolo, E. (2009). An efficient genetic algorithm with uniform crossover for air traffic control. *Computers & Operations Research*, *36*, 245–259. https://doi.org/10.1016/j.cor.2007.09.005

Huang, L., Chen, X., Huo, W., Wang, J., Zhang, F., Bai, B., & Shi, L. (2021). Branch and Bound in Mixed Integer Linear Programming Problems: A Survey of Techniques and Trends. *Discrete Optimization*. https://doi.org/https://doi.org/10.48550/arXiv.2111.06257

Intelligence, M. (2022). *Viral Vector Manufacturing Market Size & Share Analysis - Industry Research Report - Growth Trends*. https://www.mordorintelligence.com/industry-

reports/viral-vector-manufacturing-market

Jankauskas, K. (2019). Biopharmaceutical Scheduling Using a Flexible Genetic Algorithm Approach. *Doctoral Thesis, UCL (University College London).* https://discovery.ucl.ac.uk/id/eprint/10071909/

Jankauskas, K., & Farid, S. S. (2019). Multi-objective biopharma capacity planning under uncertainty using a flexible genetic algorithm approach. *Computers and Chemical Engineering*, *128*, 35–52. https://doi.org/10.1016/j.compchemeng.2019.05.023

Jankauskas, K., Papageorgiou, L. G., & Farid, S. S. (2019). Fast genetic algorithm approaches to solving discrete-time mixed integer linear programming problems of capacity planning and scheduling of biopharmaceutical manufacture. *Computers and Chemical Engineering*, *121*, 212–223. https://doi.org/10.1016/j.compchemeng.2018.09.019

Jenkins, M., Bilsland, J., Allsopp, T. E., Ho, S. V., & Farid, S. S. (2016). Patient-specific hiPSC bioprocessing for drug screening: Bioprocess economics and optimisation. *Biochemical Engineering Journal*, *108*, 84–97. https://doi.org/10.1016/j.bej.2015.09.024

Jenkins, Michael J., & Farid, S. S. (2018). Cost-effective bioprocess design for the manufacture of allogeneic CAR-T cell therapies using a decisional tool with multi-attribute decision-making analysis. *Biochemical Engineering Journal*, *137*, 192–204. https://doi.org/10.1016/J.BEJ.2018.05.014

Jenkins, Michael Joseph. (2018). Decisional Tools for Cost-effective Bioprocess Design for Cell Therapies and Patient-specific Drug Discovery Tools. *Doctoral Thesis, UCL (University College London).* http://discovery.ucl.ac.uk/10046409/1/Jenkins_10046409_thesis.Redacted.pdf

Kaabi, J., & Harrath, Y. (2019). Permutation rules and genetic algorithm to solve the

traveling salesman problem. *Arab Journal of Basic and Applied Sciences*, *26*(1), 283–291. https://doi.org/10.1080/25765299.2019.1615172

Kaplon, H., & Reichert, J. M. (2019). Antibodies to watch in 2019. *MAbs*, *11*(2), 219–238. https://doi.org/10.1080/19420862.2018.1556465

Katoch, S., Chauhan, S. S., & Kumar, V. (2021). A review on genetic algorithm: past, present, and future. *Multimedia Tools and Applications*, *80*(5), 8091–8126. https://doi.org/10.1007/s11042-020-10139-6

Kay, M. A., Glorioso, J. C., & Naldini, L. (2001). Viral vectors for gene therapy: The art of turning infectious agents into vehicles of therapeutics. *Nature Medicine*, *7*(1), 33–40. https://doi.org/10.1038/83324

Kelley, B. (2009). Industrialization of mAb production technology: The bioprocessing industry at a crossroads. *MAbs*, *1*(5), 443–452. https://doi.org/10.4161/mabs.1.5.9448

Khanal, O., & Lenhoff, A. M. (2021). Developments and opportunities in continuous biopharmaceutical manufacturing. *MAbs*, *13*(1). https://doi.org/10.1080/19420862.2021.1903664

Kouka, N., BenSaid, F., Fdhila, R., Fourati, R., Hussain, A., & Alimi, A. M. (2023). A novel approach of many-objective particle swarm optimization with cooperative agents based on an inverted generational distance indicator. *Information Sciences*, *623*, 220–241. https://doi.org/10.1016/J.INS.2022.12.021

Koziel, S., & Michalewicz, Z. (1999). Evolutionary algorithms, homomorphous mappings, and constrained parameter optimization. *Evolutionary Computation*, *7*(1), 19–44. https://doi.org/10.1162/EVCO.1999.7.1.19

Lagaros, N. D., Kournoutos, M., Kallioras, N. A., & Nordas, A. N. (2023). Constraint handling techniques for metaheuristics: a state-of-the-art review and new variants. *Optimization*

and Engineering, 1–48. https://doi.org/10.1007/S11081-022-09782-9/FIGURES/3

Lakhdar, K., Farid, S. S., Titchener-Hooker, N. J., & Papageorgiou, L. G. (2006). Medium Term Planning of Biopharmaceutical Manufacture with Uncertain Fermentation Titers. *Biotechnology Progress*, *22*(6), 1630–1636. https://doi.org/10.1021/bp0601950

Lakhdar, K., Zhou, Y., Savery, J., Titchener-Hooker, N. J., & Papageorgiou, L. G. (2005). Medium Term Planning of Biopharmaceutical Manufacture using Mathematical Programming. *Biotechnology Progress*, *21*(5), 1478–1489. https://doi.org/10.1021/bp0501571

Lakhdar, Kais, & Papageorgiou, L. G. (2008). An iterative mixed integer optimisation approach for medium term planning of biopharmaceutical manufacture under uncertainty. *Chemical Engineering Research and Design*, *86*(3), 259–267. https://doi.org/10.1016/j.cherd.2007.11.011

Li, F., Vijayasankaran, N., Shen, A. Y., Kiss, R., & Amanullah, A. (2010). Cell culture processes for monoclonal antibody production. *MAbs*, *2*(5), 466–479. https://doi.org/10.4161/mabs.2.5.12720

Lim, A. C., Washbrook, J., Titchener-Hooker, N. J., & Farid, S. S. (2006). A computer-aided approach to compare the production economics of fed-batch and perfusion culture under uncertainty. *Biotechnology and Bioengineering*, *93*(4), 687–697. https://doi.org/10.1002/bit.20757

Liu, H. F., Ma, J., Winter, C., & Bayer, R. (2010). Recovery and purification process development for monoclonal antibody production. *MAbs*, *2*(5), 480–499. https://doi.org/10.4161/mabs.2.5.12645

Lo, B., & Field, M. J. (2010). Conflict of Interest in Medical Research, Education and Practice. *Institute of Medicine of the National Academies*, *23*(4).

https://doi.org/10.1024/1012-5302/a000059

Lucas, W. (2010). Viral Capsids and Envelopes: Structure and Function. In *Encyclopedia of Life Sciences*. John Wiley & Sons, Ltd. https://doi.org/10.1002/9780470015902.a0001091.pub2

Lundgren, M. (2019). *Viral Vector Manufacturing for Gene Therapy - Developing a Platform Process*. https://cellculturedish.com/viral-vector-manufacturing-for-gene-therapy-developing-a-platform-process/

Lutz, H., Chefer, K., Felo, M., Cacace, B., Hove, S., Wang, B., Blanchard, M., Oulundsen, G., Piper, R., & Zhao, X. (2015). Robust depth filter sizing for centrate clarification. *Biotechnology Progress*, *31*(6), 1542–1550. https://doi.org/10.1002/btpr.2188

Lyle, A., Stamatis, C., Linke, T., Hulley, M., Schmelzer, A., Turner, R., & Farid, S. S. (2023). Process economics evaluation and optimization of adeno-associated virus downstream processing. *Biotechnology and Bioengineering*, 1–14. https://doi.org/10.1002/bit.28402

Mahal, H., Branton, H., & Farid, S. S. (2021). End-to-end continuous bioprocessing: Impact on facility design, cost of goods, and cost of development for monoclonal antibodies. *Biotechnology and Bioengineering*, *118*(9), 3468–3485. https://doi.org/10.1002/BIT.27774

Maier, P., Von Kalle, C., & Laufs, S. (2010). Retroviral vectors for gene therapy. In *Future Microbiology* (Vol. 5, Issue 10). https://doi.org/10.2217/fmb.10.100

Martin, J., Frederick, A., Luo, Y., Jackson, R., Joubert, M., Sol, B., Poulin, F., Pastor, E., Armentano, D., Wadsworth, S., & Vincent, K. (2013). Generation and characterization of adeno-associated virus producer cell lines for research and preclinical vector production. *Human Gene Therapy Methods*, *24*(4), 253–269. https://doi.org/10.1089/hgtb.2013.046

Masri, F., Cheeseman, E., & Ansorge, S. (2019). Viral vector manufacturing: how to address current and future demands? *Cell and Gene Therapy Insights*, *5*(5), 949–970. https://doi.org/10.18609/cgti.2019.104

Merino, S., & Brittle, S. (2023). *AAV vectors in a spin: zonal ultracentrifugation as an effective, automated and scalable downstream processing methodology*. Cell and Gene Therapy Insights. https://www.insights.bio/cell-and-gene-therapy-insights/webinars/464/AAV-vectors-in-a-spin-zonal-ultracentrifugation-as-an-effective-automated-and-scalable-downstream-processing-methodology

Merten, O.-W. (2016). AAV vector production: state of the art developments and remaining challenges. *Cell and Gene Therapy Insights*, *2*(5), 521–551. https://doi.org/10.18609/cgti.2016.067

Merten, O.-W., Schweizer, M., Chahal, P., & Kamen, A. (2014a). Manufacturing of viral vectors: part II. Downstream processing and safety aspects. *Pharmaceutical Bioprocessing*, *2*(3), 237–251. https://doi.org/10.4155/pbp.14.15

Merten, O.-W., Schweizer, M., Chahal, P., & Kamen, A. A. (2014b). Manufacturing of viral vectors for gene therapy: part I. Upstream processing. *Pharmaceutical Bioprocessing*, *2*(2), 183–203. https://doi.org/10.4155/pbp.14.16

Mietzsch, M., Grasse, S., Zurawski, C., Weger, S., Bennett, A., Agbandje-Mckenna, M., Muzyczka, N., Zolotukhin, S., & Heilbronn, R. (2014). OneBac: Platform for scalable and high-titer production of adeno-associated virus serotype 1-12 vectors for gene therapy. *Human Gene Therapy*, *25*(3), 212–222. https://doi.org/10.1089/hum.2013.184

Mikulic, M. (2021). *Clinical trial cost per drug by therapeutic class 2015-2017 | Statista*. https://www.statista.com/statistics/1197063/clinical-trial-cost-per-drug-by-therapy-area/

Mizukami, A., Pereira Chilima, T. D., Orellana, M. D., Neto, M. A., Covas, D. T., Farid, S. S.,

& Swiech, K. (2018). Technologies for large-scale umbilical cord-derived MSC expansion: Experimental performance and cost of goods analysis. *Biochemical Engineering Journal*, *135*, 36–48. https://doi.org/10.1016/j.bej.2018.02.018

Moço, P. D., Xu, X., Silva, C. A. T., & Kamen, A. A. (2023). Production of adeno-associated viral vector serotype 6 by triple transfection of suspension HEK293 cells at higher cell densities. *Biotechnology Journal*, *18*(9). https://doi.org/10.1002/biot.202300051

Mokhtari, R. B., Homayouni, T. S., Baluch, N., Morgatskaya, E., Kumar, S., Das, B., & Yeger, H. (2017). Combination therapy in combating cancer. *Oncotarget, 8(23)*, 38022–38043). https://doi.org/10.18632/oncotarget.16723

Moleirinho, M. G., Silva, R. J. S., Alves, P. M., Carrondo, M. J. T., & Peixoto, C. (2019). Current challenges in biotherapeutic particles manufacturing. *Expert Opinion on Biological Therapy*, 1–15. https://doi.org/10.1080/14712598.2020.1693541

Monge, A. N., Sigelman, D. W., Temple, R. J., & Chahal, H. S. (2022). Use of US Food and Drug Administration Expedited Drug Development and Review Programs by Orphan and Nonorphan Novel Drugs Approved From 2008 to 2021. *JAMA Network Open*, *5*(11), 2239336. https://doi.org/10.1001/jamanetworkopen.2022.39336

Moreno, F., Lip, F., Rojas, H., & Anggakusuma. (2022). Development of an insect cell-based adeno-associated virus packaging cell line employing advanced Rep gene expression control system. *Molecular Therapy - Methods & Clinical Development*, *27*, 391–403.

Mountain, A. (2000). Gene therapy: The first decade. *Trends in Biotechnology, 18(3),* 119–128. https://doi.org/10.1016/S0167-7799(99)01416-X

Mundae, M. K., & Ostor, A. J. K. (2010). The long road of biopharmaceutical drug development: from inception to marketing. *QJM*, *103*(1), 3–7. https://doi.org/10.1093/qjmed/hcp145

Nagai, S. (2019). Flexible and Expedited Regulatory Review Processes for Innovative Medicines and Regenerative Medical Products in the US, the EU, and Japan. *International Journal of Molecular Sciences*, *20*(15). https://doi.org/10.3390/ijms20153801

Naso, M. F., Tomkowicz, B., Perry, W. L., Strohl, W. R., & Strohl, W. R. (2017). Adeno-Associated Virus (AAV) as a Vector for Gene Therapy. *BioDrugs : Clinical Immunotherapeutics, Biopharmaceuticals and Gene Therapy*, *31*(4), 317–334. https://doi.org/10.1007/s40259-017-0234-5

Nass, S., Mattingly, M. A., Woodcock, D. A., Burnham, B. L., Ardinger, J. A., Osmond, S. E., Frederick, A. M., Scaria, A., Cheng, S. H., & O'Riordan, C. R. (2018). Universal Method for the Purification of Recombinant AAV Vectors of Differing Serotypes. *Molecular Therapy - Methods and Clinical Development*, *9*, 33–46. https://doi.org/10.1016/j.omtm.2017.12.004

Nie, W. (2015). *Cost Evaluation and Portfolio Management Optimisation for Biopharmaceutical Product Development* [University College London]. https://discovery.ucl.ac.uk/id/eprint/1461733/

Nitin Kashyap, U., Gupta, V., & Raghunandan, H. V. (2013). Comparison of drug approval process in united states & europe. *Journal of Pharmaceutical Sciences and Research*, *5*(6), 131–136.

Okada, T., Nonaka-Sarukawa, M., Uchibori, R., Kinoshita, K., Hayashita-Kinoh, H., Nitahara-Kasahara, Y., Takeda, S., & Ozawa, K. (2009). Scalable purification of adeno-associated virus serotype 1 (AAV1) and AAV8 vectors, using dual ion-exchange adsorptive membranes. *Human Gene Therapy*, *20*(9), 1013–1021. https://doi.org/10.1089/hum.2009.006

Paul, S. M., Mytelka, D. S., Dunwiddie, C. T., Persinger, C. C., Munos, B. H., Lindborg, S.

R., & Schacht, A. L. (2010). How to improve R&D productivity: the pharmaceutical industry's grand challenge. *Nature Reviews Drug Discovery*, *9*(3), 203–214. https://doi.org/10.1038/nrd3078

Pavan, M., & Todeschini, R. (2009). Multicriteria Decision-Making Methods. In *Comprehensive Chemometrics, 1,* 591–629. https://doi.org/10.1016/B978-044452701-1.00038-7

Penaud-Budloo, M., François, A., Clément, N., & Ayuso, E. (2018). Pharmacology of Recombinant Adeno-associated Virus Production. *Molecular Therapy - Methods & Clinical Development*, *8*, 166–180. https://doi.org/10.1016/j.omtm.2018.01.002

Pereira Chilima, T. D. (2019). Decisional Tools for Enabling Successful Manufacture and Commercialisation of Cell Therapy Products. *Doctoral Thesis, UCL (University College London).* http://discovery.ucl.ac.uk/10064247/

Pereira Chilima, T. D., Moncaubeig, F., & Farid, S. S. (2018). Impact of allogeneic stem cell manufacturing decisions on cost of goods, process robustness and reimbursement. *Biochemical Engineering Journal*, *137*, 132–151. https://doi.org/10.1016/j.bej.2018.04.017

Pereira Chilima, T. D., Moncaubeig, F., & Farid, S. S. (2020). Estimating capital investment and facility footprint in cell therapy facilities. *Biochemical Engineering Journal*, *155*, 107439. https://doi.org/10.1016/j.bej.2019.107439

Pérez-Escobedo, J. L., Azzaro-Pantel, C., & Pibouleau, L. (2011). New product development with discrete event simulation: Application to portfolio management for the pharmaceutical industry. *Industrial and Engineering Chemistry Research*, *50*(18), 10615–10629. https://doi.org/10.1021/ie200406s

Pollock, J. (2015). Evaluating the Economic and Operational Feasibility of Continuous

Processes for Monoclonal Antibodies. *Doctoral Thesis, UCL (University College London).*

Pollock, J., Coffman, J., Ho, S. V., & Farid, S. S. (2017). Integrated continuous bioprocessing: Economic, operational, and environmental feasibility for clinical and commercial antibody manufacture. *Biotechnology Progress*, *33*(4), 854–866. https://doi.org/10.1002/btpr.2492

Pollock, J., Ho, S. V., & Farid, S. S. (2013). Fed-batch and perfusion culture processes: Economic, environmental, and operational feasibility under uncertainty. *Biotechnology and Bioengineering*, *110*(1), 206–219. https://doi.org/10.1002/bit.24608

Potter, M., Lins, B., Mietzsch, M., Heilbronn, R., Van Vliet, K., Chipman, P., Agbandje-McKenna, M., Cleaver, B. D., Clément, N., Byrne, B. J., & Zolotukhin, S. (2014). A simplified purification protocol for recombinant adeno-associated virus vectors. *Molecular Therapy - Methods and Clinical Development*, *1*, 14034. https://doi.org/10.1038/mtm.2014.34

QLS. (2021). *Clinical Development Success Rates and Contribution Factors 2011 - 2020*. Biotechnology Innovation Organisation. https://www.bio.org/clinical-development-success-rates-and-contributing-factors-2011-2020

Qu, G., Bahr-Davidson, J., Prado, J., Tai, A., Cataniag, F., McDonnell, J., Zhou, J., Hauck, B., Luna, J., Sommer, J. M., Smith, P., Zhou, S., Colosi, P., High, K. A., Pierce, G. F., & Wright, J. F. (2007). Separation of adeno-associated virus type 2 empty particles from genome containing vectors by anion-exchange column chromatography. *Journal of Virological Methods*, *140*(1–2), 183–192. https://doi.org/10.1016/j.jviromet.2006.11.019

Qu, W., Wang, M., Wu, Y., & Xu, R. (2015). Scalable Downstream Strategies for Purification of Recombinant Adeno- Associated Virus Vectors in Light of the Properties. *Current Pharmaceutical Biotechnology*, *16*(8), 684–695.

https://doi.org/10.2174/1389201016666150505122228

Rahimi, I., Gandomi, A. H., Chen, F., & Mezura-Montes, E. (2023). A Review on Constraint Handling Techniques for Population-based Algorithms: from single-objective to multi-objective optimization. *Archives of Computational Methods in Engineering*, *30*(3), 2181–2209. https://doi.org/10.1007/S11831-022-09859-9/TABLES/9

Rajapakse, A., Titchener-Hooker, N. J., & Farid, S. S. (2005). Modelling of the biopharmaceutical drug development pathway and portfolio management. *Computers and Chemical Engineering*, *29*(6), 1357–1368. https://doi.org/10.1016/j.compchemeng.2005.02.010

Rajapakse, A., Titchener-Hooker, N. J., & Farid, S. S. (2006). Integrated approach to improving the value potential of biopharmaceutical R&D portfolios while mitigating risk. *Journal of Chemical Technology and Biotechnology*, *81*(10), 1705–1714. https://doi.org/10.1002/jctb.1595

Rodríguez, N., Gupta, A., Zabala, P. L., & Cabrera-Guerrero, G. (2018). Optimization algorithms combining (meta)heuristics and mathematical programming and its application in engineering. *Mathematical Problems in Engineering*, *2018*. Hindawi Limited. https://doi.org/10.1155/2018/3967457

Sachidananda, M., Erkoyuncu, J., Steenstra, D., & Michalska, S. (2016). Discrete Event Simulation Modelling for Dynamic Decision Making in Biopharmaceutical Manufacturing. *Procedia CIRP*, *49*, 39–44. https://doi.org/10.1016/j.procir.2015.07.026

Samanipour, F., & Jelovica, J. (2020). Adaptive repair method for constraint handling in multi-objective genetic algorithm based on relationship between constraints and variables. *Applied Soft Computing*, *90*, 106143. https://doi.org/10.1016/J.ASOC.2020.106143

Santos, T., & Xavier, S. (2018). A Convergence indicator for Multi-Objective Optimization Algorithms. *Trends in Computational and Applied Mathematics*, *19*(3), 437–448.

Schenone, M., Dančík, V., Wagner, B. K., & Clemons, P. A. (2013). Target identification and mechanism of action in chemical biology and drug discovery. *Nature Chemical Biology*, *9*(4), 232. https://doi.org/10.1038/NCHEMBIO.1199

Schmidt, C. W., & Grossmann, I. E. (1996). Optimization Models for the Scheduling of Testing Tasks in New Product Development. *Industrial & Engineering Chemistry Research*, *35*(10), 3498–3510. https://doi.org/10.1021/ie9601099

Segura, M. M., Kamen, A. A., & Garnier, A. (2011). Overview of current scalable methods for purification of viral vectors. *Viral Vectors for Gene Therapy: Methods and Protocols*, *737*, 89–116. https://doi.org/10.1007/978-1-61779-095-9_4

Siganporia, Cyrus C., Ghosh, S., Daszkowski, T., Papageorgiou, L. G., & Farid, S. S. (2014). Capacity planning for batch and perfusion bioprocesses across multiple biopharmaceutical facilities. *Biotechnology Progress*, *30*(3), 594–606. https://doi.org/10.1002/btpr.1860

Siganporia, Cyrus Carlos. (2016). Strategic Biopharmaceutical Production Planning for Batch and Perfusion Processes. *Doctoral Thesis, UCL (University College London).* https://discovery.ucl.ac.uk/id/eprint/1505719/

Simaria, A. S., Hassan, S., Varadaraju, H., Rowley, J., Warren, K., Vanek, P., & Farid, S. S. (2014). Allogeneic cell therapy bioprocess economics and optimization: Single-use cell expansion technologies. *Biotechnology and Bioengineering*, *111*(1), 69–83. https://doi.org/10.1002/bit.25008

Simaria, A. S., Turner, R., & Farid, S. S. (2012). A multi-level meta-heuristic algorithm for the optimisation of antibody purification processes. *Biochemical Engineering Journal*, *69*,

144–154. https://doi.org/10.1016/J.BEJ.2012.08.013

Smith, D. (2017). *Challenges & Opportunities in the Manufacturing of AAV Vectors Used in the Delivery of Gene Therapy Treatments*. https://drug-dev.com/aav-vector-manufacturing-challenges-opportunities-in-the-manufacturing-of-aav-vectors-used-in-the-delivery-of-gene-therapy-treatments/

Soon, G. K., Guan, T. T., On, C. K., Alfred, R., & Anthony, P. (2013). A comparison on the performance of crossover techniques in video game. *2013 IEEE International Conference on Control System, Computing and Engineering*, 493–498. https://doi.org/10.1109/ICCSCE.2013.6720015

Stamatis, C., & Farid, S. S. (2021). Process economics evaluation of cell-free synthesis for the commercial manufacture of antibody drug conjugates. *Biotechnology Journal*, *16*(4). https://doi.org/10.1002/biot.202000238

Stone, M. C., Borman, J., Ferreira, G., & Robbins, P. D. (2018). Effects of pH, conductivity, host cell protein, and DNA size distribution on DNA clearance in anion exchange chromatography media. *Biotechnology Progress*, *34*(1), 141–149. https://doi.org/10.1002/btpr.2556

Stonier, A. (2013). A Dynamic Decision Support Tool For Use in The Design of Bio-manufacturing Facilities and Processes. *Doctoral Thesis, UCL (University College London).* https://discovery.ucl.ac.uk/id/eprint/1409264/

Stonier, A., Simaria, A. S., Smith, M., & Farid, S. S. (2012). Decisional tool to assess current and future process robustness in an antibody purification facility. *Biotechnology Progress*, *28*(4), 1019–1028. https://doi.org/10.1002/btpr.1569

Stonier, A., Smith, M., Hutchinson, N., & Farid, S. S. (2009). Dynamic Simulation Framework for Design of Lean Biopharmaceutical Manufacturing Operations. *Computer Aided*

Chemical Engineering, *26*, 1069–1073. https://doi.org/10.1016/S1570-7946(09)70178-6

Strobel, B., Miller, F. D., Rist, W., & Lamla, T. (2015). Comparative Analysis of Cesium Chloride- and Iodixanol-Based Purification of Recombinant Adeno-Associated Viral Vectors for Preclinical Applications. *Human Gene Therapy Methods*, *26*(4), 147–157. https://doi.org/10.1089/hgtb.2015.051

Strobel, B., Zuckschwerdt, K., Zimmermann, G., Mayer, C., Eytner, R., Rechtsteiner, P., Kreuz, S., & Lamla, T. (2019). Standardized, Scalable, and Timely Flexible Adeno-Associated Virus Vector Production Using Frozen High-Density HEK-293 Cell Stocks and CELLdiscs. *Human Gene Therapy Methods*, *30*(1), 23–33. https://doi.org/10.1089/hgtb.2018.228

Terova, O., Soltys, S., Hermans, P., De Rooij, J., & Detmers, F. (2018). Overcoming Downstream Purification Challenges for Viral Vector Manufacturing: Enabling Advancement of Gene Therapies in the Clinic. *Cell and Gene Therapy Insights*, *4*(2), 101–111. https://doi.org/10.18609/cgti.2018.017

Thomas, D., Burns, J., Audette, J., Carroll, A., Dow-Hygelund, C., & Hay, M. (2016). Clinical Development Success Rates. *BioMedTracker*, *June*. https://www.bio.org/sites/default/files/Clinical Development Success Rates 2006-2015 - BIO, Biomedtracker, Amplion 2016.pdf

Thomas, D. L., Wang, L., Niamke, J., Liu, J., Kang, W., Scotti, M. M., Ye, G. J., Veres, G., & Knop, D. R. (2009). Scalable recombinant adeno-associated virus production using recombinant herpes simplex virus type 1 coinfection of suspension-adapted mammalian cells. *Human Gene Therapy*, *20*(8), 861–870. https://doi.org/10.1089/hum.2009.004

Tsai, M. W., Hong, T. P., & Lin, W. T. (2015). A two-dimensional genetic algorithm and its application to aircraft scheduling problem. *Mathematical Problems in Engineering*, *2015*. https://doi.org/10.1155/2015/906305

Tsuchikama, K., & An, Z. (2018). Antibody-drug conjugates: recent advances in conjugation and linker chemistries. *Protein & Cell*, *9*(1), 33–46. https://doi.org/10.1007/s13238-016-0323-0

Umscheid, C. A., Margolis, D. J., & Grossman, C. E. (2011). Key concepts of clinical trials: A narrative review. In *Postgraduate Medicine* (Vol. 123, Issue 5, pp. 194–204). https://doi.org/10.3810/pgm.2011.09.2475

Urabe, M., Xin, K.-Q., Obara, Y., Nakakura, T., Mizukami, H., Kume, A., Okuda, K., & Ozawa, K. (2006). Removal of Empty Capsids from Type 1 Adeno-Associated Virus Vector Stocks by Anion-Exchange Chromatography Potentiates Transgene Expression. *Molecular Therapy*, *13*(4), 823–828. https://doi.org/10.1016/J.YMTHE.2005.11.024

van der Loo, J. C. M., & Wright, J. F. (2016). Progress and challenges in viral vector manufacturing. *Human Molecular Genetics*, *25*(R1), R42–R52. https://doi.org/10.1093/hmg/ddv451

Van Norman, G. A. (2019). Phase II Trials in Drug Development and Adaptive Trial Design. *JACC: Basic to Translational Science*, *4*(3), 428–437. https://doi.org/10.1016/j.jacbts.2019.02.005

Vandenberghe, L. H., Xiao, R., Lock, M., Lin, J., Korn, M., & Wilson, J. M. (2010). Efficient serotype-dependent release of functional vector into the culture medium during adeno-associated virus manufacturing. *Human Gene Therapy*, *21*(10), 1251–1257. https://doi.org/10.1089/hum.2010.107

Wada, M., Uchida, N., Posadas-Herrera, G., Hayashita-Kinoh, H., Tsunekawa, Y., Hirai, Y., & Okada, T. (2023). Large-scale purification of functional AAV particles packaging the full genome using short-term ultracentrifugation with a zonal rotor. *Gene Therapy*, *30*, 641–648.

Wang, L., Blouin, V., Brument, N., Bello-Roufai, M., & Francois, A. (2012). *Production and Purification of Recombinant Adeno-Associated Vectors* (pp. 361–404). Humana Press. https://doi.org/10.1007/978-1-61779-370-7_16

Wang, W., & Sebag, M. (2013). Hypervolume indicator and dominance reward based multi-objective Monte-Carlo Tree Search. *Machine Learning*, *92*(2–3), 403–429. https://doi.org/10.1007/S10994-013-5369-0/FIGURES/17

Webb, D., Liu, Q., Alobaidi, W., & Sandgren, E. (2017). Topological Design via a Rule Based Genetic Optimization Algorithm. *American Journal of Computational Mathematics*, *07*(03), 291–320. https://doi.org/10.4236/AJCM.2017.73023

Wong, C. H., Siah, K. W., & Lo, A. W. (2019). Estimation of clinical trial success rates and related parameters. *Biostatistics*, *20*(2), 273–286. https://doi.org/10.1093/biostatistics/kxx069

Wright, J. F. (2008). Manufacturing and characterizing AAV-based vectors for use in clinical studies. *Gene Therapy*, *15*(11), 840–848. https://doi.org/10.1038/gt.2008.65

Wright, J. Fraser. (2014a). AAV empty capsids: For better or for worse? *Molecular Therapy 22*(1), 1–2. https://doi.org/10.1038/mt.2013.268

Wright, J. Fraser. (2014b). Product-related impurities in clinical-grade recombinant AAV vectors: Characterization and risk assessment. In *Biomedicines* (Vol. 2, Issue 1, pp. 80–97). MDPI AG. https://doi.org/10.3390/biomedicines2010080

Wright, J. Fraser, & Zelenaia, O. (2011). Vector characterization methods for quality control testing of recombinant adeno-associated viruses. *Methods in Molecular Biology (Clifton, N.J.)*, *737*, 247–278. https://doi.org/10.1007/978-1-61779-095-9_11

Wright, J F. (2008). Manufacturing and characterizing AAV-based vectors for use in clinical studies. *Gene Therapy*, *15*(11), 840–848. https://doi.org/10.1038/gt.2008.65

Wright, J Fraser. (2020). Quality Control Testing, Characterization and Critical Quality Attributes of Adeno-Associated Virus Vectors Used for Human Gene Therapy. *Biotechnology Journal*, *16*(1), 2000022. https://doi.org/10.1002/biot.202000022

Xiao, X., Li, J., & Samulski, R. J. (1998). Production of high-titer recombinant adeno-associated virus vectors in the absence of helper adenovirus. *Journal of Virology*, *72*(3), 2224–2232. http://www.ncbi.nlm.nih.gov/pubmed/9499080

Yamaguchi, S., Kaneko, M., & Narukawa, M. (2021). Approval success rates of drug candidates based on target, action, modality, application, and their combinations. *Clinical and Translational Science*, *14*(3), 1113–1122. https://doi.org/10.1111/CTS.12980

Yoo, H., Zavala, V. M., & Lee, J. H. (2021). A Dynamic Penalty Function Approach for Constraint-Handling in Reinforcement Learning. *IFAC Papers Online*, *54*(3), 487–491. https://doi.org/10.1016/J.IFACOL.2021.08.289

Yuan, J., Pang, H., Tong, T., Xi, D., Guo, W., & Mesenbrink, P. (2016). Seamless Phase IIa/IIb and enhanced dose-finding adaptive design. *Journal of Biopharmaceutical Statistics*, *26*(5), 912–923. https://doi.org/10.1080/10543406.2015.1094807

Yuan, Z., Qiao, C., Hu, P., Li, J., & Xiao, X. (2011). A Versatile Adeno-Associated Virus Vector Producer Cell Line Method for Scalable Vector Production of Different Serotypes. *Human Gene Therapy*, *22*(5), 613. https://doi.org/10.1089/HUM.2010.241

Zakaria, M. Z., Jamaluddin, H., Ahmad, R., & Loghmanian, S. M. (2012). Comparison between multi-objective and single-objective optimization for the modeling of dynamic systems. *Proceedings of the Institution of Mechanical Engineers. Part I: Journal of Systems and Control Engineering*, *226*(7), 994–1005. https://doi.org/10.1177/0959651812439969/ASSET/IMAGES/LARGE/10.1177_0959651812439969-FIG6.JPEG

Appendices

A: Process economic evaluation and optimisation of AAV manufacturing

Tables

Table A1 Yield and purity ranges ascertained from literature and industrial correspondence.

Step	Yield	Empty capsid reduction	HCP LRV	DNA LRV	AAV serotype	Sources
Affinity	55 – 95%	-	4.0	2.5	1, 2, 5, 10	(Florea et al., 2023; Nass et al., 2018)
AEX	30 – 90%	70 - 90%	2.5	1.5	1, 2, 5, 9	(Burova & Ioffe, 2005; Nass et al., 2018; Okada et al., 2009; G. Qu et al., 2007; Stone et al., 2018), (Linke, personal communication, 2020)
CEX	15 – 90%	-	2.5	1.5	1, 2	(Burova & Ioffe, 2005; Okada et al., 2009)
Multimodal	75%	-	2.0	1.0	Any	(Linke, personal communication, 2020)
Ultra-centrifugation	50 – 70%	99 - 100%	3.0	3.0	Any	(Linke, personal communication, 2020)

Table A2 Productivity ranges and the corresponding culture type found in the literature.

Productivity (vg/cell)	Culture type	Source
120,000	Adherent (CF10)	(Emmerling et al., 2016; Masri et al., 2019)
130,000	Adherent (CF10)	(Z. Yuan et al., 2011)
50,000	Adherent (FB)	(Emmerling et al., 2016; Masri et al., 2019)
15,000	Suspension	(Moço et al., 2023)
50,000	Suspension	(Masri et al., 2019)
100,000	Suspension	(Grieger et al., 2016b)
20,000	Suspension	(Clément & Grieger, 2016)

Table A3 Data used in FCI calculation

Parameter	Value	Units
Process support equipment costs	2,389	$/m2 of cleanroom
Logistics equipment costs	548	$/m2 of cleanroom
Environmental monitoring system unit	108,800	$
Equipment installation costs	1,920	$/unit
Building shell costs	548	$/m2
Fit out costs (Grade B)	8,320	$/m2
Fit out costs (Grade C)	6,106	$/m2
Fit out costs (Grade D)	5,082	$/m2
Fit out costs (CNC)	1,741	$/m2
Fit out costs (Unclassified)	64	$/m2
Contractor's fees	12	% of fitout costs
Land costs	6	% of shell costs
Yard costs	10	% of shell costs
Engineering, management and consultancy fees (EMC)	20	% of direct project costs
Contingency costs	20	% of direct project costs w/ EMC fees
Grade B gown	60	$/gown
Grade C gown	45	$/gown
Equipment area: Cleanroom area	0.16	ratio

Table A4 Ratios used in FCI calculation

Area	Area: Product manufacturing area (Cleanroom)	Room classification
Clean change 1	0.105	Grade C/B
Clean change 2	0.147	Grade C/B
Clean corridors	0.322	Grade C/B
Clean janitor	0.042	Grade C/B
QC labs	0.65	Grade D
Microbiology lab	0.301	Grade D
Labs corridor	0.273	Grade D
PCR room	0.294	Grade D
Janitor	0.042	Grade D
Waste corridor	0.804	Unclassified
Waste change	0.042	Unclassified
Waste treatment	0.168	Unclassified
Logistics	1.077	Unclassified
Offices	3.147	Unclassified
Meeting rooms	0.105	Unclassified
Stairs	0.231	Unclassified
Cold rooms	0.168	Unclassified
Janitor	0.042	Unclassified
General corridor	0.399	Unclassified
Lorry/Van loading docks	0.224	Unclassified
Reception	0.538	Unclassified
WC	0.392	Unclassified
Plant level	4.755	CNC

Table A5 USP technology characteristics and assumptions.

Technology	Surface area (cm^2)	Maximum working volume, V_i (L)	Consumable unit cost ($)	Maximum no. of units handled by two operator team	Incubator capacity (units/incubator)	Ancillary equipment cost ($)
SF250	-	0.1	13.26	80	100	-
SF500	-	0.2	18.24	80	100	-
T75	75	0.015	5.14	80	100	-
T225	225	0.045	11.48	80	100	-
RB850	850	0.25	11.51	40	90	-
RB1750	1750	0.53	27.70	40	90	-
CF2	1272	0.3	131.80	20	60	-
CF10	6360	1.5	650	12	12	-
FB66	660,000	70	19,000	1	-	325,000
FB133	1,330,000	70	22,300	1	-	325,000
FB333	3,330,000	70	29,400	1	-	325,000
RM1	-	0.5	328.32	2	-	92,208
RM2	-	1	418.90	2	-	92,208
RM10	-	5	1,038.96	2	-	92,208
RM20	-	10	1,168.83	2	-	92,208
RM50	-	25	1,298.70	2	-	92,208
RM100	-	50	1,657.01	2	-	223,377
RM200	-	100	2,114.19	2	-	223,377
SUB1	-	1	373.60	5	-	27,273
SUB5	-	5	978.66	5	-	55,195
SUB50	-	50	3,896.10	1	-	224,675
SUB100	-	100	4,410.00	1	-	229,870
SUB250	-	250	5,194.81	1	-	233,766
SUB500	-	500	7,792.21	1	-	253,247
SUB1000	-	1,000	10,389.61	1	-	279,221
SUB2000	-	2,000	15,584.42	1	-	389,610

Table A6 Key cost data utilised.

Unit operation	Type	Subtype	Cost ($)	Base size
Chromatography	Equipment	Column	20,000	10cm
Chromatography	Equipment	Skid	158,902	3L/min
Chromatography	Equipment	Packing system	50,000	-
Lysis	Equipment	Microfluidiser	32,000	36L/hr
Nuclease treatment	Reagent	Benzonase	0.005	1mL
Ultracentrifugation	Equipment	Batch ultracentrifuge (floor standing)	70,000	-
Ultracentrifugation	Equipment	Batch ultracentrifuge (rotor)	16,800	1.5L
Ultracentrifugation	Equipment	Continuous ultracentrifuge	350,000	9L/hr
Ultracentrifugation	Consumable	Batch ultracentrifuge (tube)	5.60	39mL
Ultracentrifugation	Reagent	Iodixanol	1.08	1mL
Filtration	Equipment	TFF skid	165,000	$5m^2$
Filtration	Equipment	Normal flow filtration skid	10,000	$1m^2$
Filtration	Consumable	Depth filter / Sterile filter	500	$0.26m^2$
Filtration	Consumable	UFDF filter	3,500	$1m^2$
Fill finish	Equipment	Fill finish machine	620,000	600 (1mL vials/hr)
Hold vessel	Equipment	Container	13,450	1,000L
Hold vessel	Consumable	Bag	829	1,000L

Table A7 Equations and assumptions regarding process timing.

Category	Assumption on time	Equations used to calculate time
Seed	k from doubling time equation	$t_{seed} = \frac{LN(\frac{N_s}{Working\ cell\ bank\ (cells/flask)})}{k\ (day^{-1})}$
TFF / UFDF	Assumed duration of 6 hours (used for area calculations	NA
Chemical lysis	Assumptions: Preparation time = 0.5hr Operation time = 1hr	Operation time = Operation time + Preparation time
Depth filtration	Assumed duration limit of **4 hours**	Recalculated processing time = $\left(\frac{V_{in}}{(A_{DF} \times J_{DF}}\right)$
Benzonase treatment	Assumptions: Preparation time = 0.5hr Operation time = 1hr	Operation time = Operation time + Preparation time
Chromatography	$t_{residence(L)} = \frac{Bed\ height}{Load\ linear\ velocity}$ $t_{residence(NL)} = \frac{Bed\ height}{Nonload\ linear\ velocity}$	Load time = $\left(\frac{(\frac{V_{in}}{N_{cycles}})}{V_{column}}\right) \times t_{residence(L)}$ Non-loading time = $Operational\ CVs \times t_{residence(NL)}$ Cycle time = Load time + Non-loading time Operation time = Cycle Time x N_{cycles}
Ultracentrifugation	Assumed duration limit (for continuous) of **6 hours (operational)** Assumed duration limit (for batch) of **3 hours (operational) –** however with two cycles conducted in a day, the total would be **6 hours** This 6 hours factors in actual processing time, as well as acceleration and deceleration time (industrial correspondence)	NA

Figures

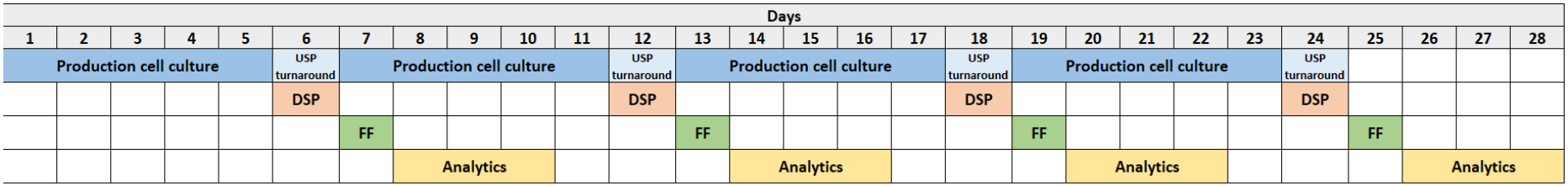

Figure A1 Gantt chart depicting one campaign without the seed time.

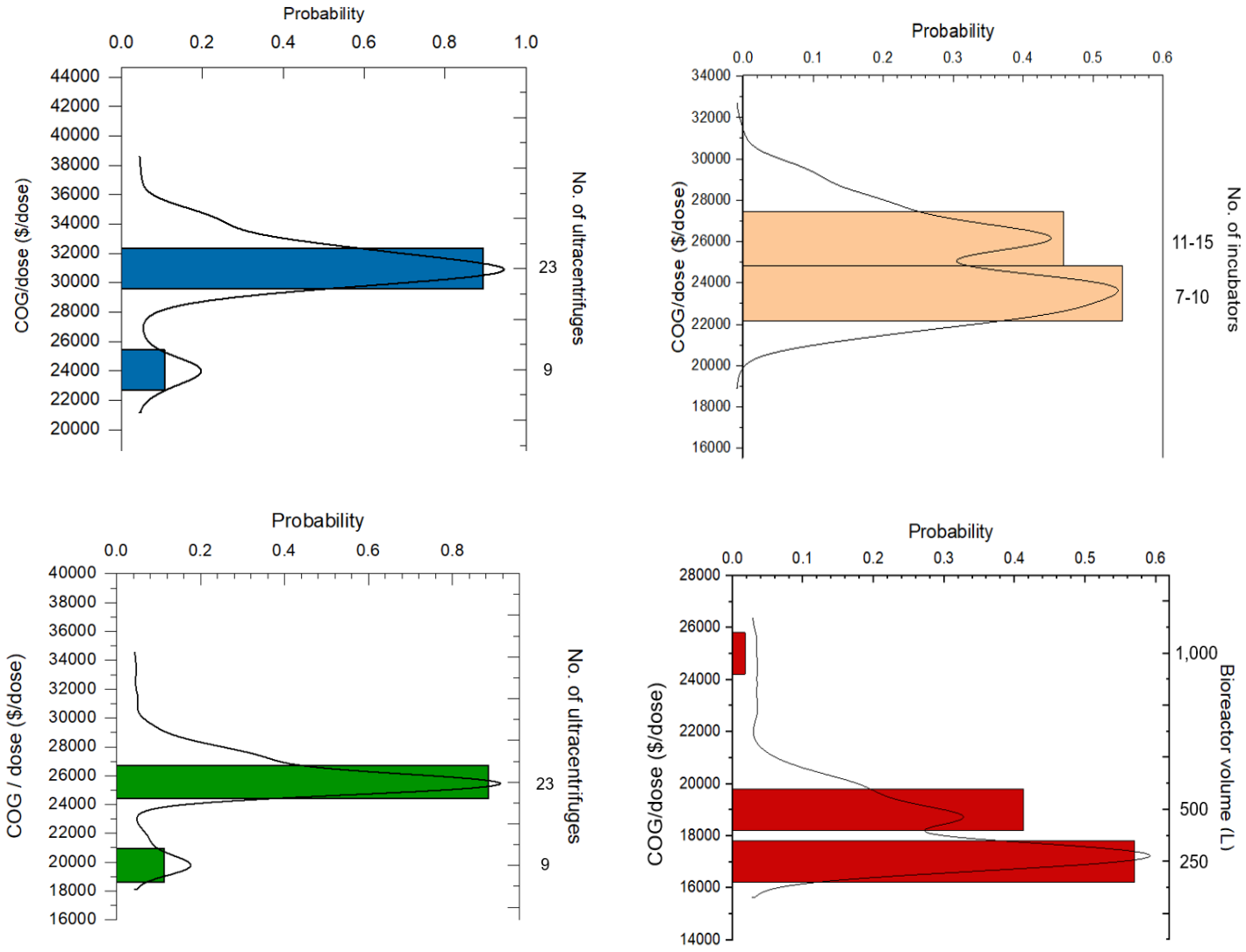

Figure A2 a) frequency distribution plots depicting the Monte Carlo output for Ad-UC, **b)** Ad-AEX **c)** Susp-UC **d)** Susp-AEX. The y-axis for each represents the key factor determining the shape of the distributions in **Figure 3.5.**

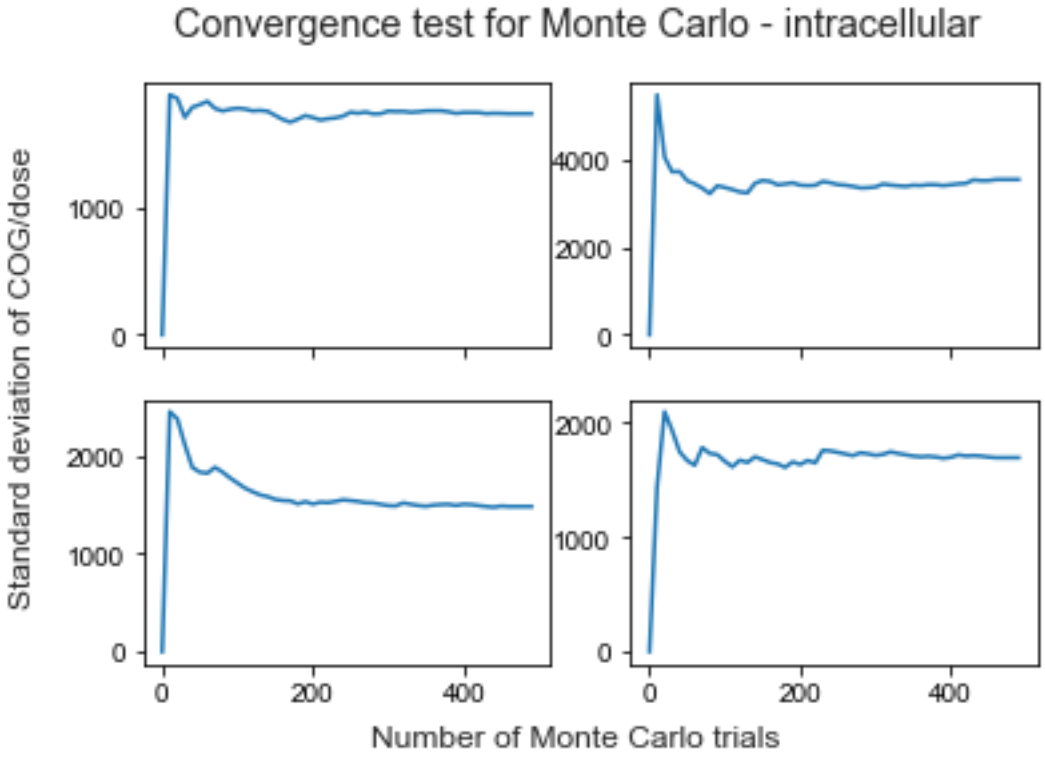

Figure A3 Confirmation of Monte Carlo convergence across all trials. Top-left: Ad-UC, top-right: Ad-AEX, bottom-left: Susp-UC, bottom-right: Susp-AEX.

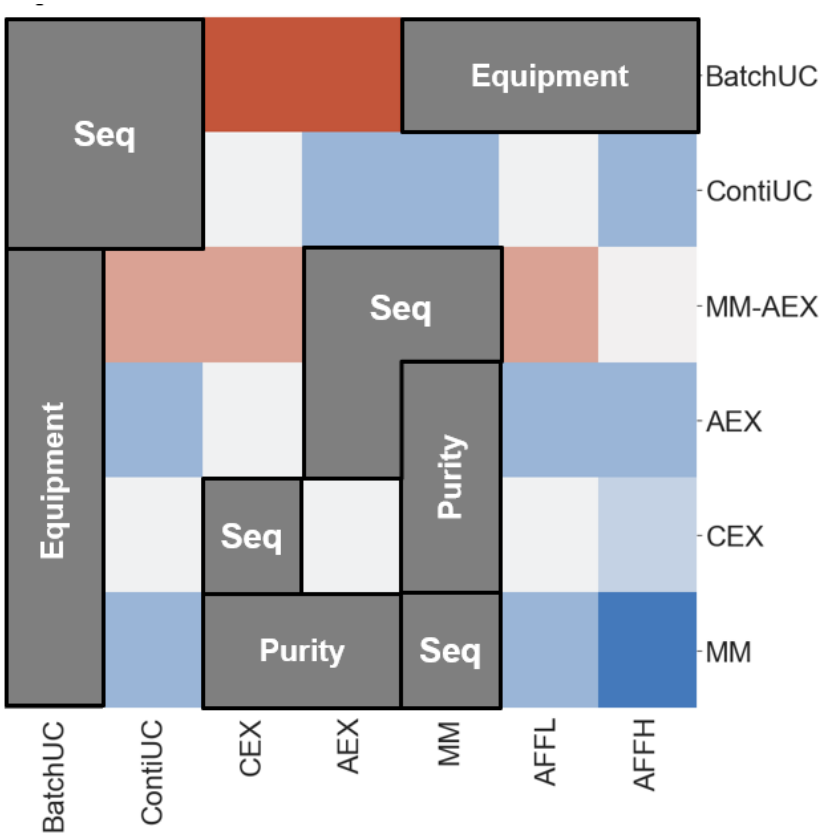

Figure A4 Specific constraints violated by purifications sequences in the optimisation work.

Seq = sequence.

Equations

Seed

The constant *k* in the above equation was generated through the doubling time equation, that is, the time for the initial cell population to double.

$$k = \frac{ln\,(2)}{\tau} \qquad (A.0.1)$$

where τ = doubling time (days)

USP

The key basis for comparison is an equal cell productivity (vg/cell) across all scenarios, hence this value can be utilised to calculate the corresponding adherent and suspension titres, as outlined in Section 3.2.

$$Titre_{adherent} = P \times d_{h_a} \qquad (A.0.2)$$

$$Titre_{suspension} = P \times d_{h_s} \qquad (A.0.3)$$

Finally, as the process models outlined in Chapter 3 assume a plasmid transfection method of gene delivery into the cells, calculation of the mass of plasmid required is pertinent, particularly for later costing purposes. The equation differs between adherent or suspension cell culture, and the difference is outlined below.

$$m_{plasmid} = m_{plasmid,1Mcells} \times d_{h_a} \times \frac{1}{1{,}000{,}000} \times A_n \times N_{units} \qquad (A.0.4)$$

$$m_{plasmid} = m_{plasmid,1Mcells} \times d_{h_s} \times \frac{1}{1{,}000{,}000} \times V_n \times N_{units} \qquad (A.0.5)$$

where $m_{plasmid,1Mcells}$ = mass of plasmid required per 1 million cells (ug/1M cells)

d_{h_a} = adherent harvest cell density (cells/cm^2)

d_{h_s} = suspension harvest cell density (cells/mL)

A_n = surface area of adherent USP technology (stage n)

V_i = working volume of suspension USP technology (stage n)

Depth filtration

In calculating the processing time for the step.

$$t_{filtration} = \frac{V_{in}}{A_{NFF} \times J_{NFF}} \quad (A.0.6)$$

where J_{NFF} = flux (LMH) for specific NFF step

UFDF

Primarily for costing purposes, the volume of diafiltration buffer utilised was corrected, to account for the extra needed due to losses from volume that is held up on the filter and the portion of such that is eventually recovered.

$$V_{buffer(actual)} = V_{buffer} + (A_{total(UFDF)} \times H \times R) \quad (A.0.7)$$

Microfluidisation

Moreover, a duration limit for the whole microfluidisation stage is typically set, so that in scenarios where t_{lysis} (the actual duration of the stage) for a single microfluidiser unit exceeds the assumed duration limit (t_{max}), the number of parallel units is corrected as follows.

$$N_{units} = \frac{(\frac{V_{in}}{Q})}{t_{max}} \quad (A.0.8)$$

where Q = volumetric flowrate (L/h) through microfluidiser

The corrected time for the process can therefore be ascertained.

$$t_{lysis} = \frac{V_{in}}{Q \times N_{units}} \quad (A.0.9)$$

Ultracentrifugation

Therefore, the total number of tubes used per batch was generated.

$$N_{tubes} = CEILING\left(\frac{V_{in}}{\frac{V_{tube}}{R_{total}}}\right) \quad (A.0.10)$$

The continuous mode ultracentrifuge features a limited capacity core, however large volumes can be processed through high flowrates.

The flowrate required when assuming a maximum duration limit for the step allows for determination of the required flowrate ($Q_{required}$). This in turn gives information as to whether multiple parallel ultracentrifuge units are needed.

$$Q_{required} = \frac{V_{in}}{Duration\ limit\ (hr)}$$

If $Q_{required}$ exceeds the maximum flowrate of the largest model in the database, then the number of parallel units is calculated as follows.

$$N_{units} = CEILING(\frac{Q_{required}}{Max\ flowrate\ of\ largest\ model})$$

Fill finish

As the final stage of the process in any case, it is essential to calculate the number of doses that have been generated in a single batch and hence evaluate the number of annual doses produced. This also serves as something of a check, to ensure the mass balance aligns with the expected product out.

$$Doses\ per\ batch = \frac{vg_{out}}{vg_{dose}} \quad (A.0.11)$$

The sizing of the fill finish is contingent on the volume of each dose, along with what available vial sizes exist within the database. The dose volume is calculated by accounting for the drug product concentration, thus the target concentration to reach in the final UFDF stage.

$$V_{dose} = \frac{vg_{dose}}{C_{DP}} \quad (A.0.12)$$

$$N_{vials} = CEILING\left(\frac{V_{dose}}{Max.vial\ size}\right) \quad (A.0.13)$$

The actual vial volume/size is selected by matching the dose volume per vial to the nearest vial size that is greater than the volume.

The sizing metric used for fill finish equipment is the number of vials that can be filled per hour (u_{vial}), hence allowing for a specific machine type to be selected. As long as the number of doses filled per batch is less than the maximum vial output per filling operation. An operation is defined by the following.

$$t_{fill\ operation} = t_{fill\ shift} \times N_{shifts_{max}} \quad (A.0.14)$$

$$N_{machines} = CEILING(\frac{Doses\ per\ batch}{Max\ vials\ per\ operation}) \quad (A.0.15)$$

$$t_{fill} = CEILING(\frac{Doses\ per\ batch \times N_{vials}}{u_{vial} \times N_{machines}}) \quad (A.0.16)$$

$$N_{shifts} = CEILING(\frac{t_{fill}}{t_{fill\ shift}}) \quad (A.0.17)$$

For fill finish, the conditions for calculating number of operators depended on that defined in the fill finish process model (see Appendix). In general however, a team of two operators are assumed to work one shift and can handled one filling machine.

$$N_{operators,FF} = N_{machines} \times N_{shifts} \times 2 \quad (A.0.18)$$

If the required filling time exceeds the maximum number of shifts that can be carried out in one day, then the equation takes the following form.

$$N_{operators,FF} = N_{machines} \times N_{shifts/day} \times 2 \quad (A.0.19)$$

Novel method for facility footprint calculation

Cleanroom area

$$Cleanroom\ area\ = \frac{Equipment\ footprint}{Equipment\ area: Cleanroom\ area} \quad (A.0.20)$$

If the USP technology is semi-closed (e.g. roller bottle or CF10), the equations for grade D and C footprint are as follows.

$$Grade\ B\ footprint = USP\ footprint + Fill\ finish\ footprint \quad (A.0.21)$$

$$Grade\ C\ footprint = DSP\ footprint \quad (A.0.22)$$

Alternatively.

$$Grade\ B\ footprint = Seed\ footprint + Fill\ finish\ footprint \quad (A.0.23)$$

$$Grade\ C\ footprint = DSP\ footprint + Production\ footprint \quad (A.0.24)$$

Grade D area

$$No.of\ QC\ labs\ \times Cleanroom\ area\ \times Grade\ D\ specific\ Ratios \quad (A.0.25)$$

CNC area

$$CNC\ area\ \times CNC\ specific\ ratios \quad (A.0.26)$$

Unclassified area

$$Unclassified\ area\ \times Unclassified\ specific\ ratios \quad (A.0.27)$$

Process support equipment cost

$$Cleanroom\ area\ \times Cost\ (per\ m^2 of\ cleanroom) \quad (A.0.28)$$

Equipment logistic cost

$$Cleanroom\ area\ \times Cost\ (per\ m^2 of\ cleanroom) \quad (A.0.29)$$

Equipment installation cost

$$Cleanroom\ area\ \times Cost\ (per\ m^2 of\ cleanroom) \quad (A.0.30)$$

QC lab cost

$$No.of\ labs\ \times Cost\ per\ lab \quad (A.0.31)$$

Total cleanroom change area

$$No.of\ gowns\ per\ operator\ per\ day\ \times (Ratio\ of\ clean\ in\ +\ out)$$

$$\times Cleanroom\ area \quad (A.0.32)$$

Grade B cleanroom change area

$$Total\ cleanroom\ change\ area\ \times (\frac{Grade\ B\ area}{Total\ cleanroom\ area}) \quad (A.0.33)$$

Total facility footprint

$$Grade\ D\ area\ +\ CNC\ area\ +\ Unclassified\ area\ +\ Cleanroom\ area$$

$$+\ Clean\ change\ area \quad (A.0.34)$$

Shell costs

$$Cost\ (\$/m^2)\ \times\ Total\ facility\ footprint \quad (A.0.35)$$

B: Estimation of research & development budgets for novel modalities

Figures

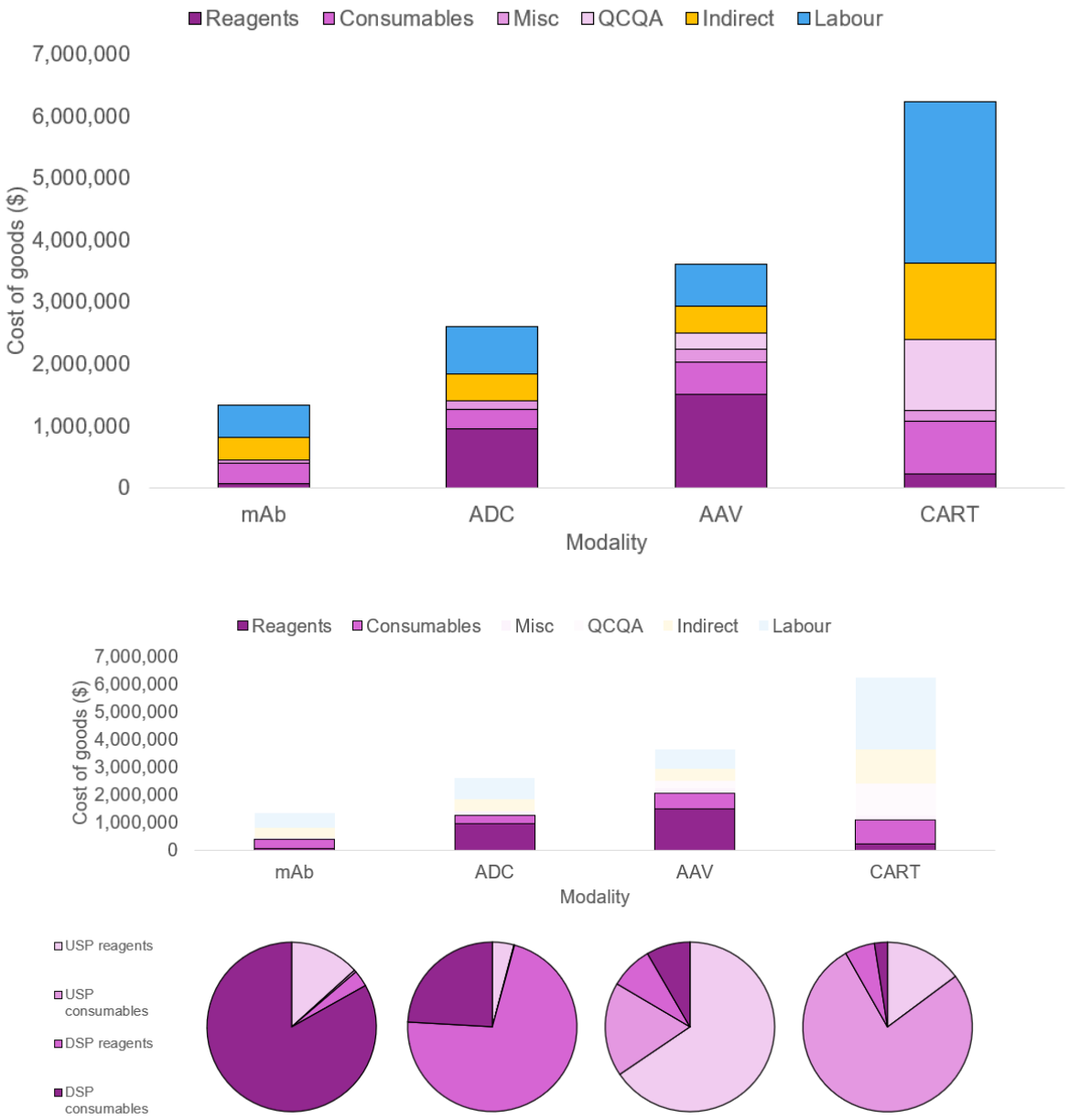

Figure B1 Cost of goods breakdowns across modalities for Phase I manufacturing.

Tables

Table B1 Range of success rates by modality found in the literature.

Source	Modalities studied	LOA from Phase I
(Hay et al., 2014)	mAb	14%
(Hassan et al., 2016),	AAV [1]	36%
(Comisel et al., 2021a)	CART [1]	36%
(Kaplon & Reichert, 2019)	mAb	17%
(Suzanne S. Farid et al., 2020)	mAb	12%
(Yamaguchi et al., 2021)	mAb	12%
	AAV [2]	3.3%
	CAR T [2]	3.3%
(Roo, 2021)	mAb	12%
	ADC	10.5%
	AAV	10%
	CAR T	17.3%

[1] Collectively studied cell therapies, however was later used for AAV and CAR T in (Comisel et al., 2021a).

[2] Study referred to these as novel modalities, stating this included nucleic acids, cell and gene therapies and viral medicines.

Table B2 Range of success rates by indication found in the literature.

Indication	Source	Phase I to II	Phase II to III	Phase III to NDA	NDA to LOA	Number of drug studied
Haematology	(D. Thomas et al., 2016)	70%	48%	77%	93%	352
	(Roo, 2021)	73%	57%	75%	84%	283
Ophthalmology	(D. Thomas et al., 2016)	85%	45%	58%	78%	267
	(Roo, 2021)	72%	36%	51%	91%	415
	(Wong et al., 2019)	89%	58%	74%	100%	437
Oncology	(D. Thomas et al., 2016)	63%	25%	40%	82%	3163
	(Roo, 2021)	49%	25%	48%	92%	4179
	(Hay et al., 2014)	69%	42%	55%	83%	919
	(Wong et al., 2019)	79%	54%	49%	100%	3107
	(Kaplon & Reichert, 2019)	68%	38%	67%	100%	176
	(Kaplon & Reichert, 2019)	61%	45%	75%	100%	274
Neurology / CNS	(D. Thomas et al., 2016)	59%	30%	57%	83%	1304
	(Roo, 2021)	48%	27%	53%	87%	1411
	(Hay et al., 2014)	63%	34%	67%	85%	301

C: Portfolio optimisation and capacity planning for mixed modality portfolios

Table C1 Detailed characteristics of the mAbs and ADCs considered in the pipeline (20% continuous pipeline).

Index	Product ID	Entry year	Manufacturing (batch / continuous)	Titre (g/L) or productivity (g/L/day)	Commercial demand (kg)	Patient population	Selling price ($/patient/annum)
1	mAb1	1	B	6	175	10938	61469
2	mAb2	1	B	9	472	29500	193841
3	mAb3	1	C	3	146	9125	18367
4	mAb4	1	B	5	274	17125	113816
5	mAb5	1	B	6	640	40000	86267
6	mAb6	1	B	8	164	10250	87720
7	mAb7	1	B	5	490	30625	77604
8	mAb8	1	C	4	400	25000	70650
9	ADC1	1	B	8	311	44429	62518
10	ADC2	1	B	9	448	64000	34165
11	mAb9	2	B	6	129	8063	145192
12	mAb10	2	B	7	122	7625	74550
13	mAb11	2	C	4	691	43188	41585
14	mAb12	2	B	10	448	28000	115634
15	mAb13	2	B	9	546	34125	150417
16	mAb14	2	B	7	211	13188	116607
17	mAb15	2	B	10	621	38813	162396
18	mAb16	2	C	4	433	27063	78103
19	ADC3	2	B	9	525	75000	162461
20	ADC4	2	B	7	476	68000	123021
21	mAb17	3	B	8	406	25375	147628
22	mAb18	3	B	10	254	15875	59176

23	mAb19	3	C	4	684	42750	185711
24	mAb20	3	B	8	400	25000	44564
25	mAb21	3	B	8	539	33688	54498
26	mAb22	3	B	9	187	11688	41803
27	mAb23	3	B	10	472	29500	49882
28	mAb24	3	C	4	579	36188	98012
29	ADC5	3	B	6	519	74143	108162
30	ADC6	3	B	6	698	99714	104515
31	mAb25	4	B	10	609	38063	125921
32	mAb26	4	B	10	273	17063	147546
33	mAb27	4	C	4	355	22188	108157
34	mAb28	4	B	10	582	36375	102254
35	mAb29	4	B	9	277	17313	158239
36	mAb30	4	B	5	635	39688	69744
37	mAb31	4	B	9	244	15250	22848
38	mAb32	4	C	3	210	13125	113558
39	ADC7	4	B	7	348	49714	127804
40	ADC8	4	B	5	311	44429	61046
41	mAb33	5	B	5	129	8063	63541
42	mAb34	5	B	10	479	29938	92600
43	mAb35	5	C	4	664	41500	21839
44	mAb36	5	B	9	673	42063	176647
45	mAb37	5	B	10	101	6313	195333
46	mAb38	5	B	5	283	17688	38141
47	mAb39	5	B	9	354	22125	55385
48	mAb40	5	C	4	665	41563	53472
49	ADC9	5	B	6	364	52000	199561
50	ADC10	5	B	10	132	18857	60418

Table C2 Detailed characteristics of the mAbs and ADCs considered in the pipeline (80% continuous pipeline).

Index	Product ID	Entry year	Manufacturing (batch / continuous)	Titre (g/L) or productivity (g/L/day)	Commercial demand (kg)	Patient population	Selling price ($/patient/annum)
1	mAb1	1	C	2	175	10938	61469
2	mAb2	1	C	3	472	29500	193841
3	mAb3	1	C	4	146	9125	18367
4	mAb4	1	B	2	274	17125	113816
5	mAb5	1	C	3	640	40000	86267
6	mAb6	1	C	4	164	10250	87720
7	mAb7	1	C	2	490	30625	77604
8	mAb8	1	C	4	400	25000	70650
9	ADC1	1	B	2	311	44429	62518
10	ADC2	1	C	3	448	64000	34165
11	mAb9	2	C	2	129	8063	145192
12	mAb10	2	C	2	122	7625	74550
13	mAb11	2	C	4	691	43188	41585
14	mAb12	2	B	4	448	28000	115634
15	mAb13	2	C	3	546	34125	150417
16	mAb14	2	C	2	211	13188	116607
17	mAb15	2	C	4	621	38813	162396
18	mAb16	2	C	4	433	27063	78103
19	ADC3	2	B	3	525	75000	162461
20	ADC4	2	C	2	476	68000	123021
21	mAb17	3	C	3	406	25375	147628

22	mAb18	3	C	3	254	15875	59176
23	mAb19	3	C	4	684	42750	185711
24	mAb20	3	B	2	400	25000	44564
25	mAb21	3	C	2	539	33688	54498
26	mAb22	3	C	3	187	11688	41803
27	mAb23	3	C	3	472	29500	49882
28	mAb24	3	C	4	579	36188	98012
29	ADC5	3	B	2	519	74143	108162
30	ADC6	3	C	2	698	99714	104515
31	mAb25	4	C	3	609	38063	125921
32	mAb26	4	C	3	273	17063	147546
33	mAb27	4	C	4	355	22188	108157
34	mAb28	4	B	3	582	36375	102254
35	mAb29	4	C	3	277	17313	158239
36	mAb30	4	C	2	635	39688	69744
37	mAb31	4	C	3	244	15250	22848
38	mAb32	4	C	4	210	13125	113558
39	ADC7	4	B	2	348	49714	127804
40	ADC8	4	C	2	311	44429	61046
41	mAb33	5	C	2	129	8063	63541
42	mAb34	5	C	3	479	29938	92600
43	mAb35	5	C	4	664	41500	21839
44	mAb36	5	B	3	673	42063	176647
45	mAb37	5	C	3	101	6313	195333
46	mAb38	5	C	2	283	17688	38141
47	mAb39	5	C	3	354	22125	55385
48	mAb40	5	C	4	665	41563	53472
49	ADC9	5	B	2	364	52000	199561
50	ADC10	5	C	3	132	18857	60418

Table C3 AAV products considered throughout the case study.

Product ID	Entry year	Manufacturing (batch / continuous)	Titre (vg/L)	Commercial demand (doses)	Patient population	Dose size (vg/dose)	Selling price ($/patient)
AAV1	1	B	6×10^{13}	5,000	5,000	7×10^{13}	800,000
AAV2	1	B	6×10^{13}	5,000	5,000	1×10^{14}	1,500,000
AAV3	1	B	6×10^{13}	5,000	5,000	7×10^{14}	2,100,000
AAV4	2	B	1×10^{14}	1,000	1,000	2×10^{14}	1,500,000
AAV5	2	B	1×10^{14}	1,000	1,000	6×10^{14}	2,000,000
AAV6	3	B	8×10^{13}	5,000	5,000	8×10^{13}	800,000
AAV7	3	B	8×10^{13}	5,000	5,000	1×10^{14}	1,500,000
AAV8	3	B	8×10^{13}	5,000	5,000	3×10^{14}	2,100,000
AAV9	4	B	6×10^{13}	1,000	1,000	1×10^{14}	1,500,000
AAV10	4	B	6×10^{13}	1,000	1,000	1×10^{14}	2,000,000
AAV11	5	B	8×10^{13}	5,000	5,000	7×10^{13}	800,000
AAV12	5	B	8×10^{13}	5,000	5,000	1×10^{14}	1,500,000
AAV13	5	B	8×10^{13}	5,000	5,000	7×10^{14}	2,100,000

Table C4 CAR T products considered throughout the case study.

Product ID	Entry year	Manufacturing (batch / continuous)	Commercial demand (doses)	Patient population	Dose size (vg/dose)	Selling price ($/patient)
CAR1	1	B	1,000	1,000	1×10^7	300,000
CAR2	1	B	1,000	1,000	2.5×10^8	600,000
CAR3	2	B	500	500	3×10^7	450,000
CAR4	2	B	5,000	5,000	9×10^7	500,000
CAR5	2	B	2,000	2,000	2.5×10^8	750,000
CAR6	3	B	1,000	1,000	5×10^7	350,000
CAR7	3	B	500	500	1×10^8	600,000
CAR8	4	B	5,000	5,000	4×10^7	450,000
CAR9	4	B	1,000	1,000	8×10^7	500,000
CAR10	4	B	2,000	2,000	1×10^8	750,000
CAR11	5	B	5,000	5,000	1×10^7	300,000
CAR12	5	B	1,000	1,000	2.5×10^8	600,000

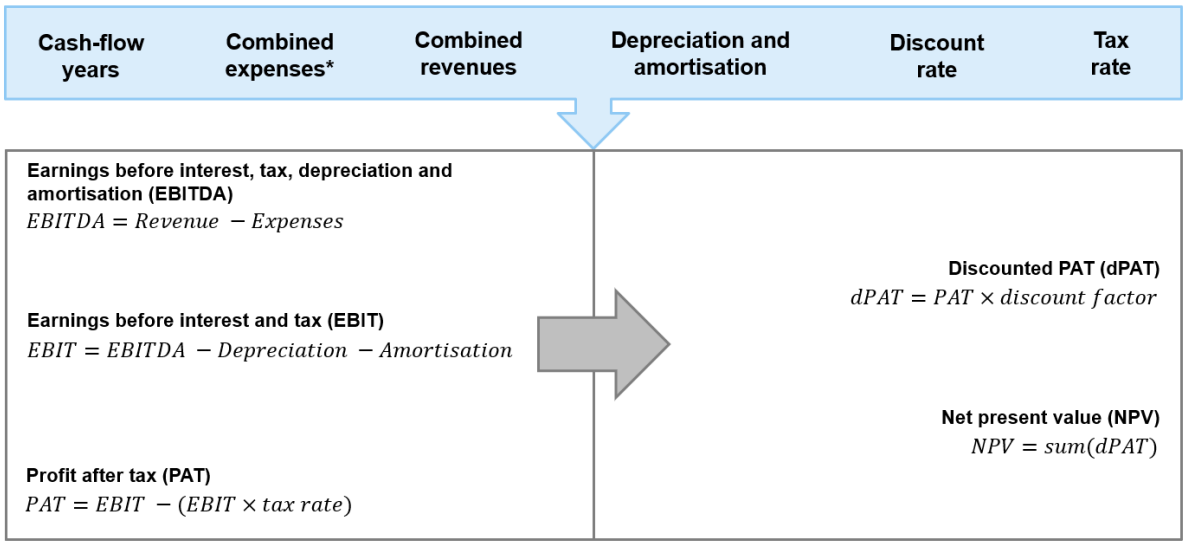

Figure C1 Flow of calculations required for determining the net present value (NPV).

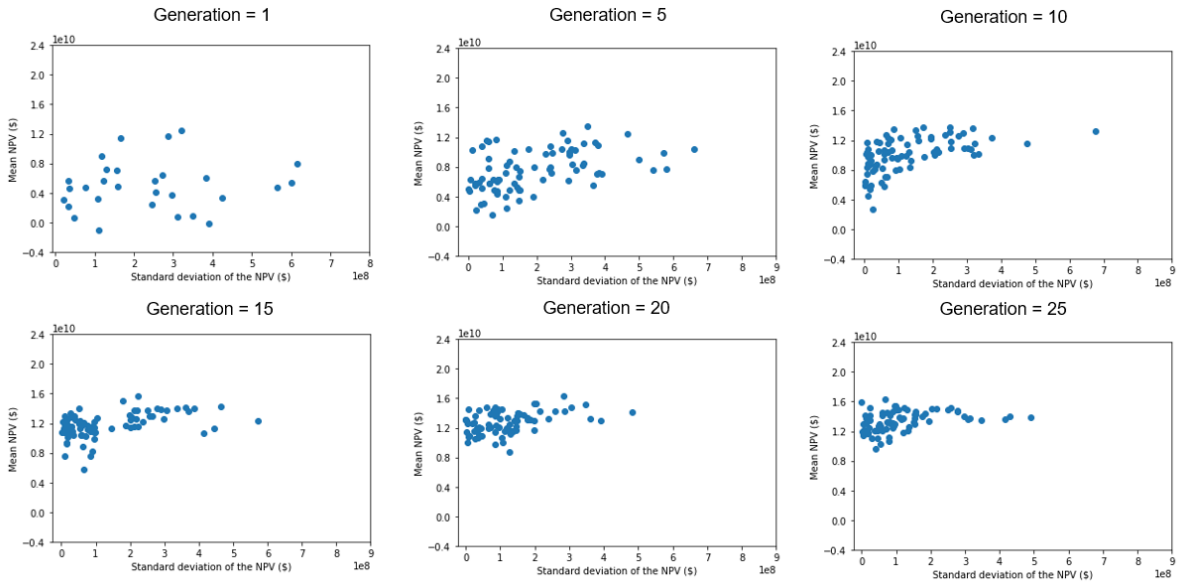

Figure C2 Progression of the objective space and Pareto discovery and for a non-risk adjusted scenario over generations when a 20% continuous pipeline was assumed, **a)** generation number 1**, b)** generation number 5**, c)** generation number 10**, d)** generation number 15**, e)** generation number 20, **f)** generation number 25.

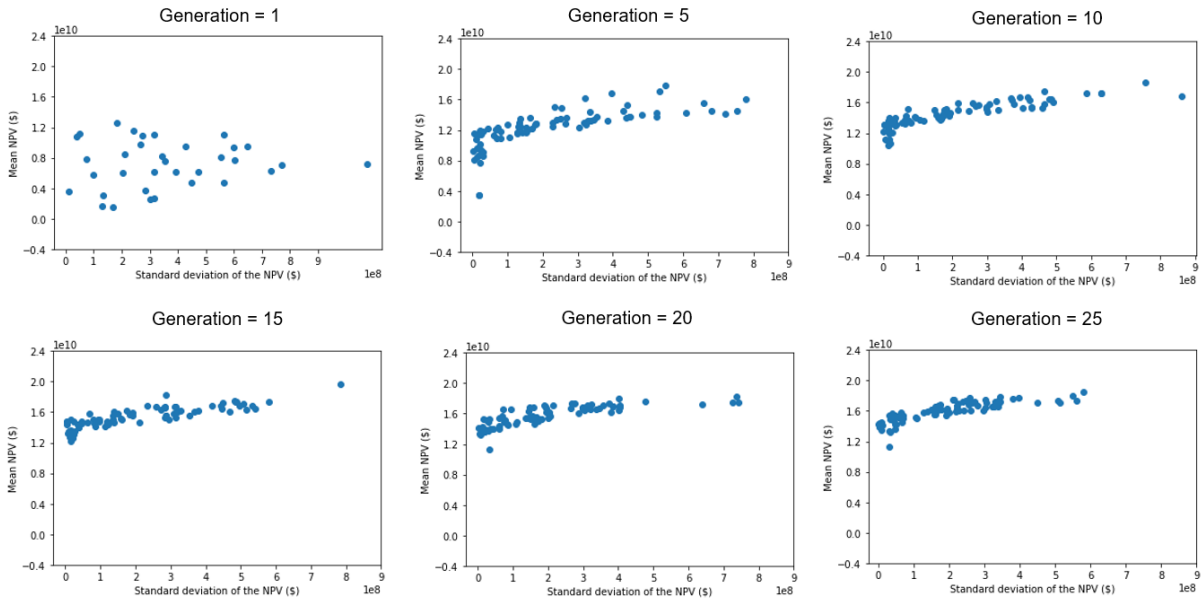

Figure C3 Progression of the objective space and discovery of the Pareto for a non-risk adjusted scenario over generations when an 80% continuous pipeline was assumed, **a)** generation number 1**, b)** generation number 5**, c)** generation number 10**, d)** generation number 15**, e)** generation number 20, **f)** generation number 25.

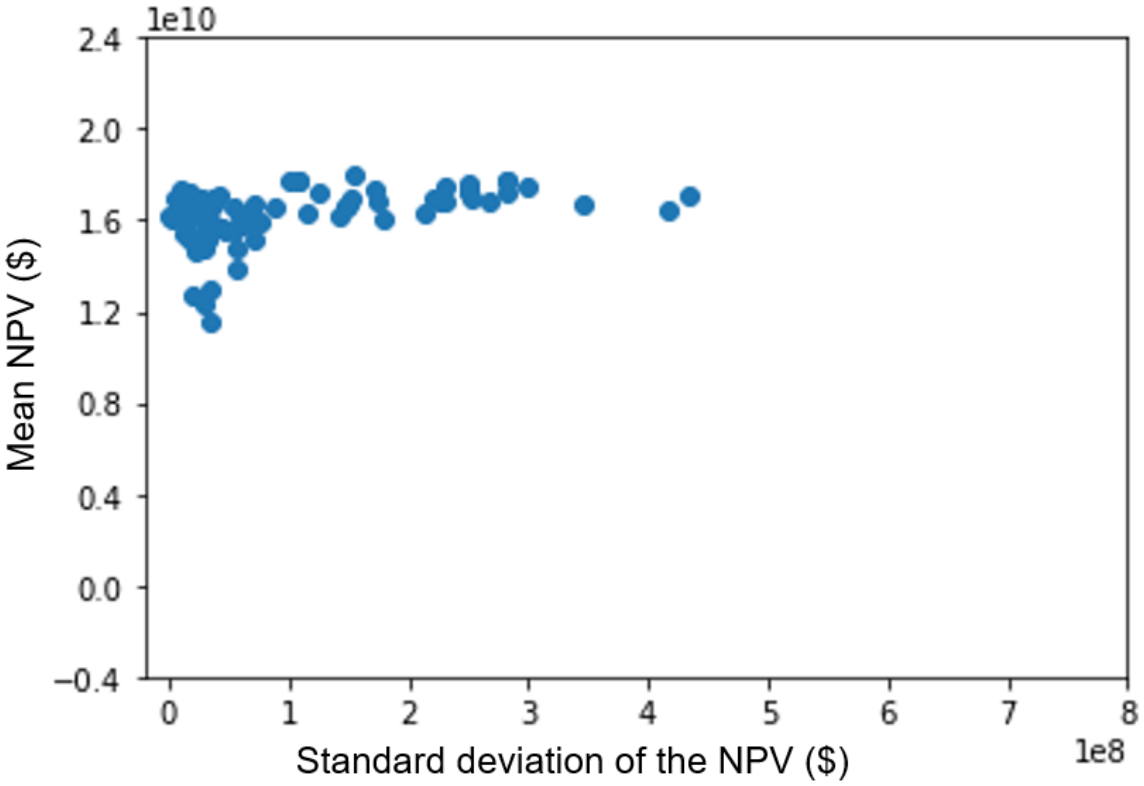

Figure C4 Final plot of the objective space when the repair strategy is implemented on the 20% pipeline scenario.

Solution 1 - $s_{30,1}$

M2	M8	A1	A2	M9	M10	M11	M14	M16	M17	M18	M19	M20	M21	M22	M23	M24	A5	A6	M25	M27	M28	M29	M30	M31	M32	A7	M33	M34	M35	M36	M38	M40
I	C	C	I	C	C	C	I	F	C	C	C	I	C	C	I	F	C	C	F	C	I	C	F	C	C	I	F	F	C	I	C	C

Solution 2 - $s_{30,2}$

M1	M2	M8	A1	M9	M10	M11	M13	M15	M16	A3	M17	M19	M20	M22	M23	M24	A5	A6	M25	M26	M27	M28	M30	M32	A8	M34	M35	M37	M38	M40	A9	A10
I	I	C	C	C	C	F	I	C	F	C	C	F	F	C	C	C	C	I	F	C	C	C	I	C	C	C	C	I	C	F	F	I

Solution 3 - $s_{30,3}$

M3	M4	M7	A1	A2	M10	M11	M13	M15	M16	M17	M19	M22	M23	M24	A5	A6	M25	M26	M27	M28	M30	M31	M32	A7	A8	M34	M35	M37	M39	M40	A9
C	C	C	C	I	C	F	C	I	F	C	F	C	I	F	I	C	C	I	F	F	I	C	C	I	C	F	F	C	I	F	I

Figure C5 Structure of the candidate portfolios arising from the repair strategy implemented on the 20% continuous pipeline. M = mAb product and A = ADC product. I = in-house, C = CMO and F = future facility. Green shading = external capacity options selected (CMO or build), orange shading = internal capacity options selected (in-house), grey shading = products that are manufactured continuously (over batch).

Algorithm C1 Crowding distance calculation in the NSGA-II.

Require: $R(solutions\ organised\ into\ Pareto\ ranks), f_1(objective\ function\ 1\ values)$, $f_2(objective\ function\ 2\ values)$

Objective function values were also organised by ranks and hence can be indexed by r

for r in R

  sort solutions in r by each objective in descending order

  generate two lists with the sorted S_g for both objectives

  assign large crowding distances to boundary solutions to preserve them

  for x in r

    $CD_{x,f_1} = \frac{{f_{1,r}}^{x+1} - {f_{1,r}}^{x-1}}{{f_{1,r}}^{max} - {f_{1,r}}^{min}}$

    $CD_{x,f_2} = \frac{{f_{2,r}}^{x+1} - {f_{2,r}}^{x-1}}{{f_{2,r}}^{max} - {f_{2,r}}^{min}}$

    $CD_x = CD_{x,f_1} + CD_{x,f_2}$

Algorithm C2 Batch assignment during capacity constraint considerations.

Require: $No.drugs$ $(number\ of\ drugs\ in\ the\ facility\ in\ the\ same\ year, from\ a\ given\ candidate\ portfolio), T\ (trains)$

$Shared\_trains\ = ceil(\frac{No.drugs}{T})$ # Maximum number of drugs handled by a train

$rem = No.drugs\ \%\ T$ # % in Python calculates remainder, which translates to how many drugs have to share a train

if $rem\ != 0$ # There is a remainder

  $arr_1 = [0, shared\_trains \ldots (shared\_trains \times rem)]$

  arr_2 , $arr_3 = [1, \ldots rem + 1]$,

  $arr_3 = [(shared\_trains \times rem),\ (shared\_trains - 1), \ldots,\ No.drugs]$

  for i, j in (arr_1, arr_2)

    append $sum(C[i: (shared\_trains \times j)])$ to $C_{combined}$

  for k in arr_3

    append $sum(C[k: (k \times (shared\_trains - 1))])$ to $C_{combined}$

else

  for i in $[0,\ shared\_trains \ldots No.drugs]$

    append $sum(C[i: (i + (shared\_trains))])$ to $C_{combined}$

Explanation

rem is used to identify how many drugs would have to share a train for that year. arr_1 is a constructed array with values ranging from 0 to the product of $shared\_trains$ and rem, in increments of $shared\_trains$. Use of both arrays together ensures where shared trains are required, appropriately grouping of drugs is performed

Using a numerical example to highlight why extra arrays were required, if the number of drugs utilising the manufacturing facility in a given year was **7** and the number of trains was equal to **4,** $shared\_trains$ became **2**, meaning the maximum number of drugs allocated to a single train is **2**. The rem is therefore equal to **3**. This value relates to the number of drugs that have to

share a train with another drug. In this case, as rem does not equal 0, $arr_1 = [0,\ 2,\ 4]$, $arr_2 = [1,\ 2,\ 3]$, $arr_3 = [6]$. It must be noted that when defining a range in Python, the length of the array is not included in the array itself, as can be seen in this example of arr_1, where the final value was specified as **6**, in increments of **2**, but the last value of the array was **4** not **6**. This was also seen for arr_2 and arr_3.

Line 9 then sum the batches stored in C by utilising Python indexing to group drugs, i.e. $[0:2]$ (in Python, this means the index of 0 and 1 are summed) and then $[2:4]$ and $[4:6]$. By this point, drugs in indices from 0 to 5 (i.e. 6 drugs) have been grouped. This leaves one remaining drug to use a train to itself, evidenced in Lines 10 and 11.

Papers by the author

Lyle A., Stamatis C., Linke T., Hulley M., Schmelzer A., Turner R., Farid SS (2023). **Process economics evaluation and optimisation of adeno-associated virus downstream processing.** *Biotechnology and Bioengineering*